Ponnuswamy Mohanasundaram

The Role of Vimentin in Tissue Repair and Cell Growth

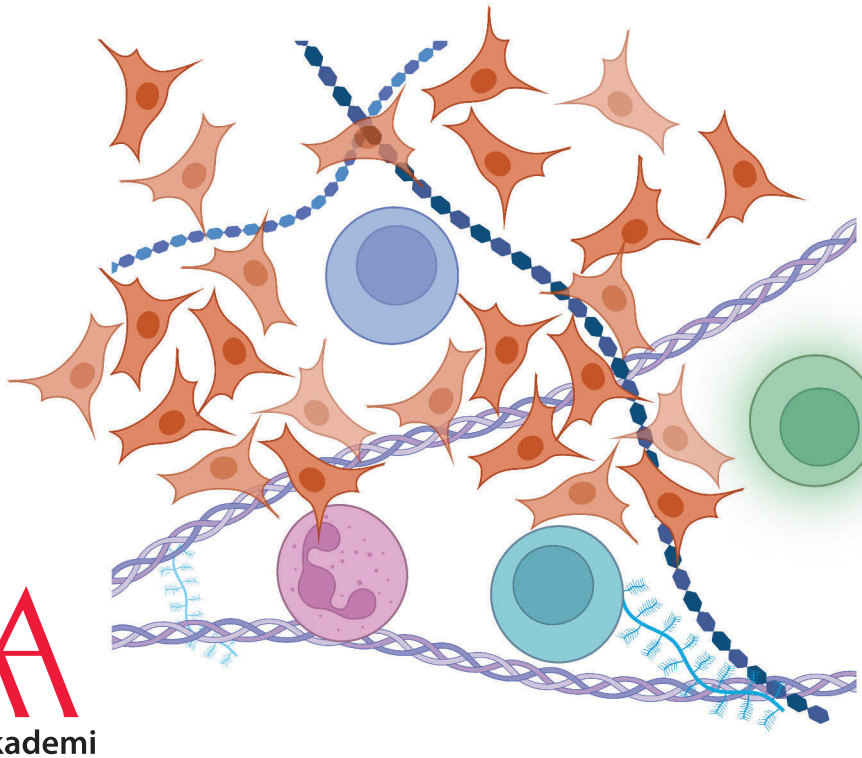

Åbo Akademi University

Ponnuswamy Mohanasundaram

Born in 1988 in Karur India

Previous study and degree

Master of Science in Biomedical Science Bharathidasan University India 2010

The cover image was designed through BioRender software by the author

The Role of Vimentin in Tissue Repair and Cell Growth

Ponnuswamy Mohanasundaram

Cell Biology
Faculty of Science and Engineering
Åbo Akademi University
Turku Bioscience Centre
University of Turku and Åbo Akademi University
Åbo Finland
2023

From the Faculty of Science and Engineering Cell Biology
Turku Doctoral Network in Molecular Biosciences Åbo Akademi University
Turku Bioscience Centre University of Turku and Åbo Akademi University

Supervised by

Professor John E. Eriksson PhD
Faculty of Science and Engineering
Åbo Akademi University
Turku Bioscience Centre University of Turku and Åbo Akademi University
Turku Finland

Co-supervised by

Associate Professor Fang Cheng PhD
School of Pharmaceutical Sciences (Shenzhen)
Sun Yat-Sen University
Shenzhen China

Pre-examiners

Docent Minna Poukkula PhD
Academy of Finland Research Fellow
Institute of Biotechnology
University of Helsinki
Helsinki Finland

Docent Emilia Peuhu PhD
Academy of Finland Research Fellow
Institute of Biomedicine
University of Turku
Turku Finland

Opponent

Professor Ville Hietakangas PhD
Molecular and Integrative Biosciences Research Programme
Faculty of Biological and Environmental Sciences
University of Helsinki
Helsinki Finland

ISBN 978-952-12-4262-5 (printed)
ISBN 978-952-12-4263-2 (digital)
Painosalama, Åbo, Finland 2023

It is better to identify with our ignorance than knowledge, because knowledge implies a boundary

Our lives become beautiful not because we are perfect. Our lives become beautiful because we put our heart into whatever we do

May your dreams not come true. May things that you could never dream of happen to you.

ABSTRACT

Microfilaments, microtubules, and intermediate filaments serve as the cytoskeleton of the cell and form a complex network by interacting with cytoskeleton-associated proteins. The cytoskeleton provides a framework for the cell and regulates different cellular functions. Intermediate filaments form a large family of proteins, which are classified into different groups based on their structure and tissue expression pattern. Epithelial cells undergo epithelial-mesenchymal transitions (EMT) during embryonic development, wound healing, cancer, and fibrosis, to become proliferative, and migratory in nature. Vimentin is a well-known EMT marker, but its role in EMT is not well characterized. This thesis work investigated the role of vimentin in EMT during the wound healing process, cell growth, and autoimmunity. In *Vim*$^{-/-}$ mice, delayed wound healing due to defects in EMT signaling, keratinocyte cell migration, fibroblast cell proliferation, and collagen deposition. Fibroblasts play an essential role in normal development and wound healing. We observed that a lack of vimentin resulted in reduced fibroblast cell size and due to deficient mTOR signaling. Vimentin affected mTOR signaling by modulating Rag GTPase activity, consequently regulating cell size and autophagy. We also found that vimentin expression was increased in regulatory Treg cells, which control autoimmune response, and this increase in expression was mediated through TGF-β1. This thesis work provides evidence for the new roles of vimentin in tissue repair and cellular growth.

SAMMANFATTNING

Mikrofilament, mikrotubuli och intermediära filament utgör cellens cytoskelett och formar ett komplext nätverk genom att interagera med cytoskelett-associerade proteiner. Cytoskelettet förser cellen med ett ramverk och reglerar olika cellulära funktioner. Intermediära filament utgör en stor proteinfamilj, som delats upp i olika grupper baserat på proteinets struktur och vävnadsuttryck. Vimentin är ett typ-III intermediärfilamentprotein, som uttrycks i stor grad i mesenkymala celler. Epitelceller genomgår epitelial-mesenkymal transition (EMT) under embryonalutvecklingen, vid sårläkning, cancer och fibros för att erhålla stamhet och en mer dynamisk och rörlig fenotyp. Vimentin är en välkänd EMT-markör, men dess roll i EMT är inte väl karaktäriserad. Detta examensarbete har undersökt vimentins roll i EMT under sårläkningsprocessen, vid celltillväxt och vid skydd mot oxidativ stress. I *Vim*$^{-/-}$ möss fördröjs sårläkningen till följd av defekter i EMT signaleringen, keratinocyt-migrationen, fibroblast-proliferationen och depositionen av kollagen. Medan vi kunde påvisa att vimentin är essentiell för funktionen av fibroblaster vid normal utveckling och sårläkning, vi observerade också att en avsaknad av vimentin reducerar fibroblasters storlek till följd av bristfällig mTOR signalering. Vimentin påverkar mTOR signalering genom att modulera aktiviteten av Rag GTPas, vilket i sin tur reglerar cellstorlek och autofagi. Vimentin stimulerar proliferation och skyddar cellerna mot oxidativ stress genom att upprätthålla redoxtillståndet. Vi har även påvisat att uttrycket av vimentin ökade i reglerande Treg celler, vilka kontrollerar immunresponsen och autoimmuna sjukdomar och detta förhöjda uttryck är medierat genom TGF-β1. Detta examensarbete påvisar nya roller för vimentin i vävnadsregenerering och celltillväxt.

TABLE OF CONTENTS

LIST OF ORIGINAL PUBLICATIONS

This thesis is based on the following original publications that are referred to in the text by their Roman numerals (**I-III**). In addition, unpublished results are also included in the thesis.

I. Cheng F, Shen Y, **Mohanasundaram P**, Lindström M, Ivaska J, Ny T, Eriksson JE. 2016. Vimentin coordinates fibroblast proliferation and keratinocyte differentiation in wound healing via TGF-β-Slug signaling. *Proc Natl Acad Sci USA* 113:E4320-4327.

II. **Mohanasundaram P**#, Coelho-Rato LS#, Modi MK, Urbanska M, Lautenschläger F, Cheng F, Eriksson JE. 2022. Cytoskeletal vimentin regulates cell size and autophagy through mTORC1 signaling. *PLOS Biology* 20:e3001737. # Equal contributions

III. Mohammad I, Nousiainen K, Bhosale SD, Starskaia I, Moulder R, Rokka A, Cheng F, **Mohanasundaram P**, Eriksson JE, Goodlett DR, Lähdesmäki H, Chen Z. 2018. Quantitative proteomic characterization and comparison of T helper 17 and induced regulatory T cells. *PLOS Biology* 16:e2004194.

Publication not included in the thesis

IV. Wang L, **Mohanasundaram P**, Lindström M, Asghar MN, Sultana G, Misiorek JO, Jiu Y, Chen H, Chen Z, Toivola DM, Cheng F, Eriksson JE. 2022. Vimentin suppresses inflammation and tumorigenesis in the mouse intestine. *Front Cell Dev Biol* 10:862237.

AUTHOR CONTRIBUTIONS

1. Author contributed to the concept, performing research, analyzing data, and writing the manuscript. LSCR performed research, data analysis, and wrote the manuscript. MM helped with image analysis. UM, and FL did BMDCs experiments. FC contributed to mice data and reviewed the manuscript. JEE contributed to funding acquisition, concept, and writing the manuscript.

2. Author contributed to performing research and analyzing data along with F.C., Y.S., and M.L. Concept and research work were designed by FC, JI and JEE. Reagents/analytic tools were provided by JI and TN. The manuscript was written by FC and JEE. Funding acquisition by JEE.

3. Author was involved in mice experiments and reviewing-editing the manuscript. IM was involved in performing research, analyzing data, and reviewing manuscripts. KN was involved in data visualization and review & editing of the manuscript. IS performed research and reviewed a manuscript. SDB, RM, and AR were involved in mass spectrometry methodology and reviewing-editing the manuscript. FC was involved in performing research and reviewing-editing the manuscript. JEE was involved in funding acquisition and reviewing-editing the manuscript. DRG methodology, supervision, reviewing-editing the manuscript. HL contributed to resources, supervision, and reviewing-editing the manuscript. ZC was involved in conceptualization, funding acquisition, investigation, project administration, resources, supervision, visualization, writing the original draft, review & editing the manuscript.

ABBREVIATIONS

BMDCs - Bone marrow-derived dendritic cells

BMI – Body mass index

CDK1 - Cyclin-dependent kinase1

Deptor - DEP domain-containing mTOR-interacting protein

DLD - Dihydrolipoamide dehydrogenase

DSS - Dextran sodium sulfate

EAAs - Essential amino acids

eEF-2K - Eukaryotic elongation factor 2 kinase

EGF - Epidermal growth factor

eIF4B - Eukaryotic initiation factor 4B

EMT - Epithelial-mesenchymal transition

FAK - Focal adhesion kinase

FGF - Fibroblast growth factor

GDFs - Growth and differentiation factors

GDP - Guanosine diphosphate

GEFs - Guanine nucleotide exchange factors

GFAP - Glial fibrillary acidic protein

GGF - Glial growth factor

GTP - Guanosine triphosphate

HGF - Hepatocyte growth factor

HIF1α - Hypoxia inducible factor 1α

HK2 - Hexokinase 2

HLH – Helix-loop-helix factors

IFs - Intermediate filaments

IGF 1/ 2 – Insulin-like growth factor 1/2

LC3 - microtubule-associated protein light chain 3

LDHA - Lactate dehydrogenase A

LDHB - Lactate dehydrogenase B

MAP - Microtubule-associated protein

MDFs - Mouse dermal fibroblasts

MEFs - Mouse embryonic fibroblasts

MET - Mesenchymal-epithelial transition

MINPP1 - Multiple inositol-polyphosphate phosphatase 1

mLST8 - Mammalian lethal with SEC13 protein 8

MMPs - Matrix metalloproteinases

mSin1 – Stress-activated protein kinase-interacting protein 1

mTOR - Mechanistic target of rapamycin

mTORC1 - Mechanistic target of rapamycin complex 1

mTORC2 - Mechanistic target of rapamycin complex 2

NEAAs - Non-essential amino acids

NLS - Nuclear localization signal

Pak1 - p21-activated kinase

PDCD4 - Programmed cell death 4

PDGFs - Platelet-derived growth factors

PDK1 - Phosphoinositide-dependent kinase-1

PE - Phosphatidylethanolamine

PEP - Phosphoenolpyruvate

PFKL - Phosphofructokinase, liver type

PGAM2 - Phosphoglycerate mutase 2

PGK1 - Phosphoglycerate kinase 1

PIP2 - Phosphatidylinositol 4,5-bisphosphate

PIP3 - Phosphatidylinositol 3,4,5-trisphosphate

PK - Pyruvate kinase

PKM2 - Pyruvate kinase M2

PPP - Pentose phosphate pathway

PRAS40 - Proline-rich Akt/PKB substrate 40 kDa

Protor - Protein observed with Rictor

PtdIns3K - Phosphatidylinositol 3-kinase

PTMs - Post-translational modifications

Raptor - Regulatory-associated protein of mTOR

Rictor - Rapamycin-insensitive companion of mTOR

ROS - Reactive oxygen species

RTKs - Receptor tyrosine kinases

SDS-PAGE - Sodium dodecyl-sulfate polyacrylamide gel electrophoresis

S1P - Sphingosine 1-phosphate

SHP2 - SH2 containing protein tyrosine phosphatase-2

SKAR - S6K1 Aly/REF-like substrate

SPC - Sphingosylphosphorylcholine

SREBP-1 - Sterol regulatory element binding protein 1

TCA - Tricarboxylic acid cycle

TGF-β1 - Transforming growth factors β1

TNF-α - Tumor necrosis factor-α

TPI1 - Triosephosphate isomerase

TSC2 - Tuberous sclerosis complex 2

ULFs - Unit length filaments

ULK1 - Unc-51 like autophagy activating kinase 1

VEGF -Vascular endothelial growth factor

Vim $^{-/-}$ -Vimentin knock out

WT - Wild type

1 INTRODUCTION

Initially, life emerged as a single-celled organism by transforming inanimate matter into living things. Then single-celled organisms subsequently evolved into multicellular organisms by increasing their complexity (Colizzi *et al*, 2020). To make cells fully functional and dynamic, thousands of proteins communicate and interact with each other (Aebersold *et al*, 2018). The cytoskeleton is a filamentous network of proteins, which provides structure and integrity to the cell (Fletcher & Mullins, 2010). In most eukaryotic unicellular organisms, microfilaments and microtubules constitute the cytoskeleton of the cell. Multicellular organisms possess one more cytoskeletal protein family called intermediate filaments (IFs) (Preisner *et al*, 2018). More than 70 genes comprise the IFs family and they are classified into six groups based on their structure and tissue expression patterns (Szeverenyi *et al*, 2008). Besides providing a structural framework, IFs support cells adhering to adjacent cells and extracellular matrix. This property brings complexity and integrity to the tissue (Jones *et al*, 2017). Vimentin is a type III intermediate filament protein, expressed mainly in mesenchymal cells. It is involved in different cellular functions, such as proliferation, migration, invasion, autophagy, and protection from oxidative stress (Ridge *et al*, 2022). Vimentin occurs in soluble forms (monomer, dimer, tetramer, and unit-length filaments) and fibrous network structures. The dynamics of vimentin filaments are regulated mainly by post-translational modifications through which they control various cellular functions such as proliferation, migration, invasion, and signaling (Snider & Omary, 2014; Ramos *et al*, 2020).

The epithelial-mesenchymal transition (EMT) occurs during embryonic development and in pathological conditions such as cancer, wound healing, and fibrosis. During EMT, polarized epithelial cells undergo morphological changes from a cuboidal shape into spindle-like shaped mesenchymal cells (Dongre & Weinberg, 2019). The cell's transcriptome and proteome change from epithelial-specific into mesenchymal-specific, and cell detach itself from the basement membrane. EMT increases the proliferative and migratory capacity of cells and secretion of extracellular matrix. These characteristics provide versatility to the mesenchymal cells and support growth and development (Mani *et al*, 2008; Francou & Anderson, 2020). Mesenchymal cells also can switch to epithelial cells by undergoing a mesenchymal-epithelial transition (MET) (Pei *et al*, 2019). Both EMT and MET play a significant role in maintaining homeostasis during tissue

regeneration and embryonic development. Dysregulation in the EMT can cause chronic wounds, fibrosis, and cancer (Dongre & Weinberg, 2019; Pei *et al*, 2019).

Defects in the formation of connective tissue, cell proliferation, and migration mainly affect tissue regeneration (Stone *et al*, 2016). Growth factors, nutrient availability, oxygen level, and other factors, influence cell growth and proliferation (Saxton & Sabatini, 2017). Cells require nutrients and growth factors to maintain rapid cell growth and proliferation. Cancer cells have evolved to adapt and modify their metabolism to overcome nutrient and growth factor restrictions. In some cancers, most glucose molecules are converted into metabolic intermediates to support nucleotides, fatty acids, and non-essential amino acids synthesis, instead of undergoing oxidative phosphorylation. This helps to maintain the redox level and reduces the metabolic burden (Pavlova & Thompson, 2016; Pavlova *et al*, 2022).

Vimentin expression in mesenchymal and cancer cells supports cell proliferation and migration. Vimentin is one of the widely used mesenchymal markers in EMT. As a cytoskeletal protein, it provides structural and mechanical support to the cells. It is also involved in cell proliferation, migration, and invasion; however, molecular mechanisms have not been explored in depth (Satelli & Li, 2011; Ridge *et al*, 2022). This thesis work investigated the involvement of vimentin in EMT during wound healing, autoimmune disorders, and how vimentin regulates cell growth and proliferation.

2 REVIEW OF THE LITERATURE

2.1 Cytoskeleton of the cell

Animal cells look like fluid-filled bags, enclosed by a lipid bilayer plasma membrane (Clegg, 1984). The plasma membrane selectively allows the cell to exchange molecules and nutrients and also separates the cell from its external surroundings (Lillemeier *et al*, 2006). The cell is a very delicate structure and needs special structural support (Luna & Hitt, 1992). The cytoskeletal network proteins provide structure and form to the cells. They also hold the plasma membrane and internal organelles in place (Koppers *et al*, 2020). Assembly and disassembly of the cytoskeletal network enable cells to respond to surrounding signals by changing cell morphology and properties (Fletcher & Mullins, 2010). Besides providing structural support, the cytoskeleton also plays a vital role in mitosis, cell division, mechanosensing, migration, invasion, as well as organelle positioning, and vesicle trafficking (Fletcher & Mullins, 2010; Fife *et al*, 2014; Rogers & Gelfand, 2000).

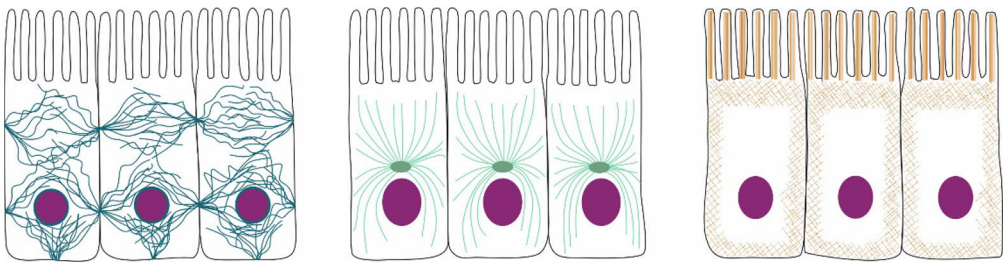

Figure 1. **Cytoskeleton of the cell.** Intermediate filaments, microtubules, and microfilaments are the three filament structures that form the cytoskeleton of the cell. The image is adapted from (Pollard & Goldman, 2018).

In most eukaryotes, microfilaments, microtubules, and intermediate filaments (IFs) form the cell's cytoskeleton (Figure 1). They form fibrous filament structures by assembling simple subunits into long thread-like strands. Along with filamentous structures, the cell also possesses cytoskeletal-associated proteins, which support complex cytoskeletal network formation (Hohmann & Dehghani, 2019). These three cytoskeletal filament proteins regulate cell function either collectively or individually depending upon the type of functions in which they are involved (Schoumacher *et al*, 2010; Gan *et al*, 2016; Fletcher & Mullins, 2010).

2.2 Intermediate filaments

Intermediate filaments are prevalent in metazoans (multicellular animals), there are some studies claim that bacteria possess intermediate-like filaments but their functional role needs to be studied further (Pollard & Goldman, 2018; Ausmees *et al*, 2003). Based on the localization of IFs in the cell compartment, IFs are classified into cytoplasmic IFs and nuclear IFs. Cytoplasmic IFs are located in the cytoplasm and nuclear IFs form a nuclear lamina along with nuclear lamin-associated membrane proteins, which envelope the nucleus (Szeverenyi *et al*, 2008). In *Dictyostelium,* lamin-like protein NE81 was identified and it shares lamin function, however cytoplasmic intermediate filament presence in lower eukaryotes is not reported (Chang & Goldman, 2004; Osmanagic-Myers & Foisner, 2019). Based on this, it has been hypothesized that the IFs protein family emerged from the primordial *lamin* gene (Dittmer & Misteli, 2011).

2.2.1 Types of intermediate filaments

The IFs are the largest cytoskeletal protein family. It comprises more than 70 genes with distinct tissue-specific expression patterns (Szeverenyi *et al*, 2008). Based on their sequence homology, the IFs are classified into six types, they are Type I, Type II, Type III, Type IV, Type V and Type VI (Table 1) (Chang & Goldman, 2004). Type I IFs are acidic keratins and type II IFs are basic keratins; both are expressed in epithelial cells (Omary *et al*, 2006). Vimentin, desmin, glial fibrillary acidic protein (GFAP), peripherin, and syncoilin are classified as type III IFs. Vimentin is expressed mainly in cells of mesenchymal origin, leukocytes, and endothelial cells; GFAP expression is primarily seen in astrocytes and glial cells. Desmin and syncoilin are found mainly in muscle cells. Peripherin is expressed in peripheral neurons (Robert *et al*, 2016). Neurofilament-L, neurofilament-M, neurofilament-H, nestin, synemin, and α-internexin fall under type IV IFs. Neurofilaments-L, M, and H are specific to central and peripheral neurons, α-internexin is present in nervous system; synemin occurs in astrocytes and neurons; and nestin is mainly expressed in neuroepithelial progenitor cells (Godsel *et al*, 2008). Lamins A, B, and C are classified under type V IFs proteins. Lamins A, a small splice variant, and C are encoded by the *LMNA* gene. They are expressed in most of the differentiated cells. Lamins B1 and B2 are encoded by two different genes and expressed in all cell types (Chang & Goldman, 2004; Osmanagic-Myers & Foisner, 2019). Lastly, phakinin and filensin are orphan type VI IFs, and their expression is specific to eye lenses (Szeverenyi *et al*, 2008).

Table:1 Intermediate filaments classification based on their homology and assembly property.

Types	Intermediate filaments	Assembly group	Distribution
Type I	Keratins (K9-K20)	Group I	Epithelia, hair and nails
Type II	Keratins (K1-K8)		Epithelia, hair and nails
Type III	Vimentin	Group II	Mesenchyme
	Desmin		Cardiac, skeletal and smooth muscles
	Syncoilin		Muscles
	GFAP		Glia, astrocytes
	Peripherin		Peripheral neurons
Type IV	Neurofilaments: NF-L, NF-M, NF-H		Central nervous system and peripheral neurons
	α-Internexin		Nervous system
	Synemin		Neurons and astrocytes
	Nestin		Neuroepithelial progenitor cells
Type V	Lamins A, B and C	Group III	Nucleus
Type VI	Filensin	Unknown	Lens
	Phakinin		Lens

Among these types, some filament types can form either homopolymer or heteropolymer filaments with other filament types; based on this assembly property, they are further categorized into three groups (Table 1). Type I and II keratins exist as heteropolymeric filaments; they cannot form homopolymeric filaments. Based on the nature of the filament assembly property, Types I and II are grouped under assembly group I. Types III and IV IFs can form homopolymers or heteropolymers between these two groups, based on this property, they are grouped into assembly groups II. Type V Lamins form homodimers and cannot form heterodimers with other IFs family members, so they are grouped under the type assembly group III (Chang & Goldman, 2004).

2.2.2 Intermediate filament's structure and assembly

The basic unit of IFs comprises a central alpha-helix rod domain and it is flanked by a non-helical domain at the N-terminus head region and C-terminus tail region (Herrmann & Aebi, 2004). The central rod domain contains three coiled structures. These coiled structures are connected through linkers. Coil 1A and coil 1B are connected through linker L1, and coil 2 is closely associated with coil 1B through linker L12 (Conway & Parry, 1988). Along with these structures, lamins possess a nuclear localization signal and an Ig-fold, which are specific to the nuclear intermediate filaments (Figure 2) (Herrmann & Aebi, 2016). The central rod domain has a hydrophobic heptad repeat sequence, which is highly conserved in all IFs. This sequence plays an important role in dimer formation (Herrmann & Aebi, 2004). Formation of IF filaments from monomers is described in Figure 3. Two alpha-helical rod domains form a coiled-coil dimer. Dimers align opposite each other and form a tetramer; because of this antiparallel arrangement, IFs lack polarity. Then tetramers align laterally and form unit length filaments (ULFs), which then assemble into a filament (Figure 3). These filaments form complex networks by interacting with cytoskeletal-associated proteins and other members of the cytoskeleton (Chang & Goldman, 2004; Herrmann *et al*, 2007; Herrmann & Aebi, 2016). The diameter of the IFs is between the sizes of microfilaments and microtubules, i.e., around 10 to 12 nm. The assembly of a dimer into long filaments is mainly regulated by a consensus motif on either side of the alpha-helical domain (Strelkov *et al*, 2002). The assembly of IFs is well-studied using *in vitro* systems. By adding divalent metal ions or increasing the concentration of sodium chloride to physiological levels, soluble IF monomers spontaneously assemble into dimers, tetramers, and ULFs (Herrmann *et al*, 1999). In cells, post-translational modifications on their head and tail domains mainly regulate IF assembly and disassembly (Snider & Omary, 2014).

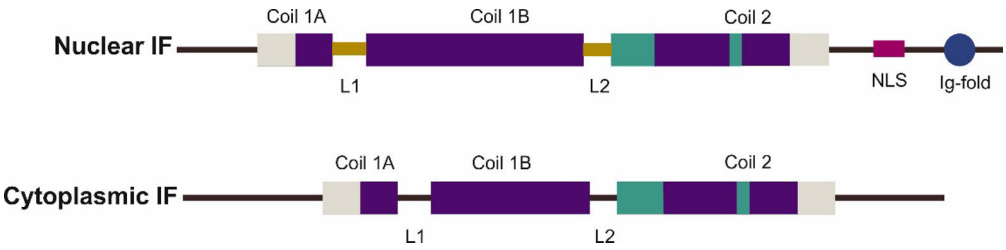

Figure 2: Intermediate filaments structure. Cytoplasmic and nuclear IFs possess coil 1A, coil 1B, and coil 2 domains, which form the basic units of IFs and are connected through linker L1 and L12. The nuclear localization signal (NLS) and Ig fold are unique to nuclear IFs. Image adapted from (Herrmann & Aebi, 2016).

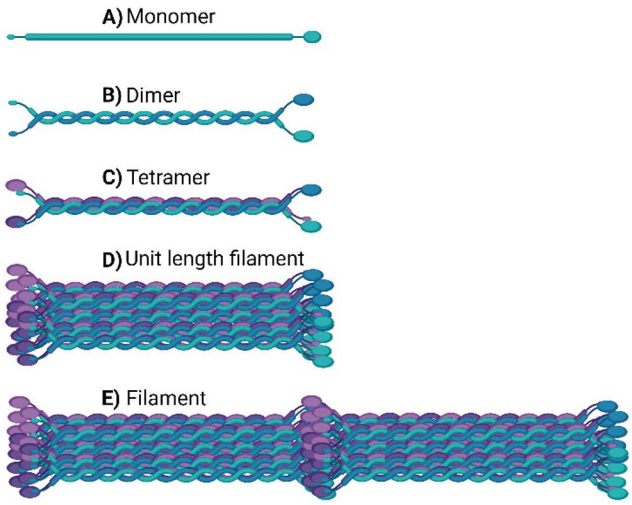

Figure 3. **Assembly of IFs** A) IF monomer. B) Two monomers align each other and form a coiled-coil dimer. C) Two dimers align antiparallel to each other and form tetramer. D) Tetramers form a unit length filament. E) Unit length filaments assemble to form a ropelike filament. Images adapted from (Herrmann & Aebi, 2016).

IFs form a thick rope-like structure that can resist more stress and strain than microfilaments and microtubules. These enable cells and tissues to withstand various physical and mechanical strains (Goldman *et al*, 2008). Flexibility and elasticity are unique characteristics of IFs that distinguish them from other cytoskeletal proteins (Charrier & Janmey, 2016). IFs can increase their length by extending their dimer structures along the axis of the filament and transforming its secondary structure from α helical to β sheet, which provides elasticity and flexibility to the filament (Qin *et al*, 2009).

2.2.3 Intermediate filaments regulation and diseases

The length and composition of the head and tail domains vary within the IFs protein family, which allows them to function uniquely (Kornreich *et al*, 2015). In order to regulate a vast array of functions, IFs undergo a wide range of post-translational modifications (PTMs), such as phosphorylation, sumoylation, glycosylation, acetylation, and ubiquitylation (Hyder *et al*, 2008; Snider & Omary, 2014). IFs act as prime substrates for different kinases; they possess numerous phosphorylation sites, especially in their head and tail domains (Omary *et al*, 2006; Snider & Omary, 2014). Some phosphorylation sites are highly conserved

in all IF proteins; for instance, the cyclin-dependent kinase1 (CDK1) phosphorylation site which regulates lamin disassembly during mitosis is highly conserved in all IF proteins (Omary *et al*, 2006; Köster *et al*, 2015; Machowska *et al*, 2015). Likewise, different kinases can phosphorylate IFs on the same site (Hyder, 2014). Initially, it was reported that phosphorylation mainly regulates the assembly and disassembly of IFs. However, more evidence suggests that phosphorylation of IFs plays a role in a wide range of cellular functions, such as cell motility, cell-cell interaction, cell adhesion, scaffolding, metabolism, mitosis, cell survival, and cell death (Ivaska *et al*, 2005; Snider & Omary, 2014; Robert *et al*, 2016). Mutations in IFs can affect specific organs, such as muscle, nerves, skin, or organ systems in the body (Omary *et al*, 2004). Especially mutation in the lamins causes serious pathological conditions, such as premature aging, muscular dystrophy, cardiomyopathy, and neuropathy (Worman, 2012).

2.3 Vimentin

2.3.1 Vimentin expression

Vimentin belongs to the type III intermediate filament protein family (Szeverenyi *et al*, 2008). It is found in kidney, lung, liver, heart, eye, brain, ovary, testis, and various tissue such as adipose tissue, connective tissue, vascular tissue, and bone marrow; and it is expressed mainly in mesenchymal cells and fibroblasts (Uhlén *et al*, 2015). During embryonic development, vimentin expression is initially seen in mesenchymal cells at the primitive streak region, on embryonic day 8.5 (Franke *et al*, 1982). Mesenchymal cells act as precursor cells for adipose tissues, bone, cartilage, muscles, skin, and liver (Bianco, 2014). Although vimentin is known to occur in the cytoplasm, however number of reports showed that vimentin also occurs on the cell surface or secreted into the extracellular space or exosomes. Vimentin present outside of the cell is called extracellular vimentin (Ramos *et al*, 2020; Mor-Vaknin *et al*, 2003; Parvanian *et al*, 2021). It is secreted by various cells such as macrophages, endothelial cells, neutrophils, and platelets. Extracellular vimentin involves in different cellular processes such as infection, immune response, wound healing, and hemostasis (Mor-Vaknin *et al*, 2003; Zou *et al*, 2006; Da *et al*, 2014; Xu *et al*, 2004).

2.3.2 Vimentin and cell organelles

Vimentin filament can withstand a higher degree of mechanical stress than actin and microtubule. This property provides mechanical integrity and localizes organelle in place (Guo *et al*, 2013). In confined migration, vimentin prevents

nuclear deformation and protects the cell from DNA damage by regulating nuclear shape and perinuclear stiffness (Patteson *et al*, 2019). Mitochondria are highly dynamic organelles, which undergo fusion and fission to maintain normal functions and bioenergetics (Gao & Hu, 2021). Deletion of vimentin disturbs mitochondria distribution, decreases membrane potential, and increases mitochondrial motility and reactive oxygen species generation (Tang *et al*, 2008; Nekrasova *et al*, 2011; Chernoivanenko *et al*, 2014). To prevent mitochondrial motility, vimentin anchors mitochondria at proline 57 sites (Chernoivanenko *et al*, 2015). The Golgi complex can interact with vimentin, through which it regulates nucleus and cell body orientation during migration. Vimentin also interacts with the AP3 complex, which is involved in the endolysosomal transport system (Gao & Sztul, 2001; Gao *et al*, 2002; Styers *et al*, 2004). During pre-adipose cells differentiation, vimentin forms cage-like structures around lipid droplets, which is mediated by perilipin for lipid droplet formation. Vimentin also regulates lipid accumulation in late endosomes by interacting with Rab9 (Walter *et al*, 2009; Heid *et al*, 2014).

2.3.3 Function and post-translational modifications of vimentin

Vimentin possesses several post-translational modification sites in both head and tail domains; especially phosphorylation sites are abundant (Hyder *et al*, 2008; Hyder, 2014). Different kinases, such as PKC, PKA, CaM kinase II, Cdk1, ROCK, Aurora-B kinase, PLK-1, and Akt phosphorylate vimentin (Snider & Omary, 2014; Virtakoivu *et al*, 2015a; Hyder, 2014; Ivaska *et al*, 2005). These kinases can phosphorylate vimentin on single or multiple sites, through which they regulate vimentin assembly, interaction, and different cellular functions such as proliferation, migration, invasion, and autophagy. Some of the phosphorylation sites in vimentin can act as a target for different kinases and also some kinases can phosphorylate vimentin on multiple sites (Hyder, 2014; Zhu *et al*, 2011). Phosphorylated vimentin can bind to 14-3-3, which could enable other protein interactions. For instance, vimentin mediates the interaction of 14-3-3 ε with GFAP, or it can limit other proteins' interaction with 14-3-3 (Tzivion *et al*, 2000, 2001; Satoh *et al*, 2004). During mitosis, the mitotic kinase, CDK1 phosphorylates vimentin at serine 55, leading to the activation of PIk1. In turn, Plk1 phosphorylates vimentin at serine 82, which allows ROCK and Aurora B to phosphorylate vimentin at S71 and S72. This consecutive phosphorylation of vimentin regulates cytokinesis and the segregation of IFs into two daughter cells (Goto *et al*, 2003; Yamaguchi *et al*, 2005; Yokoyama *et al*, 2005). Mutation of mitotic-specific phosphorylation sites from serine to alanine causes cataract

formation, chromosome instability, aneuploidy, and decreased lens size (microphthalmia) in transgenic mice (Matsuyama *et al*, 2013). Phosphatases balance vimentin assembly and disassembly dynamics and functions by removing phosphate groups in vimentin. Protein phosphatase 2A (PP2A) and protein phosphatase 1 (PP1) are enzymes known to dephosphorylate vimentin (Li *et al*, 2016; Turowski *et al*, 1999). Apart from phosphorylation, vimentin also undergo other types of post-translational modifications such as SUMOylation, glycosylation, and acetylation (Guo *et al*, 2018; Tarbet *et al*, 2018; Wang *et al*, 2010).

2.4 Cell growth and proliferation

Mass accumulation increases cell size, which allows cells to store nutrients and energy and produce equal-sized daughter cells after cell division (Amodeo & Skotheim, 2016). Although an increase in cell size and cell division are two separate processes, however, they are very connected to each other. In some cases, such as in postmitotic neurons, cells increase their size without undergoing cell division, whereas zygote undergo a series of cell divisions without increasing their size (Lloyd, 2013; Niklas, 2015). Cell proliferation is a division of cells after attaining a considerable size (NCI Dictionary of Cancer Terms, 2011). In embryonic development, cells undergo rapid proliferation and reproduce fully developed organisms. In adults, cells undergo proliferation to maintain organ and organism homeostasis. In both cases, cell proliferation is very strictly regulated. Any defects in this process can cause cancer, chronic wounds, and various diseases (Lloyd, 2013; Pavlova & Thompson, 2016).

In unicellular organisms, cell proliferation is mainly regulated by nutrient availability (Jorgensen & Tyers, 2004). In contrast, in multicellular organisms, abundant nutrients alone do not stimulate cell growth or proliferation. Along with nutrients, cells also require growth factor signals and mitogenic signals (Efeyan & Sabatini, 2013; Saxton & Sabatini, 2017). Conlon and his coworkers showed how two distinct signaling pathways regulate cell size and cell division in Schwann cells (Figure 4). They found that serum starvation arrests cell cycle and reduces cell size. After serum starvation, stimulation of cells with insulin-like growth factor-1 (IGF1) increases their cell size without undergoing cell division. In contrast, glial growth factor (GGF) stimulation triggers cell division without increasing the cell size. However, in the presence of both IGF1 and GGF, a synergistic effect of cell growth and cell division is seen. Cells undergo cell divisions rapidly and produce more cells with optimal size when compared to GGF alone. At the molecular level, growth factor IGF-1 stimulation sustains PI3K-

AKT signaling for an extended period, whereas mitogen GGF activation maintains ERK signaling for a long duration (Conlon *et al*, 2001). Integrating nutrients and growth signals is essential in cell growth regulation, and it is coordinated by mTOR complex 1 (Saxton & Sabatini, 2017; Laplante & Sabatini, 2012a). In the next section, the mTOR signaling pathway is discussed in more detail.

Figure 4: Regulation of cell size and cell division. Growth factors insulin, IGF1, and IGF2 regulate cell growth; mitogens EGF and FGF regulate cell division. Cell size and division are two separate phenomena controlled by specific signaling cascades and ligands (Conlon *et al*, 2001).

2.4.1 The mTOR signaling pathway

mTOR is a serine/threonine protein kinase, highly conserved from yeast to mammals. Initially called a mammalian target of rapamycin, it is now officially renamed as a mechanistic target of rapamycin (Laplante & Sabatini, 2012a). mTOR is a component of two distinct protein complexes, mTORC1 and mTORC2 (Figure 5). mTORC1 is composed of mTOR, a regulatory associated protein of mTOR (Raptor), mammalian lethal with SEC13 protein 8 (mLST8), DEP domain-containing mTOR-interacting protein (Deptor), and proline-rich Akt/PKB substrate 40 kDa (PRAS40). mTOR forms the catalytic unit of the complex, whereas raptor regulates the mTORC1 complex assembly, localization, and recruitment of different mTORC1 specific substrates for phosphorylation. mLST8 regulates the catalytic activity of the kinase domain by stabilizing the activation loop, while PRAS40 and Deptor inhibit the mTORC1 complex by associating with it. Phosphorylation of PRAS40 and Deptor inhibit its interaction with mTORC1 complex (Laplante & Sabatini, 2009, 2012a; Saxton & Sabatini, 2017). mTORC2 possesses mTOR, rapamycin-insensitive companion of mTOR (Rictor), mLST8, mSin1 (MAPKAP1), Protor (PRR5), and Deptor. Like the raptor in mTORC1, rictor is specific to the mTORC2 complex; it recruits specific

substrates for its activation and phosphorylation. mSin1 and mLST8 are essential for mTORC2 complex integrity and kinase activity. Deptor inhibits the mTORC2 complex, and the role of protor is not clearly known (Laplante & Sabatini, 2012a; Saxton & Sabatini, 2017). Rapamycin is an antifungal agent; it inhibits cell growth and proliferation by forming a complex with FKBP12 (Chung *et al*, 1992; Cafferkey *et al*, 1993). Later, found that rapamycin inhibits mTORC1 activity by directly interacting with mTOR. However, mTORC2 is insensitive to rapamycin; it requires more extended periods of treatment for its inhibition. The molecular mechanism of rapamycin inhibition is not clearly known (Ballou & Lin, 2008; Schreiber *et al*, 2015). Nonetheless, it is widely used as an inhibitor to study mTORC1 complex signaling and biochemical actions (Laplante & Sabatini, 2012a).

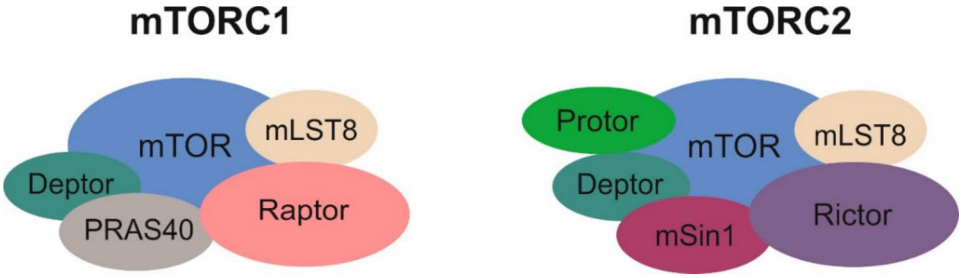

Figure 5. mTORC1 and mTORC2 Complexes. Both mTORC1 and mTORC2 complexes share mTOR, deptor, mLST. Raptor and PRAS40 are unique to the mTORC1 complex. Rictor, mSin1, and protor are present only in the mTORC2 complex (Saxton & Sabatini, 2017).

2.4.2 mTORC1 upstream regulators

mTORC1 senses different cues such as amino acids, glucose, oxygen, stress, energy level, and growth factors or mitogen signals (Figure 6). mTORC1 helps to decide whether the cell needs to activate anabolic or survival pathways by sensing and integrating different cues (Saxton & Sabatini, 2017; Liu & Sabatini, 2020). Growth factors such as insulin and insulin-like growth factors act as prime signaling molecules in regulating anabolic processes by activating the PI3K/AKT/mTOR signaling pathway. This helps to convert nutrients into cell mass or cellular components, which is pivotal for normal growth and development (Laplante & Sabatini, 2009; Boucher *et al*, 2014). Growth factors initiate signals through the binding of a ligand (insulin) to RTKs, which causes a receptor conformational change and leads to transphosphorylation of the intracellular domain of the receptor. Phosphorylated insulin receptor tyrosine

kinase recruits and phosphorylates the adaptor protein insulin receptor substrate (IRS)(Boucher *et al*, 2014; Laplante & Sabatini, 2012a). IRS activates PI3 kinase, and that leads to the conversion of phosphatidylinositol 4,5-bisphosphate (PIP2) into phosphatidylinositol 3,4,5-trisphosphate (PIP3) (Boucher *et al*, 2014). PIP3 is anchored at the plasma membrane, and it contains a pleckstrin homology domain which helps to recruit inactive AKT from the cytosol to the plasma membrane (Czech, 2000). Phosphoinositide-dependent kinase-1 (PDK1) at the plasma membrane activates AKT by phosphorylating at Thr308 (Boucher *et al*, 2014; Dangelmaier *et al*, 2014). A few reports have shown that PIP3 can regulate mTORC2 complex activity, however, the mechanism of action is not clear (Gan *et al*, 2011; Liu *et al*, 2015b). Active mTORC2 fully activates the AKT kinase by phosphorylating at serine 473 (Sarbassov *et al*, 2005). Phosphorylated AKT activates the mTORC1 complex by phosphorylating the Tuberous Sclerosis Complex 2 (TSC2) (Inoki *et al*, 2002). TSC2 forms heterodimer complexes with TSC1 and also possesses a GTPase-activating protein domain that acts as a negative regulator of mTORC1 by inhibiting Rheb activity (Inoki *et al*, 2003). Rheb is an essential component for mTORC1 activation, and TSC2 inhibits mTOR activity by converting active GTP-bound Rheb to inactive GDP-bound (Figure 6) (Yang *et al*, 2006; Lu *et al*, 2010). The TSC2 complex acts as a molecular switch for mTORC1 by transducing different growth factors and mitogenic signals. It has been shown that TSC2 knockout increases mTORC1 activity without growth factor stimulation (Li *et al*, 2002; Zhang *et al*, 2003; Menon *et al*, 2014). The mitogen signal Ras also regulates mTORC1 activity through MAPK and p90RSK1 by phosphorylating the TSC2 complex (Miyazaki & Takemasa, 2017). Depending upon the type of signal, the TSC2 complex gets phosphorylated at different sites, but how it integrates these signaling pathways needs to be explored (Laplante & Sabatini, 2012a; Liu & Sabatini, 2020).

Although growth factors and mitogens activate mTORC1 mainly through the TSC2 complex, however, low energy levels, hypoxia, and DNA damage can inhibit growth factor-induced mTORC1 activation by inhibiting the dissociation of TSC2 from the mTORC1 complex (Saxton & Sabatini, 2017). Apart from TSC2, another negative regulator of mTORC1 is PRAS40. During growth factor stimulation, Akt phosphorylates PRAS40 at T246, which mediates the interaction of PRAS40 with 14-3-3 and causes dissociation from the mTORC1 complex. This dissociation prevents its inhibitory activity (Vander Haar *et al*, 2007; Nascimento *et al*, 2010).

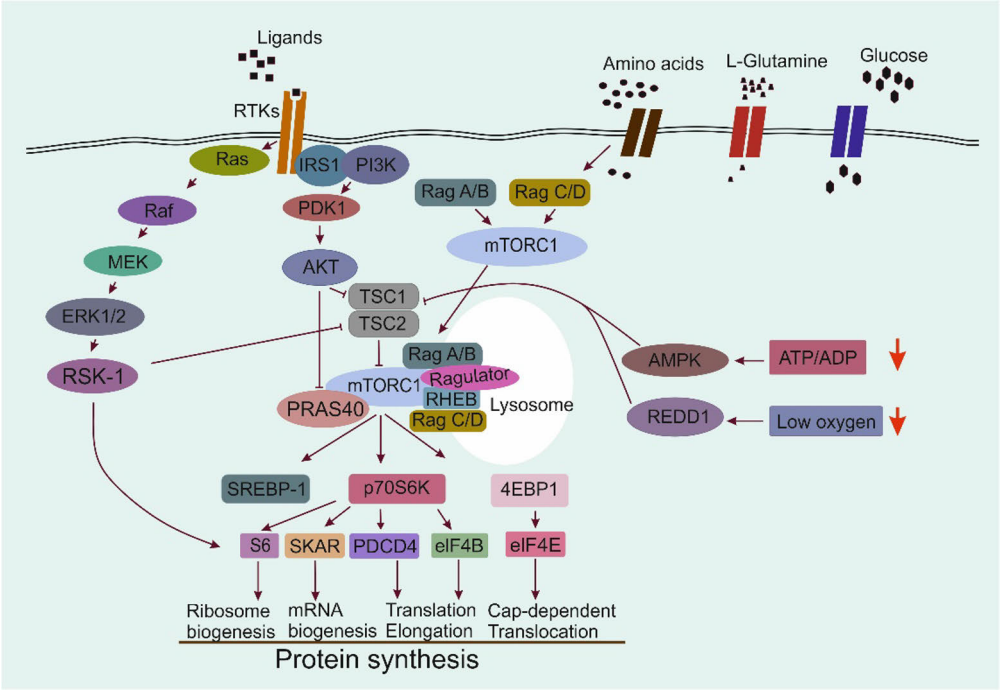

Figure 6. The mTORC1 signaling pathway. mTORC1 complex integrates signals from different cues and activates downstream effectors for protein synthesis. Image adapted from (Laplante & Sabatini, 2009; Saxton & Sabatini, 2017).

It has been shown that growth factors regulate mTORC1 activity through TSC2. However, mTORC1 requires amino acids for its activation. Amino acids not only act as building blocks for protein synthesis but also regulate mTORC1 signaling (Efeyan *et al*, 2013a; Sancak *et al*, 2008). To mediate the mTORC1 signal, cells need to sense both intracellular and extracellular amino acid levels. It is not clear how the cell senses specific amino acid levels in the cell, although, a few studies demonstrated that cells have specific sensor molecules for amino acids (Kim *et al*, 2013a; Hu & Guo, 2021; Gumerov *et al*, 2022). The mTORC1 complex needs to translocate from the cytosol to the lysosomal membrane for its activation and this process is mediated through amino acids. Rag A, Rag B, Rag C, and Rag D, are Rag GTPases that belong to the Ras family of proteins and form the heterodimers Rag A/B and Rag C/D. GTP levels. Under amino acid deprivation conditions, Rag A/B is bound to GDP, whereas Rag C/D is GTP bound, which results in inactive Rag. The presence of amino acids activate Rag GTPase, by switching the nucleotide-bound state from GDP to GTP in Rag A/B and from GTP to GDP in Rag C/D. Activated Rag GTPases recruit mTORC1 through interacting with raptor

protein. This complex is translocated to the lysosomal membrane, a process mediated through the ragulator protein (Figure 6) (Kim *et al*, 2008; Sancak *et al*, 2008, 2010).

Apart from lysosomal membrane protein, amino acids inside the lysosome also regulate mTORC1 signaling through vATPase (Zoncu *et al*, 2011). Ragulator is a multimeric protein that docks the Rag-mTORC1 complex on lysosomal membranes near the Rheb protein by direct physical interaction with v ATPase. v ATPase acts as a guide for mTORC1 translocation to the lysosome. Disruption of vATPase inhibits both mTORC1 translocation and its downstream signaling (Düvel *et al*, 2010; Peña-Llopis *et al*, 2011). Similarly, knockdown of either Rag or Ragulator completely inhibits mTORC1 signaling, even in TSC2 knockout cells (Laplante & Sabatini, 2012b; Schweitzer *et al*, 2015). Amino acids play a pivotal role in mTORC1 signaling; among the 20 amino acids, leucine, arginine, and glutamine play a significant role in mTOR signaling (Jewell *et al*, 2015; Tan *et al*, 2017).

Glucose acts as an energy supplier and a precursor for macromolecule synthesis. Studies showed that glucose is also involved in mTOR signaling, but its functional role is unclear. Glucose deprivation dispersed mTORC1 localization from the lysosomal membrane to the cytosol, and also inhibits mTORC1 activity by inducing the association of hexokinase-II and mTORC1 (Efeyan *et al*, 2013a; Roberts *et al*, 2014). It has been reported that glucose is involved in Rag GTPase signaling; nevertheless, its mechanism needs to be further explored. The glycolysis metabolic intermediate dihydroxyacetone phosphate can activate mTORC1 signaling without the glucose molecule (Orozco *et al*, 2020). Only a few papers have reported the involvement of glucose in mTORC1 signaling, but its mechanism of action is not well known yet. How glucose regulates mTOR signaling either directly or via its metabolic intermediates needs to be explored (Liu & Sabatini, 2020).

2.4.3 mTORC1 downstream signaling

Once mTORC1 is activated, it promotes different anabolic processes, such as protein, lipid, and nucleotide synthesis, by phosphorylating various downstream targets. S6Ks and 4EBP1 are two well-known mTORC1 substrates through which it regulates protein synthesis. mTORC1 can regulate protein synthesis globally or a specific set of proteins involved in cell growth and metabolism (Laplante & Sabatini, 2009, 2012b). Non-phosphorylated 4EBP1 usually binds to the eukaryotic initiation factor eIF4E, which inhibits the formation of the eIF4E cap-

binding complex and prevents cap-dependent mRNA translation (Laplante & Sabatini, 2009). mTORC1 phosphorylates 4EBP1 on different sites causing it to dissociate from eIF4E and disrupting its protein translation inhibitory action. This leaves eIF4E free and promotes protein synthesis. mTORC1 phosphorylates 4EBP1 at four different sites, T37, T46, T70, and S65. The T37/ T46 sites do not disrupt the interaction but facilitate the phosphorylation of other sites. Hypophosphorylated 4EBP1 isoforms continue to interact with eIF4E, whereas hyperphosphorylated 4EBP1 isoforms completely lose their interaction with eIF4E and thus promote mRNA translation (Figure 6) (Gingras *et al*, 1999; Hinnebusch, 2012; Qin *et al*, 2016).

mTORC1 also promotes mRNA translation via S6K1 (p70S6K1) and S6K2. mTORC1 phosphorylates S6K1 at Thr 389 and S6K1 phosphorylates ribosomal protein S6, which is a component of the 40S ribosomal subunit (Magnuson *et al*, 2012; Wu *et al*, 2022). It has been shown that the ribosomal protein S6 is involved in protein synthesis; however, phospho-deficient ribosomal S6 increases protein synthesis rates. Thus, the role of ribosomal protein S6 in protein synthesis is not very clear. Furthermore, ribosomal S6 knockout disrupts glucose homeostasis and reduces cell size (Ruvinsky *et al*, 2005). Apart from S6K1 (p70S6K1), p90S6k also phosphorylates ribosomal S6 protein and it is regulated by MAP kinase signaling through ERK1/2 (Esnault *et al*, 2015). S6K1 also phosphorylates different substrates such as SKAR, eukaryotic elongation factor 2 kinase (eEF-2K), eukaryotic initiation factor 4B (eIF4B), and programmed cell death 4 (PDCD4), through which it regulates mRNA translation and protein synthesis (Figure 6)(Laplante & Sabatini, 2012b; Saxton & Sabatini, 2017). mTORC1 is an anabolic regulator and inhibition of mTOR through rapamycin reduces the gene expression of different metabolic enzymes that are involved in glycolysis, as well as lipid, nucleotide, and amino acid metabolism.

2.4.4 Autophagy

To maintain rapid growth and proliferation, mTORC1 not only increases the anabolic process, it also decreases catabolic processes by inhibiting autophagy (Jung *et al*, 2010). Autophagy is a degradative and recycling process through which cells regenerate amino acids and energy from defective organelles and proteins. It occurs during protein aggregation, stress, and nutrient and growth factor starvation (Glick *et al*, 2010). In general, defective organelles and proteins are degraded in the lysosomes; however, depending on how they are transported into lysosomes, the degradation is categorized as macroautophagy, microautophagy, and chaperone-mediated autophagy (Mizushima, 2007; Jung *et*

al, 2010). In macroautophagy, organelles and cytosolic components are sequestered into membrane vesicles and form an autophagosome. Then, the autophagosome fuses with a lysosome for the degradation and recycling of the cargo (Glick *et al*, 2010). In microautophagy, lysosomes engulf cellular components through their membrane surface, whereas in chaperone-mediated autophagy, proteins are translocated into lysosomes. Macroautophagy is the most widely studied process (Parzych & Klionsky, 2014), and the molecules regulating this process are explained below.

Under nutrient starvation, cells initiate autophagy by forming the ULK complex, which translocate to the endoplasmic reticulum and forms a pre-autophagosomal structure. This pre-autophagosomal structure acts as a recruitment place for different autophagy-related complexes to promote phagophore formation and maturation (Glick *et al*, 2010). The ULK complex regulates class III phosphatidylinositol 3-kinase (PI3KC3–C1) complex formation, which contains Vps34 and Beclin-1 (Trelford & Di Guglielmo, 2021). Vps34 is involved in different membrane sorting processes. Beclin-1 usually interacts with Bcl-2, and their interaction can be disrupted either through phosphorylation of Beclin-1 or Bcl-2, through which it regulates both autophagy and apoptosis (Kang et al, 2011). Beclin-1 directs membrane activity in autophagic processes and also regulates PIP3 generation. Then PIP3 binds with WIPI2 and recruits the Atg5–Atg12–Atg16L complex (Mizushima & Komatsu, 2011; Lu *et al*, 2022). After recruitment, Atg5–Atg12–Atg16L complex conjugates phosphatidylethanolamine (PE) to mATG8 protein LC3I, and it forms LC3-II. Phosphatidylethanolamine helps to anchor LC3II on the phagophore membrane and it promote maturation into an autophagosome (Lu *et al*, 2022). Finally, autophagosomes fuse with lysosomes and form autolysosomes, where proteins get degraded for recycling (Mizushima & Komatsu, 2011). LC3 plays an important role in sorting the cargo and fusing autophagosomes with lysosomes. Although conversion of LC3I to LC3II is used as a readout for autophagy, however it also occur during non autophagy conditons, its role and molecular mechanisms are not clear elucidated (Lee & Lee, 2016; Kar *et al*, 2009; Nakamura *et al*, 2021). LC3II occurs on both the inner and outer surface of the autophagosomes and it acts as a receptor for the selective degradation of specific molecules through the adaptor molecule p62/SQSTM1 (Mizushima, 2007; Mizushima & Komatsu, 2011; Bento *et al*, 2016). p62/SQSTM1 contains a ubiquitin-associated domain through which it interacts with ubiquitinated or polyubiquitinated proteins and directs them towards autophagosomes for selective degradation of protein molecules. By measuring the p62/SQSTM1 level, we can infer autophagy flux. However, in

some cases, the p62 level does not correlate with the number of autophagy vacuoles or flux. In order to know whether cells are undergoing autophagy, both LC3 and p62 need to be measured (Katsuragi *et al*, 2015; Sánchez-Martín & Komatsu, 2018; Tanida & Waguri, 2010). Apart from autophagy, p62 also regulates amino acid signaling and oxidative stress (Rusten & Stenmark, 2010; Carroll *et al*, 2018; Duran *et al*, 2011). Growth factor stimulation inhibits autophagy through mTORC1; however, autophagy can activate mTORC1 by releasing amino acids from damaged protein after protein degradation (Yu *et al*, 2010). Numerous molecules are required for autophagy, but the serine/threonine kinases ULK1/2 are key molecules in pre-autophagosome formation. It is not well known how mTORC1 inhibits autophagy, but a few observations indicate that phosphorylating ULK1/2 and Atg13 prevents pre-autophagosome formation (Jung *et al*, 2010; Laplante & Sabatini, 2012b; Dunlop & Tee, 2014).

2.4.5 Vimentin and autophagy

In fibrogenic lung injury model, inhibition of vimentin assembly with withaferin A increases autophagy level. It also reduces fibrosis by clearing collagen I level (Surolia *et al*, 2019). Akt regulates vimentin by phosphorylating at serine 38. This increases cell invasion and protects vimentin from proteasomal degradation (Zhu *et al*, 2011). Moreover, Akt-mediated vimentin phosphorylation leads to the formation of a vimentin-beclin-14-3-3 complex, which inhibits autophagy and promotes tumor growth (Wang *et al*, 2012). Vimentin also interacts with p62, one of the well-known markers for autophagy; this interaction promotes tumor progression and metastasis in breast cancer (Li *et al*, 2017). Although vimentin is known to interact and regulate beclin and p62 functions, how this interaction is regulated needs to be elucidated to explore vimentin's role in autophagy.

2.5 Epithelial cell junctions and polarity

Epithelial cells are tightly packed and compactly arranged sheet-like layer. Cells are held tightly together through epithelial cell junctions; adherens junction, tight junction, desmosome, hemidesmosome, and gap junction. These junctions provide mechanical support and act as a barrier to the tissue and organs (Adil *et al*, 2021). A tight junction is located at the lateral apical region of the cell; it helps to seal space in between the cells and prevent the entry of ions, water, and small molecules. Claudin and occludin form tight junctions, they connect to the actin cytoskeleton through adaptor proteins PSD-95/discs-large/zonula occludens-1

(PDZ) domain proteins (Zihni *et al*, 2016). Adherens junctions help to connect cells with adjacent cells through cadherin transmembrane protein and also act as a hub for cell signaling and gene expression. E-cadherin is very characteristic of epithelial cells; it forms a ternary complex with β-catenin, p120-Catenin, and α-catenin. This ternary complex bind with the actin cytoskeleton and forms adherens junctions (Garcia *et al*, 2018). In desmosomes, cadherin subtypes transmembrane protein desmoglein and desmocollin interact with plakoglobin and plakophilin. Plakophilin connects with intermediate filament keratin through the desmoplakin adaptor protein and forms desmosomes (Müller *et al*, 2021; Garcia *et al*, 2018). Integrin α6β4 and plectin form hemidesmosome, integrin establishes a connection with extracellular matrix and cytoskeletal cross-linker plectin, which ties the intermediate filament keratin with hemidesmosome (Walko *et al*, 2015). Gap junctions regulate ions and small molecules transport between two cells through the channel (Villanelo *et al*, 2017).

Apico-basal polarity is a unique feature of epithelial cells and is vital for epithelial cell function. The apical region of the cell faces the lumen or outside of the body and the basal part of the cell is attached to a specialized extracellular matrix, the basement membrane (Buckley & St Johnston, 2022). To achieve distinct cell polarity, several proteins such as PAR complex, aPKC, crumbs complex, PALSI, and PATJ, are in an apical region of the cell. Scribble complex, lethal giant larvae, and Disc large located in a basal region of the cell (Martin *et al*, 2021). These polarity protein complexes provide mechanical and functional integrity to the epithelial cells by associating with cell junctions (St Johnston & Ahringer, 2010). Unlike epithelial cells, mesenchymal cells are highly dynamic lack apical-basal polarity and possess front-rear polarity, and occur as single cells (Kalluri & Weinberg, 2009a; Nieto *et al*, 2016).

2.6 Epithelial-mesenchymal transition

Elizabeth Hay first identified the epithelial-mesenchymal transition in a chick embryo's primitive streak (Hay, 1995). Initially, it was referred to as epithelial to mesenchymal transformation, later renamed as epithelial-mesenchymal transition (EMT) to distinct from neoplastic transformation. Apart from embryonic development, EMT also occurs during wound healing, fibrosis, and cancer (Yang *et al*, 2020). EMT signaling and regulations are different in biological processes; based on this, they are classified into three types (Kalluri & Weinberg, 2009b; Marconi *et al*, 2021).

EMT which occurs during organ formation and embryonic development is named as Type I. It wouldn't cause any invasive phenotype or fibrosis.

Type II EMT occurs during tissue regeneration and fibrosis. It is triggered by inflammatory signals after injuries to promote tissue generation and wound healing. However, impaired or prolonged inflammatory signals would cause excessive extracellular matrix deposition in organ tissue and lead to fibrosis.

Type III EMT occurs in neoplastic cells, and it promotes invasion and metastasis. Epigenetic changes, mutations, and tumor-associated stroma secretions (HGF, EGF, PDGF, and TGF-β1) support carcinoma to acquire mesenchymal-like phenotypes (Kalluri & Weinberg, 2009b; Marconi *et al*, 2021).

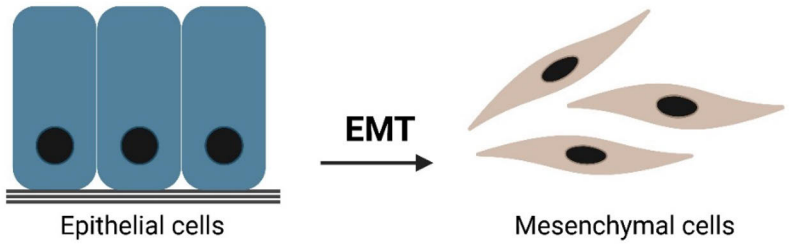

Figure 7. EMT changes cellular characteristics. During EMT epithelial cells change their morphology from a cuboidal into a spindle-like shape (Yang *et al*, 2020).

During EMT, epithelial cells undergo various changes within and around the cells. Initially, cells change their gene expression from epithelial to mesenchymal-specific genes; then, the cells lose their apical-basal polarity through dissociation of cell adhesion proteins (Stone *et al*, 2016). Cells acquire front-to-rear-end polarity and motility by changing their cytoskeletal proteins. Finally, mesenchymal cells detach and migrate out of the epithelial cell layer (Figure 7) (Xu *et al*, 2009a; Nieto *et al*, 2016). Mesenchymal cells are proliferative and migratory and produce an extracellular matrix. These properties play a crucial role in the development, regeneration, and cancer (Kalluri & Weinberg, 2009a).

2.6.1 Modulation of gene expression from epithelial to mesenchymal specific

EMT initiates through the repression of epithelial genes and activation of mesenchymal genes. Various transcription factors regulate gene expression

during EMT; the most well-known transcription factor families are SNAIL, bHLH, and ZEB (Lamouille *et al*, 2014). These transcription factors regulate both epithelial gene repression and mesenchymal gene activation simultaneously. Depending on the upstream signal and cell type, these transcription factors produce distinct gene expression profile (Nieto *et al*, 2016).

Transcription factors SNAIL1 and SNAIL2 (also known as a slug) induce EMT in normal development and pathological conditions, such as cancer and fibrosis(Medici *et al*, 2008; Craene & Berx, 2013). TGF-β1 is very known to regulate SNAIL1 and SNAIL2, however other pathways, WNT, Notch, RAS-MAPK, and receptor tyrosine kinases (RTKs) can also regulate them (Lamouille *et al*, 2014; Dhasarathy *et al*, 2011).

Helix-loop-helix (HLH) factors are a large transcription factor protein family mainly involved in normal development and differentiation (Craene & Berx, 2013). Twist1 and Twist2 are well-known transcription factors from this family to involve in EMT. Twist induces EMT mainly during cancer and development. The hypoxia-inducible factor 1α (HIF1 α) induces Twist expression in hypoxic conditions stimulating EMT and tumor invasion (Yang & Wu, 2008).

ZEB1 and ZEB2 form the ZEB transcription factor family. ZEB expression is regulated by TGF-β and other signaling pathways, such as RAS-MAPK, Wnt, and other growth factors (Lamouille *et al*, 2014).

2.6.2 TGF-β signaling during EMT

The TGF-β family is comprised of a large group of proteins, including different types of ligands, such as TGF-β, activin, nodal, bone morphogenetic protein, growth and differentiation factors (GDFs), and the anti-müllerian hormone (Massagué, 2012). These ligands transduce signals through the TGF-β receptor family. Binding of the TGF-β ligand to the transmembrane type II TGF-β receptor recruits the type I TGF-β receptor and activates it through phosphorylation. Active type I receptor conveys its signal to the nucleus through phosphorylating SMAD2 and 3. SMAD2 and 3 form a trimer with SMAD4 and translocate to the nucleus, where the complex regulates gene expression by binding to a DNA regulatory sequence. SMAD6 and SMAD7 inhibit complex formation by preventing the interaction of SMAD2, SMAD3, and SMAD4 with the type I receptor (Feng & Derynck, 2005; Xu *et al*, 2009a). TGF-β family signaling through the SMAD complex is the canonical pathway. However, TGF-β also induces EMT

by activating other signaling cascades, such as RAS-MAPK, PI3K-AKT, and Rho GTPases via non-SMAD pathways (Figure 8)(Lamouille *et al*, 2014).

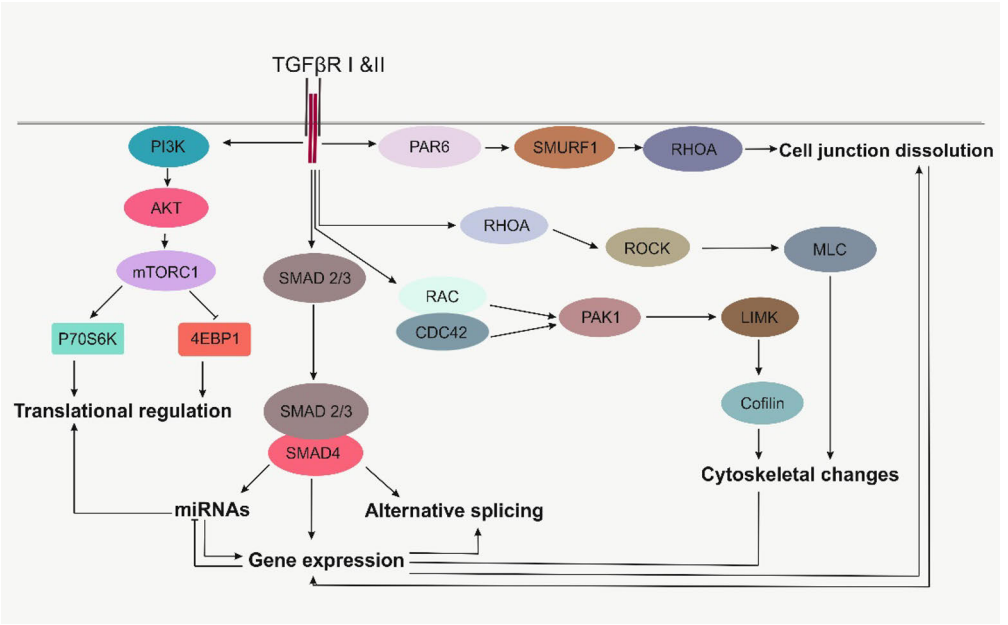

Figure 8: TGFβ signaling pathways that are activated and regulated during the EMT. Image adapted from (Lamouille *et al*, 2014).

2.6.3 Loosing cell junctions and polarity, cell migration

Epithelial cells are tightly held together by different cell junction proteins. Degradation of the epithelial cell-cell junction proteins is an essential step in EMT. Downregulation of claudin and occludin destabilizes tight junctions (Stone *et al*, 2016). Cleavage and degradation of E-Cadherin disturb adherens junctions and release β-catenin from cell junctions, which either regulate transcription or undergo degradation. P120 Catenin is also an adherens junction protein; it translocates into the nucleus and represses E-cadherin expression after cell junction destabilization (Brieher & Yap, 2013; Nieto *et al*, 2016). Cell junction proteins in desmosomes and gap junctions are also get degraded. Repression of epithelial cell junction genes not only disturb cell junctions, and also prevents the reformation of epithelial cell junctions, which helps to acquire mesenchymal phenotype (Huang *et al*, 2012).

During EMT, epithelial-specific E-cadherin is replaced by mesenchymal-specific N-cadherin, which enables cell migration by weakening cell-cell interaction with

adjacent cells (Grünert *et al*, 2003; Cavallaro & Christofori, 2004). Disruption of cell junctions and the replacement of cytokeratin with mesenchymal-specific cytoskeletal filament vimentin affect cell polarity (Kalluri & Weinberg, 2009b). Vimentin alters the cytoskeletal network and dynamics and does not interact with E-cadherin, thus facilitating cell migration and invasion (Huang *et al*, 2012). The cells switch their polarity from apical-basal to front-rear polarity by changing the localization of polarity complexes, actin reorganization, and modulating Rac1 and RhoA activity (Lamouille *et al*, 2014). The polarity complexes PAR and scribble relocalize to the edge of the cell, where actin forms membrane protrusions; this is regulated by RAC1 and CDC42. On the rear end, the RhoA protein mediates the adhesion complex disassembly and the cell withdraws its attachment from the surface, facilitating cell migration (Nelson, 2009; Godde *et al*, 2010; Whale *et al*, 2011).

Integrin is a transmembrane cell surface protein that enables cells to attach to an extracellular matrix. Remodeling the extracellular matrix from epithelial-specific laminin to mesenchymal-specific collagen and fibronectin is crucial for EMT progression (Lamouille *et al*, 2014; Marconi *et al*, 2021). Cells also change their integrin expression from epithelial to mesenchymal specific and increase the levels of matrix metalloproteinases (MMPs). MMPs are involved in matrix degradation, remodeling, and invasion (McNiven, 2013; Nieto *et al*, 2016). Sometimes, cells show epithelial-mesenchymal plasticity by expressing both epithelial and mesenchymal markers. Thus, enabling cells to switch their phenotype to either epithelial or mesenchymal cells, depending on the circumstances. Epithelial-mesenchymal plasticity occurs in development, wound healing, and cancer (Yang *et al*, 2020).

Cells attach to the ECM substrate through integrins, and these points of contact are called focal adhesion. They comprise more than 150 different proteins and act as regulatory centers for cell migration (Kuo *et al*, 2012). Integrin is one of the well-studied proteins in focal adhesions; it links the extracellular matrix and the actin cytoskeleton of the cell and also regulates different cell signaling such as PI3K-Akt, MAPK, Rac (Barczyk *et al*, 2010). Focal adhesions control both migration signals and cell traction forces. During cell migration, cells exert their force on traction points, and actin undergoes polymerization at the leading edge of the migrating cell (Wozniak *et al*, 2004; Vicente-Manzanares *et al*, 2005; Trepat *et al*, 2012). Actin also forms cell membrane protrusions, such as lamellipodia and filopodia; it helps to navigate and sense the environment. Rho-GTPase protein family mainly regulate cytoskeletal reorganization and actin

polymerization; they are Rac, RhoA, and Cdc42 (Vicente-Manzanares *et al*, 2005; Trepat *et al*, 2012). In focal adhesions, the paxillin and focal adhesion kinase (FAK) signaling complex regulates the Rho-GTPases protein family and activates MAPK, PI3K, and PKC signaling (Devreotes & Horwitz, 2015).

2.6.4 EMT and vimentin expression

Vimentin is one of the well-known marker for EMT and is used to assess EMT progression, but its role in EMT is not well-reported (Liu *et al*, 2015a). Mesenchymal cells are proliferative, migratory, invasive, and produce an extracellular matrix. Vimentin could be necessary for the mesenchymal cell phenotype, but how it regulates these features is unclear (Kalluri & Weinberg, 2009b; Vuoriluoto *et al*, 2011). Many studies have shown that vimentin is required for morphological changes and cell migration during EMT (Ivaska, 2011; Ridge *et al*, 2022). Exogenous expression of vimentin in epithelial cells induces cell morphological changes from highly ordered polarized cells into spindle-like shaped mesenchymal cells. This is accompanied by a loss of cell-cell adhesion and increased cell motility (Mendez *et al*, 2010). TGF-β1 is one of the well-known EMT inducer and activates downstream transcription factors such as snail and slug (Lamouille *et al*, 2014). TGF-β1 stimulation increases vimentin expression and cell migration, whereas vimentin silencing inhibits TGF-β1 induced cell migration (Rogel *et al*, 2011).

In normal mammary epithelial MCF10A cells, exogenous expression of either *slug or H-Ras^{G12V}* induces EMT, which increases vimentin expression and promotes cell migration. Vimentin is required for both *slug* and *H-Ras^{G12V}* induced EMT and cell migration (Vuoriluoto *et al*, 2011). It is well known that *slug* induces vimentin expression; however, a study showed that vimentin could indirectly activate the slug transcription factor by recruiting active ERK and scaffolding it. Formation of the vimentin-ERK complex inhibits ERK dephosphorylation, which helps to recruit slug. Active ERK phosphorylates slug at serine S87, which in turn induces EMT and vimentin expression (Virtakoivu *et al*, 2015b). HIF-1α is activated during hypoxia conditions and is also a potential inducer of EMT in cancer. HIF-1α activation increases vimentin expression and cell invasion, which supports tumor growth and metastasis (Zhang *et al*, 2015).

2.7 Vimentin in cell migration

The role of vimentin in cell migration has not been explored in great detail, although several studies have showed that vimentin is involved in different

aspects of cell migration such as polarization, adhesion, protrusion, and retraction (Tsuruta & Jones, 2003; Phua *et al*, 2009; Dave & Bayless, 2014). Vimentin has been found in focal adhesions and interacts with focal adhesion complex proteins. Additionally, the knockdown of vimentin affects both cell adhesion and migration (Tsuruta & Jones, 2003; Kreis *et al*, 2005; Havel *et al*, 2015).

The expression of the integrin β1 subunit on the cell surface is crucial for cell migration and cell adhesion on fibronectin and collagen (Barczyk *et al*, 2010; Ostrowska-Podhorodecka *et al*, 2021). Interestingly, phosphorylation of vimentin at serine S6 by PKC ε regulates integrin β1 subunit recycling and cell migration (Ivaska *et al*, 2005). Later, several studies showed that vimentin interacts with filamin A; silencing of vimentin or filamin A reduces the surface expression of integrin β1 and cell spreading (Kim *et al*, 2010b, 2010a; MacPherson & Fagerholm, 2010). Vimentin knock-out also reduces the expression of cell surface adhesion molecules such as ICAM-1 and VCAM-1 in endothelial cells, and integrin β1 in peripheral blood mononuclear cells (Nieminen *et al*, 2006).

Activation of Rac1 leads to vimentin phosphorylation at S38, causing vimentin disassembly near the plasma membrane, which makes space for actin polymerization and lamellipodia formation (Helfand *et al*, 2011). VAV2 activates Rac1 by acting as a guanine nucleotide exchange factor (GEF). Vimentin knockdown reduces VAV2 activity and the number of focal adhesions, which can be rescued by Rac1 overexpression. Therefore, vimentin could activate and stabilizes focal adhesions through VAV2 (Havel *et al*, 2015).

Propulsion of the membrane towards the leading edge requires contraction forces. Actin filaments and myosin form a contractile structure that produces the necessary contraction force for cell migration. The association of vimentin and actomyosin arc causes a retrograde flow of vimentin (Jiu *et al*, 2015, 2017). Another study made similar observations that vimentin coaligns with actin stress fibers, which slow down the retrograde flow of actin. In addition, vimentin also absorbs the actin traction force by acting as a stress-bearing structure and redistributes actin forces uniformly to the substrate to support cell single migration (Costigliola *et al*, 2017).

Podosomes are small protruding actin-rich adhesion structures, which contain actin, integrin, and other kinases. They are involved in cell motility, invasion, extracellular matrix degradation, and matrix remodeling (Linder & Kopp, 2005;

Murphy & Courtneidge, 2011). FAK promotes the formation of podosome rosettes by inhibiting ROCK-mediated phosphorylation of vimentin at serine S38 and serine S71 (Pan *et al*, 2011). In contrast, sphingosine 1-phosphate (S1P) and sphingosylphosphorylcholine (SPC) increase ROCK-mediated phosphorylation on vimentin at serine S71. It inhibits cell migration by promoting vimentin assembly (Hyder *et al*, 2015).

2.8 Wound healing

Skin is the largest organ in our body, in our day-to-day life, we may expose to different kinds of threats, which can be physical, mechanical, chemical, or thermal injuries (Dhivya *et al*, 2015). These can cause minor or major lesions, and if they are not healed properly it may lead to chronic wounds, amputation of body parts, or even death (Demidova-Rice *et al*, 2012b; Frykberg & Banks, 2015). Wound healing is a vital process for the survival of the organism. The rate of wound healing depends upon the external environment and internal factors (Demidova-Rice *et al*, 2012b; Gonzalez *et al*, 2016).

Wound healing is a complex multistep process, and it is categorized into four different phases, namely 1) Hemostasis, 2) Inflammation, 3) Proliferation and migration, and 4) Remodeling (Figure 9) (Guo & DiPietro, 2010).

2.8.1 Hemostasis

A wound is a disruption of tissue continuity and rupture of blood vessels, and it affects tissue integrity and functions (Broughton *et al*, 2006). Depending on the size and depth of the wound, blood loss can be mild to severe; in some cases, it can be lethal. Therefore, preventing blood loss is one of the crucial steps in wound healing, and this process is called hemostasis (Gale, 2011). Disruption of blood vessels releases blood cells and activates pain receptors around the blood vessels. It also induces smooth muscle contraction, which constricts blood vessels and reduces blood flow (Robson *et al*, 2001a). Blood cells in the wounded area contact with the extracellular matrix, which triggers platelet activation, releasing blood clotting factors and the aggregation of platelets. This aggregation forms platelet plugs by converting soluble fibrinogen into an insoluble fibrin mesh network. Platelets and other blood cells are trapped in the fibrin mesh network and form blood clots (Broughton *et al*, 2006; Demidova-Rice *et al*, 2012b; Gonzalez *et al*, 2016). Blood clots completely cover the damaged blood vessels and prevent blood loss, which triggers the next phase of wound healing by releasing chemo-attractants, cytokines, and growth factors, such as

transforming growth factor-beta 1 (TGF-β1) and platelet-derived growth factors (PDGF) from platelets. These factors initiate an inflammatory response by attracting different inflammatory cells, such as neutrophils, leukocytes, and macrophages (Velnar *et al*, 2009; Demidova-Rice *et al*, 2012b).

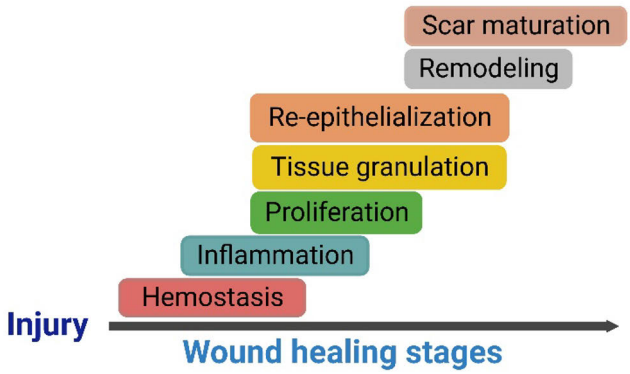

Figure 9. **Different stages of the wound healing process**. Wound healing includes hemostasis, inflammation, proliferation, and tissue remodeling (Gonzalez *et al*, 2016).

2.8.2 Inflammation

Inflammation is one of the protective mechanisms of the immune system. It results in the migration of immune cells toward the site of injuries or foreign bodies, which helps to remove toxins, pathogens, and damaged cells from the affected area (Hart, 2002; Frykberg & Banks, 2015). It is triggered by pathogens, noxious chemicals, and tissue injuries (Hart, 2002; Landén *et al*, 2016). Platelet degranulation, pathogens, and complement systems attract neutrophils toward the wound site during the inflammatory phase (Gonzalez *et al*, 2016; Landén *et al*, 2016). Neutrophils clear away pathogens and cell debris by phagocytosis. Neutrophils also release different cytokines, reactive oxygen species, proteases, and antimicrobial peptides that enhance clearing in the wounded area (Dovi *et al*, 2004). Then, monocytes infiltrate the injury site and later differentiate into macrophages (Eming *et al*, 2007). These macrophages act as antigen-presenting cells and also assist neutrophils. They are recruited to the wound site by complement factors, collagen debris, elastin, and cytokines, other factors such as PDGF, TGF-β1, and platelet factor IV (Velnar *et al*, 2009; Gonzalez *et al*, 2016). Once the bacterial level is reduced, neutrophils gradually reduce their activity

and are eliminated by apoptosis (Hart, 2002; Eming *et al*, 2007). Macrophages clear cell debris and apoptotic bodies through phagocytosis (Rodero & Khosrotehrani, 2010). Macrophages play a very crucial role in the production of potent growth factors, such as TGF-β1, epidermal growth factor (EGF), vascular endothelial growth factor (VEGF), and fibroblast growth factor (FGF) to promote EMT, cell proliferation, and growth in the proliferative phase (Gonzalez *et al*, 2016; Landén *et al*, 2016). Reduction in the number of macrophages and monocytes causes impairment of fibroblast proliferation, angiogenesis, extracellular matrix production, and deposition (Witte & Barbul, 1997; Ennis & Meneses, 2000).

2.8.3 Proliferation and migration

In the last phase of inflammation, extracellular matrix debris, damaged cells, and pathogens get cleared from the wound site (Li *et al*, 2007). The next step is the closure of the wound area through the formation of granulation tissue (new connective tissue and blood vessel in the wound area), angiogenesis, and re-epithelialization (Guo & DiPietro, 2010). Different cytokines and growth factors produced from immune cells and platelets during the inflammatory phase initiate proliferation and migration (Velnar *et al*, 2009; Gonzalez *et al*, 2016). TGF-β1 and PDGF attract fibroblasts toward the injury site (Witte & Barbul, 1997). Once fibroblasts reach the wound area, they proliferate rapidly and secrete extracellular matrix, which is crucial for granulation tissue formation, repairing, and remodeling (Bainbridge, 2013). Collagen is the major component of the extracellular matrix produced by fibroblasts (Guo & DiPietro, 2010; Demidova-Rice *et al*, 2012b).

Initially, the wound receives nutrients from the surrounding undamaged blood vessels and interstitium. At the center of the wound, nutrients and oxygen availability are very limited; hence, to support fibroblast proliferation and tissue viability, blood vessels and granulation tissue need to be formed (Servold, 1991; DiPietro, 2016; Gonzalez *et al*, 2016). Angiogenesis and tissue granulation occur simultaneously. Under hypoxic conditions, angiogenic factors activate endothelial cells, which cause a detachment of endothelial cells from blood vessels; these cells then migrate toward the wounded area. Once the endothelial cells reach the wound area, they proliferate and form blood vessels and capillaries through differentiation and remodeling. Tissue granulation fills the wound, but the wound is still exposed to the external environment and needs to be protected from different external threats. Consequently, epithelial cells form a sheet-like layer of tissue to act as a barrier against the external environment

(Guo & DiPietro, 2010; Tonnesen *et al*, 2000; Barrientos *et al*, 2008; Demidova-Rice *et al*, 2012a). Keratinocytes in the epidermis undergo EMT by dissolving cell-cell junctions and changing their cytoskeletal proteins. This enables keratinocytes to change their morphology from a cuboidal to a flattened shape, promoting cell migration (Velnar *et al*, 2009; Pastar *et al*, 2014). Keratinocytes that have undergone EMT migrate toward the wound area and cover the wound. After this, epithelial cells form a protective sheet by forming adherens junctions, desmosomes, and tight junctions between adjacent cells and hemidesmosomes with the basement membrane underneath the epithelial cells. This process is called re-epithelialization (Broughton *et al*, 2006; Stone *et al*, 2016). Many growth factors, such as TGF-β1, FGF, hepatocyte growth factor (HGF), and EGF, regulate the EMT process (Lamouille *et al*, 2014).

2.8.4 Extracellular matrix remodeling

Remodeling is the last phase of the wound healing process and it can last up to 1 to 2 years (Velnar *et al*, 2009). During remodeling, the tissue increases its tensile strength. To increase tissue tensile strength, the extracellular matrix in the granulation tissue needs to undergo degradation, re-synthesis, and reorganization. Fibrin, fibronectin, hyaluronic acid, and collagen III make up the extracellular matrix of the newly formed granulation tissue (Werner *et al*, 2007; Guo & DiPietro, 2010; Gonzalez *et al*, 2016). These will be replaced mainly with collagen I during the remodeling phase, which provides strength and integrity to the tissue. In the unwounded dermis, collagen I constitute 80% of the extracellular matrix (Clark, 1993; Robson *et al*, 2001b).

Synthesis and degradation of the extracellular matrix need to be delicately balanced. These processes are regulated by TGF-β1, FGF and matrix metalloproteinases (MMPs) (Pierce *et al*, 1991; Bainbridge, 2013; Gonzalez *et al*, 2016). Fibroblasts in the granulation tissue differentiate into myofibroblasts, which form stress fibers by acquiring smooth muscle actin. These fibers help to contract the wound area. Along with synthesis and degradation of extracellular matrix, contraction of the wound area supports matrix reorganization and remodeling (Gabbiani *et al*, 1972; Grinnell, 2000; Van De Water *et al*, 2013). Finally, blood flow and metabolic activity decline steadily. At the end of the wound healing process, the number of cells and blood vessels in the wound area diminishes, and the tissue acquires high tensile strength and forms a mature scar (Robson *et al*, 2001a; Broughton *et al*, 2006; Velnar *et al*, 2009).

2.8.5 Vimentin in wound healing

According to Colucci-Guyon and co-workers, vimentin knockout mice reproduced and developed normally without any visible phenotype (Colucci-Guyon *et al*, 1994). The later report showed that reducing renal mass in the kidney disrupts vascular adaptation in vimentin knockout mice (Terzi *et al*, 1997). Likewise, induction of excision wound in vimentin null mice delayed the wound healing process and it is due to defects in fibroblast migration (Eckes *et al*, 2000). In *ex vivo* lens epithelial wound healing model, vimentin regulate wound healing by promoting migration and release soluble vimentin into extracellular space, which activates mesenchymal leader cell to promote wound closure and myofibroblast formation (Menko *et al*, 2014; Walker *et al*, 2018). The presence of vimentin in adipose stem cell-derived exosomes accelerates the wound-healing process in a mouse model. Treating wounds with exosomes carrying vimentin increases TGF-β1 and collagen I mRNA levels in the mice wound. It also regulates fibroblast functions (Parvanian *et al*, 2020). In injury sites, fibroblasts play an essential role in healing mechanisms that fill the wound area by secreting extracellular matrix (Bianco, 2014; Nieto *et al*, 2016). How vimentin regulates fibroblast function needs to be studied to explore the role of vimentin in wound healing mechanisms.

2.9 Vimentin in immune cells

In 2013, Mor-Vaknin and coworkers induced a bacterial infection in a mouse model by injecting *E. coli* intraperitoneally, then monitored the bacterial clearance for a few days in WT and vimentin null mice. They found that vimentin knockout mice showed more effective clearing of bacteria than WT. This effect was mainly due to excessive ROS production in vimentin null mice. They propose that vimentin may inhibit ROS production by binding to the subunit p47phox of NADPH oxidase, however, this finding was not validated with genetic and biochemical studies. They also showed the phenotype in a dextran sodium sulfate (DSS) induced colitis mouse model, the vimentin null mice showed less bacterial extravasation than WT (Mor-Vaknin *et al*, 2013). Similarly, in an acute lung injury mouse model, bleomycin, asbestos, and LPS treatment triggered NLRP3 inflammasome activation, increases inflammation, IL-1β level, and fibrosis in WT. In vimentin null mice, inflammatory responses to LPS, bleomycin, and asbestos were lower than WT. They proposed that the direct interaction of vimentin with NLRP3 increases inflammasome formation (dos Santos *et al*, 2015).

T cells play a significant role in acquired immunity by secreting cytokines and activating B cells (Cano & Lopera, 2013). Depending upon cytokine stimulation, naïve T cells differentiate into different subpopulations, such as Th1, Th2, Th17, Treg, Th9, Th22, and Tfh. T cell lineage is classified into conventional helper cells and regulatory cells. Conventional T helper cells promote the immune response by secreting cytokines and activating effector cells; in contrast, regulatory T cells suppress T cell proliferation and cytokine production to maintain immune homeostasis and inhibit autoimmune disorders (Wan, 2010). Initially, Th1 and Th2 were the two known T subpopulations; later the Th17 helper cells were identified. TGF-β1, IL-6, IL-21, and IL-23 induce differentiation of CD4+ T cells into Th17 cells, which help fight against microbial infection, mainly by preventing extracellular bacteria and fungi infection. Th17 cells produce IL-17A cytokine, which triggers an inflammatory response and is also involved in autoimmune diseases (Tesmer *et al*, 2008). Treg cells derived from thymus and other parts of the body are called natural Treg cells. If Treg cells are induced to differentiate from *in vitro* are called induced Treg cells. The presence of TGF-β1 and IL-2 induces the differentiation of CD4+ T cells into induced Treg cells. Antigens which activate Treg cells suppress T helper cell activity to balance immune cell activity during allergy, oral tolerance toward foods, maternal tolerance of a fetus and suppresses autoimmune disorders (Vignali *et al*, 2008).

PKC-θ play a key role in regulating effector T cells, and Treg cells function. In effector T cells PKC-θ gets recruited to the immunological synapse and it supports the full activation of T cells. However, in Treg Cells, PKC-θ localizes in the distal pole complex (DPC) which is away from the immunological synapse. The presence of PKC-θ in DPC inhibits Treg cell function (Zanin-Zhorov *et al*, 2010; Brezar *et al*, 2015). A recent study showed that vimentin forms a superstructure in DPC and it supports PKC-θ localization. Vimentin knockdown prevents PKC-θ localization in DPC, and activates Treg cells and supports autoimmune function (McDonald-Hyman *et al,* 2018). The role of vimentin in Treg function needs to be fully elucidated to exploit Treg cells in preventing cancer progression and autoimmune disorders.

3 OUTLINE OF THE STUDY

Earlier studies showed that vimentin knockout mice did not exhibit distinct phenotypes; however, later studies showed delayed wound healing and blood vessel disruption (Colucci-Guyon *et al*, 1994; Terzi *et al*, 1997; Eckes *et al*, 2000). Defect in wound healing is mainly due to defects in fibroblast stability and cell stiffness (Eckes *et al*, 2000). In the *ex vivo* lens wound healing model, vimentin affects wound healing by regulating mesenchymal leader cell's function (Walker *et al*, 2018). Vimentin is widely used as a mesenchymal marker and its expression is predominate in mesenchymal cells (Jung *et al*, 2019; Uhlén *et al*, 2015; Stone *et al*, 2016). Epithelial-mesenchymal transition plays a major role in wound healing by enabling re-epithelization (Stone *et al*, 2016). An *in vitro* study showed that vimentin supports TGF-β1-induced EMT (Rogel *et al*, 2011). In mice model, the role of vimentin in the wound-healing process has not been explored in the context of EMT.

- This thesis project aimed to identify the role of vimentin in EMT, especially during wound healing, using *in vivo* skin injury mice model.

Vimentin regulates autophagy in an AKT-dependent manner (Wang *et al*, 2012). mTORC1 is the downstream target of AKT and cell size regulatory complex (Fingar *et al*, 2002). The role of vimentin in cell size regulation has not been previously reported, however, keratin 17 intermediate filaments have been shown to regulate cell size through mTORC1 (Kim *et al*, 2006). It has been reported that vimentin knock-out mice look lean and weigh less (Wilhelmsson et al, 2019). We also made similar observations in vimentin knockout mice. Along with that, vimentin knockout mice resist high-fat diet induced obesity (Kim et al, 2021). Accumulation of mass is important for nutrient storage and rapid cell proliferation.

- As vimentin knockout MEFs were found to appear smaller than WT, mTORC1 signaling was studied in this thesis using WT and *Vim*$^{-/-}$ MEFs cell models to explore the role of vimentin in cell size regulation and autophagy.

Vimentin's role in immune cell functions has been previously reported in number of studies (Ramos *et al*, 2020; Su *et al*, 2019; Li *et al*, 2015). However, vimentin's role in Treg cells has been shown in only one article. Vimentin regulates Treg cell function by affecting PKC-θ localization. Polarized Treg

cells show strong vimentin protein expression than naïve T-cells, how vimentin expression is regulated has not been studied (McDonald-Hyman *et al* 2018).

- This thesis project aimed to identify how vimentin expression was regulated in Treg cells.

4 MATERIALS AND METHODS

Detailed experimental procedures are available in the original publications section at the end of the thesis.

4.1 Mice (I, II & III)

Mice were maintained in a Biocity animal facility and sacrificed according to ethical guidelines provided by the laboratory animal research facility. Wild type (WT) and vimentin knockout mice (*Vim*$^{-/-}$) were generated by crossbreeding heterozygous mice (129/Sv × C57BL/6). The mouse genotype was identified by the PCR reaction. Body mass index, Lee's index, and fat mass were measured from 6 months old mice. Body weight was measured from 3 and 6-months old mice. Organ weight was measured from 3 months old mice. Wound healing experiments were carried out at Umeå University, Sweden, according to the ethical committee for animal studies guidelines.

4.2 Experimental procedure for wound healing (I)

Before making the wound, mice were anesthetized. Then the hair on the dorsal region of the mouse was shaved. After shaving, either burn or excisional wounds were induced on 8 to10-week-old wild type (WT) and *Vim*$^{-/-}$ mice with a standard size. Wound healing was monitored in both WT and *Vim*$^{-/-}$ mice by taking photographs of the wound area contraction on different days. For histology, immunohistochemistry and immunofluorescence staining wound tissue samples were collected from different time points. To examine the tissue ultrastructure, protein, and mRNA expression during wound healing.

4.3 Cell culture (I & II)

WT and *Vim*$^{-/-}$ keratinocytes and mouse dermal fibroblasts (MDFs) were isolated from newborn mice. Primary mouse embryonic fibroblasts (MEFs) were isolated from a mouse embryo at 13.5 days post coitum. Keratinocytes were grown in FAD media (DMEM/Ham's F-12 Nutrient Mixture; 3.5:1.1) supplemented with Chelex-treated fetal bovine serum (FBS) (10%) (Invitrogen), insulin (5 µg/mL), hydrocortisone (0.5 µg/mL), adenine (0.18 mM), cholera toxin (100 pM) (from Sigma), EGF (10 ng/mL), sodium pyruvate (1 mM), penicillin (100 IU/mL)/ streptomycin (100 µg/ml), and glutamax (2 mM) (from Invitrogen) on a cell plate coated with collagen I (Invitrogen). Keratinocytes were incubated at 32 °C with 5% CO_2. MDFs, MEFs, and primary MEFs were grown in Dulbecco's Modified

Eagle Medium (DMEM) (Sigma) supplemented with L-glutamine (2 mM) (Invitrogen), penicillin (100 IU/mL) and streptomycin (100 µg/ml) (Invitrogen), and heat-inactivated FBS (10%) (Invitrogen/Biowest) at 37 °C with 5% CO_2. Macrophages were generated by inducing differentiation of cells isolated from the bone marrow of WT and *Vim*$^{-/-}$ mice. DMEM/F12 medium supplemented with heat-inactivated FBS (10%), L-glutamine (2 mM), penicillin (100 IU/mL), and streptomycin (100 µg/ml) (Invitrogen) were used to grow macrophages with 5% CO_2 at 37 °C. Bone marrow-derived dendritic cells were grown using Iscove's Modified Dulbecco's Medium (Gibco) containing FBS (10%), glutamine (20 mM), penicillin (100 IU/ml), streptomycin (100 µg/ml), 2-mercaptoethanol (50 µm) supplemented with granulocyte-macrophage colony-stimulating factor (50 ng/ml).

Cell lines
MEFs WT and *Vim*$^{-/-}$ (I & II)
Mouse keratinocytes WT and *Vim*$^{-/-}$ (I)
Macrophage WT and *Vim*$^{-/-}$ (I)
MDFs WT and *Vim*$^{-/-}$ (I)
Primary MEFs WT and *Vim*$^{-/-}$ (II)
Bone marrow-derived dendritic cells WT and *Vim*$^{-/-}$ (II)

4.3.1 CD4+ T cell isolation (III)

To obtain naïve T cells, mouse splenocytes were isolated from WT and *Vim*$^{-/-}$mice spleen. Then naïve T (Th0) cells were isolated using CD4+CD62L+ T cell Isolation Kit II (Miltenyi Biotec). Th0 cells were cultured for 3 days in IL6 (30 ng/ml) (PeproTech), TGF-β1 (5 ng/ml) (R&D system), and neutralizing antibodies anti-IL4 and anti-IFNγ (both at 10 µg/mL) (BD PharMingen), to induce Th17 polarization. To differentiate Th0 to iTreg cells, cells were grown in IL2 (10 ng/ml) (R&D system) and TGF-β1 (20 ng/ml) (R&D system) for 7 days and then restimulated with anti-CD3/CD28 and cultured for another 3 days with a fresh cytokine-containing medium. To perform cell culture, Iscove's Modified Dulbecco's Medium (Gibco) supplemented with FBS (10%), glutamine (2 mM), penicillin (100 IU/mL), streptomycin (0.1 mg/mL) (Sigma), and β-

mercaptoethanol (2.5 μM) were used. After polarization, Th17 and iTreg cells were subjected to proteomic and RNA-seq analysis along with control Th0 cells.

Plasmids and siRNA
pCDNA3 (I)
pCDNA3-vimentin (I)
pCMV-script-vimentin (Ivaska *et al*, 2005) (II)
pMRX-IP-GFP-LC3-RFP-LC3ΔG (Addgene) (II)
pRK5-HA GST RagB WT (Addgene) (II)
pRK5-HA GST RagC WT (Addgene) (II)
pRK5-HA GST RagB 99L (Addgene) (II)
pRK5-HA GST RagC 75L (Addgene) (II)
Scrambled siRNA (Dharmacon) (I)
Slug siRNA (Dharmacon) (I)
pCMV4-HA (Addgene) (II)
pME18S-3HA-mULK1(K46N) (Addgene) (II)

4.3.2 Transfection (I & II)

pcDNA3-vimentin and its empty vector were transfected into *Vim*$^{-/-}$ MDFs by electroporation. pCMV vimentin, pCMV4-HA and pME18S-3HA-mULK1(K46N) were transfected in *Vim*$^{-/-}$ MEFs; pMRX-IP-GFP-LC3-RFP-LC3ΔG, pRK5-HA GST RagB WT, pRK5-HA GST RagC WT, pRK5-HA GST RagB 99L and pRK5-HA GST RagC 75L were transfected in WT and *Vim*$^{-/-}$ MEFs using Xfect transfection reagent (Clontech) according to the manufacturer's protocol. To transfect scrambled siRNA and *slug* siRNA, lipofectamine RNAiMAX (Thermo Fisher Scientific) was used according to the manufacturer's protocol.

Reagents	**Study**
50X Essential amino acids mix (Thermo Fisher Scientific)	(II)
Glucose (Thermo Fisher Scientific)	(II)
Insulin (Sigma)	(II)
LY2109761 (Santa Cruz Biotechnology)	(I)
100X Nonessential amino acids mix (Sigma)	(II)
Rapamycin (Tocris Bioscience)	(II)
SB 431542 (Tocris Bioscience)	(I)
TGF-β1 (R&D Systems)	(I)
Thymidine (Sigma)	(II)
AKTVIII (Calbio)	(II)
TRAM (Selleckchem)	(II)

4.3.3 Treatments (I & II)

To induce EMT *in vitro*, mouse keratinocytes were stimulated with TGF-β1 (5–10 ng/mL) for 0, 3, or 5 d. After treatment, cells were lysed and collected for western blotting. WT and *Vim*$^{-/-}$ MDFs grown in media for six days were used as conditioned media for treatments. Cells grown in WT and *Vim*$^{-/-}$ conditioned media were treated with pan–TGF-β neutralizing antibody 1D11 (10 μg/mL), TGF-β I/II receptors inhibitor LY2109761 (2 μM), and SMAD inhibitor SB431542

(2 μM) for 3 days to inhibit TGF-β1 signaling, DMSO (2 μM) and IgG (10 μg/mL) were used as a control.

Cell synchronization in the G1/S phase was achieved by treating cells with thymidine (2 mM) overnight. Thymidine arrests cells in the G1/S phase by inhibiting DNA synthesis (Chen & Deng, 2018). To determine whether vimentin regulates growth factor signaling, both WT and *Vim*$^{-/-}$ MEFs were serum-starved for two to three days. Then, the media was changed to fresh serum-free DMEM media and stimulated with insulin (100 μg/ml) or fetal bovine serum (5%) for 24 h. To measure mTORC1 activation and translocation, WT and *Vim*$^{-/-}$ MEFs were serum-starved for 16 h and then stimulated with insulin (100 nM) or FBS (5%) for 15 minutes. Samples were then immunostained and immunoblotted. To investigate whether vimentin modulates mTORC1 upstream regulators nutrients and growth factor signals or not, WT and *Vim*$^{-/-}$ MEFs were starved for one hour without amino acids, glucose and serum, then cells were stimulated with L-glutamine (1 mM) plus 1X minimum essential amino acids mix, either presence or absence of 1X non-essential amino acids mix, glucose (2.5 mM), and insulin (100 nM) for 30 minutes. To further validate vimentin role in nutrient and growth signals, after 40 minutes of amino acids, glucose and serum starvation, cells were treated with rapamycin (100 nM)/ AKT VIII (1, 1.5 μM)/ TRAM (ERK 1/2 inhibitor) (0.1, 0.2 μM) for 20 minutes. Then cells were stimulated with L-glutamine (1 mM) plus 1X minimum essential amino acids mix, either presence or absence of 1X non-essential amino acids mix, glucose (2.5 mM), and insulin (100 nM) for 30 minutes. To study vimentin role in autophagy, WT and *Vim*$^{-/-}$ MEFs were grown in normal DMEM media containing FBS (10%) and L-glutamine (2 mM) for overnight. The next day after PBS wash, the media was replaced with RPMI media without amino acids, glucose, and serum. Then L-glutamine (1 mM) plus 1x minimum essential amino acids mix, 1X non-essential amino acids mix, and glucose (2.5 mM) was added alone or in combination with essential/ and non-essential amino acids mix and allowed to grow for one hour.

4.3.4 Antibodies

The following primary antibodies were used in this study.

Antibodies	Study	Host and Isotype	Usage
4EBP1 (53H11) (CST)	(II)	Rabbit IgG	WB
4EBP1 T37/38 (236B4) (CST)	(II)	Rabbit IgG	WB
Akt (C67E7) (CST)	(II)	Rabbit IgG	WB
Akt S473 (D9E) (CST)	(II)	Rabbit IgG	WB
Akt T308 (D25E6) (CST)	(II)	Rabbit IgG	WB
CD11b (AbD Serotec)	(I)	Rat IgG2b	IHC
Desmoplakin (gifts from Thomas Schulz, University of Leipzig)	(I)	Mouse IgG	WB
E-cadherin (GeneTex)	(I)	Rat IgG1	WB
GAPDH (14C10) (CST)	(I)	Rabbit IgG	WB
Hsc70 (Enzo Life Sciences)	(I, II)	Rat IgG2a	WB
HA-Tag (6E2)	(II)	Mouse IgG1	IF
HA-Tag (C29F4)	(II)	Rabbit IgG	IF
Insulin Receptor (4B8) (CST)	(II)	Rabbit IgG	WB
Insulin Receptor Y1150/1151 (19H7) (CST)	(II)	Rabbit IgG	WB
Keratin 14 (gifts from Thomas Schulz, University of Leipzig)	(I)	Mouse IgG	IF
Keratin 5 (AF 138) (Covance)	(I)	Rabbit IgG	IF
Keratin 6 (gifts from Thomas Schulz, University of Leipzig)	(I)	Mouse IgG	IF
Ki67 (Abcam)	(I)	Rabbit IgG	IF
LAMP1 (1D4B) (Santa Cruz)	(II)	Rat IgG2a	IF
LC3A/B (CST)	(II)	Rabbit IgG	WB
MPO (Thermo Fisher Scientific)	(I)	Rabbit IgG	IHC
mTOR (7C10) (CST)	(II)	Rabbit IgG	IF
N-cadherin (EPR1792Y) (Millipore)	(I)	Rabbit IgG	WB & IF
p44/42 MAPK (ERK1/2) (137F5) (CST)	(I & II)	Rabbit IgG	WB
p44/42 MAPK (ERK1/2) (Thr202/Tyr204) (CST)	(I & II)	Rabbit IgG	WB

Antibodies	Study	Host and Isotype	Usage
P70S6K (49D7) (CST)	(II)	Rabbit IgG	WB
P70S6K T389 (108D2) (CST)	(II)	Rabbit IgG	WB
Pan-keratin (Abcam)	(I)	Rabbit IgG	IHC & IF
S6 (5G10) (CST)	(II)	Rabbit IgG	WB
S6 S235/236 (D57.2.2E) (CST)	(II)	Rabbit IgG	WB
S6 Ser235/236 (2F9) (CST)	(II)	Rabbit IgG	Flow cytometry
Slug (C19G7) (CST)	(I)	Rabbit IgG	WB
Smad2 (Ser465/467)/Smad3 (Ser423/425) (D27F4)	(I)	Rabbit IgG	WB
Smad2/3 (D7G7) (CST)	(I)	Rabbit IgG	WB
SQSTM1/p62 (D1Q5S) (CST)	(II)	Rabbit IgG	WB
Vimentin (Covance)	(I, II)	Chicken IgY	IF
Vimentin (D21H3) (CST)	(I, II)	Rabbit IgG	WB
Zap-70 (99F2)	(I)	Rabbit IgG	IHC
α-SMA (BD)	(I)	Mouse IgG	IF
ULK1(CST)	(II)	Rabbit IgG	WB
ULK1 Ser757 (CST)	(II)	Rabbit IgG	WB
FOXP3 (eBioscience)	(III)	Mouse IgG1	WB
β-actin (CalBioChem)	(III)	Mouse IgG	WB
PKM2 (D78A4) (CST)		Rabbit IgG	WB
Vimentin Alexa Flour 647 Conjugate	(II)	Rabbit IgG	Flow cytometry

4.3.5 Western blot analysis (I, II & III)

Cells were lysed in Laemmli buffer or Triton X-100 lysis buffer (50 mM Tris-HCl, pH 7.5, 150 mM NaCl, 0.5% Triton X-100, 5% Glycerol, 1% SDS) with protease and phosphatase inhibitors (Roche). Samples were boiled with Laemmli buffer at 95°C for 5 to 10 minutes. Then proteins were separated by SDS-PAGE. After separation by SDS-PAGE, proteins were transferred to nitrocellulose or polyvinylidene difluoride (PVDF) membranes through wet transfer. PVDF membranes were activated in methanol before the transfer. Then the membrane was blocked with 5% milk in TBS, 0.3% tween20; after blocking, the membrane was washed with 0.3% tween20 TBS buffer. Then, proteins on the membrane were probed using a specific primary antibody and a secondary antibody conjugated with HRP. Enhanced chemiluminescence was used to detect antibody

on the membrane and its signal intensity was measured by chemiluminescence imaging (Biorad).

4.4 Microscopy

4.4.1 Collagen, haematoxylin and eosin staining (I&II)

Adipocyte tissue, normal and wounded skin tissue from mice were fixed in 4 % paraformaldehyde for 6 to 12 hr. After fixation, the tissues were embedded and sectioned, and then sections were stained using eosin and haematoxylin. Normal and wounded skin sections were also stained for collagen fibers using picro-sirius red staining. After staining, the H&E samples were imaged under a Leica DM LB microscope (Leica) or using panoramic digital slide scanners, and the collagen-stained samples were imaged using polarized light microscopy.

4.4.2 Immunohistochemistry and Immunofluorescence (I&II)

Cells plated on a coverslip were fixed with 3% paraformaldehyde for 10 to 20 minutes. The fixed cells were blocked with 3-5% Bovine serum albumin/PBS /0.3% tween-20 and labeled with a primary antibody and a secondary fluorescent antibody; the samples were stained with or without DAPI. Before performing immunostaining, paraffin-embedded tissue sections were deparaffinized and rehydrated. The antigens in the tissue section were unmasked by antigen retrieval method using 0.1 M citrate buffer (pH 6.0). Tissue sections were blocked with 5% goat serum and then labeled with the primary antibody. For immunofluorescence, the tissue was labeled with fluorescent secondary antibody and then stained with DAPI. To do immunohistochemistry, after primary antibody labeling, tissue sections were labeled with HRP-conjugated secondary antibodies and then antibody labeling was detected by the ABC staining system. Finally, the tissue was counterstained with haematoxylin. After staining, the samples were imaged under a Zeiss LSM780 confocal microscope using plan-apochromat 10× (NA 0.45, air), plan-apochromat 40× (NA 1.30, oil) objective or Leica SP5 confocal microscope using 63X objective/ Pannoramic digital slide scanners (3DHISTECH)/ Leica DM LB microscope.

4.4.3 Image analysis and quantification (I&II)

Cell area and diameter were measured from phase contrast image of attached cells and trypsinized cells using Fiji Image J hand tool. For cell volume analysis, cells were fixed in 3% paraformaldehyde for 15 minutes, after trypsinization. Then cells were stained with cell tracker dye (2 μm) (Thermo Fisher Scientific).

To measure cell volume, Z stack images series were taken from Leica SP5 confocal microscope using 63X objective, and then cell volume was measured by Imaris software. Fluorescent intensity and nuclei were measured in tissue sections using Bioimagexd image analysis software. Colocalization of LAMP1 and mTOR was analyzed from 12 to 18 cells per experiment, by using Bioimagexd software or Fiji using the JACoP tool. To measure cell area and volume in deformed cells, real-time deformability cytometry was used. Experiment and analysis were performed in bone marrow-derived dendritic cells as described previously (Vargas *et al*, 2016; Urbanska *et al*, 2018).

4.5 Wound healing (I)

In 24 or 96 well plates, scratch wounds were made on a monolayer of cells, and closure was monitored by incuCyte live-cell imaging instruments or a Cell IQ imaging system. After imaging, the wound closure area was measured using IncuCyte analysis software and an Image J or Cell IQ analyzer. To prevent proliferation, mitomycin C (10 μg/mL) was added to the media.

4.6 ELISA assay (I)

TGF-β1 level was measured from MDFs or macrophage filtered cell-free supernatant using an ELISA Ready-SET-Go! kit (eBioscience).

4.7 Quantitative Real-Time PCR (I)

To measure gene expression, a FFPE Total RNA Isolation Kit (Invitrogen) was used to isolate total RNA from the skin tissue section. RNeasy mini kit (Qiagen) was used to extract total RNA from cells. After RNA isolation, cDNA was synthesized using a High-Capacity cDNA Reverse Transcription Kit (Applied Biosystems). Then the transcript level of specific genes was measured by reverse transcription-quantitative polymerase chain reaction (RT-qPCR). Standard curve and melting curve analysis were done to measure the quality of the quantitative PCR run; GAPDH was used as a housekeeping gene for normalization.

Gene name (protein name)	**Forward sequence**	**Reverse sequence**	**NCBI Gene ID**
Vim (Vimentin)	CGTCCACACGCACCTACAG	GGGGGATGAGGAATAGAGGCT	22352
Fn1 (Fibronectin)	GATGTCCGAACAGCTATTTACCA	CCTTGCGACTTCAGCCACT	14268
S100a4 (FSP-1)	TCCACAAATACTCAGGCAAAGAG	GCAGCTCCCTGGTCAGTAG	20198
Cdh2 (N-Cadherin)	AGCGCAGTCTTACCGAAGG	TCGCTGCTTTCATACTGAACTTT	12558
Snai2 (Slug)	TGGTCAAGAAACATTTCAACGCC	GGTGAGGATCTCTGGTTTTGGTA	20583
Gapdh (GAPDH)	AGGTCGGTGTGAACGGATTTG	TGTAGACCATGTAGTTGAGGTCA	14433
Il6 (IL-6)	TAGTCCTTCCTACCCCAATTTCC	TTGGTCCTTAGCCACTCCTTC	16193
Il23 (IL-23)	ATGCTGGATTGCAGAGCAGTA	ACGGGGCACATTATTTTTAGTCT	83430
Tgfb1 (TGF-β1)	CTCCCGTGGCTTCTAGTGC	GCCTTAGTTTGGACAGGATCTG	21803
Tnf (TNF-α)	CCCTCACACTCAGATCATCTTCT	GCTACGACGTGGGCTACAG	21926
Il1a (IL-1α)	CGTCAGGCAGAAGTTTGTCA	TGATGAGTTTTGGTGTTTCTGG	16175
Il1b (IL-1β)	GCAACTGTTCCTGAACTCAACT	ATCTTTTGGGGTCCGTCAACT	16176

4.8 Measurement of protein content (II)

Cells were trypsinized from 6 well plates with 80% confluence and counted. Then 300,000 cells were lysed in RIPA buffer with protease inhibitor (Thermo Fisher Scientific) and the protein concentration was measured using the BCA assay kit (Pierce).

4.9 Protein synthesis assay (II)

Click-iT HPG Alexa Fluor Protein Synthesis Assay Kit (Thermo Fisher Scientific) was used to measure protein synthesis. Cells were serum-starved for 16 hours, and then the media was changed to methionine-free media without serum. The cells were stimulated with insulin in the presence of methionine analog for 30 minutes. Then cells were fixed and stained according to the manufacturer's instructions, stained cells were imaged and analyzed by Cell IQ imaging and analysis system.

4.10 Autophagy flux (II)

To measure the autophagic flux, WT and *Vim*$^{-/-}$ MEFs were transfected with pMRX-IP-GFP-LC3-RFP-LC3ΔG vector. Then cells were seeded on glass coverslips and allowed to grow overnight. Later media was changed to serum-free DMEM or media with L-glutamine (1 mM) plus minimum essential amino acid mix and glucose (2.5 mM) for 3 hours. Cells were imaged using Leica SP5 TCS confocal microscope under a 63× immersion oil objective after fixing with 3% PFA for 15 minutes. By using Fiji, GFP and RFP fluorescent intensity were measured.

4.11 Flow cytometry (II)

For flow cytometry analysis, trypsinized cells were fixed and permeabilized using 3% PFA for 20 minutes and 0.2% Triton X-100/PBS for 10 minutes. Cells were blocked with 3% BSA 0.2% Tween20 for 1 hour. Proteins were probed and labeled with specific primary antibody/primary antibody conjugated with fluorescent dye and fluorescent conjugated secondary antibody. Flow cytometry data were acquired through BD LSRFortessa (BD Biosciences) using FITC 530/30 (515 to 545 nm) and APC 670/14 (663 to 677 nm) filter. The data were analyzed with FlowJo software.

4.12 Cell proliferation assay

To measure cell proliferation, 15000 cells of WT and *Vim*$^{-/-}$ MEFs were seeded on 12 well plate and grow them in Dulbecco's Modified Eagle Medium (DMEM) (25 mM glucose) (Sigma) supplemented with L-glutamine (2 mM) (Invitrogen), penicillin (100 IU/mL) and streptomycin (100 µg/ml) (Invitrogen), and heat-inactivated FBS (10%). Then cells were counted on day 1, 2, 3 and 4 by using burker chamber. To measure glucose-dependent cell proliferation, 15000 cells of WT and *Vim*$^{-/-}$ MEFs were plated on 12 well plates with media containing glucose (0, 5, 10, 15, 20 and 25mM) and allowed to grow for three days. Cell proliferation rate was measured by crystal violet staining, everyday samples were collected and washed with PBS, then fixed in 4% paraformaldehyde for 15 minutes and stained with 0.2% crystal violet. After staining, cells were washed with PBS three times and lysed with 1% SDS. Then crystal violet dye absorbance was measured at 570 nm, using the Hidex instrument (Hidex Oy, Finland).

4.13 GSH and GSSG assay

WT and *Vim*$^{-/-}$ MEFs were plated on 96 well plates and then GSH and GSSG levels in the cells were measured using a GSH and GSSG Promega assay kit. The protocol was followed according to the manufacturer's instructions.

4.14 Pull-down assay

WT and *Vim*$^{-/-}$ MEFs were seeded on a 10 cm cell culture plate and allowed to grow overnight in DMEM (25 mM glucose) with L-glutamine (2 mM) and FBS (10%) and reach 80% confluency. The next day cells were washed with ice-cold PBS three times and lysed in lysis buffer containing 25 mM HEPES buffer pH 7.4, 150 mM NaCl, 2 mM EDTA, 1% NP40, 10 mM sodium pyrophosphate, 10 mM β-glycerophosphate, 1.5 mM sodium orthovanadate and protease inhibitor cocktail mix (Pierce). Cell lysates were centrifuged at 12,000 g for 15 minutes. Then the supernatant was transferred to a fresh tube and the protein amount was measured using a BCA assay kit (Pierce). Then 1 µg of purified recombinant His-tagged PKM2 was incubated with 1mg/ml of cell lysate for one hour at 4° C. After one hour, His-Tag Dynabeads (Pierce) was added and allowed to incubate for another 30 minutes. Then beads were washed with lysis buffer three times and boiled in Laemmli buffer for 10 minutes. The samples were analyzed by immunoblotting.

4.15 Statistical analysis (I, II & III)

All the statistical analyses were carried out by graph pad software. All the observations and measurements were obtained from three independent repeats unless stated. To determine statistical significance, the student T-test was used between two samples; for multiple samples, one-way ANOVA was used.

5 RESULTS

5.1 Vimentin in the wound healing process and fibroblast proliferation

5.1.1 *Vim*$^{-/-}$ delays the wound healing process (I)

Vimentin role in physiology got attention only after identifying vimentin role in wound healing process (Eckes *et al*, 2000). However, no one studied further about vimentin in wound healing process using *in vivo* mouse model (Ridge *et al*, 2022). Here we induced either burn or excisional wounds on mice skin to study the wound healing process in a *Vim*$^{-/-}$ mouse model. In WT mice, the wound area completely closed within 15 days, but in *Vim*$^{-/-}$ mice the wound area was not completely closed (Figure 1 I). Histological sections of wound area at different time points were analyzed to assess how molecular and cellular events were affected in different phases of the wound healing process. In WT mice, on day 9 post-injury, 32% of the wound area was re-epithelialized but in *Vim*$^{-/-}$ mice only 17% of the wound area was re-epithelialized. On day 15 post-injury, a layer of epithelial cells completely covered the wound area in WT. However, in *Vim*$^{-/-}$ mice only ~56% of wound area was re-epithelialized (Figure 1 A, B, and C I). By measuring the closure of the wound area at different time points, we found that in WT the wound area begins to heal on day 4 post-injury; however, *Vim*$^{-/-}$ mice showed delays in the wound healing process (Figure 1 D I). Like burn-induced wounds, excisional wound healing was also severely impaired in *Vim*$^{-/-}$ mice (Figure S1 I). To examine the basal conditions of mouse skin, we also compared the tissue sections of uninjured WT with *Vim*$^{-/-}$ from prenatal mice (E14), preweaning (18 days postnatal) mice, and adult mice. We did not find any morphological or structural abnormalities in WT and *Vim*$^{-/-}$ mice (Figure S2 A-D I). Based on those observations, we have concluded that delayed reepithelization retarded wound closure in *Vim*$^{-/-}$ mice. EMT coordinates and regulates the re-epithelization of skin; impairment of re-epithelization could result from vimentin deletion, thereby delaying the process of wound healing.

5.1.2 EMT program is dysregulated in *Vim*$^{-/-}$ mice wound site (I)

Re-epithelialization of the wound area was delayed in *Vim*$^{-/-}$ mice. To further evaluate the molecular mechanism behind this impairment, we measured keratin 6 and 14 protein expression in keratinocytes from wound tissue sections. Keratinocytes form sheet-like layers on the dermis; tissue injury induces the

expression of keratin 6, 14 and 16 (DePianto & Coulombe, 2004; Lessard *et al*, 2013). On day 9 and 15 post-injury, keratin 6 and 14 fluorescence signals were stronger in WT than *Vim*$^{-/-}$ mice. Expression of keratin 6 and keratin 14 were upregulated in mitotically active cells (Figure 2 A & B I). Likewise, pan keratin intensity was also stronger in WT mice than *Vim*$^{-/-}$ counterparts. On day 15 in WT mice, keratinocytes were fused to form a stratified mature epidermis, whereas in *Vim*$^{-/-}$ mice, a very thin epithelial layer was developed under the large scab. Pan-Keratin labeling showed that the average thickness of the epithelial layer in *Vim*$^{-/-}$ mice was three times less than in WT mice. Furthermore, the organization of keratinocytes were affected in *Vim*$^{-/-}$ mice (Figure 2 C and D I). This effect could likely be due to a defect in keratinocyte migration and EMT. To replace the damaged epithelium, keratinocytes undergo EMT by losing their epithelial junctions and acquiring mesenchymal-like phenotype.

Vimentin is an EMT marker, but its role in EMT is not very clear. However, there are several reports on the involvement of vimentin in EMT and cell migration (Satelli & Li, 2011b; Kidd *et al*, 2014). Slug is a transcription factor and an EMT inducer. Here we found that slug mRNA was maintained at the same level in both WT and *Vim*$^{-/-}$ mice on day 0 (Figure 2 E I) (Xu *et al*, 2009b). On day 3 post-injury, the slug mRNA level was upregulated in WT, however in *Vim*$^{-/-}$ mice the slug mRNA level was 4.7 fold lower than in WT mice. On day 9 post-injury, slug mRNA expression was upregulated drastically in WT mice compared to day 0, but in *Vim*$^{-/-}$ mice the slug mRNA level was 11.5 fold lower than in WT. On day 15, the slug mRNA level returned to the same levels in both WT and *Vim*$^{-/-}$ mice (Figure 2 E I). To assess whether the slug mRNA level correlated with EMT induction, we measured expression levels of EMT markers on the corresponding days. Slug regulates the expression of mesenchymal specific markers N-Cadherin (Cdh2), fibroblast-specific protein 1 (S100a4) and fibronectin (Fn1) (Acloque *et al*, 2008; Jägle *et al*, 2017). On day 0, the expression of mesenchymal markers was at basal levels in both WT and *Vim*$^{-/-}$ mice. In WT mice, we found that on day 9 mesenchymal marker expression levels were upregulated and correlated with slug level and then returned to the baseline level on day 15. However, there was no upregulation of slug and mesenchymal markers in *Vim*$^{-/-}$ mice on day 9 (Figure 2E I). On day 9 post-injury, the number of keratin-positive cells at the epidermis-dermis interface were significantly less in *Vim*$^{-/-}$ mice than WT (Figure S3 A and B, I). WT mice expressed significantly more keratin and the mesenchymal marker alpha-smooth muscle actin at the dermal wound site than *Vim*$^{-/-}$ mice (Figure S3 C I). The intermediate EMT phenotype is crucial for wound healing, but we didn't find many cells expressing both epithelial (keratin) and mesenchymal protein (alpha-smooth

muscle actin) in *Vim*$^{-/-}$ mice (Figure S3 C and F I). On day 15 post-injury, co-expression of N-Cadherin and keratin 6 was mainly seen in the WT epidermal layer (Figure S3 E and F I). Slug expression was not upregulated in the *Vim*$^{-/-}$ wound site on day 9 post-injury, which is an active phase of the wound healing process and crucial for EMT induction and epithelial cell migration. We also found that mesenchymal markers were not upregulated in *Vim*$^{-/-}$ mice. Based on these observations, vimentin could be involved in the EMT process in cells by regulating the EMT inducer slug or facilitating the acquisition of mesenchymal properties.

5.1.3 TGF-β1 regulates the EMT inducer slug and epithelial cell migration (I)

Various growth factors regulate EMT induction. TGF-β1 is one of the well-known EMT regulators during development and wound healing, so we assessed the TGF-β1 mRNA expression level in both WT and *Vim*$^{-/-}$ mice (Derynck & Zhang, 2003; Xu *et al*, 2009b). We found that the TGF-β1 mRNA expression level was significantly lower in *Vim*$^{-/-}$ than WT mice, especially on day 3 and 9 (Figure 3A I). In mouse keratinocytes, recombinant TGF-β1 stimulation suppressed epithelial markers desmoplakin and E-cadherin and also activated mesenchymal proteins slug, N-cadherin and vimentin (Figure 3B-D I). To investigate whether TGF-β1 induces EMT through slug, we knocked down slug in keratinocytes and then stimulated with TGF-β1. Silencing slug reduced TGF-β1 induced upregulation of N-cadherin and vimentin expression levels; repression of desmoplakin was not prominent compared to scr siRNA (Figure 3E-G I). This suggests that slug is a downstream effector of TGF-β1, through which it induces EMT. We hypothesized that active fibroblasts in the dermal region could produce TGF-β1, which can induce EMT in epidermal keratinocytes. To support our hypothesis, we found that TGF-β1 expression was lower in mouse dermal fibroblasts (MDFs) isolated from *Vim*$^{-/-}$ mice than in WT (Figure 4A I). We also found that the active TGF-β1 level in *Vim*$^{-/-}$ cell culture supernatant was significantly lower than WT supernatant (Figure 4B I). WT MDFs cell culture supernatant contained an abundance of TGF-β1 molecules, and it induced significantly more EMT in a mouse keratinocyte cell line than cell culture supernatant from *Vim*$^{-/-}$ MDFs (Figure 4C I). Similarly, in a scratch wound assay, mouse keratinocytes migrated faster and closed the wound area more quickly with WT MDFs conditioned cell supernatant stimulation than with *Vim*$^{-/-}$ MDFs conditioned cell supernatant (Figure 4 C and D I). We measured different inflammatory cytokine levels to rule out whether cytokines produced by immune cells influence the EMT process. We found that cytokines IL-6, IL-1 alpha, and TNF alpha mRNA levels were similar in both WT and *Vim*$^{-/-}$ mice on day 3 and

9 post-injury (Figure S4A I). On day 9 post-injury, *Vim*$^{-/-}$ mice showed 1.5-fold higher neutrophil infiltration in the wound edge than WT (Figure S4B and C I); however, there was no significant difference in neutrophil myeloperoxidase activity between WT and *Vim*$^{-/-}$ mice (Figure S4D and E I). Likewise, on day 9 post-injury, there was no difference in the number of macrophages (CD11b+) and activated T cells (Zap-70+) in both WT and *Vim*$^{-/-}$ mice (Figure S4D and E I). In cell culture, both WT and *Vim*$^{-/-}$ macrophages released the same amount of TGF-β1 secretion in the media (Figure SF I). These results suggest that vimentin knockout in fibroblasts affects TGF-β1 production and its downstream signaling. To check whether TGF-β1 ligand produced from MDFs regulated EMT in keratinocytes, we blocked TGF-β1 signaling in keratinocytes by using pan TGF-β1 neutralizing antibody and chemical inhibitors LY2109761 (TGFβ receptor I/II inhibitor) and SB431542 (inhibit SMAD signaling), and then stimulated cells with the MDFs-derived conditioned medium. As a readout, we measured TGF-β1 downstream signaling of SMAD phosphorylation by immunoblotting and it showed the inhibition of TGF-β1 downstream signal in *Vim*$^{-/-}$ MDFs (Figure 4F I). In addition to the downregulation of EMT markers slug and N-cadherin, TGF-β1 inhibition also reduced the keratinocytes cell migration rate (Figure 4G and H I). Inhibition of TGF-β1 signaling and cell migration was more prominent in WT-conditioned MDFs medium than *Vim*$^{-/-}$ potentially due to the high levels of TGF-β1 present in the cell culture media (Figure 4G I). We also found that silencing of slug reduced the cell migration rate in keratinocytes (Figure 4J I). Based on this we propose that vimentin could play a role in the EMT program induced by TGF-β1 and slug signaling. TGF-β1 is the key growth factor for normal development and growth, and an EMT inducer. Here we found that TGF-βl level and its signaling was reduced in *Vim*$^{-/-}$ MDFs. During the wound-healing process, active fibroblasts produced TGF-β1. In both WT and *Vim*$^{-/-}$ mice, inflammatory cell activity and cytokine production were at the same level on day 3 and 9 post injury. *In vitro*, TGF-β1 production and slug expression and mesenchymal proteins were reduced in *Vim*$^{-/-}$ MDFs. This suggests that vimentin is required for active TGF-β1 production, which in turn stimulates and acts as a paracrine signal for the wound healing process by regulating EMT and cell migration.

5.1.4 Vimentin mediates fibroblast proliferation, collagen deposition, and paracrine EMT signal (I)

In *Vim*$^{-/-}$ mice wound sections, fibroblast cell numbers were very low compared to WT, especially during the late stage of wound healing. This could be due to a defect in fibroblast cell proliferation. In support of this hypothesis, we found that the

proliferation marker Ki67 was significantly reduced in the *Vim*$^{-/-}$ wound area (Figure 5 A and B I). Since fibroblasts are the main producers of the extracellular matrix, to ascertain whether a defect in fibroblast proliferation affects extracellular matrix production and deposition. We stained collagen in the tissue sections using picro-sirius red staining. WT granulation tissue showed thick collagen fibers in the wound area. However, in *Vim*$^{-/-}$ mice, collagen fibers were either very thin or completely absent (Figure 5 C I). On day 15 post-injury, in WT mice, most of the dermis layer (95%) was completely occupied with collagen fibers, however, vimentin loss resulted in a striking loss of collagen deposition (Figure 5 D I). We also examined the collagen deposition in both adult WT and *Vim*$^{-/-}$ uninjured mouse tissue and did not notice any differences. It implies that a low level of collagen deposition during wound healing could be a defect in fibroblast proliferation and collagen production. *In vivo* results indicate that there could be a defect in fibroblast proliferation. To ascertain this, we measured the MDFs cell proliferation rate in both WT and *Vim*$^{-/-}$. We found reduced cell proliferation rate in *Vim*$^{-/-}$ MDFs (Figure 6A I), but did not increase apoptosis (Figure S5A I). To determine whether vimentin rescue the cell proliferation rate, we exogenously expressed human wild-type vimentin in *Vim*$^{-/-}$ MDFs cells and observed an increased cell proliferation rate (Figure 6A I). Also, rescuing *Vim*$^{-/-}$ MDF cells with human WT vimentin increased the phosphorylation of ERK1/2, one of the key molecules for cell proliferation (Figure 6B I). In addition, we found that exogenous expression of vimentin in *Vim*$^{-/-}$ keratinocytes rescued the EMT phenotype and cell migration delay (Figure 6C and D I). Fibroblast and extracellular matrix fill the wound area and TGF-β1 acts as a paracrine signal for EMT induction through which it regulates re-epithelization. Based on our results fibroblasts require vimentin for active cell proliferation, extracellular matrix production, and TGF-β1 secretion.

5.1.5 Reduced form of glutathione was decreased in *Vim*$^{-/-}$ MEFs

Similar to our observation in dermal fibroblasts, cell proliferation rate was significantly reduced in *Vim*$^{-/-}$ MEFs (Figure 10A). Related to our observation, a previous study showed that in primary *Vim*$^{-/-}$ MEFs cell cycle progression was arrested at a much earlier passage than WT. The earlier arrest of cell cycle progression is due to an increase of reactive oxygen species levels and also it shows signs of oxidative stress such as an enlarged nucleus and defective mitochondria with low membrane potential (Tolstonog *et al*, 2001). Previous studies showed that vimentin protects mitochondria from oxidative stress (Nekrasova *et al*, 2011; Chernoivanenko *et al*, 2014, 2015). The molecular mechanism of its regulation has been not studied. Reduced glutathione(GSH) is

the frontline defense against reactive oxygen species (Ceballos-Picot *et al*, 1996). In some cells, most of the glucose molecules are diverted to the pentose phosphate pathway (PPP) rather than oxidative phosphorylation. It helps to maintain the redox state by generating NADPH and also supports macromolecular synthesis. NADPH replenishes oxidized glutathione(GSSG) into reduced GSH (Dayton *et al*, 2016; Pavlova & Thompson, 2016). Here we found that GSH level was significantly reduced in *Vim*$^{-/-}$ MEFs (Figure 10 B). This implies that vimentin could protect the cells from oxidative stress.

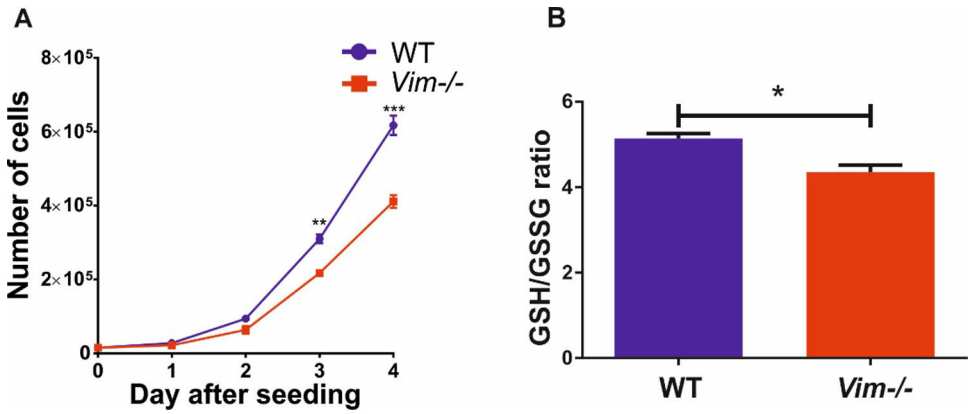

Figure 10. Vimentin affects the rate of cell proliferation and GSH/GSSG ratios. A) Graph plot showing number of cells from WT and *Vim*$^{-/-}$ MEFs were counted on day 0, 1, 2, 3 and 4 (n=3), error bars were plotted from standard mean error, statistical significance was calculated by unpaired T test *p<0.01, ***p<0.001. B) Bar graph showing the ratio of GSH and GSSG from WT and *Vim*$^{-/-}$ MEFs without any treatment (n=3), error bars were plotted from standard mean error, statistical significance was calculated by unpaired T test *p<0.1.

5.1.6 Vimentin interacts with PKM2

To investigate, whether vimentin is involved in glucose metabolism, we grew MEFs in the media containing increasing concentrations of glucose varying from 0, 5, 10, and 25 mM. At 0 mM glucose, both WT and *Vim*$^{-/-}$ MEFs were proliferating at the same rate, whereas increasing glucose concentration gradually increases the cell proliferation rate in both WT and *Vim*$^{-/-}$ MEFs. However, the proliferation rate was very significantly higher in WT than *Vim*$^{-/-}$ MEFs. The cell proliferation rate of *Vim*$^{-/-}$ MEFs grown in 25 mM glucose was equal to WT grown in 10 mM glucose (Figure 11A). This suggests that vimentin could take part in glucose metabolism or uptake. We also observed that vimentin interacted with pyruvate

kinase M2 (PKM2), which is one of the key enzymes in regulating the pentose phosphate pathway (Figure 11 B).

PKM2 occurs in three different forms: a completely inactive monomer, a partially active dimer, and a highly active tetramer (Dayton *et al*, 2016). PKM2 converts phosphoenolpyruvate to pyruvate which enters mitochondria for oxidative phosphorylation. However, inhibition of PKM2 diverts glucose metabolites to the pentose phosphate pathway. Cells can modulate glucose metabolism by regulating the activity of PKM2 (Dong *et al*, 2016). The activity of PKM2 can be modulated by its substrate and tyrosine-phosphorylated peptide/protein. The binding of tyrosine-phosphorylated protein inhibits substrate binding and converts it to the dimer form (Christofk *et al*, 2008). We speculate that vimentin a phosphorylation-rich protein, may regulate PKM2 activity through which it could influence the pentose phosphate pathway and redox state of the cell. Vimentin's role in PKM2 activity needs to be studied using genetic and biochemical approaches.

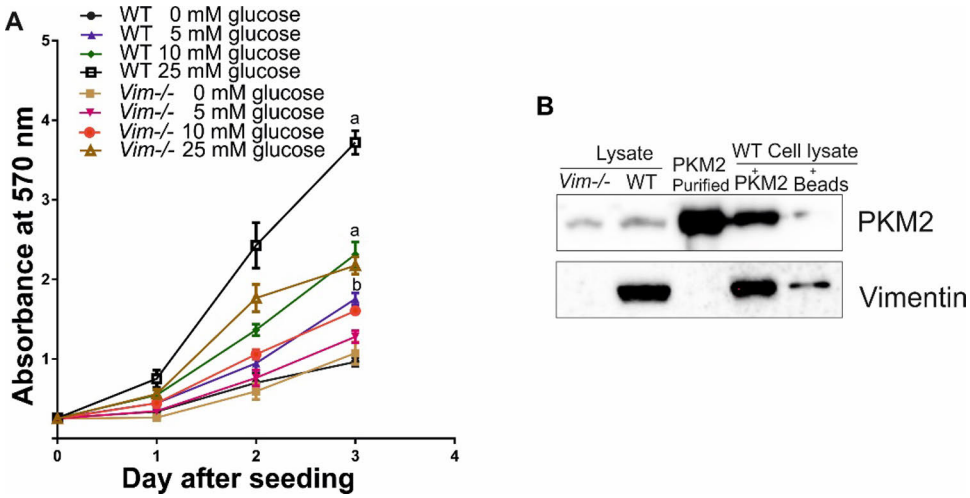

Figure 11. Vimentin affects cell proliferation and PMK2 interaction. A) WT and *Vim*$^{-/-}$ MEFs were grown in media containing different amounts of glucose 0, 5, 10 and 25 mM for three days. Cell proliferation rate was measured by crystal violet staining and absorbance at 595 nm (n=3), error bars were plotted from standard mean error**,** statistical significance was calculated by two-way ANOVA **a** indicates $p<0.001$ difference between WT and *Vim*$^{-/-}$ in 10 mM and 25 mM glucose conditions, **b** indicates $p<0.01$ difference between WT and *Vim*$^{-/-}$ in the 5 mM glucose condition. B) Purified His tagged PKM2 was incubated with WT MEFs cell lysate and then PKM2 was pull down with Dynabeads. PKM2 binding protein vimentin was identified by immunoblotting.

5.2 Vimentin regulates cell growth and autophagy

5.2.1 Lack of vimentin decreases the cell size (II)

While measuring the cell proliferation rate using Cell-IQ, we found that *Vim*$^{-/-}$ MEFs look smaller than WT (Extended video 1 II). We also observed that *Vim*$^{-/-}$ mice look leaner and weigh less than WT mice. Some internal organs such as heart and kidneys were smaller in size in *Vim*$^{-/-}$ mice. A low level of body weight is due to less fat content, and it was reflected in BMI, Lee index, total fat, and fat/body weight ratio. Like MEFs, we also found that *Vim*$^{-/-}$ adipocytes were smaller in size in adipose tissue sections compared to WT (Figure 1 A-F II). To study cell size differences in WT and *Vim*$^{-/-}$ MEFs, we measured the cell area from phase-contrast images, using the Fiji ImageJ analyzer. Our results indicate that *Vim*$^{-/-}$ MEFs cell area was significantly smaller than WT. This could be due to a lack of the cytoskeletal protein vimentin, which affects cell morphology and spreading (Figure 2A-B II). So we measured cell volume using 3D rendering of confocal microscopy Z stack images to ascertain whether vimentin knockout affects cell morphology or cell size. Cell volume measurement from the 3D projection of Z-stack images showed that *Vim*$^{-/-}$ MEFs were smaller in size, and the volume of the cells was significantly reduced (Figure 2 C II). Cells are not same size in all phases of the cell cycle, and it varies from one phase to another. To rule out whether *Vim*$^{-/-}$ knockout causes a defect in cell cycle progression or accumulation of cells in one phase of the cell cycle. We arrested cells in the G1/S phase by thymidine treatment. Thymidine-treated cells show a cell volume difference between the groups and likewise, *Vim*$^{-/-}$ MEFs were smaller in size (Figure 2 D II). To address whether vimentin affects cell size, we expressed wild-type vimentin exogenously in *Vim*$^{-/-}$ MEFs and this rescued the cell size phenotype in *Vim*$^{-/-}$ MEFs (Figure 2 E II). We also measured cell volume in primary MEFs and obtained similar results as in immortalized MEFs (Figure 2 F II). Since the cytoskeleton provides structure and form to the cells, to analyze whether vimentin increases cell size by supporting the cell spreading through cytoskeleton network or increasing cell mass. We measured cell size in non-adherent primary bone marrow-derived dendritic cells (BMDCs) by passing them through a narrow-constricted channel. Passing cells through a narrow constriction affects cell morphology, but it didn't affect cell mass. There is a clear cell size difference between WT and *Vim*$^{-/-}$ BMDCs. This suggests that vimentin not only provides structure and form to the cell but also supports cell size (Extended Data Fig. 1a, b II). Vimentin provides dynamics and structural support

to the cell, but its role in cell size regulation has never been reported. Based on these observations, vimentin could be involved in cell size regulation.

5.2.2 Vimentin is involved in cell growth through mTORC1 signaling (II)

Growth factors such as IGF1, IGF2, and insulin transduce their signal mainly through tyrosine receptor kinases (RTKs) and activate PI3K/AKT/mTOR signaling pathway (Lodish *et al*, 2000; Efeyan & Sabatini, 2013; Boucher *et al*, 2014). We found that *Vim*$^{-/-}$ MEFs were smaller in size, possibly due to a defect in growth factor signaling. To examine whether vimentin knockout impairs cell growth signaling, both WT and *Vim*$^{-/-}$ MEFs were serum-starved for two to three days and then the media was replaced with serum-free media and stimulated with either insulin or FCS for 24 hours. Serum starvation reduces cell size in both WT and *Vim*$^{-/-}$ MEFs; insulin stimulation increases cell size in WT, but we did not observe any increase of cell size in *Vim*$^{-/-}$ MEFs. In contrast, serum stimulation increased cell size in both WT and *Vim*$^{-/-}$ MEFs, however, *Vim*$^{-/-}$ MEFs were significantly smaller than WT (Figure 3 A-II). We also measured the protein content in MEFs and found that the protein content in *Vim*$^{-/-}$ MEFs was ~25 % less than WT (Figure 3B II). Insulin stimulation activates protein and lipid synthesis. We measured protein synthesis after insulin stimulation to investigate whether vimentin promotes cell growth by supporting protein synthesis through growth signaling. We found that protein synthesis was relatively low in *Vim*$^{-/-}$ compared to WT MEFs (Figure 3C II). This suggests that vimentin plays a role in insulin-dependent protein synthesis, and it could regulate protein synthesis through the PI3K/mTOR signaling pathway. mTORC1 is a complex protein that regulates cell growth by activating different anabolic processes. The major regulators of mTORC1 activity are nutrients and growth factors (Laplante & Sabatini, 2009). Next, we analyzed whether vimentin regulates protein synthesis through the mTORC1 signaling pathway. To study that, we serum-starved MEFs WT and *Vim*$^{-/-}$ overnight and then stimulated with either insulin or FCS. We found that mTORC1 downstream P70S6K1 and S6 phosphorylation was relatively low in *Vim*$^{-/-}$ MEFs (Figure 3 D II). This implies that vimentin regulates mTORC1 activity either directly or indirectly, affecting its upstream signaling.

5.2.3 Vimentin modulates mTORC1 signaling through Rag GTPase (II)

We found that mTORC1 activity was reduced in *Vim*$^{-/-}$ MEFs, but the mechanism of regulation is unclear. To understand how vimentin modulates mTORC1

signaling, we starved both WT and *Vim*$^{-/-}$ MEFs without amino acids, glucose, and serum for one hour and then the cells were stimulated with different combinations of L-glutamine, minimum essential amino acids (EAAs), non-essential amino acids (NEAAs), glucose and insulin for 30 minutes. Along with amino acids, we also included glucose in the stimulation. It is well known that amino acids regulate mTORC1 signaling and few reports indicate that glucose also affects mTORC1 signaling through Rag GTPase (Efeyan *et al*, 2013b). We found that under a combination of insulin, amino acids and glucose stimulation, the phosphorylation level of mTORC1 downstream signaling molecules such as P70S6K1, 4EBP1 and S6 was lower in *Vim*$^{-/-}$ MEFs compared to WT.

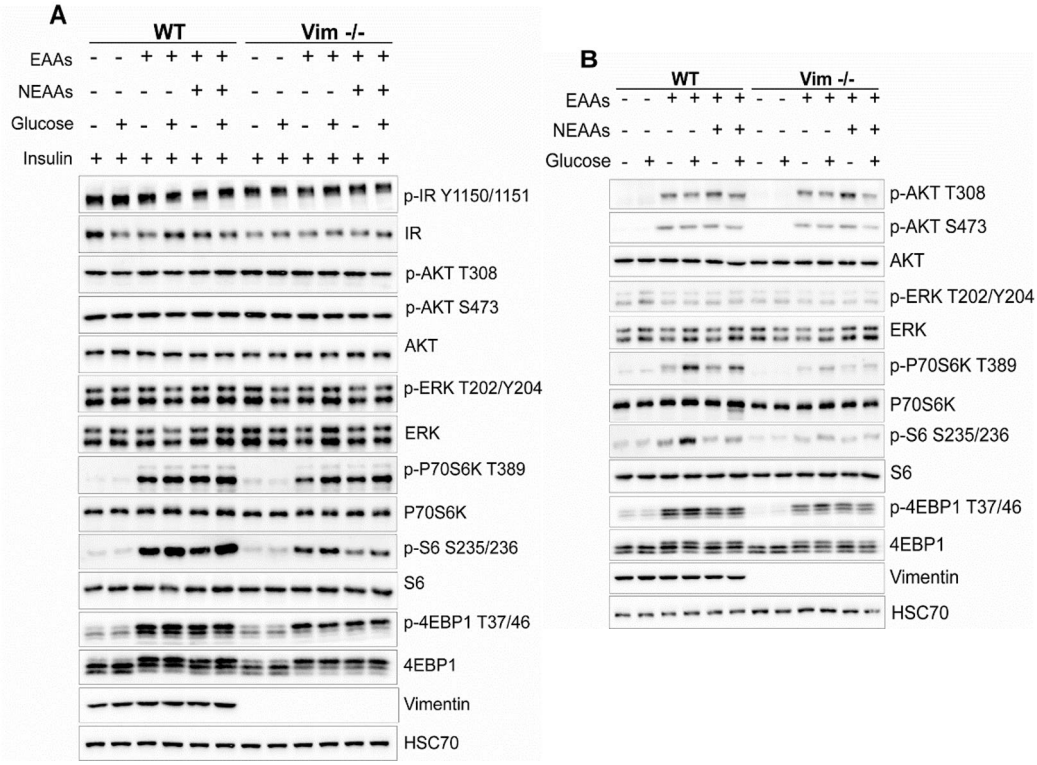

Figure 12. mTORC1 signaling effects of vimentin after nutrients and insulin stimulation. A) Western blot analysis showing WT and *Vim*$^{-/-}$ MEFs were starved for one hour in an RPMI media without amino acids, glucose, and growth factors and then stimulated with 1 mM L-glutamine plus 1x EAAs alone or with NEAAs, either with 2.5 mM glucose or without glucose and 100 nM insulin for 30 minutes (n=3). B) Treatment was performed as mentioned in Figure A without insulin (n=3). Above western blot images were extracted from (Mohanasundaram *et al*, 2022) under **creative commons attribution license**.

However, the Thr308 and S473 phosphorylation levels of AKT, mTORC1 upstream regulator, were very similar in both WT and *Vim*$^{-/-}$ MEFs (Figure 12 A). Glucose alone did not activate mTORC1 but in combination with amino acids amplify P70S6K1 and S6 phosphorylation. Especially, S6 phosphorylation was stronger in WT than *Vim*$^{-/-}$ MEFs (Figure 12 A). We also performed nutrient stimulation without insulin to identify how amino acids and glucose affect mTORC1 activation without growth factors. Here we found, similar to nutrient and growth factor stimulation, phosphorylation levels of mTORC1 downstream regulators P70S6K1 and S6 were low in *Vim*$^{-/-}$ MEFs (Figure 12 B). However, activation was not as prominent as compared with amino acids, glucose, and insulin stimulation. Similarly, glucose alone did not activate any signaling molecules, but in combination with amino acids, it increased the phosphorylation of mTORC1 downstream targets, especially S6. S6 activation was more substantial in WT than *Vim*$^{-/-}$ (Figure 12 B). Transfection of wild-type vimentin in *Vim*$^{-/-}$ MEFs rescued pS6 activity after nutrients and insulin stimulation (Extended figure 1 C-E II). Interestingly, we found that in WT MEFs, essential amino acids and glucose stimulation produced a greater increase in phosphorylation level of S6 compared to the EAAs plus NEAAs and glucose mixture (Figure 12 B). This could result from non-essential amino acids in an amino acid mixture inhibiting mTORC1 activation or essential amino acids and glucose treatment sustain mTOR activation.

Rapamycin treatment inhibited amino acids, glucose, and insulin-mediated phosphorylation of mTORC1 downstream targets in both WT and *Vim*$^{-/-}$ MEFs (Extended Figure 2 A-B II). This suggests that vimentin could modulate growth signals through the mTORC1 complex. Both P70S6K1 and P90S6K can phosphorylate S6 at serine 234/235. P70S6K phosphorylates S6 in a mTORC1 dependent manner. On the other hand, MAPK signaling regulates P90S6K which also phosphorylates S6 at serine 234/235 (Magnuson *et al*, 2012). It is known that vimentin regulates MAPK signaling by scaffolding ERK 1/2 (Virtakoivu *et al*, 2015b). To ascertain whether vimentin amplifies S6 phosphorylation by scaffolding ERK1/2 molecules, MEFs were treated with an ERK inhibitor before nutrients and growth factor stimulation. ERK inhibition did not make any changes in the S6 phosphorylation level in both WT and *Vim*$^{-/-}$ MEFs after stimulation. ERK1/2 inhibitor did not affect mTORC1 signaling molecules such as Akt, P70S6K1, and 4EBP1. However, AKT inhibition affects all the mTORC1 downstream signaling targets (Extended Figure 2C II). This suggests that vimentin didn't affect S6 phosphorylation through MAPK signaling.

mTORC1 needs to translocate from the cytosol to the lysosome membrane for its activation. In the presence of amino acids, Rag GTPase recruits mTORC1 from the cytosol to lysosome membranes containing the mTORC1 activator Rheb. Growth factors cannot activate mTORC1 in the absence of amino acids (Kim *et al*, 2013b), and blocking mTORC1 translocation can inhibit mTORC1 signaling. To determine whether vimentin promotes mTORC1 activation by regulating mTORC1 translocation, we allowed WT and *Vim*$^{-/-}$ MEFs to grow overnight in the absence of serum to disperse the mTOR complex from the lysosome to the cytosol. Insulin stimulation triggered the translocation of mTOR from the cytosol to lysosomes in both WT and *Vim*$^{-/-}$ MEFs; however, in *Vim*$^{-/-}$ MEFs, mTOR translocation to lysosomes was ~30% less than WT MEFs. We also observed a similar phenotype under steady-state conditions (Figure 4 C-E II). This indicates that vimentin plays a role in mTORC1 signaling by regulating mTORC1 translocation.

Amino acids cause Rag GTPase to recruit mTORC1 from the cytosol to lysosome membranes for its activation. To study whether vimentin affects mTORC1 translocation by regulating Rag GTPase, we exogenously expressed normal Rag GTPase and constitutively active Rag GTPase, which can recruit and translocate mTORC1 to lysosomes without any amino acid activation. mTOR localization on lysosomal membranes is significantly higher in WT than *Vim*$^{-/-}$ when expressing normal Rag GTPase. However, this phenotype can be recused in *Vim*$^{-/-}$ MEFs by expressing constitutively active Rag GTPase (Figure 5 A-B). This provides evidence that vimentin regulates mTORC1 translocation and activation through Rag GTPase. Amino acids in the cytosol and lysosome contribute to Rag GTPase activation; however, the level of amino acids in the lysosome plays a major role in Rag GTPase activation. Vimentin could modulate Rag GTPase activity through either nutrient signaling or lysosomal function.

5.2.4 Vimentin protects fibroblasts from nutrient limitation and inhibits autophagy (II)

Amino acids play a vital role in cell growth and autophagy by regulating mTORC1 signaling. Here we found that nutrients and growth factors starvation reduced p62 level in *Vim*$^{-/-}$ compared to WT MEFs (Figure 6A II). p62 directs ubiquitinated proteins to the lysosome lumen for degradation, during this process p62 also gets degraded. Autophagy decreases the p62 level; in contrast, inhibition of autophagy increases the p62 level (Katsuragi *et al*, 2015). These results showed that vimentin could protect cells from undergoing autophagy under starvation. To further investigate whether vimentin inhibits autophagy under nutrient-limited conditions, we switched cell culture media from complete

DMEM medium (10% FBS, P/S, and L-glutamine) to RPMI media without any growth factors or mitogens, with limited nutrients containing either essential amino acids alone or with non-essential amino acids, with or without glucose/ glucose alone. In WT, p62 level was maintained at the same level, either absence of nutrients or presence of amino acids mix with or without glucose. However, presence of glucose alone in the media reduced p62 level in WT, compared to other conditions (Figure 13). It could be the presence of glucose alone induces autophagy which helps to replenish amino acids. In *Vim*$^{-/-}$ MEFs, p62 protein level was gradually reduced if we limit the nutrients availability in the media. In *Vim*$^{-/-}$ p62 was maintained at higher level in the media which contains essential amino acids, non-essential amino acids mix and glucose, however limiting glucose, non-essential amino acids and essential amino acids reduces p62 level. Compared to WT, limiting amino acids or glucose reduces p62 level in *Vim*$^{-/-}$ MEFs (Figure 13). This suggests that vimentin could help to sustain fibroblasts in nutrient-limited conditions.

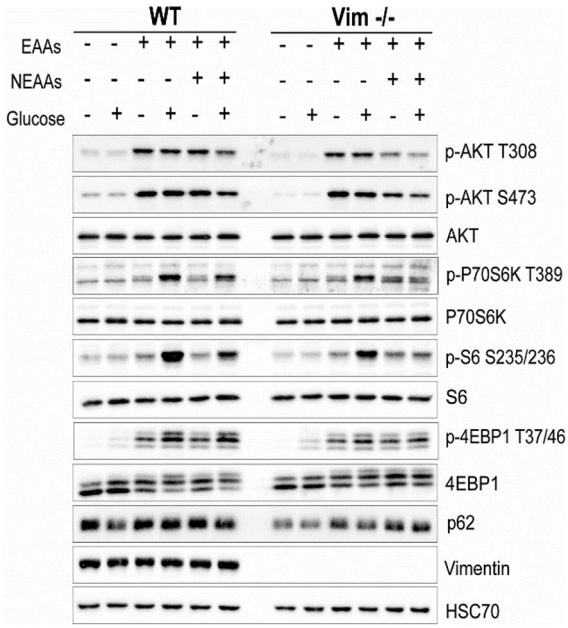

Figure 13: mTORC1 signaling effects of vimentin under nutrients limitation. WT and *Vim*$^{-/-}$ MEFs were allowed to grow in RPMI media containing different combination of amino acids and glucose alone (1 mM of L-glutamine plus EAAs alone or with NEAAs and 2.5 mM glucose or without glucose) for one hour and then samples were collected for western blot analysis (n=3). Above western blot image was extracted from (Mohanasundaram *et al*, 2022) under **creative commons attribution license**.

We also found that S6 phosphorylation was more abundant in WT under EAAs and glucose conditions than with EAAs plus NEAAs and glucose (Figure 13). It could be that non-essential amino acids in the amino acid mix could reduce S6 phosphorylation or EAAs and glucose conditions maintain S6 phosphorylation level. To further support our results, we also measured autophagy markers LC3I and LC3II levels by western blotting. Our immunoblot showed that the LC3 II level was slightly higher in both WT and *Vim*$^{-/-}$ even under normal conditions and nutrient limitations. On the other hand, LC3I decreased in both WT and *Vim*$^{-/-}$ when nutrients were limited (Extended figure 5B). Although these results give LC3 I and II levels, they did not provide detailed information about LC3 I and LC3 II turnover. Measuring LC3 I and LC3II turnover give an autophagic rate, and we used a GFP-LC3-RFP-LC3ΔG construct to study that. During autophagy, the GFP-LC3-RFP-LC3ΔG recombinant protein is cleaved to yield GFP-LC3 and RFP-LC3ΔG. GFP-LC3 is degraded in the autolysosome; however, RFP-LC3ΔG is retained in the cytosol because it cannot undergo lipidation. By measuring the GFP and RFP fluorescent intensity ratio, we can plot the LC3I to LC3II conversion rate. Nutrient limitations and serum starvation increase LC3I to LC3II conversion in WT and *Vim*$^{-/-}$ MEFs; however, the LC3 conversion rate is very significantly higher in *Vim*$^{-/-}$ than WT MEFs. This suggests that vimentin could protect cells from undergoing autophagy under nutrient-limited conditions (Figure 6 C II).

Amino acid signals regulate cell size and autophagy through mTORC1. To determine whether vimentin promotes mTORC1 signaling by activating mTORC1 signaling or inhibiting autophagy signaling, we also measured the ULK1 serine 757 phosphorylation level, which is mediated by the mTORC1 complex to inhibit autophagy. The ULK1 serine 757 phosphorylation level was higher in WT than in *Vim*$^{-/-}$ cells under insulin, amino acids and glucose stimulation, and nutrient limitations (Figure 6 A&D II). Transfection of dominant negative ULK1 didn't rescue cell size in *Vim*$^{-/-}$ MEFs (extended figure 6 II) (Hara *et al*, 2008). This suggests that vimentin inhibits autophagy by regulating mTORC1 signaling.

5.3 Vimentin in autoimmune disorders

5.3.1 Proteomics analysis of Th17 and Treg cells (III)

In our day-to-day life, our body is exposed to various threats such as bacteria, viruses, and injuries. The immune system plays a significant role in the fight against foreign bodies and removing damaged cells (Cooper & Alder, 2006). In some cases, immune cells may damage our own cells and cause autoimmune disorders. Rheumatoid arthritis, systemic lupus erythematosus, inflammatory

bowel disease, and multiple sclerosis are major autoimmune diseases (Wang *et al*, 2015). Th17 cells are T helper cells that can mediate autoimmune disorders, and Treg cells suppress autoimmune dysfunction. The proteomic profiles of Th17 and Treg cells were analyzed from spleen murine samples to study autoimmune disorders. For proteomics analysis, naïve CD4+ T cells were treated with TGF-β1, IL-6, anti-IL-4 anti-CD3, anti-CD28, and anti-IFN-γ for three days to induce differentiation into Th17 cells. To produce Treg cells, naïve CD4+ T cells were treated with IL-2 and TGF-β1 for ten days. After differentiation, 414 proteins were upregulated and 591 proteins were downregulated in Th17 cells; in Treg cells, 308 proteins were upregulated, and 367 proteins were downregulated. Nearly 978 proteins showed higher abundance in Treg cells when comparing protein abundance between Th17 and Treg. ITGAE, TGF-β1, CD44, IL2RA, TRAF6, and vimentin are among those highly upregulated in Treg cells. Vimentin protein abundance was further validated by western blotting analysis. Using KEGG (Kyoto Encyclopedia of Genes and Genomes) databases, highly active signaling pathways and biological functional relevance were determined using the differential protein expression of Th17 and Treg cells. Proteins involved in spliceosome, ribosome, and oxidative phosphorylation were abundant in Th17 cells. Aminoacyl-tRNA biosynthesis, fatty acid metabolism, alanine, aspartate, and glutamate metabolism pathways were abundant in Treg cells.

5.3.2 TGF-β1 increases vimentin expression in Treg cells (III)

Compared to naïve CD+4 T cells, the vimentin protein level was higher in Treg cells. To study the role of vimentin in Treg cells' differentiation, wild-type and vimentin null naïve CD+4 T cells were induced to differentiate into Treg cells. Then, we measured Foxp3 protein level, which is a specific marker for Treg cells (Rudensky, 2011). Vimentin deletion did not affect Foxp3 expression level. To further evaluate Foxp3 expression and the role of vimentin in Treg cells; wild-type and vimentin null naïve CD+4 T cells were allowed to grow either with TGF-β1 or IL-2 or both. After TGF-β1 treatment, the Foxp3 protein level was relatively low in vimentin null Treg cells compared to WT. This effect can be reversed by adding IL-2 along with TGF-β1. To study the role of TGF-β1 in Foxp3 expression, Wild type naïve CD+4 T cells were treated with TGF-β1 inhibitor, which reduces vimentin and Foxp3 protein levels. Based on this, vimentin requires for TGF-β1 induced polarization of naïve CD+4 T cells and Foxp3 expression. The role of vimentin in Treg cells regulation and autoimmune disease needs to be explored further.

6 DISCUSSION

6.1 Fibroblast proliferation, extracellular matrix secretion, and EMT signaling were reduced in *Vim*$^{-/-}$ mice

In 2000, vimentin's role in wound healing was first identified in a mouse skin *in vivo* model. Delayed wound healing in vimentin knockout mice is due to defects in fibroblast migration (Eckes *et al*, 2000). In the *ex vivo* model, vimentin helps to heal the lens epithelial wound by regulating mesenchymal cell migration and myofibroblasts formation (Menko *et al*, 2014; Walker *et al*, 2018). Related to the previous observation, we also found delayed wound healing in *Vim*$^{-/-}$ mouse skin model. Our novel finding was the low level of EMT inducer TGF-β1 and slug during wound healing. EMT plays a major role in re-epithelialization by inducing a change of keratinocyte morphology to mesenchymal-like and increasing cell migration. The previous study showed that exogenous expression of vimentin in breast cancer epithelial cell line (MCF7) induces cell morphological changes and acquires a mesenchymal-like phenotype (Mendez *et al*, 2010). Vimentin is one of the well-known marker for EMT. There are number of papers reported about vimentin's role in EMT and cell migration using *in vitro* model (Rogel *et al*, 2011; Vuoriluoto *et al*, 2011; Grasset *et al*, 2022; Liu *et al*, 2015a). Here we were able to show that EMT inducer slug and TGF-β1 mRNA expression level were lower in *Vim*$^{-/-}$ mice. On day 0 and 15, both WT and *Vim*$^{-/-}$ mice showed similar levels of slug mRNA, however, on day 9 slug mRNA expression level was significantly lower in *Vim*$^{-/-}$ than WT mice. Similarly, on day 9, mesenchymal markers such as N-Cadherin, S400a4 and fibronectin were upregulated in WT but not in *Vim*$^{-/-}$ mice. The impairment of slug expression possibly affects EMT induction, which in turn affects re-epithelialization in *Vim*$^{-/-}$ mice. TGF-β1 is a master regulator of EMT signaling; it regulates slug expression through SMAD signaling (Frick *et al*, 2017; Thuault *et al*, 2006). Here we found that the TGF-β1 mRNA expression level was also low in *Vim*$^{-/-}$ mice. Previous studies showed that TGF-β1 and slug increase vimentin expression in an epithelial cell line. Conversely, knockdown of vimentin reduces TGF-β1 or slug-induced cell migration and EMT (Vuoriluoto *et al*, 2011; Rogel *et al*, 2011). Although we showed low TGF-β1 secretion in *Vim*$^{-/-}$ MDFs, the molecular mechanism of TGF-β1 secretion in fibroblasts needs to be explored. Fibroblasts fill the wound area through proliferation and extracellular matrix production (Rodrigues *et al*, 2019; Mariggiò *et al*, 2009). Vimentin regulates cell proliferation in cancer cells (Zhu *et al*, 2011; Lindsay *et al*, 2016); however, its role in fibroblast proliferation is not elucidated yet. The previous

study showed that vimentin supports collagen production by stabilizing collagen mRNA (Challa & Stefanovic, 2011). Our experimental results align with the previous observation that fibroblast cell proliferation and collagen levels in the wound areas were reduced in *Vim*$^{-/-}$ mice. This suggests that vimentin could help in forming granulation tissue in the wound area by promoting fibroblast proliferation and collagen synthesis. Similarly, *Vim*$^{-/-}$ MDFs showed reduced cell proliferation rate and ERK phosphorylation level. The exogenous expression of WT vimentin rescue this phenotype. ERK kinase signaling pathway promotes cell proliferation and growth. Previous work showed that vimentin maintains ERK activity by preventing it from dephosphorylation, through scaffolding (Perlson *et al*, 2006). In mammary epithelial cell model (MCF10A), vimentin regulates slug phosphorylation through ERK kinase by scaffolding ERK (Virtakoivu *et al*, 2015a). Based on these, vimentin could promote cell proliferation and EMT by regulating slug through ERK.

During wound healing, immune cells produce TGF-β1 for EMT induction. Here we observed that both WT and *Vim*$^{-/-}$ macrophages produced same amount of TGF-β1 in *in vitro*. However, neutrophil levels and cytokines levels were elevated in *Vim*$^{-/-}$ mice at the late stage of wound healing. Several studies showed that vimentin regulates immune cells functions (Mor-Vaknin *et al*, 2003; Su *et al*, 2019; Li *et al*, 2015). Immune cells' activity and function are crucial in wound healing, progressing from the inflammatory to the proliferative phase. Impairment of immune cells function would cause chronic wounds or fibrosis. In this study, the role of vimentin was not explored from an immunological point of view. How immune cells affect and regulate the wound healing process in vimentin knockout conditions needs to be elucidated in the future.

6.2 Vimentin regulated the mTORC1 signaling through Rag GTPase

The role of cytoskeletal intermediate filament in cell size regulation was not widely studied (Etienne-Manneville, 2018). Initially, intermediate filament keratin 17 was identified in cell size regulation. Deletion of keratin 17 reduces protein synthesis and mTORC1 signaling. To maintain mTORC1 signaling, keratin 17 supports 14-3-3-σ localization from the nucleus to the cytoplasm (Kim *et al*, 2006). The role of vimentin in cell size regulation has not been previously reported (Strouhalova *et al*, 2020; Ridge *et al*, 2022). Here we identified that vimentin regulates cell size and inhibits autophagy through mTORC1 signaling by regulating Rag GTPase activity. A previous study has shown that AKT promotes invasion by phosphorylating vimentin at serine 38

(Zhu *et al*, 2011). Akt also inhibits autophagy by promoting beclin/14-3-3/vimentin complex formation, which prevents beclin from autophagy induction (Wang *et al*, 2012). Akt is a direct upstream of the mTORC1 target, and growth factor signals mainly regulate Akt. Apart from growth signals, amino acids and glucose also regulate mTOR signaling. Akt regulates mTORC1 by phosphorylating the TSC2 complex, which releases the mTORC1 complex from inhibition (Inoki *et al*, 2002). We assumed that vimentin regulates mTORC1 through Akt signaling pathway, however, we found that mTOR translocation from cytosol to lysosome in both steady state and insulin stimulation was reduced in *Vim*$^{-/-}$ MEFs. The translocation of mTOR from cytosol to lysosome is regulated by Rag GTPase amino acid sensor. Presence of amino acids activates Rag GTPase and recruits mTORC1 to lysosome for its activation (Sancak *et al*, 2008). Insulin stimulation causes same level of AKT phosphorylation in both WT and *Vim*$^{-/-}$ MEFs, however, mTORC1 downstream signaling P70S6K1 and S6 phosphorylation were lower in *Vim*$^{-/-}$ than WT. This implies that vimentin could promote mTORC1 activation through amino acid sensing signaling. Expression of consecutively active Rag GTPase rescued mTOR translocation phenotype in *Vim*$^{-/-}$ MEFs. It supports our hypothesis that vimentin regulates mTORC1 through Rag GTPase. The recent finding showed that mTORC1 gets translocated to focal adhesion and activated there (Rabanal-Ruiz *et al*, 2021). Likewise, in our lab we found that vimentin regulates cell directionality through focal adhesion (Venu *et al*, 2022). Whether vimentin coordinates mTORC1 signaling at focal adhesion needs to be explored in the future.

mTORC1 inhibits autophagy. However, autophagy can activate mTORC1 by replenishing amino acids through recycling the proteins (Yu *et al*, 2010). Under limited nutrient conditions, mTORC1 downstream signaling was slightly higher in WT than *Vim*$^{-/-}$ MEFs and p62 level was maintained at a high level compared to *Vim*$^{-/-}$ MEFs. Previous work showed that vimentin interacts with p62 and enhances cancer metastasis (Li *et al*, 2017). p62 is known to regulate mTORC1 signaling by supporting Rag GTPase heterodimer formation (Duran *et al*, 2011). Based on previous findings and our observation, vimentin may regulate the nutrient-sensing mechanism of mTORC1 through p62. How vimentin helps to withstand nutrient limitations and maintain mTORC1 downstream signaling needs to be further explored.

Vimentin expression is elevated in cancer and the site of injury, although its role and mechanism have not been explored yet (Xue *et al*, 2017; Handra-Luca *et al*, 2011). The nutrients and growth factors are crucial in wound healing and cancer

progression (Pavlova *et al*, 2022; Grada & Phillips, 2022; Werner & Grose, 2003). Overall mTORC1 downstream signaling was lower in *Vim*$^{-/-}$ MEFs, however in WT MEFs mTORC1 downstream signaling molecules P70S6K1, S6, and 4EBP1 show different responses depending upon amino acids mixtures, as well as presence and absence of glucose. Whether vimentin promotes metabolic plasticity by coordinating nutrient and growth signaling needs to be explored to improve wound healing and prevent cancer progression.

6.3 Vimentin protein expression increased in polarized iTreg cells

T cells undergo metabolic reprogramming during activation and differentiation. Different subsets of T cells acquire different metabolic patterns to support cell proliferation, effector functions, and cytokine production (Slack *et al*, 2015). By proteomic analysis, we identified several metabolic regulators which were upregulated along with cytokines, transcription factors and transmembrane proteins. KEGG pathway analysis suggests that Th17 cells could use oxidative phosphorylation and Treg cells possibly utilize fatty acid metabolism. However, previous studies showed that differentiation of naïve T cells switches its metabolism from oxidative phosphorylation to glycolysis in Th17 cells (Qiu *et al*, 2020) and fatty acid oxidation in Treg cells (Cluxton *et al*, 2019; Berod *et al*, 2014). Although the KEGG pathway analysis showed upregulation in the oxidative phosphorylation in Th17 cells. However, we were able to identify many proteins involved in glycolysis that were upregulated in Th17 cells such as PGK1, HK2, DLD, LDHB, PFKL, PGAM2, TPI1, LDHA, PKM, and MINPP1. With protein expression level we were able to predict possible upregulated pathways. In future studies, including post-translational modifications along with protein expression levels could provide more insight into signaling pathways and metabolism. PI3K-AKT-mTOR signaling axis promotes differentiation of Th17 cells by increasing glycolysis and GLUT1 expression, which generate precursors for nutrient synthesis (Qiu *et al*, 2020; Cluxton *et al*, 2019). Rapamycin treatment reduces the differentiation of naïve cells into Th17 cells (Kopf *et al*, 2007). Similarly, the deletion of raptor increases the differentiation of naïve T cells to Treg cells than Th17 cells, Treg cells utilize most of their energy mainly through fatty acid oxidation (Kurebayashi *et al*, 2012). By using WT and *Vim*$^{-/-}$ cell model we found that vimentin and Foxp3 expression is regulated by TGF-β1. Foxp3 is a transcription factor and its expression is very abundant in Treg cells and it is one of the characteristic marker of Treg cells. Foxp3 regulates autoimmune function in Treg cells (Fontenot *et al*, 2003). AKT and mTOR signaling axis suppresses

TGF-β1 induced Foxp3 expression, conversely inhibition of PI3K signaling increases Foxp3 expression (Haxhinasto *et al*, 2008). We and others have shown vimentin involvement in AKT and mTOR signaling (Wang et al, 2012; Zhu et al, 2011). Based on this vimentin could support glycolysis in Th17 cells through AKT/mTOR signaling. However in Treg cells, evidence showed that vimentin inhibits Treg cells function by supporting PKC-θ localization in DPC (McDonald-Hyman *et al* 2018). Exploring vimentin's role in Th17 and Treg cells could provide new insight into autoimmune disease. How vimentin expression and function in Treg cells are regulated need to be studied to treat autoimmune disease and improve organ transplant.

7 CONCLUDING REMARKS AND FUTURE PERSPECTIVES

Skin tissue is a complex structure; it possesses parenchymal cells which are specialized to perform specific functions, and stromal cells which are composed of mesenchymal cells, extracellular matrix, blood vessels, and immune cells. Stromal cells support parenchymal cells by providing nutrients and oxygen through the blood vessels, immune cells clear damaged/mutated parenchymal cells and foreign bodies, and mesenchymal cells produce extracellular matrix to give mechanical support and also act as stem cells for tissue regeneration (Man *et al*, 2017; Pavlova & Thompson, 2016). Disruption of stromal cells' function would cause delayed wound healing, chronic inflammation, or cancer (Pavlova *et al*, 2022; Zhu & Thompson, 2019). Vimentin expression is predominant in stromal cells such as immune cells, endothelial cells, fibroblasts, and mesenchymal cells (Uhlén *et al*, 2015). In this thesis, the delayed wound healing in vimentin knockout mice was found to be caused by defects in EMT signaling. We have found that vimentin regulates autoimmune cells and inflammation. In fibroblast, vimentin supports cell growth, proliferation, migration, and extracellular secretion. Studies reported that in blood vessel formation, vimentin regulates sprouting, endothelial cells differentiation and provides resistance to shear stress (Boraas & Ahsan, 2016; Dave & Bayless, 2014; van Engeland *et al*, 2019). To understand the clinical and physiological relevance of vimentin, we need to explore how vimentin regulates and support stromal cells functions.

The data in this thesis demonstrate that vimentin promotes cell growth and inhibits autophagy by regulating mTORC1 activity through Rag GTPase and also we found that glucose affects cell proliferation in a vimentin-dependent manner (Figure 14). We and other have shown that vimentin protects cells from oxidative stress (Chernoivanenko *et al*, 2015). Reactive oxygen species are by-products of metabolism, a moderate amount of ROS sustains growth signals by inhibiting phosphatase, however excessive amounts of ROS cause damage to cells (Ostman *et al*, 2011; Panieri & Santoro, 2016). Our preliminary results showed that vimentin interacted with PKM2, based on this vimentin could regulate PKM2 activity, through which it could divert most glucose molecules to the pentose phosphate pathway than energy production, which supports biosynthesis and maintains the redox state of the cell. To support the metabolism; nutrients, growth factor signals, and reactive oxygen species need to be coordinated which in turn promotes cell growth and proliferation. Based

on our observations, propose a hypothesis that vimentin could coordinate nutrients, growth signals, reactive oxygen species, and metabolism, to promote cell growth and proliferation (Figure 15), whether vimentin regulates and supports plasticity in the metabolic process needs to be explored.

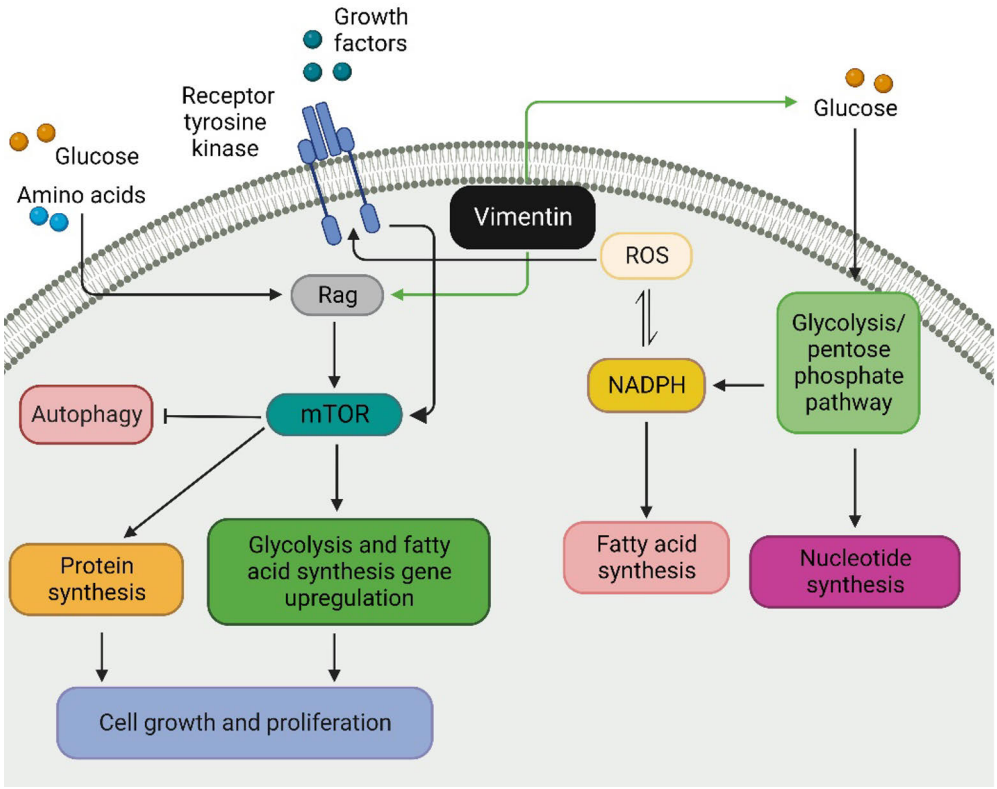

Figure 14. Summary of vimentin-mediated signaling effects. Vimentin promotes cell growth by regulating amino acid sensor Rag GTPase activity and is also involved in the glucose metabolic pathway.

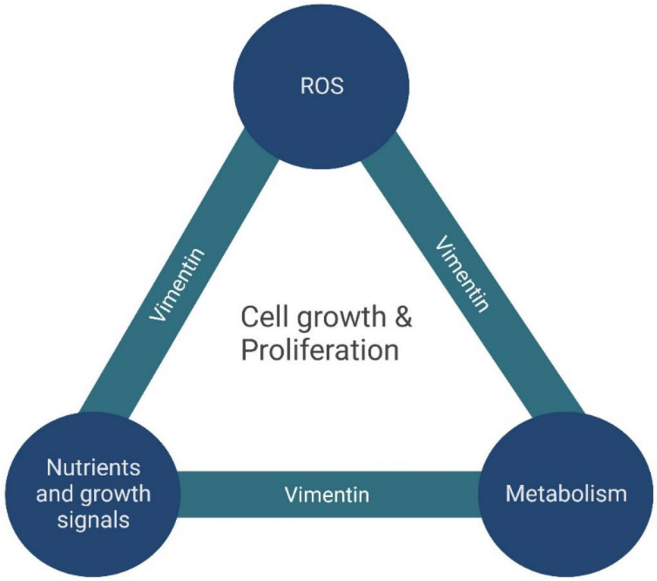

Figure 15: Proposed hypothesis of the relationship between vimentin and metabolic signaling. Vimentin supports cell growth and proliferation possibly by integrating nutrients, growth factors, metabolism, and ROS signaling.

8 ACKNOWLEDGMENTS

The thesis work was performed in the Faculty of Science and Engineering, Åbo Akademi University and Turku Bioscience Centre, University of Turku and Åbo Akademi University. I thank Annika Meinander, the Head of Subjects in Biochemistry and Cell Biology, and her predecessors, faculty members, Professors Lea Sistonen, Cecilia Sahlgren, Eleanor Coffey, Associate Professors Diana Toivola, Guillaume Jacquemet, University Lecturers Malin Åkerfelt, and Eva Henriksson for providing high-end research and education. I also want to thank Professor Riitta Lahesmaa the Director of Turku Bioscience Centre, and her predecessors, group leaders, for enabling access to cutting-edge instruments and infrastructure at the doorstep. Turku Doctoral network in Molecular Biosciences monitored my thesis work progress and facilitated in acquiring soft skills during PhD studies. I am very thankful to Biocenter Finland, Åbo Akademi University, Academy of Finland, Sigrid Jusélius Stiftelse, Magnus Ehrnrooth Foundation, K. Albin Johanssons stiftelse and Liv och Hälsa for providing funding support for this research work.

I am very grateful to John for providing an opportunity to perform my Ph.D. in his laboratory and also for supporting me during my studies. John not only gives us the freedom to pursue our research interest and also provides surplus funding to explore and unravel the mystery of the cytoskeletal filament protein vimentin. John's great articulation and presentation skills inspires me all the time. He also supports us in developing pitching skills during our studies, which immensely helped me to present research work at international conferences. My Ph.D. studies was a great endeavor because of your freedom and support.

I am very thankful to Fang Cheng (Rose) for supporting my work in the early stage of my PhD and allowing me to work on the projects. She helped me acquire skills in mice models, and I am glad to be part of a novel work published in PNAS. Your project work on vimentin's role in the wound healing process set the stage to extend my project work and other projects in our lab.

I am very delighted that Docent Emilia Peuhu and Docent Minna Poukkula were agreed to review my thesis in their tight schedule. Thank you very much for going through my thesis very extensively and gave me critical comments and suggestions. It improved my thesis quite a lot after your comments and corrections. I am also very thankful to Professor Ville Hietakangas for accepting to be my opponent.

I am very happy to have Professor Pekka Taimen and Adjunct Professor Fuping Zhang as my thesis committee members. Both of them were very flexible in having the meeting and their comments were very valuable to shaping my thesis work.

I thank Leila, Mayank, Michelle, Imran, Marta Urbanska, Franziska Lautenschläger, and other co-authors for their immense contributions and support in this research work. I am very thankful to Leila for involving in the project and Mayank for being an imaging expert.

Emilia and Jenny thank you very much for the translation. I am also thankful to Vinodh, Alexandra, Peiru and Leila for go through my thesis.

All the technical personnel in Åbo Akademi and Turku Biosciences Centre play a vital role in running the research institute seamlessly. I am very thankful for them helping us either directly or indirectly. It was wonderful to have Markku Sari, Juoko Standholm, Jari knonan and Ketlin Adel as technical persons to assist and train microscope and flow cytometry. I am thankful to Sten Lindholm for ordering reagents, Gunilla Henriksson played a vital role in ordering reagents and taking care of us during my studies, and I am very grateful for that. Thomas Bymark streamlines our work whenever things go wrong in our lab. I thank all the researchers on the 2nd and 5th floors for sharing their knowledge and reagents.

I express my gratitude to Eriksson lab members of the past and present, Claire, Julia, Tomoko, Elin, Kimmo, Josef, Erik, Senthil, Preethy, Arun, Alia, Num, Hend, Henok, Giulia, Emilia, Leila, Mayank, Silvia, Peiru, Navid, Elnaz, Micheal, Sepideh and Pallavi for helping and supporting me during the study. Each of us have very different aspirations, ideas, and projects, but we are functioning as a one lab is a great thing.

I am very glad to have Kamesh, Pramod, Pasi, Senthil, Hariharan, Gopinath, Dhayakumar, Aravind, Dhanaprakash, Venkat, Partiban and Neeraj as friends. I am very thankful for your support and cheerful moments.

My BDU gangs Ashik, Arafat, Vinodh, Muniesh and Yashwanth. It seems like we met recently but our friendship will cross two decades soon. Thanks for constantly in touch with me and giving your time. Ashik, you helped and uplifted me in many ways; I am very indebted for that. Arafat, my consultant, and with your help I started the cell size project. Vinodh, although you get angry very easily, I admire your helping tendency and working for openness in science.

Yashwanth and Muniesh, very good old friends, now both of you landed on the west coast. Muniesh very hard-working guy. Yashwanth, you were sharing with me a quote from old text in 2012. At that time, I didn't pay attention to that; it took me seven years to realize the depth and profoundness of the quote.

I am very blessed to have constant support and love from my family members, mom, dad, brother, and wife.

Ponnuswamy Mohanasundaram

9 REFERENCES

Acloque H, Thiery JP & Nieto MA (2008) The physiology and pathology of the EMT. Meeting on the Epithelial–Mesenchymal Transition. *EMBO Rep* 9: 322–326

Adil MS, Narayanan SP & Somanath PR (2021) Cell-cell junctions: structure and regulation in physiology and pathology. *Tissue Barriers* 9: 1848212

Aebersold R, Agar JN, Amster IJ, Baker MS, Bertozzi CR, Boja ES, Costello CE, Cravatt BF, Fenselau C, Garcia BA, *et al* (2018) How many human proteoforms are there? *Nat Chem Biol* 14: 206–214

Amodeo AA & Skotheim JM (2016) Cell-Size Control. *Cold Spring Harb Perspect Biol* 8: a019083

Ausmees N, Kuhn JR & Jacobs-Wagner C (2003) The Bacterial Cytoskeleton: An Intermediate Filament-Like Function in Cell Shape. *Cell* 115: 705–713

Bainbridge P (2013) Wound healing and the role of fibroblasts. *J Wound Care* 22: 407–408, 410–412

Ballou LM & Lin RZ (2008) Rapamycin and mTOR kinase inhibitors. *J Chem Biol* 1: 27–36

Barczyk M, Carracedo S & Gullberg D (2010) Integrins. *Cell Tissue Res* 339: 269–280

Barrientos S, Stojadinovic O, Golinko MS, Brem H & Tomic-Canic M (2008) PERSPECTIVE ARTICLE: Growth factors and cytokines in wound healing. *Wound Repair and Regeneration* 16: 585–601

Bento CF, Renna M, Ghislat G, Puri C, Ashkenazi A, Vicinanza M, Menzies FM & Rubinsztein DC (2016) Mammalian Autophagy: How Does It Work? *Annual Review of Biochemistry* 85: 685–713

Berod L, Friedrich C, Nandan A, Freitag J, Hagemann S, Harmrolfs K, Sandouk A, Hesse C, Castro CN, Bähre H, *et al* (2014) De novo fatty acid synthesis controls the fate between regulatory T and T helper 17 cells. *Nat Med* 20: 1327–1333

Bianco P (2014) 'Mesenchymal' stem cells. *Annu Rev Cell Dev Biol* 30: 677–704

Boraas LC & Ahsan T (2016) Lack of vimentin impairs endothelial differentiation of embryonic stem cells. *Sci Rep* 6: 30814

Boucher J, Kleinridders A & Kahn CR (2014) Insulin Receptor Signaling in Normal and Insulin-Resistant States. *Cold Spring Harb Perspect Biol* 6: a009191

Brezar V, Tu WJ & Seddiki N (2015) PKC-theta in regulatory and effector T-cell functions. *Frontiers in Immunology* 6: 530

Brieher WM & Yap AS (2013) Cadherin junctions and their cytoskeleton(s). *Curr Opin Cell Biol* 25: 39–46

Broughton G, Janis JE & Attinger CE (2006) The basic science of wound healing. *Plast Reconstr Surg* 117: 12S-34S

Buckley CE & St Johnston D (2022) Apical–basal polarity and the control of epithelial form and function. *Nat Rev Mol Cell Biol* 23: 559–577

Cafferkey R, Young PR, McLaughlin MM, Bergsma DJ, Koltin Y, Sathe GM, Faucette L, Eng WK, Johnson RK & Livi GP (1993) Dominant missense mutations in a novel yeast protein related to mammalian phosphatidylinositol 3-kinase and VPS34 abrogate rapamycin cytotoxicity. *Mol Cell Biol* 13: 6012–6023

Cano RLE & Lopera HDE (2013) Introduction to T and B lymphocytes El Rosario University Press

Carroll B, Otten EG, Manni D, Stefanatos R, Menzies FM, Smith GR, Jurk D, Kenneth N, Wilkinson S, Passos JF, *et al* (2018) Oxidation of SQSTM1/p62 mediates the link between redox state and protein homeostasis. *Nat Commun* 9: 256

Cavallaro U & Christofori G (2004) Cell adhesion and signalling by cadherins and Ig-CAMs in cancer. *Nat Rev Cancer* 4: 118–132

Ceballos-Picot I, Witko-Sarsat V, Merad-Boudia M, Nguyen AT, Thévenin M, Jaudon MC, Zingraff J, Verger C, Jungers P & Descamps-Latscha B (1996) Glutathione antioxidant system as a marker of oxidative stress in chronic renal failure. *Free Radic Biol Med* 21: 845–853

Challa AA & Stefanovic B (2011) A novel role of vimentin filaments: binding and stabilization of collagen mRNAs. *Mol Cell Biol* 31: 3773–3789

Chang L & Goldman RD (2004) Intermediate filaments mediate cytoskeletal crosstalk. *Nat Rev Mol Cell Biol* 5: 601–613

Charrier EE & Janmey PA (2016) Mechanical properties of intermediate filament proteins. *Methods Enzymol* 568: 35–57

Chen G & Deng X (2018) Cell Synchronization by Double Thymidine Block. *Bio Protoc* 8: e2994

Chernoivanenko I, Zerkalenkova E, Gelfand V, Goldman R & Minin A (2014) Mitochondrial membrane potential is regulated by vimentin intermediate filaments. *FASEB journal : official publication of the Federation of American Societies for Experimental Biology* 29.3: 820

Chernoivanenko IS, Matveeva EA, Gelfand VI, Goldman RD & Minin AA (2015) Mitochondrial membrane potential is regulated by vimentin intermediate filaments. *FASEB J* 29: 820–827

Christofk HR, Vander Heiden MG, Wu N, Asara JM & Cantley LC (2008) Pyruvate kinase M2 is a phosphotyrosine-binding protein. *Nature* 452: 181–186

Chung J, Kuo CJ, Crabtree GR & Blenis J (1992) Rapamycin-FKBP specifically blocks growth-dependent activation of and signaling by the 70 kd S6 protein kinases. *Cell* 69: 1227–1236

Clark RAF (1993) Regulation of Fibroplasia in Cutaneous Wound Repair. *The American Journal of the Medical Sciences* 306: 42–48

Clegg JS (1984) Properties and metabolism of the aqueous cytoplasm and its boundaries. *Am J Physiol* 246: R133-151

Cluxton D, Petrasca A, Moran B & Fletcher JM (2019) Differential Regulation of Human Treg and Th17 Cells by Fatty Acid Synthesis and Glycolysis. *Frontiers in Immunology* 10: 215

Colizzi ES, Vroomans RM & Merks RM (2020) Evolution of multicellularity by collective integration of spatial information. *eLife* 9: e56349

Colucci-Guyon E, Portier MM, Dunia I, Paulin D, Pournin S & Babinet C (1994) Mice lacking vimentin develop and reproduce without an obvious phenotype. *Cell* 79: 679–694

Conlon IJ, Dunn GA, Mudge AW & Raff MC (2001) Extracellular control of cell size. *Nat Cell Biol* 3: 918–921

Conway JF & Parry DAD (1988) Intermediate filament structure: 3. Analysis of sequence homologies. *International Journal of Biological Macromolecules* 10: 79–98

Cooper MD & Alder MN (2006) The Evolution of Adaptive Immune Systems. *Cell* 124: 815–822

Costigliola N, Ding L, Burckhardt CJ, Han SJ, Gutierrez E, Mota A, Groisman A, Mitchison TJ & Danuser G (2017) Vimentin fibers orient traction stress. *PNAS* 114: 5195–5200

Craene BD & Berx G (2013) Regulatory networks defining EMT during cancer initiation and progression. *Nature Reviews Cancer* 13: 97–110

Czech MP (2000) PIP2 and PIP3: Complex Roles at the Cell Surface. *Cell* 100: 603–606

Da Q, Behymer M, Correa JI, Vijayan KV & Cruz MA (2014) Platelet adhesion involves a novel interaction between vimentin and von Willebrand factor under high shear stress. *Blood* 123: 2715–2721

Dangelmaier C, Manne BK, Liverani E, Jin J, Bray P & Kunapuli SP (2014) PDK1 selectively phosphorylates Thr(308) on Akt and contributes to human platelet functional responses. *Thromb Haemost* 111: 508–517

Dave JM & Bayless KJ (2014) Vimentin as an Integral Regulator of Cell Adhesion and Endothelial Sprouting. *Microcirculation* 21: 333–344

Dayton TL, Jacks T & Vander Heiden MG (2016) PKM2, cancer metabolism, and the road ahead. *EMBO Rep* 17: 1721–1730

Demidova-Rice TN, Durham JT & Herman IM (2012a) Wound Healing Angiogenesis: Innovations and Challenges in Acute and Chronic Wound Healing. *Adv Wound Care (New Rochelle)* 1: 17–22

Demidova-Rice TN, Hamblin MR & Herman IM (2012b) Acute and Impaired Wound Healing: Pathophysiology and Current

Methods for Drug Delivery, Part 1: Normal and Chronic Wounds: Biology, Causes, and Approaches to Care. *Adv Skin Wound Care* 25: 304–314

DePianto D & Coulombe PA (2004) Intermediate filaments and tissue repair. *Exp Cell Res* 301: 68–76

Derynck R & Zhang YE (2003) Smad-dependent and Smad-independent pathways in TGF-beta family signalling. *Nature* 425: 577–584

Devreotes P & Horwitz AR (2015) Signaling networks that regulate cell migration. *Cold Spring Harb Perspect Biol* 7: a005959

Dhasarathy A, Phadke D, Mav D, Shah RR & Wade PA (2011) The transcription factors Snail and Slug activate the transforming growth factor-beta signaling pathway in breast cancer. *PLoS One* 6: e26514

Dhivya S, Padma VV & Santhini E (2015) Wound dressings – a review. *Biomedicine (Taipei)* 5.4 : 22

DiPietro LA (2016) Angiogenesis and wound repair: when enough is enough. *Journal of Leukocyte Biology* 100: 979–984

Dittmer TA & Misteli T (2011) The lamin protein family. *Genome Biol* 12: 222

Dong G, Mao Q, Xia W, Xu Y, Wang J, Xu L & Jiang F (2016) PKM2 and cancer: The function of PKM2 beyond glycolysis (Review). *Oncology Letters* 11: 1980–1986

Dongre A & Weinberg RA (2019) New insights into the mechanisms of epithelial–mesenchymal transition and implications for cancer. *Nat Rev Mol Cell Biol* 20: 69–84

Dovi JV, Szpaderska AM & DiPietro LA (2004) Neutrophil function in the healing wound: adding insult to injury? *Thromb Haemost* 92: 275–280

Dunlop EA & Tee AR (2014) mTOR and autophagy: a dynamic relationship governed by nutrients and energy. *Semin Cell Dev Biol* 36: 121–129

Duran A, Amanchy R, Linares JF, Joshi J, Abu-Baker S, Porollo A, Hansen M, Moscat J & Diaz-Meco MT (2011) p62 is a key regulator of nutrient sensing in the mTORC1 pathway. *Mol Cell* 44: 134–146

Düvel K, Yecies JL, Menon S, Raman P, Lipovsky AI, Souza AL, Triantafellow E, Ma Q, Gorski R, Cleaver S, *et al* (2010) Activation of a metabolic gene regulatory network downstream of mTOR complex 1. *Mol Cell* 39: 171–183

Eckes B, Colucci-Guyon E, Smola H, Nodder S, Babinet C, Krieg T & Martin P (2000) Impaired wound healing in embryonic and adult mice lacking vimentin. *J Cell Sci* 113 (Pt 13): 2455–2462

Efeyan A & Sabatini DM (2013) Nutrients and growth factors in mTORC1 activation. *Biochem Soc Trans* 41: 902–905

Efeyan A, Zoncu R, Chang S, Gumper I, Snitkin H, Wolfson RL, Kirak O, Sabatini DD & Sabatini DM (2013a) Regulation of mTORC1 by the Rag GTPases is necessary for neonatal autophagy and survival. *Nature* 493: 679–683

Efeyan A, Zoncu R, Chang S, Gumper I, Snitkin H, Wolfson RL, Kirak O, Sabatini DD & Sabatini DM (2013b) Regulation of mTORC1 by the Rag GTPases is necessary for neonatal autophagy and survival. *Nature* 493: 679–683

Eming SA, Krieg T & Davidson JM (2007) Inflammation in wound repair: molecular and cellular mechanisms. *J Invest Dermatol* 127: 514–525

van Engeland NCA, Suarez Rodriguez F, Rivero-Müller A, Ristori T, Duran CL, Stassen OMJA, Antfolk D, Driessen RCH, Ruohonen S, Ruohonen ST, *et al* (2019) Vimentin regulates Notch signaling strength and arterial remodeling in response to hemodynamic stress. *Sci Rep* 9: 12415

Ennis WJ & Meneses P (2000) Wound healing at the local level: the stunned wound. *Ostomy Wound Manage* 46: 39S-48S; quiz 49S-50S

Esnault S, Kelly EAB, Shen Z-J, Johansson MW, Malter JS & Jarjour NN (2015) IL-3 maintains activation of the P90S6K/RPS6 pathway and increases translation in human eosinophils. *J Immunol* 195: 2529–2539

Etienne-Manneville S (2018) Cytoplasmic Intermediate Filaments in Cell Biology. *Annual Review of Cell and Developmental Biology* 34: 1–28

Feng X-H & Derynck R (2005) Specificity and versatility in tgf-beta signaling through Smads. *Annu Rev Cell Dev Biol* 21: 659–693

Fife CM, McCarroll JA & Kavallaris M (2014) Movers and shakers: cell cytoskeleton in cancer metastasis. *British Journal of Pharmacology* 171: 5507–5523

Fingar DC, Salama S, Tsou C, Harlow E & Blenis J (2002) Mammalian cell size is controlled by mTOR and its downstream targets S6K1 and 4EBP1/eIF4E. *Genes Dev* 16: 1472–1487

Fletcher DA & Mullins RD (2010) Cell mechanics and the cytoskeleton. *Nature* 463: 485

Fontenot JD, Gavin MA & Rudensky AY (2003) Foxp3 programs the development and function of CD4+CD25+ regulatory T cells. *Nat Immunol* 4: 330–336

Francou A & Anderson KV (2020) The Epithelial-to-Mesenchymal Transition in Development and Cancer. *Annual Review of Cancer Biology* 4: 197–220

Franke WW, Schmid E, Schiller DL, Winter S, Jarasch ED, Moll R, Denk H, Jackson BW & Illmensee K (1982) Differentiation-related patterns of expression of proteins of intermediate-size filaments in tissues and cultured cells. *Cold Spring Harbor Symposia on Quantitative Biology* 46: 431–453

Frick CL, Yarka C, Nunns H & Goentoro L (2017) Sensing relative signal in the Tgf-β/Smad pathway. *Proceedings of the National Academy of Sciences* 114: E2975–E2982

Frykberg RG & Banks J (2015) Challenges in the Treatment of Chronic Wounds. *Adv Wound Care (New Rochelle)* 4: 560–582

Gabbiani G, Hirschel BJ, Ryan GB, Statkov PR & Majno G (1972) Granulation Tissue as a Contractile Organ: A Study of Structure and Function. *Journal of Experimental Medicine* 135: 719–734

Gale AJ (2011) Current Understanding of Hemostasis. *Toxicologic pathology* 39: 273

Gan X, Wang J, Su B & Wu D (2011) Evidence for Direct Activation of mTORC2 Kinase Activity by Phosphatidylinositol 3,4,5-Trisphosphate. *J Biol Chem* 286: 10998–11002

Gan Z, Ding L, Burckhardt CJ, Lowery J, Zaritsky A, Sitterley K, Mota A, Costigliola N, Starker CG, Voytas DF, *et al* (2016) Vimentin Intermediate Filaments Template Microtubule Networks to Enhance Persistence in Cell Polarity and Directed Migration. *Cell Syst* 3: 252-263.e8

Gao S & Hu J (2021) Mitochondrial Fusion: The Machineries In and Out. *Trends in Cell Biology* 31: 62–74

Gao Y & Sztul E (2001) A Novel Interaction of the Golgi Complex with the Vimentin Intermediate Filament Cytoskeleton. *J Cell Biol* 152: 877–894

Gao Y-S, Vrielink A, MacKenzie R & Sztul E (2002) A novel type of regulation of the vimentin intermediate filament cytoskeleton by a Golgi protein. *Eur J Cell Biol* 81: 391–401

Garcia MA, Nelson WJ & Chavez N (2018) Cell–Cell Junctions Organize Structural and Signaling Networks. *Cold Spring Harb Perspect Biol* 10: a029181

Gingras AC, Raught B & Sonenberg N (1999) eIF4 initiation factors: effectors of mRNA recruitment to ribosomes and regulators of translation. *Annu Rev Biochem* 68: 913–963

Glick D, Barth S & Macleod KF (2010) Autophagy: cellular and molecular mechanisms. *J Pathol* 221: 3–12

Godde NJ, Galea RC, Elsum IA & Humbert PO (2010) Cell polarity in motion: redefining mammary tissue organization through EMT and cell polarity transitions. *J Mammary Gland Biol Neoplasia* 15: 149–168

Godsel LM, Hobbs RP & Green KJ (2008) Intermediate filament assembly: dynamics to disease. *Trends in Cell Biology* 18: 28–37

Goldman RD, Grin B, Mendez MG & Kuczmarski ER (2008) Intermediate filaments: versatile building blocks of cell structure. *Curr Opin Cell Biol* 20: 28–34

Gonzalez AC de O, Costa TF, Andrade Z de A & Medrado ARAP (2016) Wound healing - A literature review. *An Bras Dermatol* 91: 614–620

Goto H, Yasui Y, Kawajiri A, Nigg EA, Terada Y, Tatsuka M, Nagata K & Inagaki M (2003) Aurora-B regulates the cleavage furrow-specific vimentin phosphorylation in the cytokinetic process. *J Biol Chem* 278: 8526–8530

Grada A & Phillips TJ (2022) Nutrition and cutaneous wound healing. *Clinics in Dermatology* 40: 103–113

Grasset EM, Dunworth M, Sharma G, Loth M, Tandurella J, Cimino-Mathews A, Gentz M, Bracht S, Haynes M, Fertig EJ, *et al* (2022) Triple-negative breast cancer metastasis involves complex epithelial-mesenchymal transition dynamics and requires vimentin. *Sci Transl Med* 14: eabn7571

Grinnell F (2000) Fibroblast–collagen-matrix contraction: growth-factor signalling and mechanical loading. *Trends in Cell Biology* 10: 362–365

Grünert S, Jechlinger M & Beug H (2003) Diverse cellular and molecular mechanisms contribute to epithelial plasticity and metastasis. *Nat Rev Mol Cell Biol* 4: 657–665

Gumerov VM, Andrianova EP, Matilla MA, Page KM, Monteagudo-Cascales E, Dolphin AC, Krell T & Zhulin IB (2022) Amino acid sensor conserved from bacteria to humans. *Proceedings of the National Academy of Sciences* 119: e2110415119

Guo D, Song X, Guo T, Gu S, Chang X, Su T, Yang X, Liang B & Huang D (2018) Vimentin acetylation is involved in SIRT5-mediated hepatocellular carcinoma migration. *Am J Cancer Res* 8: 2453–2466

Guo M, Ehrlicher AJ, Mahammad S, Fabich H, Jensen MH, Moore JR, Fredberg JJ, Goldman RD & Weitz DA (2013) The Role of Vimentin Intermediate Filaments in Cortical and Cytoplasmic Mechanics. *Biophys J* 105: 1562–1568

Guo S & DiPietro LA (2010) Factors Affecting Wound Healing. *J Dent Res* 89: 219–229

Handra-Luca A, Hong S-M, Walter K, Wolfgang C, Hruban R & Goggins M (2011) Tumour epithelial vimentin expression and outcome of pancreatic ductal adenocarcinomas. *Br J Cancer* 104: 1296–1302

Hara T, Takamura A, Kishi C, Iemura S-I, Natsume T, Guan J-L & Mizushima N (2008) FIP200, a ULK-interacting protein, is required for autophagosome formation in mammalian cells. *J Cell Biol* 181: 497–510

Hart J (2002) Inflammation 1: its role in the healing of acute wounds. *J Wound Care* 11: 205–209

Havel LS, Kline ER, Salgueiro AM & Marcus AI (2015) Vimentin regulates lung cancer cell adhesion through a VAV2-Rac1 pathway to control focal adhesion kinase activity. *Oncogene* 34: 1979–1990

Haxhinasto S, Mathis D & Benoist C (2008) The AKT–mTOR axis regulates de novo differentiation of CD4+Foxp3+ cells. *Journal of Experimental Medicine* 205: 565–574

Hay ED (1995) An overview of epithelio-mesenchymal transformation. *Acta Anat (Basel)* 154: 8–20

Heid H, Rickelt S, Zimbelmann R, Winter S, Schumacher H, Dörflinger Y, Kuhn C & Franke WW (2014) On the Formation of Lipid Droplets in Human Adipocytes: The Organization of the Perilipin–Vimentin Cortex. *PLoS One* 9.2 : e90386

Helfand BT, Mendez MG, Murthy SNP, Shumaker DK, Grin B, Mahammad S, Aebi U, Wedig T, Wu YI, Hahn KM, *et al* (2011) Vimentin organization modulates the formation of lamellipodia. *Mol Biol Cell* 22: 1274–1289

Herrmann H & Aebi U (2004) Intermediate filaments: molecular structure, assembly mechanism, and integration into functionally distinct intracellular Scaffolds. *Annu Rev Biochem* 73: 749–789

Herrmann H & Aebi U (2016) Intermediate Filaments: Structure and Assembly. *Cold Spring Harb Perspect Biol* 8: a018242

Herrmann H, Bär H, Kreplak L, Strelkov SV & Aebi U (2007) Intermediate filaments: from cell architecture to nanomechanics. *Nat Rev Mol Cell Biol* 8: 562–573

Herrmann H, Häner M, Brettel M, Ku NO & Aebi U (1999) Characterization of distinct early assembly units of different intermediate filament proteins. *J Mol Biol* 286: 1403–1420

Hinnebusch AG (2012) Translational homeostasis via eIF4E and 4E-BP1. *Mol Cell* 46: 717–719

Hohmann T & Dehghani F (2019) The Cytoskeleton—A Complex Interacting Meshwork. *Cells* 8: 362

Hu X & Guo F (2021) Amino Acid Sensing in Metabolic Homeostasis and Health. *Endocrine Reviews* 42: 56–76

Huang RY-J, Guilford P & Thiery JP (2012) Early events in cell adhesion and polarity during epithelial-mesenchymal transition. *J Cell Sci* 125: 4417–4422

Hyder C (2014) Tuning cell motility : roles of nestin and vimentin in cancer cell invasion and motility.

Hyder CL, Kemppainen K, Isoniemi KO, Imanishi SY, Goto H, Inagaki M, Fazeli E, Eriksson JE & Törnquist K (2015) Sphingolipids inhibit vimentin-dependent cell migration. *J Cell Sci* 128: 2057–2069

Hyder CL, Pallari H-M, Kochin V & Eriksson JE (2008) Providing cellular signposts – Post-translational modifications of intermediate filaments. *FEBS Letters* 582: 2140–2148

Inoki K, Li Y, Xu T & Guan K-L (2003) Rheb GTPase is a direct target of TSC2 GAP activity and regulates mTOR signaling. *Genes Dev* 17: 1829–1834

Inoki K, Li Y, Zhu T, Wu J & Guan K-L (2002) TSC2 is phosphorylated and inhibited by Akt and suppresses mTOR signalling. *Nat Cell Biol* 4: 648–657

Ivaska J (2011) Vimentin: Central hub in EMT induction? *Small GTPases* 2: 51–53

Ivaska J, Vuoriluoto K, Huovinen T, Izawa I, Inagaki M & Parker PJ (2005) PKCepsilon-mediated phosphorylation of vimentin controls integrin recycling and motility. *EMBO J* 24: 3834–3845

Jägle S, Busch H, Freihen V, Beyes S, Schrempp M, Boerries M & Hecht A (2017) SNAIL1-mediated downregulation of FOXA proteins facilitates the inactivation of transcriptional enhancer elements at key epithelial genes in colorectal cancer cells. *PLOS Genetics* 13: e1007109

Jewell JL, Kim YC, Russell RC, Yu F-X, Park HW, Plouffe SW, Tagliabracci VS & Guan K-L (2015) Differential regulation of mTORC1 by leucine and glutamine. *Science* 347: 194–198

Jiu Y, Lehtimäki J, Tojkander S, Cheng F, Jäälinoja H, Liu X, Varjosalo M, Eriksson JE & Lappalainen P (2015) Bidirectional Interplay between Vimentin Intermediate Filaments and Contractile Actin Stress Fibers. *Cell Rep* 11: 1511–1518

Jiu Y, Peränen J, Schaible N, Cheng F, Eriksson JE, Krishnan R & Lappalainen P (2017) Vimentin intermediate filaments control actin stress fiber assembly through GEF-H1 and RhoA. *J Cell Sci* 130: 892–902

Jones JCR, Kam CY, Harmon RM, Woychek AV, Hopkinson SB & Green KJ (2017) Intermediate Filaments and the Plasma Membrane. *Cold Spring Harb Perspect Biol* 9: a025866

Jorgensen P & Tyers M (2004) How Cells Coordinate Growth and Division. *Current Biology* 14: R1014–R1027

Jung CH, Ro S-H, Cao J, Otto NM & Kim D-H (2010) mTOR regulation of autophagy. *FEBS Lett* 584: 1287–1295

Jung HJ, Hong SJ & Kim SH (2019) Immunohistochemical Expression of Epithelial-Mesenchymal Transition Markers in Early Gastric Cancer: Cancer Tissue versus Noncancer Tissue. *Clin Endosc* 52: 464–471

Kalluri R & Weinberg RA (2009a) The basics of epithelial-mesenchymal transition. *J Clin Invest* 119: 1420–1428

Kalluri R & Weinberg RA (2009b) The basics of epithelial-mesenchymal transition. *J Clin Invest* 119: 1420–1428

Kar R, Singha PK, Venkatachalam MA & Saikumar P (2009) A novel role for MAP1 LC3 in nonautophagic cytoplasmic vacuolation death of cancer cells. *Oncogene* 28: 2556–2568

Katsuragi Y, Ichimura Y & Komatsu M (2015) p62/SQSTM1 functions as a signaling hub and an autophagy adaptor. *FEBS J* 282: 4672–4678

Kidd ME, Shumaker DK & Ridge KM (2014) The role of vimentin intermediate filaments in the progression of lung cancer. *Am J Respir Cell Mol Biol* 50: 1–6

Kim E, Goraksha-Hicks P, Li L, Neufeld TP & Guan K-L (2008) Regulation of TORC1 by Rag GTPases in nutrient response. *Nat Cell Biol* 10: 935–945

Kim H, Nakamura F, Lee W, Hong C, Pérez-Sala D & McCulloch CA (2010a) Regulation of cell adhesion to collagen via beta1 integrins is dependent on interactions of

filamin A with vimentin and protein kinase C epsilon. *Exp Cell Res* 316: 1829–1844

Kim H, Nakamura F, Lee W, Shifrin Y, Arora P & McCulloch CA (2010b) Filamin A is required for vimentin-mediated cell adhesion and spreading. *Am J Physiol, Cell Physiol* 298: C221-236

Kim S, Wong P & Coulombe PA (2006) A keratin cytoskeletal protein regulates protein synthesis and epithelial cell growth. *Nature* 441: 362–365

Kim SG, Buel GR & Blenis J (2013a) Nutrient regulation of the mTOR complex 1 signaling pathway. *Mol Cells* 35: 463–473

Kim SG, Buel GR & Blenis J (2013b) Nutrient Regulation of the mTOR Complex 1 Signaling Pathway. *Mol Cells* 35: 463–473

Kopf H, de la Rosa GM, Howard OMZ & Chen X (2007) Rapamycin inhibits differentiation of Th17 cells and promotes generation of FoxP3+ T regulatory cells. *Int Immunopharmacol* 7: 1819–1824

Koppers M, Özkan N & Farías GG (2020) Complex Interactions Between Membrane-Bound Organelles, Biomolecular Condensates and the Cytoskeleton. *Frontiers in Cell and Developmental Biology* 8 : 618733

Kornreich M, Avinery R, Malka-Gibor E, Laser-Azogui A & Beck R (2015) Order and disorder in intermediate filament proteins. *FEBS Letters* 589: 2464–2476

Köster S, Weitz D, Goldman RD, Aebi U & Herrmann H (2015) Intermediate filament mechanics in vitro and in the cell: From coiled coils to filaments, fibers and networks. *Curr Opin Cell Biol* 0: 82–91

Kreis S, Schönfeld H-J, Melchior C, Steiner B & Kieffer N (2005) The intermediate filament protein vimentin binds specifically to a recombinant integrin alpha2/beta1 cytoplasmic tail complex and co-localizes with native alpha2/beta1 in endothelial cell focal adhesions. *Exp Cell Res* 305: 110–121

Kuo J-C, Han X, Yates JR & Waterman CM (2012) Isolation of focal adhesion proteins for biochemical and proteomic analysis. *Methods Mol Biol* 757: 297–323

Kurebayashi Y, Nagai S, Ikejiri A, Ohtani M, Ichiyama K, Baba Y, Yamada T, Egami S, Hoshii T, Hirao A, *et al* (2012) PI3K-Akt-mTORC1-S6K1/2 axis controls Th17 differentiation by regulating Gfi1 expression and nuclear translocation of RORγ. *Cell Rep* 1: 360–373

Lamouille S, Xu J & Derynck R (2014) Molecular mechanisms of epithelial–mesenchymal transition. *Nat Rev Mol Cell Biol* 15: 178–196

Landén NX, Li D & Ståhle M (2016) Transition from inflammation to proliferation: a critical step during wound healing. *Cell Mol Life Sci* 73: 3861–3885

Laplante M & Sabatini DM (2009) mTOR signaling at a glance. *Journal of Cell Science* 122: 3589–3594

Laplante M & Sabatini DM (2012a) mTOR signaling in growth control and disease. *Cell* 149: 274–293

Laplante M & Sabatini DM (2012b) mTOR signaling in growth control and disease. *Cell* 149: 274–293

Lee Y-K & Lee J-A (2016) Role of the mammalian ATG8/LC3 family in autophagy: differential and compensatory roles in the spatiotemporal regulation of autophagy. *BMB Rep* 49: 424–430

Lessard JC, Piña-Paz S, Rotty JD, Hickerson RP, Kaspar RL, Balmain A & Coulombe PA (2013) Keratin 16 regulates innate immunity in response to epidermal barrier breach. *Proc Natl Acad Sci U S A* 110: 19537–19542

Li D, Rebecca P, Cruz MA, Molldrem JJ, Champlin RE & Ma Q (2015) Intermediate Filament (IF) Protein Vimentin Regulates T Cell Mediated Immune Response in Gvhd. *Blood* 126: 3073

Li J, Chen J & Kirsner R (2007) Pathophysiology of acute wound healing. *Clin Dermatol* 25: 9–18

Li J, Wang R & Tang DD (2016) Vimentin dephosphorylation at ser-56 is regulated by type 1 protein phosphatase in smooth muscle. *Respiratory Research* 17: 91

Li S-S, Xu L-Z, Zhou W, Yao S, Wang C-L, Xia J-L, Wang H-F, Kamran M, Xue X-Y, Dong L, *et al* (2017) p62/SQSTM1 interacts with vimentin to enhance breast cancer metastasis. *Carcinogenesis* 38: 1092–1103

Li Y, Inoki K, Yeung R & Guan K-L (2002) Regulation of TSC2 by 14-3-3 binding. *J Biol Chem* 277: 44593–44596

Lillemeier BF, Pfeiffer JR, Surviladze Z, Wilson BS & Davis MM (2006) Plasma membrane-associated proteins are clustered into islands attached to the cytoskeleton. *Proceedings of the National Academy of Sciences* 103: 18992–18997

Linder S & Kopp P (2005) Podosomes at a glance. *J Cell Sci* 118: 2079–2082

Lindsay CR, Le Moulec S, Billiot F, Loriot Y, Ngo-Camus M, Vielh P, Fizazi K, Massard C & Farace F (2016) Vimentin and Ki67 expression in circulating tumour cells derived from castrate-resistant prostate cancer. *BMC Cancer* 16: 168

Liu C-Y, Lin H-H, Tang M-J & Wang Y-K (2015a) Vimentin contributes to epithelial-mesenchymal transition cancer cell mechanics by mediating cytoskeletal organization and focal adhesion maturation. *Oncotarget* 6: 15966–15983

Liu GY & Sabatini DM (2020) mTOR at the nexus of nutrition, growth, ageing and disease. *Nat Rev Mol Cell Biol* 21: 183–203

Liu P, Gan W, Chin YR, Ogura K, Guo J, Zhang J, Wang B, Blenis J, Cantley LC, Toker A, *et al* (2015b) PtdIns(3,4,5)P3-dependent Activation of the mTORC2 Kinase Complex. *Cancer Discov* 5: 1194–1209

Lloyd AC (2013) The Regulation of Cell Size. *Cell* 154: 1194–1205

Lodish H, Berk A, Zipursky SL, Matsudaira P, Baltimore D & Darnell J (2000) Receptor Tyrosine Kinases and Ras. *Molecular Cell Biology 4th edition*

Lu G, Wang Y, Shi Y, Zhang Z, Huang C, He W, Wang C & Shen H-M (2022) Autophagy in health and disease: From molecular mechanisms to therapeutic target. *MedComm* 3: e150

Lu Z, Shvartsman M, Lee A, Shao J, McGahren Murray M, Kladney R, Fan D, Krajewski S (Stan), Chiang G, Mills G, *et al* (2010) Mammalian Target of Rapamycin Activator RHEB Is Frequently Overexpressed in Human Carcinomas and Is Critical and Sufficient for Skin Epithelial Carcinogenesis. *Cancer research* 70: 3287–98

Luna EJ & Hitt AL (1992) Cytoskeleton—Plasma Membrane Interactions. *Science* 258: 955–964

Machowska M, Piekarowicz K & Rzepecki R (2015) Regulation of lamin properties and functions: does phosphorylation do it all? *Open Biol* 5.11: 150094

MacPherson M & Fagerholm SC (2010) Filamin and filamin-binding proteins in integrin-regulation and adhesion. Focus on: 'FilaminA is required for vimentin-mediated cell adhesion and spreading'. *Am J Physiol, Cell Physiol* 298: C206-208

Magnuson B, Ekim B & Fingar DC (2012) Regulation and function of ribosomal protein S6 kinase (S6K) within mTOR signalling networks. *Biochem J* 441: 1–21

Man K, Kutyavin VI & Chawla A (2017) Tissue immunometabolism: development, physiology, and pathobiology. *Cell metabolism* 25: 11

Mani SA, Guo W, Liao M-J, Eaton ENg, Ayyanan A, Zhou AY, Brooks M, Reinhard F, Zhang CC, Shipitsin M, *et al* (2008) The epithelial-mesenchymal transition generates cells with properties of stem cells. *Cell* 133: 704–715

Marconi GD, Fonticoli L, Rajan TS, Pierdomenico SD, Trubiani O, Pizzicannella J & Diomede F (2021) Epithelial-Mesenchymal Transition (EMT): The Type-2 EMT in Wound Healing, Tissue Regeneration and Organ Fibrosis. *Cells* 10: 1587

Mariggiò MA, Cassano A, Vinella A, Vincenti A, Fumarulo R, Muzio LL, Maiorano E, Ribatti D & Favia G (2009) Enhancement of Fibroblast Proliferation, Collagen Biosynthesis and Production of Growth Factors as a Result of Combining Sodium Hyaluronate and Aminoacids. *Int J Immunopathol Pharmacol* 22: 485–492

Martin E, Girardello R, Dittmar G & Ludwig A (2021) New insights into the organization and regulation of the apical polarity network in mammalian epithelial cells. *The FEBS Journal* 288: 7073–7095

Massagué J (2012) TGFβ signalling in context. *Nat Rev Mol Cell Biol* 13: 616–630

Matsuyama M, Tanaka H, Inoko A, Goto H, Yonemura S, Kobori K, Hayashi Y, Kondo E, Itohara S, Izawa I, *et al* (2013) Defect of

mitotic vimentin phosphorylation causes microophthalmia and cataract via aneuploidy and senescence in lens epithelial cells. *J Biol Chem* 288: 35626–35635

McDonald-Hyman C, Muller JT, Loschi M, Thangavelu G, Saha A, Kumari S, Reichenbach DK, Smith MJ, Zhang G, Koehn BH, *et al* The vimentin intermediate filament network restrains regulatory T cell suppression of graft-versus-host disease. *J Clin Invest* 128: 4604–4621

McNiven MA (2013) Breaking away: matrix remodeling from the leading edge. *Trends Cell Biol* 23: 16–21

Medici D, Hay ED & Olsen BR (2008) Snail and Slug Promote Epithelial-Mesenchymal Transition through β-Catenin–T-Cell Factor-4-dependent Expression of Transforming Growth Factor-β3. *Mol Biol Cell* 19: 4875–4887

Mendez MG, Kojima S-I & Goldman RD (2010) Vimentin induces changes in cell shape, motility, and adhesion during the epithelial to mesenchymal transition. *FASEB J* 24: 1838–1851

Menko AS, Bleaken BM, Libowitz AA, Zhang L, Stepp MA & Walker JL (2014) A central role for vimentin in regulating repair function during healing of the lens epithelium. *Mol Biol Cell* 25: 776–790

Menon S, Dibble CC, Talbott G, Hoxhaj G, Valvezan AJ, Takahashi H, Cantley LC & Manning BD (2014) Spatial control of the TSC complex integrates insulin and nutrient regulation of mTORC1 at the lysosome. *Cell* 156: 771–785

Miyazaki M & Takemasa T (2017) TSC2/Rheb signaling mediates ERK-dependent regulation of mTORC1 activity in C2C12 myoblasts. *FEBS Open Bio* 7: 424–433

Mizushima N (2007) Autophagy: process and function. *Genes Dev* 21: 2861–2873

Mizushima N & Komatsu M (2011) Autophagy: renovation of cells and tissues. *Cell* 147: 728–741

Mohanasundaram P, Coelho-Rato LS, Modi MK, Urbanska M, Lautenschläger F, Cheng F & Eriksson JE (2022) Cytoskeletal vimentin regulates cell size and autophagy through mTORC1 signaling. *PLOS Biology* 20: e3001737

Mor-Vaknin N, Legendre M, Yu Y, Serezani CHC, Garg SK, Jatzek A, Swanson MD, Gonzalez-Hernandez MJ, Teitz-Tennenbaum S, Punturieri A, *et al* (2013) Murine Colitis is Mediated by Vimentin. *Scientific Reports* 3: 1–8

Mor-Vaknin N, Punturieri A, Sitwala K & Markovitz DM (2003) Vimentin is secreted by activated macrophages. *Nat Cell Biol* 5: 59–63

Müller L, Hatzfeld M & Keil R (2021) Desmosomes as Signaling Hubs in the Regulation of Cell Behavior. *Frontiers in Cell and Developmental Biology* 9: 745670

Murphy DA & Courtneidge SA (2011) The 'ins' and 'outs' of podosomes and invadopodia: characteristics, formation and function. *Nat Rev Mol Cell Biol* 12: 413–426

Nakamura S, Akayama S & Yoshimori T (2021) Autophagy-independent function of lipidated LC3 essential for TFEB activation during the lysosomal damage responses. *Autophagy* 17: 581–583

Nascimento EBM, Snel M, Guigas B, van der Zon GCM, Kriek J, Maassen JA, Jazet IM, Diamant M & Ouwens DM (2010) Phosphorylation of PRAS40 on Thr246 by PKB/AKT facilitates efficient phosphorylation of Ser183 by mTORC1. *Cell Signal* 22: 961–967

NCI Dictionary of Cancer Terms (2011) *National Cancer Institute*

Nekrasova OE, Mendez MG, Chernoivanenko IS, Tyurin-Kuzmin PA, Kuczmarski ER, Gelfand VI, Goldman RD & Minin AA (2011) Vimentin intermediate filaments modulate the motility of mitochondria. *Mol Biol Cell* 22: 2282–2289

Nelson WJ (2009) Remodeling Epithelial Cell Organization: Transitions Between Front–Rear and Apical–Basal Polarity. *Cold Spring Harb Perspect Biol* 1

Nieminen M, Henttinen T, Merinen M, Marttila-Ichihara F, Eriksson JE & Jalkanen S (2006) Vimentin function in lymphocyte adhesion and transcellular migration. *Nat Cell Biol* 8: 156–162

Nieto MA, Huang RY-J, Jackson RA & Thiery JP (2016) EMT: 2016. *Cell* 166: 21–45

Niklas KJ (2015) A Phyletic Perspective on Cell Growth. *Cold Spring Harb Perspect Biol* 7

Omary MB, Coulombe PA & McLean WHI (2004) Intermediate Filament Proteins and Their Associated Diseases. *New England Journal of Medicine* 351: 2087–2100

Omary MB, Ku N-O, Tao G-Z, Toivola DM & Liao J (2006) 'Heads and tails' of intermediate filament phosphorylation: multiple sites and functional insights. *Trends Biochem Sci* 31: 383–394

Orozco JM, Krawczyk PA, Scaria SM, Cangelosi AL, Chan SH, Kunchok T, Lewis CA & Sabatini DM (2020) Dihydroxyacetone phosphate signals glucose availability to mTORC1. *Nat Metab* 2: 893–901

Osmanagic-Myers S & Foisner R (2019) The structural and gene expression hypotheses in laminopathic diseases—not so different after all. *MBoC* 30: 1786–1790

Ostman A, Frijhoff J, Sandin A & Böhmer F-D (2011) Regulation of protein tyrosine phosphatases by reversible oxidation. *J Biochem* 150: 345–356

Ostrowska-Podhorodecka Z, Ding I, Lee W, Tanic J, Abbasi S, Arora PD, Liu RS, Patteson AE, Janmey PA & McCulloch CA (2021) Vimentin tunes cell migration on collagen by controlling β1 integrin activation and clustering. *J Cell Sci* 134: jcs254359

Pan Y-R, Chen C-L & Chen H-C (2011) FAK is required for the assembly of podosome rosettes. *J Cell Biol* 195: 113–129

Panieri E & Santoro MM (2016) ROS homeostasis and metabolism: a dangerous liason in cancer cells. *Cell Death Dis* 7: e2253–e2253

Parvanian S, Yan F, Su D, Coelho-Rato LS, Venu AP, Yang P, Zou X, Jiu Y, Chen H, Eriksson JE, *et al* (2020) Exosomal vimentin from adipocyte progenitors accelerates wound healing. *Cytoskeleton* 77: 399–413

Parvanian S, Zha H, Su D, Xi L, Jiu Y, Chen H, Eriksson JE & Cheng F (2021) Exosomal Vimentin from Adipocyte Progenitors Protects Fibroblasts against Osmotic Stress and Inhibits Apoptosis to Enhance Wound Healing. *International Journal of Molecular Sciences* 22: 4678

Parzych KR & Klionsky DJ (2014) An Overview of Autophagy: Morphology, Mechanism, and Regulation. *Antioxid Redox Signal* 20: 460–473

Pastar I, Stojadinovic O, Yin NC, Ramirez H, Nusbaum AG, Sawaya A, Patel SB, Khalid L, Isseroff RR & Tomic-Canic M (2014) Epithelialization in Wound Healing: A Comprehensive Review. *Adv Wound Care (New Rochelle)* 3: 445–464

Patteson AE, Vahabikashi A, Pogoda K, Adam SA, Mandal K, Kittisopikul M, Sivagurunathan S, Goldman A, Goldman RD & Janmey PA (2019) Vimentin protects cells against nuclear rupture and DNA damage during migration. *J Cell Biol* 218: 4079–4092

Pavlova NN & Thompson CB (2016) THE EMERGING HALLMARKS OF CANCER METABOLISM. *Cell Metab* 23: 27–47

Pavlova NN, Zhu J & Thompson CB (2022) The hallmarks of cancer metabolism: Still emerging. *Cell Metabolism* 34: 355–377

Pei D, Shu X, Gassama-Diagne A & Thiery JP (2019) Mesenchymal–epithelial transition in development and reprogramming. *Nature Cell Biology* 21: 44–53

Peña-Llopis S, Vega-Rubin-de-Celis S, Schwartz JC, Wolff NC, Tran TAT, Zou L, Xie X-J, Corey DR & Brugarolas J (2011) Regulation of TFEB and V-ATPases by mTORC1. *EMBO J* 30: 3242–3258

Perlson E, Michaelevski I, Kowalsman N, Ben-Yaakov K, Shaked M, Seger R, Eisenstein M & Fainzilber M (2006) Vimentin binding to phosphorylated Erk sterically hinders enzymatic dephosphorylation of the kinase. *J Mol Biol* 364: 938–944

Phua DCY, Humbert PO & Hunziker W (2009) Vimentin regulates scribble activity by protecting it from proteasomal degradation. *Mol Biol Cell* 20: 2841–2855

Pierce GF, Vande Berg J, Rudolph R, Tarpley J & Mustoe TA (1991) Platelet-derived growth factor-BB and transforming growth factor beta 1 selectively modulate glycosaminoglycans, collagen, and myofibroblasts in excisional wounds. *Am J Pathol* 138: 629–646

Pollard TD & Goldman RD (2018) Overview of the Cytoskeleton from an Evolutionary Perspective. *Cold Spring Harbor Perspectives in Biology* 10: a030288

Preisner H, Habicht J, Garg SG & Gould SB (2018) Intermediate filament protein evolution and protists. *Cytoskeleton (Hoboken)* 75: 231–243

Qin X, Jiang B & Zhang Y (2016) 4E-BP1, a multifactor regulated multifunctional protein. *Cell Cycle* 15: 781–786

Qin Z, Kreplak L & Buehler MJ (2009) Nanomechanical properties of vimentin intermediate filament dimers. *Nanotechnology* 20: 425101

Qiu R, Yu X, Wang L, Han Z, Yao C, Cui Y, Hou G, Dai D, Jin W & Shen N (2020) Inhibition of Glycolysis in Pathogenic TH17 Cells through Targeting a miR-21–Peli1–c-Rel Pathway Prevents Autoimmunity. *The Journal of Immunology* 204.12 : 3160-70

Rabanal-Ruiz Y, Byron A, Wirth A, Madsen R, Sedlackova L, Hewitt G, Nelson G, Stingele J, Wills JC, Zhang T, *et al* (2021) mTORC1 activity is supported by spatial association with focal adhesions. *Journal of Cell Biology* 220: e202004010

Ramos I, Stamatakis K, Oeste CL & Pérez-Sala D (2020) Vimentin as a Multifaceted Player and Potential Therapeutic Target in Viral Infections. *International Journal of Molecular Sciences* 21: 4675

Ridge KM, Eriksson JE, Pekny M & Goldman RD (2022) Roles of vimentin in health and disease. *Genes Dev* 36: 391–407

Robert A, Hookway C & Gelfand VI (2016) Intermediate filament dynamics: What we can see now and why it matters. *Bioessays* 38: 232–243

Roberts DJ, Tan-Sah VP, Ding EY, Smith JM & Miyamoto S (2014) Hexokinase-II positively regulates glucose starvation-induced autophagy through TORC1 inhibition. *Mol Cell* 53: 521–533

Robson MC, Steed DL & Franz MG (2001a) Wound healing: biologic features and approaches to maximize healing trajectories. *Curr Probl Surg* 38: 72–140

Robson MC, Steed DL & Franz MG (2001b) Wound healing: Biologic features and approaches to maximize healing trajectories. *Current Problems in Surgery* 38: A1-140

Rodero MP & Khosrotehrani K (2010) Skin wound healing modulation by macrophages. *Int J Clin Exp Pathol* 3: 643–653

Rodrigues M, Kosaric N, Bonham CA & Gurtner GC (2019) Wound Healing: A Cellular Perspective. *Physiological Reviews* 99: 665–706

Rogel MR, Soni PN, Troken JR, Sitikov A, Trejo HE & Ridge KM (2011) Vimentin is sufficient and required for wound repair and remodeling in alveolar epithelial cells. *FASEB J* 25: 3873–3883

Rogers SL & Gelfand VI (2000) Membrane trafficking, organelle transport, and the cytoskeleton. *Curr Opin Cell Biol* 12: 57–62

Rudensky AY (2011) Regulatory T Cells and Foxp3. *Immunol Rev* 241: 260–268

Rusten TE & Stenmark H (2010) p62, an autophagy hero or culprit? *Nat Cell Biol* 12: 207–209

Ruvinsky I, Sharon N, Lerer T, Cohen H, Stolovich-Rain M, Nir T, Dor Y, Zisman P & Meyuhas O (2005) Ribosomal protein S6 phosphorylation is a determinant of cell size and glucose homeostasis. *Genes Dev* 19: 2199–2211

Sancak Y, Bar-Peled L, Zoncu R, Markhard AL, Nada S & Sabatini DM (2010) Ragulator-Rag complex targets mTORC1 to the lysosomal surface and is necessary for its activation by amino acids. *Cell* 141: 290–303

Sancak Y, Peterson TR, Shaul YD, Lindquist RA, Thoreen CC, Bar-Peled L & Sabatini DM (2008) The Rag GTPases bind raptor and mediate amino acid signaling to mTORC1. *Science* 320: 1496–1501

Sánchez-Martín P & Komatsu M (2018) p62/SQSTM1 – steering the cell through health and disease. *J Cell Sci* 131.21: jcs222836

dos Santos G, Rogel MR, Baker MA, Troken JR, Urich D, Morales-Nebreda L, Sennello JA, Kutuzov MA, Sitikov A, Davis JM, *et al* (2015) Vimentin regulates activation of the NLRP3 inflammasome. *Nature Communications* 6: 1–13

Sarbassov DD, Guertin DA, Ali SM & Sabatini DM (2005) Phosphorylation and regulation of Akt/PKB by the rictor-mTOR complex. *Science* 307: 1098–1101

Satelli A & Li S (2011a) Vimentin in cancer and its potential as a molecular target for cancer therapy. *Cell Mol Life Sci* 68: 3033–3046

Satelli A & Li S (2011b) Vimentin in cancer and its potential as a molecular target for cancer therapy. *Cell Mol Life Sci* 68: 3033–3046

Satoh J, Yamamura T & Arima K (2004) The 14-3-3 Protein ε Isoform Expressed in Reactive Astrocytes in Demyelinating Lesions of Multiple Sclerosis Binds to Vimentin and Glial Fibrillary Acidic Protein in Cultured Human Astrocytes. *Am J Pathol* 165: 577–592

Saxton RA & Sabatini DM (2017) mTOR Signaling in Growth, Metabolism, and Disease. *Cell* 168: 960–976

Schoumacher M, Goldman RD, Louvard D & Vignjevic DM (2010) Actin, microtubules, and vimentin intermediate filaments cooperate for elongation of invadopodia. *J Cell Biol* 189: 541–556

Schreiber KH, Ortiz D, Academia EC, Anies AC, Liao C-Y & Kennedy BK (2015) Rapamycin-mediated mTORC2 inhibition is determined by the relative expression of FK506-binding proteins. *Aging Cell* 14: 265–273

Schweitzer LD, Comb WC, Bar-Peled L & Sabatini DM (2015) Disruption of the Rag-Ragulator Complex by c17orf59 Inhibits mTORC1. *Cell Reports* 12: 1445–1455

Servold SA (1991) Growth factor impact on wound healing. *Clin Podiatr Med Surg* 8: 937–953

Slack M, Wang T & Wang R (2015) T cell metabolic reprogramming and plasticity. *Mol Immunol* 68: 507–512

Snider NT & Omary MB (2014) Post-translational modifications of intermediate filament proteins: mechanisms and functions. *Nat Rev Mol Cell Biol* 15: 163–177

St Johnston D & Ahringer J (2010) Cell polarity in eggs and epithelia: parallels and diversity. *Cell* 141: 757–774

Stone RC, Pastar I, Ojeh N, Chen V, Liu S, Garzon KI & Tomic-Canic M (2016) Epithelial-Mesenchymal Transition in Tissue Repair and Fibrosis. *Cell Tissue Res* 365: 495–506

Strelkov SV, Herrmann H, Geisler N, Wedig T, Zimbelmann R, Aebi U & Burkhard P (2002) Conserved segments 1A and 2B of the intermediate filament dimer: their atomic structures and role in filament assembly. *The EMBO Journal* 21: 1255–1266

Strouhalova K, Přechová M, Gandalovičová A, Brábek J, Gregor M & Rosel D (2020) Vimentin Intermediate Filaments as Potential Target for Cancer Treatment. *Cancers (Basel)* 12: 184

Styers ML, Salazar G, Love R, Peden AA, Kowalczyk AP & Faundez V (2004) The Endo-Lysosomal Sorting Machinery Interacts with the Intermediate Filament Cytoskeleton. *Mol Biol Cell* 15: 5369–5382

Su L, Pan P, Yan P, Long Y, Zhou X, Wang X, Zhou R, Wen B, Xie L & Liu D (2019) Role of vimentin in modulating immune cell apoptosis and inflammatory responses in sepsis. *Sci Rep* 9: 5747

Surolia R, Li FJ, Wang Z, Li H, Dsouza K, Thomas V, Mirov S, Pérez-Sala D, Athar M, Thannickal VJ, *et al* (2019) Vimentin intermediate filament assembly regulates fibroblast invasion in fibrogenic lung injury. *JCI Insight* 4.7: e123253

Szeverenyi I, Cassidy AJ, Chung CW, Lee BTK, Common JEA, Ogg SC, Chen H, Sim SY, Goh WLP, Ng KW, *et al* (2008) The Human Intermediate Filament Database: comprehensive information on a gene family involved in many human diseases. *Hum Mutat* 29: 351–360

Tan HWS, Sim AYL & Long YC (2017) Glutamine metabolism regulates autophagy-dependent mTORC1 reactivation during amino acid starvation. *Nature Communications* 8: 1–10

Tang HL, Lung HL, Wu KC, Le A-HP, Tang HM & Fung MC (2008) Vimentin supports mitochondrial morphology and organization. *Biochem J* 410: 141–146

Tanida I & Waguri S (2010) Measurement of autophagy in cells and tissues. *Methods Mol Biol* 648: 193–214

Tarbet HJ, Dolat L, Smith TJ, Condon BM, O'Brien ET, Valdivia RH & Boyce M (2018) Site-specific glycosylation regulates the form and function of the intermediate filament cytoskeleton. *Elife* 7: e31807

Terzi F, Henrion D, Colucci-Guyon E, Federici P, Babinet C, Levy BI, Briand P & Friedlander G (1997) Reduction of renal mass is lethal in mice lacking vimentin. Role of endothelin-nitric oxide imbalance. *J Clin Invest* 100: 1520–1528

Tesmer LA, Lundy SK, Sarkar S & Fox DA (2008) Th17 cells in human disease. *Immunol Rev* 223: 87–113

Thuault S, Valcourt U, Petersen M, Manfioletti G, Heldin C-H & Moustakas A (2006) Transforming growth factor-beta employs HMGA2 to elicit epithelial-mesenchymal transition. *J Cell Biol* 174: 175–183

Tolstonog GV, Shoeman RL, Traub U & Traub P (2001) Role of the intermediate filament protein vimentin in delaying senescence and in the spontaneous immortalization of mouse embryo fibroblasts. *DNA Cell Biol* 20: 509–529

Tonnesen MG, Feng X & Clark RA (2000) Angiogenesis in wound healing. *J Investig Dermatol Symp Proc* 5: 40–46

Trelford CB & Di Guglielmo GM (2021) Molecular mechanisms of mammalian autophagy. *Biochemical Journal* 478: 3395–3421

Trepat X, Chen Z & Jacobson K (2012) Cell Migration. *Compr Physiol* 2: 2369–2392

Tsuruta D & Jones JCR (2003) The vimentin cytoskeleton regulates focal contact size and adhesion of endothelial cells subjected to shear stress. *J Cell Sci* 116: 4977–4984

Turowski P, Myles T, Hemmings BA, Fernandez A & Lamb NJ (1999) Vimentin dephosphorylation by protein phosphatase 2A is modulated by the targeting subunit B55. *Mol Biol Cell* 10: 1997–2015

Tzivion G, Luo ZJ & Avruch J (2000) Calyculin A-induced Vimentin Phosphorylation Sequesters 14-3-3 and Displaces Other 14-3-3 Partners in Vivo. *The Journal of biological chemistry* 275: 29772–8

Tzivion G, Shen YH & Zhu J (2001) 14-3-3 proteins; bringing new definitions to scaffolding. *Oncogene* 20: 6331–6338

Uhlén M, Fagerberg L, Hallström BM, Lindskog C, Oksvold P, Mardinoglu A, Sivertsson Å, Kampf C, Sjöstedt E, Asplund A, *et al* (2015) Tissue-based map of the human proteome. *Science* 347: 1260419

Urbanska M, Rosendahl P, Kräter M & Guck J (2018) Chapter 10 - High-throughput single-cell mechanical phenotyping with real-time deformability cytometry. In *Methods in Cell Biology*, Piel M Fletcher D & Doh J (eds) pp 175–198. Academic Press

Van De Water L, Varney S & Tomasek JJ (2013) Mechanoregulation of the Myofibroblast in Wound Contraction, Scarring, and Fibrosis: Opportunities for New Therapeutic Intervention. *Adv Wound Care (New Rochelle)* 2: 122–141

Vander Haar E, Lee S-I, Bandhakavi S, Griffin TJ & Kim D-H (2007) Insulin signalling to mTOR mediated by the Akt/PKB substrate PRAS40. *Nat Cell Biol* 9: 316–323

Vargas P, Maiuri P, Bretou M, Sáez PJ, Pierobon P, Maurin M, Chabaud M, Lankar D, Obino D, Terriac E, *et al* (2016) Innate control of actin nucleation determines two distinct migration behaviours in dendritic cells. *Nat Cell Biol* 18: 43–53

Velnar T, Bailey T & Smrkolj V (2009) The Wound Healing Process: An Overview of the Cellular and Molecular Mechanisms. *J Int Med Res* 37: 1528–1542

Venu AP, Modi M, Aryal U, Tcarenkova E, Jiu Y, Jacquemet G, Minin A, Cheng F & Eriksson JE (2022) Vimentin supports directional cell migration by controlling focal adhesions. 2022.10.02.510295 doi:10.1101/2022.10.02.510295 [PREPRINT]

Vicente-Manzanares M, Webb DJ & Horwitz AR (2005) Cell migration at a glance. *Journal of Cell Science* 118: 4917–4919

Vignali DAA, Collison LW & Workman CJ (2008) How regulatory T cells work. *Nat Rev Immunol* 8: 523–532

Villanelo F, Escalona Y, Pareja-Barrueto C, Garate JA, Skerrett IM & Perez-Acle T (2017) Accessing gap-junction channel structure-function relationships through molecular modeling and simulations. *BMC Cell Biology* 18: 5

Virtakoivu R, Mai A, Mattila E, De Franceschi N, Imanishi SY, Corthals G, Kaukonen R, Saari M, Cheng F, Torvaldson E, *et al* (2015a) Vimentin-ERK Signaling Uncouples Slug

Gene Regulatory Function. *Cancer Res* 75: 2349–2362

Virtakoivu R, Mai A, Mattila E, Franceschi ND, Imanishi SY, Corthals G, Kaukonen R, Saari M, Cheng F, Torvaldson E, *et al* (2015b) Vimentin–ERK Signaling Uncouples Slug Gene Regulatory Function. *Cancer Res* 75: 2349–2362

Vuoriluoto K, Haugen H, Kiviluoto S, Mpindi J-P, Nevo J, Gjerdrum C, Tiron C, Lorens JB & Ivaska J (2011) Vimentin regulates EMT induction by Slug and oncogenic H-Ras and migration by governing Axl expression in breast cancer. *Oncogene* 30: 1436–1448

Walker JL, Bleaken BM, Romisher AR, Alnwibit AA & Menko AS (2018) In wound repair vimentin mediates the transition of mesenchymal leader cells to a myofibroblast phenotype. *Mol Biol Cell* 29: 1555–1570

Walko G, Castañón MJ & Wiche G (2015) Molecular architecture and function of the hemidesmosome. *Cell Tissue Res* 360: 529–544

Walter M, Chen FW, Tamari F, Wang R & Ioannou YA (2009) Endosomal lipid accumulation in NPC1 leads to inhibition of PKC, hypophosphorylation of vimentin and Rab9 entrapment. *Biol Cell* 101: 141–152

Wan YY (2010) Multi-tasking of helper T cells. *Immunology* 130: 166–171

Wang L, Wang F-S & Gershwin ME (2015) Human autoimmune diseases: a comprehensive update. *Journal of Internal Medicine* 278: 369–395

Wang L, Zhang J, Banerjee S, Barnes L, Sajja V, Liu Y, Guo B, Du Y, Agarwal MK, Wald DN, *et al* (2010) Sumoylation of Vimentin354 Is Associated with PIAS3 Inhibition of Glioma Cell Migration. *Oncotarget* 1: 620–627

Wang RC, Wei Y, An Z, Zou Z, Xiao G, Bhagat G, White M, Reichelt J & Levine B (2012) Akt-mediated regulation of autophagy and tumorigenesis through Beclin 1 phosphorylation. *Science* 338: 956–959

Werner S & Grose R (2003) Regulation of Wound Healing by Growth Factors and Cytokines. *Physiological Reviews* 83: 835–870

Werner S, Krieg T & Smola H (2007) Keratinocyte–Fibroblast Interactions in Wound Healing. *Journal of Investigative Dermatology* 127: 998–1008

Whale A, Hashim FN, Fram S, Jones GE & Wells CM (2011) Signalling to cancer cell invasion through PAK family kinases. *Front Biosci (Landmark Ed)* 16: 849–864

Witte MB & Barbul A (1997) GENERAL PRINCIPLES OF WOUND HEALING. *Surgical Clinics of North America* 77: 509–528

Worman HJ (2012) Nuclear lamins and laminopathies. *J Pathol* 226: 316–325

Wozniak MA, Modzelewska K, Kwong L & Keely PJ (2004) Focal adhesion regulation of cell behavior. *Biochim Biophys Acta* 1692: 103–119

Wu X, Xie W, Xie W, Wei W & Guo J (2022) Beyond controlling cell size: functional analyses of S6K in tumorigenesis. *Cell Death Dis* 13: 1–19

Xu B, deWaal RM, Mor-Vaknin N, Hibbard C, Markovitz DM & Kahn ML (2004) The Endothelial Cell-Specific Antibody PAL-E Identifies a Secreted Form of Vimentin in the Blood Vasculature. *Molecular and Cellular Biology* 24: 9198–9206

Xu J, Lamouille S & Derynck R (2009a) TGF-beta-induced epithelial to mesenchymal transition. *Cell Res* 19: 156–172

Xu J, Lamouille S & Derynck R (2009b) TGF-β-induced epithelial to mesenchymal transition. *Cell Res* 19: 156–172

Xue P, Chen L, Lu X, Zhang J, Bao G, Xu G, Sun Y, Guo X, Jiang J, Gu H, *et al* (2017) Vimentin Promotes Astrocyte Activation After Chronic Constriction Injury. *Journal of Molecular Neuroscience* 63: 91-99

Yamaguchi T, Goto H, Yokoyama T, Silljé H, Hanisch A, Uldschmid A, Takai Y, Oguri T, Nigg EA & Inagaki M (2005) Phosphorylation by Cdk1 induces Plk1-mediated vimentin phosphorylation during mitosis. *J Cell Biol* 171: 431–436

Yang J, Antin P, Berx G, Blanpain C, Brabletz T, Bronner M, Campbell K, Cano A, Casanova J, Christofori G, *et al* (2020) Guidelines and definitions for research on epithelial–mesenchymal transition. *Nat Rev Mol Cell Biol* 21: 341–352

Yang M-H & Wu K-J (2008) TWIST activation by hypoxia inducible factor-1 (HIF-1): implications in metastasis and development. *Cell Cycle* 7: 2090–2096

Yang Q, Inoki K, Kim E & Guan K-L (2006) TSC1/TSC2 and Rheb have different effects on TORC1 and TORC2 activity. *Proc Natl Acad Sci USA* 103: 6811–6816

Yokoyama T, Goto H, Izawa I, Mizutani H & Inagaki M (2005) Aurora-B and Rho-kinase/ROCK, the two cleavage furrow kinases, independently regulate the progression of cytokinesis: possible existence of a novel cleavage furrow kinase phosphorylates ezrin/radixin/moesin (ERM). *Genes Cells* 10: 127–137

Yu L, McPhee CK, Zheng L, Mardones GA, Rong Y, Peng J, Mi N, Zhao Y, Liu Z, Wan F, *et al* (2010) Termination of autophagy and reformation of lysosomes regulated by mTOR. *Nature* 465: 942–946

Zanin-Zhorov A, Ding Y, Kumari S, Attur M, Hippen KL, Brown M, Blazar BR, Abramson SB, Lafaille JJ & Dustin ML (2010) Protein kinase C-theta mediates negative feedback on regulatory T cell function. *Science* 328: 372–376

Zhang W, Shi X, Peng Y, Wu M, Zhang P, Xie R, Wu Y, Yan Q, Liu S & Wang J (2015) HIF-1α Promotes Epithelial-Mesenchymal Transition and Metastasis through Direct Regulation of ZEB1 in Colorectal Cancer. *PLoS ONE* 10: e0129603

Zhang Y, Gao X, Saucedo LJ, Ru B, Edgar BA & Pan D (2003) Rheb is a direct target of the tuberous sclerosis tumour suppressor proteins. *Nat Cell Biol* 5: 578–581

Zhu J & Thompson CB (2019) Metabolic regulation of cell growth and proliferation. *Nat Rev Mol Cell Biol* 20: 436–450

Zhu Q-S, Rosenblatt K, Huang K-L, Lahat G, Brobey R, Bolshakov S, Nguyen T, Ding Z, Belousov R, Bill K, *et al* (2011) Vimentin is a novel AKT1 target mediating motility and invasion. *Oncogene* 30: 457–470

Zihni C, Mills C, Matter K & Balda MS (2016) Tight junctions: from simple barriers to multifunctional molecular gates. *Nat Rev Mol Cell Biol* 17: 564–580

Zoncu R, Bar-Peled L, Efeyan A, Wang S, Sancak Y & Sabatini DM (2011) mTORC1 senses lysosomal amino acids through an inside-out mechanism that requires the vacuolar H(+)-ATPase. *Science* 334: 678–683

Zou Y, He L & Huang S-H (2006) Identification of a surface protein on human brain microvascular endothelial cells as vimentin interacting with Escherichia coli invasion protein IbeA. *Biochem Biophys Res Commun*51: 625–630

APPENDIX: ORIGINAL PUBLICATIONS

Cheng F, Shen Y, **Mohanasundaram P**, Lindström M, Ivaska J, Ny T, Eriksson JE. 2016. Vimentin coordinates fibroblast proliferation and keratinocyte differentiation in wound healing via TGF-β-Slug signaling. *Proc Natl Acad Sci USA* 113:E4320-4327.

I

Vimentin coordinates fibroblast proliferation and keratinocyte differentiation in wound healing via TGF-β–Slug signaling

Fang Cheng[a,b], Yue Shen[c,d,e], Ponnuswamy Mohanasundaram[a,b], Michelle Lindström[a], Johanna Ivaska[b,f], Tor Ny[c], and John E. Eriksson[a,b,1]

[a]Cell Biology, Biosciences, Faculty of Science and Engineering, Åbo Akademi University, FI-20520, Turku, Finland; [b]Turku Centre for Biotechnology, University of Turku and Åbo Akademi University, FI-20521, Turku, Finland; [c]Department of Medical Biochemistry and Biophysics, Umeå University, SE-90187 Umeå, Sweden; [d]Centre for Heart Lung Innovation, St. Paul's Hospital, Vancouver, BC, Canada V6Z 1Y6; [e]Department of Pathology and Laboratory Medicine, University of British Columbia, Vancouver, BC, Canada V6Z 1Y6; and [f]Department of Biochemistry and Food Chemistry, University of Turku, FI-20520, Turku, Finland

Edited by Pierre A. Coulombe, The Johns Hopkins University, Baltimore, MD, and accepted by Editorial Board Member Edward D. Korn June 8, 2016 (received for review December 23, 2015)

Vimentin has been shown to be involved in wound healing, but its functional contribution to this process is poorly understood. Here we describe a previously unrecognized function of vimentin in coordinating fibroblast proliferation and keratinocyte differentiation during wound healing. Loss of vimentin led to a severe deficiency in fibroblast growth, which in turn inhibited the activation of two major initiators of epithelial–mesenchymal transition (EMT), TGF-β1 signaling and the Zinc finger transcriptional repressor protein Slug, in vimentin-deficient ($VIM^{-/-}$) wounds. Correspondingly, $VIM^{-/-}$ wounds exhibited loss of EMT-like keratinocyte activation, limited keratinization, and slow reepithelialization. Furthermore, the fibroblast deficiency abolished collagen accumulation in the $VIM^{-/-}$ wounds. Vimentin reconstitution in $VIM^{-/-}$ fibroblasts restored both their proliferation and TGF-β1 production. Similarly, restoring paracrine TGF-β–Slug–EMT signaling reactivated the transdifferentiation of keratinocytes, reviving their migratory properties, a critical feature for efficient healing. Our results demonstrate that vimentin orchestrates the healing by controlling fibroblast proliferation, TGF-β1–Slug signaling, collagen accumulation, and EMT processing, all of which in turn govern the required keratinocyte activation.

vimentin intermediate filaments | wound healing | epithelial–mesenchymal transition | fibroblast proliferation | keratinocyte migration

Successful cutaneous wound repair requires a series of tightly coordinated and overlapping steps including inflammation, new tissue formation, and remodeling (1, 2). Upon injury, keratinocytes at the wound edges form epithelial tongues that move and interact with the dermal cells and collagen-rich extracellular matrix (ECM) to reestablish coverage of the wound bed via a complex process termed "reepithelialization" (2, 3). In addition, dermal fibroblasts activated by growth factors migrate into the site of injury, where they proliferate and lay down the ECM that facilitates cell migration and tissue reconstruction (2, 3).

To migrate over the wound site, keratinocytes must disengage desmosome/hemidesmosome junctions and reorganize their cytoskeleton to enable the required promigratory program (4). As reepithelialization continues, keratinocytes gradually stop migration, revert to their normal phenotype, and use hemidesmosomes to attach firmly to the reestablished basement membrane and to the underlying dermis through collagen fibrils (1, 2, 5). Some of these dramatic phenotypic changes reflect the transformation of the epithelial cells to a mesenchymal state, a critical differentiation program called "epithelial–mesenchymal transition" (EMT). During EMT, epithelial cells lose their intercellular junctions and acquire mesenchymal phenotypes as manifested, for example, by increased motility and increased production of ECM. EMT is a process that is crucial for cells requiring a shift from an epithelial state toward a more dynamic state. In addition to wound healing, EMT is involved in embryonic development, fibrosis, and tumor progression (6, 7).

The intermediate filament protein vimentin participates in numerous cellular processes, with functions in cell adhesion, migration and invasion, signaling, differentiation, cytoskeletal rearrangements, and regulation of cell morphology and plasticity (8–11). Recent data from our consortium have shown that vimentin is required to support ERK-mediated Slug phosphorylation and activation in a cancer-related model (12). With this model, we could show that vimentin–ERK–Slug interaction amplifies EMT onset via a positive-feedback loop between vimentin and the transcription factor Slug, which has an established role in skin development and the EMT-like processes of wound healing (13–15).

In relation to tissue repair, vimentin has been found in mesenchymal repair cells to regulate the collective movement of the lens epithelium in response to an injury (16). In relation to vimentin's role in maintaining lens homeostasis and integrity, vimentin mutations have also been linked with cataract formation (17, 18). Furthermore, we have demonstrated previously that vimentin is required in inflammatory cell migration; vimentin-deficient lymphocytes have a reduced transmigration capability in vivo because of the down-regulation of the adhesion molecule ICAM-1 and integrins on the cell surface (19). Although the original report on vimentin-knockout ($VIM^{-/-}$) mice reported no defects in tissue repair (20), later studies revealed defective fibroblast migration and hampered contractile capacity of fibroblasts during wound healing in $VIM^{-/-}$ embryonic

Significance

The central concept in this study is that a major cytoskeletal component, vimentin, acts as a signal integrator during wound healing, operating in both signal-triggering and signal-receiving cells. This is a previously unreported concept for intermediate filaments, with an evolving paradigm according to which intermediate filaments emerge as integrators of regeneration with specific functions in the particular tissues for which individual intermediate filaments are characteristic. Our study reveals the underlying molecular and cellular control functions of vimentin in vimentin-dependent epithelial–mesenchymal transition, regeneration, and healing.

Author contributions: F.C., J.I., and J.E.E. designed research; F.C., Y.S., P.M., and M.L. performed research; J.I. and T.N. contributed new reagents/analytic tools; F.C., Y.S., P.M., and M.L. analyzed data; and F.C. and J.E.E. wrote the paper.

The authors declare no conflict of interest.

This article is a PNAS Direct Submission. P.A.C. is a guest editor invited by the Editorial Board.

Freely available online through the PNAS open access option.

[1]To whom correspondence should be addressed. Email: john.eriksson@abo.fi.

This article contains supporting information online at www.pnas.org/lookup/suppl/doi:10.1073/pnas.1519197113/-/DCSupplemental.

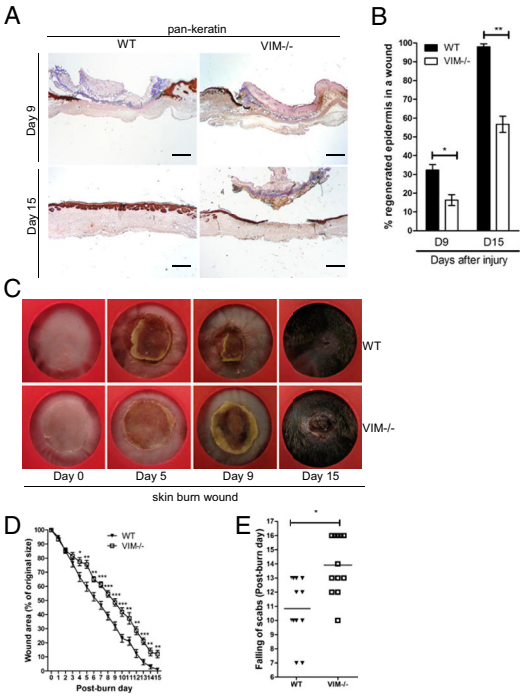

Fig. 1. VIM$^{-/-}$ mice display wound-healing defect in a burn wound model. (*A*) Representative pictures showing immunohistochemical labeling of pan-keratin in WT and VIM$^{-/-}$ wounds on days 9 (D9) and 15 (D15) postinjury. (Scale bar, 100 μm.) (*B*) Quantification of the percentage of wound reepithelialization at different time points after wounding in VIM$^{-/-}$ and WT wounds. Data are shown as means ± SEM; $n = 6$. (*C*) Representative wound pictures from VIM$^{-/-}$ and WT mice during the 15-d wound-healing period. (*D*) Quantification of the remaining wound area at different time points after wounding in WT and VIM$^{-/-}$ groups. Data are shown as means ± SEM; $n = 6$–12. (*E*) Comparison of the healing times (scab falling off) in the days after wounding. Data are shown as means ± SEM; $n = 12$. $^{*}P < 0.05$; $^{**}P < 0.01$; $^{***}P < 0.001$.

and adult mice (21, 22). In findings related, to some extent, to these results, the requirement for functional vimentin in epithelial maintenance was demonstrated by recent observations showing that compromised vimentin phosphorylation caused cellular senescence in lens epithelial cells (23), cytokinetic failure of s.c. fibroblasts upon injury (24), and skin aging (24). These studies were made in phospho-vimentin–deficient mice in which all mitotic serine-specific phosphorylation sites were replaced by alanine residues.

Because the redifferentiation following wound injury involves such a dramatic increase in vimentin expression (which has been established as a determinant of a number of signaling systems), we wanted to investigate whether vimentin could be directly involved in regulating the cellular processes and interactions that are required for proper regeneration and healing. To address this hypothesis in a physiological setting, we used a combination of two well-defined in vivo wound-healing paradigms, burn and excision injury, in genetically engineered mice lacking vimentin. Along with the in vivo experiments, we also used a number of reconstituted cellular in vitro models relevant to the wound-healing process to validate the assumptions based on observations in healing tissue. Indeed, the results show that vimentin serves as an integrator of the processes that occur during wound healing, regulating the proliferation of fibroblasts and the EMT-like transdifferentiation of keratinocytes, both crucial processes for successful wound repair. In the absence of vimentin, these cellular processes are inhibited, thereby disrupting normal tissue regeneration, reepithelialization, and the formation of a scar and an intact barrier.

Results

Loss of Vimentin Leads to Deficient Wound Healing. Burns or excisional skin wounds in mice are common experimental approaches to assess molecular, cellular, and tissue movements associated with repair. To determine whether vimentin is an important determinant in wound healing, full-thickness standardized burn wounds (1 cm in diameter) were induced in 8- to 10-wk-old VIM$^{-/-}$ mice and their WT littermates. A histological analysis of wound morphology 9 d after injury revealed epidermal healing of only 17% reepithelialization of the wounds in VIM$^{-/-}$ mice compared with 32% in the WT group (Fig. 1 *A* and *B*). At day 15 postinjury the wounds in WT mice were reepithelialized completely, with a prominent keratinized layer (Fig. 1 *A* and *B*). In contrast, the epithelium layer in VIM$^{-/-}$ mice remained open (~56% reepithelialization) and in many mice was still covered by a large scab (Fig. 1 *A* and *B*). Furthermore, the wound-closure area, quan-

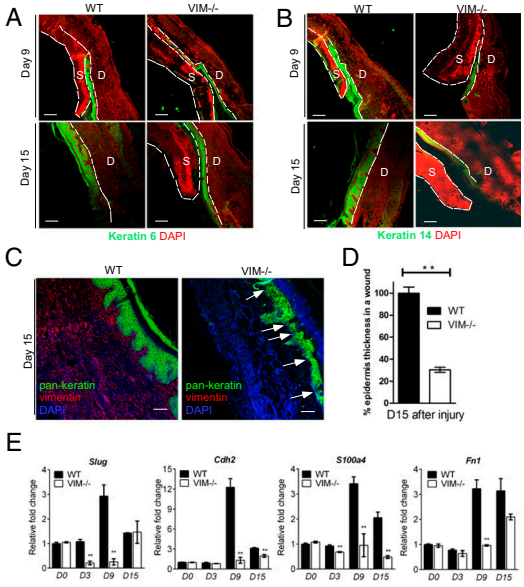

Fig. 2. Compromised reepithelialization and EMT differentiation in VIM$^{-/-}$ wounds. (*A* and *B*) Representative pictures of confocal images of keratin 6 (green) and DAPI (red) (*A*) and keratin 14 (green) and DAPI (red) (*B*) in VIM$^{-/-}$ and WT wounds on day 9 and 15 after skin burn injury. D, dermis region; S, scab region. (Scale bars, 200 μm.) (*C*) Representative confocal images of keratin expression as visualized by a pan-keratin antibody (green), vimentin (red), and DAPI (blue) in VIM$^{-/-}$ and WT wounds on day 15 postinjury. White arrows indicate the region of thin and poor keratinization in VIM$^{-/-}$ wounds. (*D*) Quantification of average epidermis thickness on day 15 after burn injury. Bars indicate the mean fold changes relative to WT ± SEM; $n = 3$. (*E*) qRT-PCR analysis of mRNA transcripts for Slug, N-cadherin (*Cdh2*), FSP-1 (*S100a4*), and fibronectin (*Fn1*) in isolated epidermal regions of VIM$^{-/-}$ and WT wounds on days 0, 3, 9, and 15 after burn injury. Bars indicate the mean fold changes ± SEM relative to day 0 WT; $^{**}P < 0.01$; $n = 3$.

tified at different time points following injury, showed that from day 4 postinjury healing was significantly slower in the VIM$^{-/-}$ group than in the WT group (Fig. 1 *C* and *D*). As shown in Fig. 1*E*, the time to healing (i.e., when the scab falls off) was ∼3 d longer in the VIM$^{-/-}$ group than in WT group. As with burn wounds, the healing of excisional wounds was severely impaired in VIM$^{-/-}$ mice (Fig. S1). To examine the possible influence of basal skin conditions on wound healing, we analyzed the overall features of uninjured control skin of prenatal mice at embryonic day 14 (E14), preweaning (18-d-old) mice, and adult mice (age 10 wk old up to 10 mo) (Fig. S2). In this examination of the uninjured skin, no striking differences in the organization of epidermis, dermis, and cell components could be observed between WT and VIM$^{-/-}$ skins (Fig. S2 *A*–*D*). The results demonstrate that loss of vimentin inhibits normal wound healing, resulting in a slow and incomplete recovery of the tissue.

The Defect in Reepithelialization Is Associated with an Inactive EMT Program in VIM$^{-/-}$ Wounds. To evaluate skin reepithelialization during wound healing further, we analyzed the keratinocytes at wound margins, which form a coordinated cell sheet with de novo production of injury-specific keratin proteins, such as keratin 6, 14, and 16 (25, 26). WT wounds had higher keratin 6 intensity than VIM$^{-/-}$ wounds at days 9 and 15 postinjury (Fig. 2*A*), and a similar tendency was observed for keratin 14 and with labeling by a pan-keratin antibody (Fig. 2 *B* and *C*). By day 15 postinjury, keratinocyte colonies had fused successfully with the newly formed stratified mature epidermis in WT wounds. In contrast, reepithelialized VIM$^{-/-}$ wound regions displayed a very thin epidermal layer with a large scab (right images in Fig. 2 *A* and *B*); the average thickness of pan-keratin^{+} epidermis was barely 30.5% of that in the WT group (Fig. 2*D*). Furthermore, certain regions of keratinocyte colonies in the epidermis of VIM$^{-/-}$ wounds were poorly organized (Fig. 2*C*). These observations imply that migration, maturation, and stratification of the epidermis, all prerequisites for fast, spontaneous wound healing, are severely compromised in the VIM$^{-/-}$ group.

EMT or an EMT-like transdifferentiation program induces the transient transition of secondary epithelial cells to a more migratory phenotype, which is critical for rapid reepithelialization of injured epithelium (27, 28). To address the role of vimentin in this process, we analyzed whether the absence of vimentin affects EMT during wound repair in injured epidermis. We found that during normal WT wound closure, the expression of a major EMT initiator, the transcription factor Slug (also termed Snai2), remained at the same levels found in samples of day 0 uninjured WT skin until day 3 (Fig. 2*E*). In the WT injured skin samples, the expression of Slug mRNA increased dramatically from day 0 until day 9 and then ceased by day 15 (Fig. 2*E*). In comparison, skin samples from VIM$^{-/-}$ mice showed significantly reduced mRNA expression of Slug during wound healing; we observed a 4.7-fold reduction on day 3 and a prominent 11.5-fold reduction on day 9 in the wounds of VIM$^{-/-}$ mice as compared with their WT littermates (Fig. 2*E*). On day 15, *Slug* expression returned to similar levels in WT and VIM$^{-/-}$ wounds (Fig. 2*E*), in accordance with previously observed kinetics of transient Slug induction in several skin-injury studies (3, 29). Correspondingly, the mRNA expression of EMT-dependent markers downstream of Slug, including N-cadherin (*Cdh2*), fibroblast-specific protein 1 (*S100a4*), and fibronectin (*Fn1*) (30), increased until day 9 and decreased by day 15 during normal WT wound closure (Fig. 2*E*). The baseline expression of these genes in skin samples from VIM$^{-/-}$ mice were at the same levels as in day 0 WT skin samples but dropped drastically during wound healing, especially at day 9 (Fig. 2*E*), further supporting the vimentin dependence of the Slug–EMT response during wound repair.

We also found keratin^{+} cell colonies at the WT epidermis–dermis interface that were absent in VIM$^{-/-}$ wounds at day 9 postinjury (Fig. S3 *A* and *B*). Additionally a significant portion of cells in the dermal regions of WT wounds coexpressed keratin and the mesenchymal marker α-SMA (Fig. S3*C*) at day 9 postinjury. Another mesenchymal marker, N-cadherin, was coexpressed with keratin 5 in WT epidermal cells on day 15 postinjury (Fig. S3 *E* and *F*). Such cells, which may be at the intermediate stages of EMT, with continued expression of epithelial markers but acquiring the expression of mesenchymal markers, were much less abundant in the healing VIM$^{-/-}$ skin (Fig. S3 *C*–*F*). Therefore, in the absence of vimentin, the consequent dysfunction of the EMT program is likely to be a primary reason for the inhibited reepithelialization during wound repair in our models.

TGF-β Derived from Dermal Fibroblasts Triggers the Slug–EMT Program and Epithelial Cell Migration. An EMT-like keratinocyte transdifferentiation program can be modulated rapidly by a variety of factors in the wound environment (31, 32). Therefore we explored the possible involvement of these signaling factors by gene-expression profiling and found that TGF-β1 (*Tgfb1*), a primary inducer of EMT,

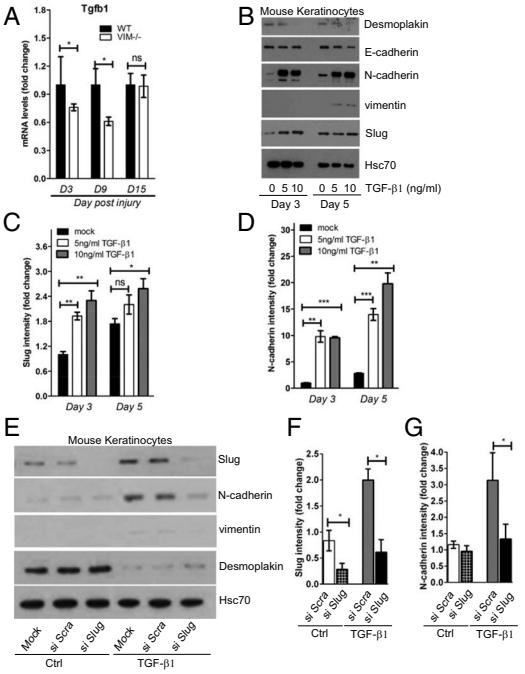

Fig. 3. TGF-β1–Slug signaling promotes keratinocyte differentiation and migration. (*A*) qRT-PCR analysis of transcripts for TGF-β1 (*Tgfb1*) in VIM$^{-/-}$ and WT wounds on days 3, 9, and 15 after wounding. Bars show mean fold changes ± SEM relative to WT; $n = 3$. (*B*) Mouse keratinocytes were stimulated with 5–10 ng/mL TGF-β1 for 0, 3, or 5 d. Cell lysates were collected and blotted with antibodies against desmoplakin, E-cadherin, N-cadherin, vimentin, and Hsc-70 as loading control. (*C* and *D*) Quantification of Slug (*C*) and N-cadherin (*D*) intensity in *B* equalized to Hsc-70. Bars show mean fold changes ± SEM relative to day 3 control mice; $n = 3$. (*E*) Mouse keratinocytes were transfected with scramble siRNA (si Scra) or Slug siRNA (si Slug) oligos for 2 d and then were stimulated with 5 ng/mL TGF-β1 for 3 d. Cell lysates were collected for Western blotting analysis of Slug, N-cadherin, vimentin, desmoplakin, and loading control Hsc-70. (*F* and *G*) Quantification of Slug (*F*) and N-cadherin (*G*) intensity in *E* equalized to Hsc-70. Bars show the mean fold changes ± SEM relative to mock transfections (Ctrl); $n = 3$; $^{*}P < 0.05$; $^{**}P < 0.01$; $^{***}P < 0.001$; ns, not significant.

had a significantly lower expression at day 3 and day 9 postinjury in VIM$^{-/-}$ wound tissues than in their WT counterparts (Fig. 3*A*). Recombinant TGF-β1 potently inhibited the expression of the epithelial markers desmoplakin and E-cadherin and induced the expression of Slug, N-cadherin, and vimentin (all hallmarks of an EMT-like transdifferentiation process) in mouse keratinocytes following cytokine stimulation (Fig. 3 *B*–*D*). To examine the involvement of Slug in wound healing-mediated EMT, we silenced Slug expression in keratinocytes using Slug siRNA in the absence or presence of TGF-β1 (Fig. 3 *E* and *F*). Keratinocytes transfected with Slug siRNA had reduced expression of N-cadherin and vimentin as well as a slight induction of desmoplakin upon TGF-β stimulation (Fig. 3 *E*–*G*), indicating that Slug is needed to induce EMT downstream of TGF-β. Taken together, these data suggest that TGF-β1 produced in WT wounds is capable of driving an active EMT transdifferentiation program via Slug.

Because vimentin as a mesenchymal marker is expressed mainly in dermal compartments, we postulated that activated dermal fibroblasts would be responsible for the TGF-β production observed upon injury, thereby triggering epidermal keratinocyte transdifferentiation. In support of this hypothesis, we found that mouse dermal fibroblasts (MDFs) isolated from VIM$^{-/-}$ mice have lower TGF-β1 gene expression than MDFs from WT mice (Fig. 4*A*). Correspondingly, the levels of active TGF-β1 in the supernatants of VIM$^{-/-}$ MDFs were significantly lower than in the supernatants of WT MDFs (Fig. 4*B*). Cell-culture supernatants of WT MDFs containing greater amounts of TGF-β1 induced a stronger EMT program in the cultivated mouse keratinocytes than did supernatants from VIM$^{-/-}$ MDFs (Fig. 4*C*). Consistently, in a scrape-wound assay, mouse keratinocytes closed the scrape wounds considerably faster in the presence of conditioned medium from WT MDFs than in conditioned medium from VIM$^{-/-}$ MDFs (Fig. 4 *D* and *E*). To exclude the involvement of other cellular effectors of inflammation that might be relevant to the keratinocyte phenotype, we assessed the expression of key cytokines and the presence of inflammatory cells during wound repair. We found that the expression of the mRNA of proinflammatory cytokines IL-6 (*Il6*), IL-1α (*Il1a*), IL-1β (*Il1b*), IL-23 (*Il23*), and TNF-α (*Tnf*) remained at similar levels (less than 1.5-fold changes) between WT and VIM$^{-/-}$ wounds on day 3 and day 9 postinjury (Fig. S4*A*). Although on day 9 postinjury, 1.5-fold fewer neutrophil cells had infiltrated to the edges of WT wounds than to the edges of VIM$^{-/-}$ wounds (Fig. S4 *B* and *C*), there was no significant change in the myeloperoxidase activity of neutrophils (MPO^{+}) in WT and VIM$^{-/-}$ wounds at day 9 postinjury (Fig. S4 *D* and *E*). In addition, the presence of macrophages (CD11b^{+}) and activated T cells (Zap-70^{+}) was comparable between WT and VIM$^{-/-}$ wounds on day 9 of wound repair (Fig. S4 *D* and *E*). Cell-culture supernatants of WT and VIM$^{-/-}$ macrophages also contained equal levels of TGF-β1 (Fig. S4*F*), demonstrating that the loss of vimentin in the regional fibroblasts, but not the infiltrated inflammatory cells, is the key effector of insufficient TGF-β production and signaling.

To test further whether TGF-β1 produced from MDFs is required to drive EMT-like changes in keratinocytes, a pan–TGF-β neutralizing antibody, 1D11, and two chemical inhibitors of TGF-β receptors, LY2109761 and SB431542, were added to MDF-conditioned medium; all effectively inhibited the phosphorylation of Smad2/3 (Fig. 4*F*), downstream effectors of the TGF-β signaling pathway. Further corroborating the involvement TGF-β signaling were the results showing that when TGF-β signaling was blocked, the expression of EMT markers (Slug and N-cadherin) in keratinocytes was reduced (Fig. 4 *G* and *H*), and cell migration was inhibited (Fig. 4*I*). This effect was prominent in cells incubated in the presence of WT MDF supernatants (Fig. 4 *G*–*I*), which contained higher levels of active TGF-β1 than VIM$^{-/-}$ MDF supernatants (Fig. 4*B*), reinforcing the notion that TGF-β signaling is a major driver in keratinocyte transdifferentiation and migration induced by fibroblast vimentin. Inhibition of Slug expression by siRNA in keratinocytes also inhibited cell migration (Fig. 4*J*), further demonstrating that vimentin regulates keratinocyte migration through *TGF-β* –Slug signaling.

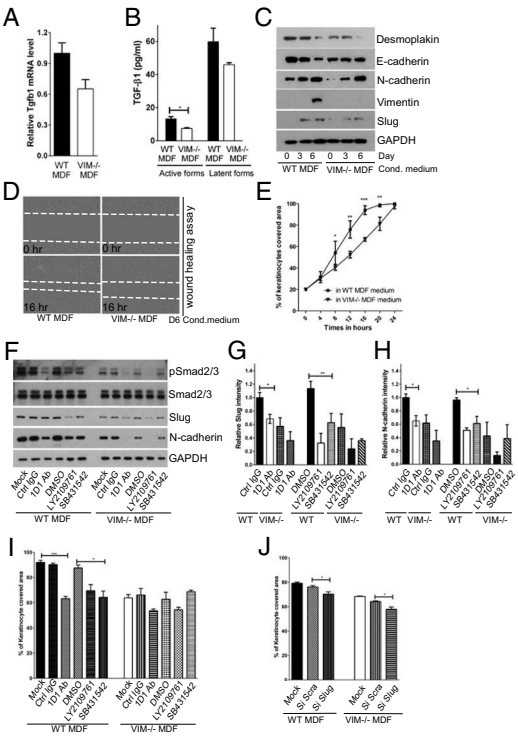

Fig. 4. Vimentin promotes TGF-β production from fibroblasts driving EMT and migration of keratinocytes. (*A*) qRT-PCR analysis of transcripts for TGF-β1 (*Tgfb1*) in VIM$^{-/-}$ and WT MDFs. Bars show mean fold changes ± SEM relative to WT; $n = 6$. (*B*) Level of active and latent forms of TGF-β1 in the supernatants of 6-d MDF cell cultures were analyzed by ELISA. Data are shown as mean ± SEM; $n = 3$. (*C*) VIM$^{-/-}$ and WT MDF cell-culture media were extracted on 0, 3, and 6 d after cell growth. The growth medium of mouse keratinocytes was replaced with the MDF-conditioned medium for 5 d. Cell lysates were collected and blotted with antibodies against desmoplakin, E-cadherin, N-cadherin, vimentin, Slug, and loading control GAPDH. (*D* and *E*) In vitro wound-healing assay of mouse keratinocytes grown in 6-d conditioned medium from VIM$^{-/-}$ MDFs and WT MDFs. The cell gap was monitored over 24 h, and the wound areas were measured and plotted against the time point. At least four wound scratches were analyzed per experiment. Data are shown as means ± SEM; $n = 3$. (*F*) Mouse keratinocytes grown in 6-d conditioned medium from the VIM$^{-/-}$ and WT MDFs were treated with control IgG (Ctrl IgG, 10 μg/mL), pan–TGF-β neutralizing antibody 1D11 (1D1 Ab, 10 μg/mL), two chemical inhibitors of TGF-β receptors [LY2109761 (2 μM) and SB431542 (2 μM)] or were grown in the corresponding DMSO control (DMSO, 2 μM) for 3 d. The cell lysates from this experiment were blotted with antibodies against pSmad2/3, total Smad2/3, Slug, N-cadherin, and loading control GAPDH. (*G* and *H*) Quantification of Slug and N-cadherin intensity in *F* equalized to GAPDH; bars show the mean fold changes relative to WT Ctrl IgG ± SEM; $n = 3$. (*I*) In vitro wound-healing assay of mouse keratinocytes (at 16 h of wound healing) in the treatments in *F*. (*J*) The *y* axis shows the percentage of area covered (at 16 h of wound healing) by keratinocytes transfected with mock, scramble siRNA (si Scra), or Slug siRNA (si Slug) oligos for 2 d and incubated in 6-d WT or VIM$^{-/-}$ MDF-conditioned medium. In *I* and *J*, at least four wound scratches were analyzed per experiment. Data are shown as means ± SEM; $n = 3$; $^{*}P < 0.05$; $^{**}P < 0.01$; $^{***}P < 0.001$.

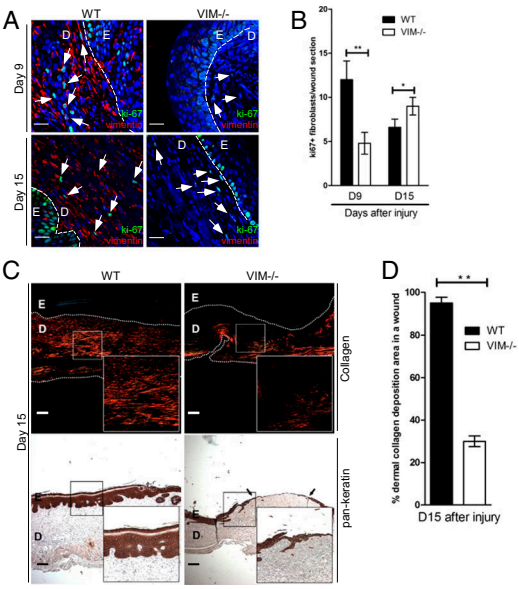

Fig. 5. Vimentin promotes mesenchymal cell proliferation and collagen accumulation in vivo. (*A*) Representative confocal images of the expression of Ki67 (punctate green signal in the nucleus) and vimentin (red) in VIM$^{-/-}$ and WT wounds on days 9 (D9) and 15 (D15) after burn wounding. Nuclei were counterstained with DAPI (blue). (Scale bars, 20 μm.) The white arrowheads indicate examples of ki67^{+} cells in dermal regions. D, dermis region; E, epidermis region. (*B*) Quantitation of ki67^{+} cells in mesenchymal/dermal regions of wounds. (*C*) Representative pictures of Picro-Sirius Red staining of collagen (*Upper*) and the immunohistochemical labeling of pan-keratin (*Lower*) in the corresponding sections of VIM$^{-/-}$ and WT wounds on day 15 postinjury. The right lower corner of each panel shows an enlarged image of the area in the white box. (Scale bars, 100 μm.) (*D*) The quantitation of collagen accumulation (Picro-Sirius Red-positive areas) in mesenchymal/dermal regions of wounds. In *B* and *D* data are shown as means ± SEM; $n = 3$; $^{*}P < 0.05$; $^{**}P < 0.01$.

Vimentin Promotes Fibroblast Proliferation, Collagen Accumulation, and Paracrine EMT Signals. At later stages of tissue repair, we found that the VIM$^{-/-}$ wounds displayed a striking reduction in s.c. proliferating fibroblasts, as indicated by the loss of cells positive for the proliferation marker nuclear antigen ki67 (Fig. 5 *A* and *B*). To assess whether this fibroblast deficiency would lead to a defect in ECM synthesis and buildup, we analyzed the accumulation of dermal collagen using Picro-Sirius Red staining (33). The normal granulation tissue with thick collagen fibers that was observed in WT wounds could not be observed in VIM$^{-/-}$ wounds, which instead showed either no fibers or at best a few scattered thin fibers (Fig. 5*C*). At 15 d postinjury, a striking difference was observed between WT and VIM$^{-/-}$ wounds: Collagen accumulation was largely absent in the dermal regions of VIM$^{-/-}$ wounds, whereas the majority (~95%) of WT dermis was occupied by collagen fibers (Fig. 5*D*). There was no striking difference in collagen accumulation between normal, uninjured WT and VIM$^{-/-}$ adult skins (Fig. S2 *E* and *F*, 10 wk), excluding the possibility of a problem in s.c. collagen distribution in uninjured basal skin. Therefore the collagen defect can be attributed entirely to events during wound healing, and the observed absence in reepithelialization in VIM$^{-/-}$ wounds is closely associated with the inhibition of fibroblast proliferation and collagen accumulation.

To investigate further whether vimentin plays a direct role in dermal fibroblast proliferation, we compared the proliferative potential of VIM$^{-/-}$ and WT MDFs. The results showed that VIM$^{-/-}$ MDFs grew much more slowly than WT MDFs (Fig. 6*A*), although the apoptotic rates in VIM$^{-/-}$ and WT MDFs were similar (Fig. S5*A*). To determine whether vimentin expression is required for the growth advantage, exogenous vimentin construct was titrated into VIM$^{-/-}$ MDFs. We found that reconstitution of vimentin in VIM$^{-/-}$ MDFs restored the cell proliferation capacity in a dose-dependent manner (Fig. 6*A*) that was associated with the reactivation of ERK1/2 signaling (Fig. 6*B*). Furthermore, the conditioned medium from these VIM$^{-/-}$ MDFs reexpressing increasing levels of vimentin gradually rescued the EMT and migration defect in keratinocytes (Fig. 6 *C* and *D*). These results suggest that the presence of vimentin in fibroblasts not only directly regulates the proliferation of these cells but also drives the transdifferentiation of keratinocytes by TGF-β1–mediated paracrine mechanisms.

Taking these results together, we have been able to validate the conceptual framework derived from in vivo observations by in vitro experiments with dermal fibroblasts and keratinocytes isolated from VIM$^{-/-}$ and WT mice. Our working model summarized in Fig. 6*E* proposes that vimentin orchestrates wound healing by regulating fibroblast proliferation and thereby both collagen accumulation and the TGF-β1–mediated Slug–EMT switch in keratinocytes.

Discussion

In this study we have demonstrated that vimentin directly coordinates four cellular activities important in the control of wound healing: fibroblast proliferation, collagen accumulation, keratinocyte transdifferentiation, and reepithelialization. Loss of vimentin disrupts this coordination, leading to slow, poor, and incomplete wound healing. Because burn and excisional wound models are very different in their character, our data demonstrate that vimentin has a general role in determining the progression of epidermal regeneration regardless of the type of epidermal injury.

TGF-β has been shown to modulate integrin expression of keratinocytes toward a more migratory phenotype (34), suggesting its supportive role in reepithelialization. TGF-β occupies a central position in the EMT signaling networks, including MEK/ERK, JNK/p38, MAP kinases, Rho GTPase, and PI3K/Akt signaling pathways (6). Vimentin plays an active role in the cellular partners that receive EMT-inducing signals (9, 10, 12), as demonstrated by previous studies showing the vimentin dependence of EMT in a cancer context and our recent observations in TGF-β1–responsive mammary epithelial (MCF10A) cells (10, 12). Because vimentin was required for the observed EMT phenotype, a common paradigm might be that vimentin, by being involved in the regulation of both TGF-β signal triggering and reception, orchestrates a dynamic balance of epithelial–stromal (epidermal–dermal) signals that induce EMT-like differentiation processes. This paradigm may be relevant not only for skin wound healing but also other physiological conditions that involve EMT.

We found that there is a kinetic expression of Slug and downstream EMT genes during normal WT wound closure. Our data imply that in WT skin these EMT genes normally are kept at a steady state in the beginning of the proliferation phase during the healing process (day 3), whereas in VIM$^{-/-}$ skin the expression of Slug drops completely. At day 9, all EMT genes are strongly induced in WT skin, but in VIM$^{-/-}$ skin, there is little or no induction and Slug remains suppressed at the day 3 level. These results emphasize the vimentin dependence of the Slug response in wound healing, as we have demonstrated previously in the context of a cancer model (12). Interestingly, after 15 d of recovery, Slug expression in VIM$^{-/-}$ skin was restored to the same levels as in WT skin. One can speculate that, in addition to the TGF-β–vimentin signaling pathway outlined in this study,

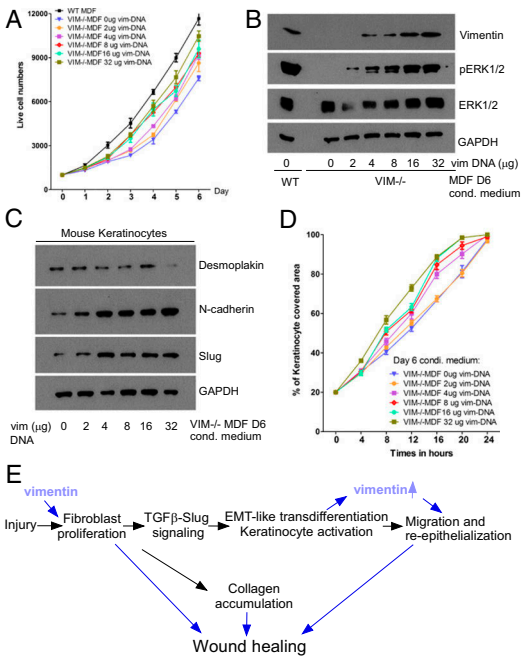

Fig. 6. Vimentin promotes mesenchymal cell proliferation and paracrine EMT signaling in vitro. (*A*) The growth curve of VIM$^{-/-}$ and WT MDF cells after transfected with different amounts of vectors encoding full-length vimentin (the total DNA per transfection was equalized with the control vector). Data are shown as mean ± SEM; $n = 3$. (*B*) Immunoblotting of vimentin, pERK1/2, total ERK1/2, and GAPDH expression of the cell lysates in *A*. (*C* and *D*) Western blotting of individual markers (*C*) and migration (*D*) of mouse keratinocytes growing in 6-d conditioned medium (D6) from VIM$^{-/-}$ and WT MDFs transfected with the indicated amount of vimentin plasmids. Data are shown as means ± SEM; $n = 3$. (*E*) Scheme showing the working model. Vimentin has a profound effect on fibroblast proliferation, which activates both collagen production and TGF-β secretion. The active fibroblast TGF-β induces Slug–EMT signaling in keratinocytes, promoting EMT-like transdifferentiation and keratinocyte migration.

Slug expression may be stimulated by other signaling modalities that could set in at this late stage to compensate for the lack of TGF-β–mediated stimulation. The dramatic induction of Slug mRNA in WT skin on day 9 postinjury that returned to normal levels when the healing was completed on day 15 is consistent with previous observations from an in vitro wound-healing model that described a transient induction of Slug with a subsequent decline upon healing of the wound (29). Thus we speculate that Slug is involved mainly in the events in the early stage of wound reepithelialization, such as triggering EMT during the proliferation phase.

We have shown previously that silencing Slug in a breast cancer model reduces vimentin expression (12). Interestingly, a recent report also revealed that keratinocytes transfected with Slug siRNA showed reduced expression of vimentin and inhibited cell migration (35). In the present study we provide further evidence demonstrating that Slug is a key mediator of TGF-β–induced expression of vimentin and other EMT markers in keratinocytes, accelerating cell migration. Our data indicate that vimentin regulates the proliferation of s.c. fibroblasts through ERK signaling; this notion is supported by our recent study on the molecular mechanisms underlying the vimentin-mediated control of growth factor signaling in the breast cancer model (12). Our current data show that the vimentin-dependent TGF-β–Slug–EMT signaling has a very steep dose–response curve, because a low level of exogenously expressed vimentin was already sufficient to rescue pERK signaling, MDF proliferation, Slug–EMT signaling, and keratinocyte migration. These results also are consistent with our previous finding that reintroducing of low levels of vimentin could fully restore EMT–ERK–Slug axis signaling in the breast cancer model (12). Taken together, our results show that the Slug–vimentin signaling axis in wound healing-related EMT is surprisingly similar to the EMT signaling we observed in the breast cancer model. Vimentin expression is dependent on Slug, and vice versa, and both contribute to ERK activation.

Vimentin-deficient wounds were conspicuously devoid of collagen accumulation, apparently as a direct consequence of the severe inhibition of fibroblast proliferation and expansion. In fact, a recent study indicated that vimentin can contribute to the posttranscriptional regulation of collagen expression (36). Furthermore, EMT also can activate fibroblasts to produce ECM (27). Based on our results, we speculate that both the slower proliferation rate of vimentin-deficient fibroblasts and the impaired EMT-like transdifferentiation of keratinocytes contribute to reduced collagen production and the observed delayed wound-healing phenotype.

Interestingly, although there were comparable levels of cytokine expression, myeloperoxidase activity of neutrophils, and macrophage and T-cell infiltration in the injured sites of WT and VIM$^{-/-}$ skin in the early stage of the healing process, we observed elevated and sustained expression of inflammatory cytokines (IL-6, IL-1α, IL-1β, IL-23, and TNF-α) at the late stage of VIM$^{-/-}$ wounds (day 15 postinjury) that correlates to a prolonged neutrophil infiltration in the VIM$^{-/-}$ wound edges. This prolonged inflammation may be a compensation mechanism in which the tissue attempts to drive healing of the VIM$^{-/-}$ wound. This hypothesis is supported by our preliminary observations showing that, although complete wound closure seemed to be achieved eventually (>20–25 d after wounding) in VIM$^{-/-}$ mice, the reepithelialization was still incomplete, as already reflected in the weak reepithelization of Vim$^{-/-}$ skin at day 15 postinjury. Future studies to assess the role of chronic inflammation in terminal healing will be warranted to understand better the possible contribution of inflammation and immune response determinants to the VIM$^{-/-}$ repair phenotype.

Recent research has rapidly expanded the knowledge of the functions of vimentin intermediate filament proteins, including their involvement in tissue repair. When organ and tissue homeostasis has been challenged in a number of different organs, vimentin has been found to participate in many processes crucial for tissue repair and regeneration, including cell migration, proliferation, differentiation, angiogenesis, extracellular matrix remodeling, and immune responses. Obviously, epidermal wound healing features many of these cellular functions. In this respect, our study demonstrates the involvement of vimentin-mediated signaling in some of the most essential aspects of the whole healing process. The results suggest that in physiological repair systems vimentin-mediated signaling is a likely target for multifactorial orchestration of the healing process. This paradigm and this model system will be a fruitful ground to explore in greater detail the molecular and cellular mechanisms that underlie signal integration in tissue repair.

Materials and Methods

Animals. All studies involving animals are reported in accordance with the Animal Research: Reporting of In Vivo Experiments (ARRIVE) guidelines for reporting experiments involving animals (37, 38). Before and during the experiments the animals were kept under standard laboratory conditions, with a 12-h light/12-h dark cycle initiated at 0600 hours, and were supplied with chow and water ad libitum. All animals were killed by cervical dislocation. All experimental protocols for the animal experiments were approved by the Umeå University Ethical Committee for Animal Studies

(A 143-00). Vimentin heterozygous mice (129/Sv × C57BL/6) were used to generate vimentin-deficient homozygotes (VIM$^{-/-}$) and WT offspring (20). The genotypes of the mice were determined by PCR genotyping methods. Eight- to ten-week-old littermates of randomly mixed sex were used for the wound-healing experiments. Ages and sex of mice used in the experiments are summarized in Table S1.

Experimental Procedures. The mice were anesthetized by i.v. injection of 100 mL of a mixture containing 5% Ketaminol Vet (Intervet) and 20% Dormitor Vet (Orion Pharma). The hair of the back of the mouse was shaved with an electric clipper followed by a depilatory cream. To make a burn wound, a metal rod (25 g, 1 cm in diameter) was heated to 95–100 °C by submersion in boiling water. The rod was immediately positioned vertically for 6 s without additional pressure on the back skin of mice that had also been depilated 3 d before wounding. To make an excisional wound, the skin was rinsed with alcohol, and full-thickness wounds extending through the panniculus carnosus were made on the dorsum on each side of midline, using an 8-mm biopsy punch. After wounding, the mice were caged individually, and the wounds were not dressed. Only Fig. 6 and Fig. S1 include dermal excisions; all other injury analyses are from burn wounds.

Measurements of Wound Contraction and Reepithelialization. Digital photographs were taken at the day of surgery and every day after wounding. A circular reference was placed alongside to permit correction for the distance between the camera and the animals. The wound area was calculated in pixels with ImageJ 1.41 software (NIH), corrected for the area of the reference circle, and expressed as percentage of the original area. Reepithelialization was defined as the area within the pan-keratin marks that was covered with epithelium. This area was calculated by scanning the slides and measuring the epithelial tongues from the computerized image using ImageJ. The percentage of reepithelialization was determined using the formula: [(sum of epithelial tongues)/(distance between tattoo marks)] × 100.

Morphologic and Collagen Staining. Five-micrometer-thick sections were taken perpendicular to the wounded skin from paraffin-fixed tissue samples and were processed for H&E staining. Images were taken with a DC300F digital camera attached to a DM LB microscope (Leica). Sirius Red, Fast Green, and picric acid (all from Sigma) were used in Picro-Sirius Red staining for histological visualization of collagen fibers in tissue sections under polarized light microscopy (33) at 20× magnification, and pictures were taken at a fixed exposure. Quantification of collagen was performed as previously described (39) using Image Pro Plus version 4.5.0.29 imaging software (Media Cybernetics Inc.).

Immunofluorescence and Immunohistochemistry. Immunofluorescence staining of the cells on coverslips was performed as described previously (40). For tissue sample analysis, skin samples were collected 24 h after wounding and injection. Paraffin-embedded wound tissues were sectioned (5-μm thickness) perpendicular to the wound. For immunostaining of paraffin-embedded skin samples, the samples were deparaffinized and rehydrated. After antigen retrieval with 0.1 M citrate buffer (pH 6.0), sections were blocked with 5% normal goat serum, stained with primary antibodies overnight at 4 °C and with secondary antibodies for 3 h at room temperature, and counterstained with DAPI for 10 min. For immunohistochemistry analysis of tissue sections, upon antigen retrieval, tissues were immunohistochemically stained with HRP-conjugated antibody and visualized using the ABC staining system (Vector Laboratories, Inc.). Finally, all sections were counterstained with Mayer's Hematoxylin (Histolab). Isotype- and concentration-matched primary antibodies were used as negative controls, and all were found to be negative.

Microscopic Image Acquisition and Quantification. Confocal images shown in all figures were acquired at room temperature using Zeiss Zen software on a Zeiss LSM780 confocal laser-scanning microscope (Carl Zeiss, Inc.) with the following objectives: Plan-Apochromat 10× (NA 0.45, air), Plan-Apochromat 40× (NA 1.30, oil). The following fluorochromes were used: Alexa-Fluor 488, Alexa-Fluor 594, and DAPI. Immunohistochemistry images were taken with a Leica DC300F digital camera attached to a Leica DM LB microscope (Leica) or using Pannoramic digital slide scanners (3DHISTECH Ltd.). Images were viewed and brightness and contrast were adjusted using Adobe Photoshop software. Fluorescent image quantification was processed and analyzed in a pipeline created in the BioImageXD framework (41). The pipeline detects the nuclei from the Hoechst channel and counts them. The cytoplasm of each cell was modeled with a 20-pixel ring around the nucleus. All cells present within the sectioned wounds were counted. To diminish the variance within samples, at least 10 consecutive sections from each wound sample and three to six samples per time point were counted, as indicated in the figure legends.

Cell Isolation and Cell Culture. Mouse skin keratinocytes were isolated from WT newborn mice and cultured in FAD medium (DMEM/Ham's F-12 Nutrient Mixture; 3.5:1.1) supplemented with 10% (vol/vol) Chelex-treated FCS (Invitrogen), 0.18 mM adenine, 0.5 μg/mL hydrocortisone, 5 μg/mL insulin, 100 pM cholera toxin (all from Sigma), 10 ng/mL EGF, 100 U/mL sodium pyruvate, 100 μg/mL penicillin/streptomycin, and 2 mM Glutamax (all from Invitrogen) in 5% CO_2 and 32 °C. Cells were cultured on collagen I (rat tail; Invitrogen)-coated cell-culture dishes in 5% CO_2 at 32 °C. The purity of keratinocytes was confirmed by immunofluorescence (Fig. S5*B*), although low-level contamination by vimentin-expressing, nonkeratinocyte cells such as melanocytes may occur in primary cultures because of the limitations of isolation and purification techniques. MDFs were isolated from WT and VIM$^{-/-}$ newborn mice and cultured in DMEM (4.5 mM glucose) supplemented with 2 mM L-glutamine, 100 IU/mL penicillin and streptomycin, and 10% heat-inactivated FBS (Invitrogen) in 5% CO_2 at 37 °C. WT and VIM$^{-/-}$ bone marrow cells were isolated and differentiated to obtain primary murine macrophage cells using L Cell conditioned medium. Macrophages were cultured in DMEM/F12 medium supplemented with 2 mM L-glutamine, 100 IU/mL penicillin and streptomycin, and 10% heat-inactivated FBS (Invitrogen) in 5% CO_2 at 37 °C. Only cells between passages 2–9 were used for the experiments.

Antibodies and Reagents. The following antibodies were used in this study: rabbit antibodies against Slug (C19G7), vimentin (D21H3), p44/42 MAPK (Erk1/2) (137F5), phospho-p44/42 MAPK (Erk1/2) (Thr202/Tyr204), Smad2/3 (D7G7), phospho-Smad2 (Ser465/467)/Smad3 (Ser423/425) (D27F4), Zap-70 (99F2), and GAPDH (14C10) (all from Cell Signaling); Pan-keratin (Abcam), Ki67 (Abcam), N-cadherin (EPR1792Y) (Millipore), MPO (Thermo Scientific), and keratin 5 (AF 138) (Covance); rat anti–E-cadherin (GeneTex), rat anti-CD11b (AbD Serotec), rat anti-Hsc70 (Abcam); chicken anti-vimentin (Covance), and mouse anti-α-SMA (BD). Antibodies against mouse keratin 6, keratin 14, and desmoplakin were gifts from Thomas Schulz, University Leipzig, Leipzig, Germany. Growth factors and inhibitors used in this study included TGF-β1 (R&D Systems), SB 431542 (Tocris Bioscience), and LY2109761 (Santa Cruz Biotechnology).

Cell Transfection. WT and VIM$^{-/-}$ MDFs were electroporated and were transfected with different amounts of pcDNA3-vimentin (full-length) plasmids with additional amounts of backbone plasmid DNA added to keep the total plasmids consistent in every transfection. For siRNA silencing, keratinocytes were plated on a 24-well plate (50,000 cells per well). For each well, 50 nM siRNA (in one Eppendorf tube) were transfected using Lipofectamine RNAiMAX Reagent (Invitrogen). The experiments were performed a few days after transfection as indicated in *Results* and in the figure legends. Slug siRNAs (ON-TARGET plus Mouse Snai2 siRNA-SMARTpool; Dharmacon) and scrambled siRNAs (AllStars Negative Control; Qiagen) were used in this study. The siRNA Slug (Snai2) oligo sequences are listed in Table S2.

Wound-Healing Assay. For in vitro wound-healing assays, cells were grown in automated 96-well cell-migration plates and imaged with IncuCyte live-cell imaging instruments (Essen BioScience). Scratch wounds were made using a 96-pin wound-making tool (WoundMaker; Essen BioScience). Mitomycin C (10 μg/mL) was included in the medium to prevent cell proliferation. The relative migration of the cells was calculated from IncuCyte analysis software and from the area measured after scratching relative to the basal area as expressed in pixels using ImageJ 1.32 (NIH) software.

Western Blot Analysis. Cells were washed three times with TBS and were lysed in SDS/PAGE loading buffer. Cells were scraped using a sterile cell scraper and then were aspirated into a fresh 1.5-mL microcentrifuge tube and boiled at 95 °C for 5 min. Protein was separated by SDS/PAGE using 10% gel at 120 V for 90 min. After separation, protein was transferred to a nitrocellulose membrane by wet transfer at 100 V for 30 min. The nitrocellulose membrane with the transferred protein was incubated in TBS containing 5% milk and 0.3% Tween 20 for 1 h at room temperature. The membrane was washed three times in 0.3% Tween 20/TBS. The membrane was incubated with primary antibodies overnight at 4 °C with shaking. The membrane was washed three times (10 min each) in 0.3% Tween 20/TBS, was incubated again with secondary antibodies for 1 h at room temperature with shaking, and then was washed three times (10 min each) in 0.3% Tween 20/TBS. Amersham ECL reagent was used to detect protein in accordance with the manufacturer's instructions.

ELISA Analysis. The filtered MDF or macrophage cell supernatant was used to determine the TGF-β1 level by a Human/Mouse TGF beta 1 ELISA Ready-SET-Go! kit (eBioscience) according to the manufacturer's instructions. For total TGF-β1 measurement, samples were first treated with 1N HCl (1 μL/50 μL supernatant) for 15 min at room temperature and were neutralized with an equal amount of 1N NaOH before analysis in the ELISA. For active TGF-β1 measurement, samples were analyzed in the ELISA without acid treatment. Active TGF-β1 was subtracted from the total TGF-β1 to determine the latent TGF-β1 values.

Quantitative Real-Time PCR. Total RNA was extracted from skin epidermal regions using the FFPE Total RNA Isolation Kit (Invitrogen) or from cells using RNeasy mini kits (Qiagen). cDNA was obtained by reverse-transcribing same amount of total RNA using the High Capacity cDNA Reverse Transcription Kit (Applied Biosystems). The transcript levels of the genes of interest were measured by quantitative RT-PCR (qRT-PCR). The qRT-PCR reactions were performed using the SYBR Green qRT-PCR reagents (Applied Biosystems) in an Applied Biosystems 7300 detection system (Bio-Rad). The quality of the quantitative PCR run was determined by standard curves and melting-curve analysis. The data were normalized to the expression of a cellular housekeeping gene, *GAPDH*. Forward and reverse primer sequences used in this study are listed in Table S3.

Statistical Analysis. The results are expressed as the mean ± SEM. Statistical differences between groups were calculated with the two-tailed unpaired *t* test, and differences were considered significant at $P \leq 0.05$. For statistical evaluation of qRT-PCR data, logarithmic values were converted to ΔΔCt values (linear $\log_2$ scale values), and *P* values were calculated using one-tailed unpaired Student's *t* test, based on the data normalized to the appropriate control.

ACKNOWLEDGMENTS. We thank H. Saarento and C. Oram for excellent technical assistance and Dr. T. Magin, Dr. D. Granville, and Dr. K. Seltmann for providing the reagents, equipment, and software needed to complete this work. This study was supported by the Academy of Finland, the Sigrid Juselius Foundation, the Endowment of Åbo Akademi University, and Swedish National Cancer Foundation Grant 150319. F.C. was supported by a postdoctoral grant from the Academy of Finland and by Åbo Akademi University, the Finnish Cultural Foundation, and the Alfred Kordelin Foundation.

1. Gurtner GC, Werner S, Barrandon Y, Longaker MT (2008) Wound repair and regeneration. *Nature* 453(7193):314–321.
2. Reinke JM, Sorg H (2012) Wound repair and regeneration. *Eur Surg Res* 49(1):35–43.
3. Hudson LG, et al. (2009) Cutaneous wound reepithelialization is compromised in mice lacking functional Slug (Snai2). *J Dermatol Sci* 56(1):19–26.
4. Windoffer R, Beil M, Magin TM, Leube RE (2011) Cytoskeleton in motion: The dynamics of keratin intermediate filaments in epithelia. *J Cell Biol* 194(5):669–678.
5. Raja SK, Sivamani K, Garcia MS, Isseroff RR (2007) Wound re-epithelialization: Modulating keratinocyte migration in wound healing. *Front Biosci* 12:2849–2868.
6. Thiery JP, Acloque H, Huang RYJ, Nieto MA (2009) Epithelial-mesenchymal transitions in development and disease. *Cell* 139(5):871–890.
7. Hanahan D, Weinberg RA (2011) Hallmarks of cancer: The next generation. *Cell* 144(5):646–674.
8. Ivaska J, Pallari HM, Nevo J, Eriksson JE (2007) Novel functions of vimentin in cell adhesion, migration, and signaling. *Exp Cell Res* 313(10):2050–2062.
9. Mendez MG, Kojima S, Goldman RD (2010) Vimentin induces changes in cell shape, motility, and adhesion during the epithelial to mesenchymal transition. *FASEB J* 24(6):1838–1851.
10. Vuoriluoto K, et al. (2011) Vimentin regulates EMT induction by Slug and oncogenic H-Ras and migration by governing Axl expression in breast cancer. *Oncogene* 30(12):1436–1448.
11. Dave JM, Bayless KJ (2014) Vimentin as an integral regulator of cell adhesion and endothelial sprouting. *Microcirculation* 21(4):333–344.
12. Virtakoivu R, et al. (2015) Vimentin-ERK signaling uncouples Slug gene regulatory function. *Cancer Res* 75(11):2349–2362.
13. Shirley SH, Hudson LG, He J, Kusewitt DF (2010) The skinny on Slug. *Mol Carcinog* 49(10):851–861.
14. Savagner P (2001) Leaving the neighborhood: Molecular mechanisms involved during epithelial-mesenchymal transition. *BioEssays* 23(10):912–923.
15. Yilmaz M, Christofori G (2009) EMT, the cytoskeleton, and cancer cell invasion. *Cancer Metastasis Rev* 28(1-2):15–33.
16. Menko AS, et al. (2014) A central role for vimentin in regulating repair function during healing of the lens epithelium. *Mol Biol Cell* 25(6):776–790.
17. Müller M, et al. (2009) Dominant cataract formation in association with a vimentin assembly disrupting mutation. *Hum Mol Genet* 18(6):1052–1057.
18. Bornheim R, et al. (2008) A dominant vimentin mutant upregulates Hsp70 and the activity of the ubiquitin-proteasome system, and causes posterior cataracts in transgenic mice. *J Cell Sci* 121(Pt 22):3737–3746.
19. Nieminen M, et al. (2006) Vimentin function in lymphocyte adhesion and transcellular migration. *Nat Cell Biol* 8(2):156–162.
20. Colucci-Guyon E, et al. (1994) Mice lacking vimentin develop and reproduce without an obvious phenotype. *Cell* 79(4):679–694.
21. Eckes B, et al. (1998) Impaired mechanical stability, migration and contractile capacity in vimentin-deficient fibroblasts. *J Cell Sci* 111(Pt 13):1897–1907.
22. Eckes B, et al. (2000) Impaired wound healing in embryonic and adult mice lacking vimentin. *J Cell Sci* 113(Pt 13):2455–2462.
23. Matsuyama M, et al. (2013) Defect of mitotic vimentin phosphorylation causes microophthalmia and cataract via aneuploidy and senescence in lens epithelial cells. *J Biol Chem* 288(50):35626–35635.
24. Tanaka H, et al. (2015) Cytokinetic failure-induced tetraploidy develops into aneuploidy, triggering skin aging in phosphovimentin-deficient mice. *J Biol Chem* 290(21):12984–12998.
25. DePianto D, Coulombe PA (2004) Intermediate filaments and tissue repair. *Exp Cell Res* 301(1):68–76.
26. Lessard JC, et al. (2013) Keratin 16 regulates innate immunity in response to epidermal barrier breach. *Proc Natl Acad Sci USA* 110(48):19537–19542.
27. Kalluri R, Weinberg RA (2009) The basics of epithelial-mesenchymal transition. *J Clin Invest* 119(6):1420–1428.
28. Weber CE, Li NY, Wai PY, Kuo PC (2012) Epithelial-mesenchymal transition, TGF-β, and osteopontin in wound healing and tissue remodeling after injury. *J Burn Care Res* 33(3):311–318.
29. Savagner P, et al. (2005) Developmental transcription factor slug is required for effective re-epithelialization by adult keratinocytes. *J Cell Physiol* 202(3):858–866.
30. Acloque H, Thiery JP, Nieto MA (2008) The physiology and pathology of the EMT. Meeting on the epithelial-mesenchymal transition. *EMBO Rep* 9(4):322–326.
31. Kusewitt DF, et al. (2009) Slug/Snai2 is a downstream mediator of epidermal growth factor receptor-stimulated reepithelialization. *J Invest Dermatol* 129(2):491–495.
32. Zavadil J, et al. (2001) Genetic programs of epithelial cell plasticity directed by transforming growth factor-beta. *Proc Natl Acad Sci USA* 98(12):6686–6691.
33. Junqueira LCU, Bignolas G, Brentani RR (1979) Picrosirius staining plus polarization microscopy, a specific method for collagen detection in tissue sections. *Histochem J* 11(4):447–455.
34. Margadant C, Sonnenberg A (2010) Integrin-TGF-beta crosstalk in fibrosis, cancer and wound healing. *EMBO Rep* 11(2):97–105.
35. Shin JU, et al. (2015) Estrogen Upregulates Slug to Enhance the Migration of Keratinocytes. *J Invest Dermatol* 135(12):3200–3203.
36. Challa AA, Stefanovic B (2011) A novel role of vimentin filaments: Binding and stabilization of collagen mRNAs. *Mol Cell Biol* 31(18):3773–3789.
37. Kilkenny C, Browne W, Cuthill IC, Emerson M, Altman DG; NC3Rs Reporting Guidelines Working Group (2010) Animal research: Reporting in vivo experiments: The ARRIVE guidelines. *Br J Pharmacol* 160(7):1577–1579.
38. McGrath JC, Drummond GB, McLachlan EM, Kilkenny C, Wainwright CL (2010) Guidelines for reporting experiments involving animals: The ARRIVE guidelines. *Br J Pharmacol* 160(7):1573–1576.
39. Hiebert PR, Wu D, Granville DJ (2013) Granzyme B degrades extracellular matrix and contributes to delayed wound closure in apolipoprotein E knockout mice. *Cell Death Differ* 20(10):1404–1414.
40. Cheng F, et al. (2011) KSHV-initiated notch activation leads to membrane-type-1 matrix metalloproteinase-dependent lymphatic endothelial-to-mesenchymal transition. *Cell Host Microbe* 10(6):577–590.
41. Kankaanpää P, et al. (2012) BioImageXD: An open, general-purpose and high-throughput image-processing platform. *Nat Methods* 9(7):683–689.

Supporting Information

Cheng et al. 10.1073/pnas.1519197113

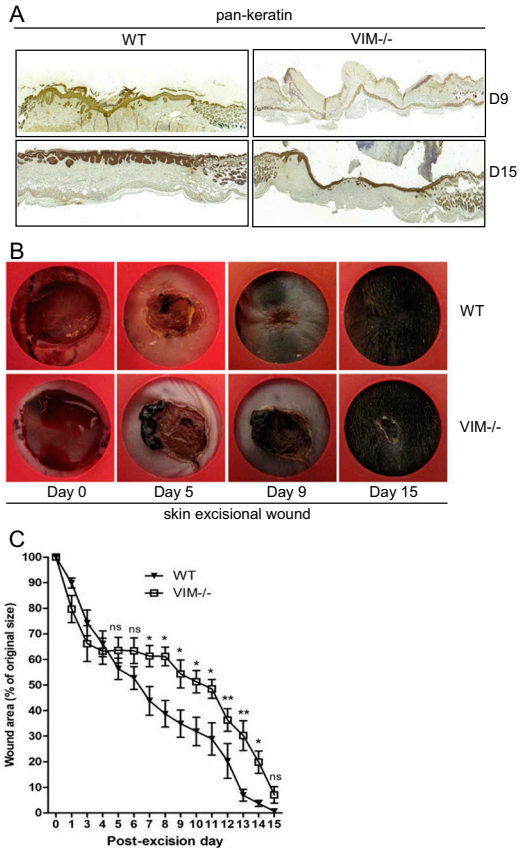

Fig. S1. VIM$^{-/-}$ mice have slower wound healing in an excisional wound model (related to Fig. 1). (*A*) Representative pictures of immunohistochemical labeling of pan-keratin in wounds in VIM$^{-/-}$ and WT mice on days 9 (D9) and 15 (D15) postinjury. (*B*) Representative pictures of wounds in WT and VIM$^{-/-}$ mice 15 d after excisional injury. (*C*) Quantification of the wound area remaining at different time points after wounding in the WT and VIM$^{-/-}$ groups. Data are shown as means ± SEM; $n = 4$. *$P < 0.05$; **$P < 0.01$; ns, not significant.

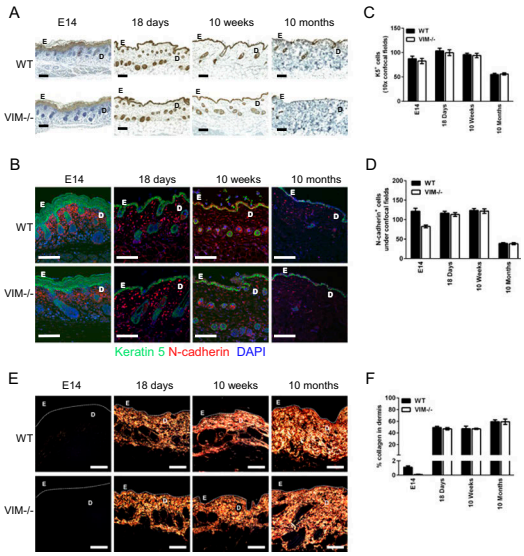

Fig. S2. Vimentin control mice have normal skin composition and collagen accumulation (related to Figs. 2 and 5). (*A*) Representative pictures showing immunohistochemical labeling of pan-keratin in uninjured skin from control mice on E14 and from 18-d-old, 10-wk-old, and 10-mo-old mice. (*B*) Representative confocal pictures of immunofluorescent labeling of N-cadherin (red) and keratin 5 (K5, green) in skins of uninjured control mice. (*C* and *D*) Quantitation of $K5^{+}DAPI^{+}$ cells (*C*) and N-$cadherin^{+}$ $DAPI^{+}$ cells (*D*) in the epidermal and dermal region. (*E*) Representative pictures of Picro-Sirius Red staining of collagen in the corresponding sections of skins from $VIM^{-/-}$ and WT control mice. (*F*) The quantitation of collagen accumulation (Picro-Sirius Red-positive areas) in the mesenchymal/dermal regions of wounds. In *A*, *B*, and *E*, D, dermis region; E, epidermis region. (Scale bars, 100 μm.) In *C*, *D*, and *F*, data are shown as means ± SD; $n = 2–4$.

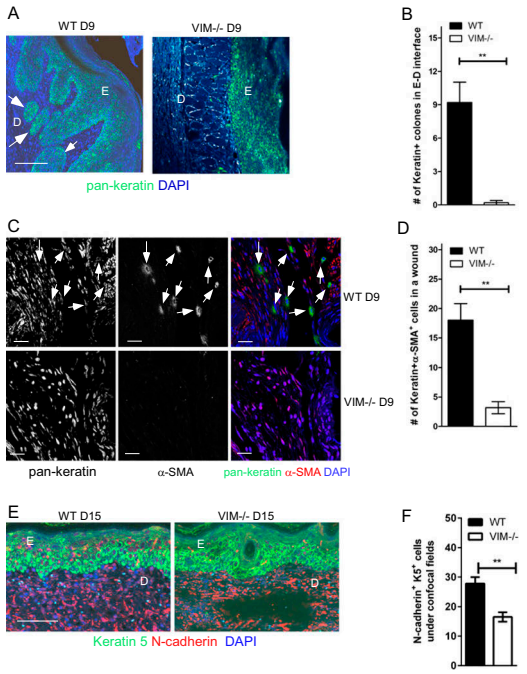

Fig. S3. Compromised reepithelialization and keratinocyte transdifferentiation in VIM$^{-/-}$ wounds (related to Fig. 2). (*A*) Representative confocal images of the expression of pan-keratin (green) and DAPI (blue) in wounds of VIM$^{-/-}$ and WT mice on day 9 postinjury (D9). The white arrowheads indicate examples of migrating pan-keratin^{+} cell colonies locating in the dermis–epidermis interface. (Scale bar, 100 μm.) (*B*) Quantitation of pan-keratin^{+} cell colony numbers in dermis–epidermis interface regions on day 9 postinjury. (*C*) Representative confocal images of the expression of α-SMA (red) and pan-keratin (green) in VIM$^{-/-}$ and WT wounds on day 9 postinjury. The white arrowheads indicate examples of pan-keratin^{+}α-SMA^{+} cells in the dermal region of WT wounds on day 9 postinjury. (Scale bars, 20 μm.) (*D*) Quantitation of pan-keratin^{+}α-SMA^{+} cells in wounds in VIM$^{-/-}$ and WT mice on day 9 postinjury. (*E*) Representative pictures of immunofluorescent labeling of keratin 5 (green) and N-cadherin (red) in wounds of VIM$^{-/-}$ and WT mice on day 15 postinjury (D15). (Scale bar, 100 μm.) (*F*) Quantitation of N-cadherin^{+} K5^{+} cells in epidermis in day 15 wounds. In *A* and *E*, E: epidermis region; D: dermis region. In *B*, *D*, and *F*, data are shown as means ± SEM; $n = 3$. $^{**}P < 0.01$.

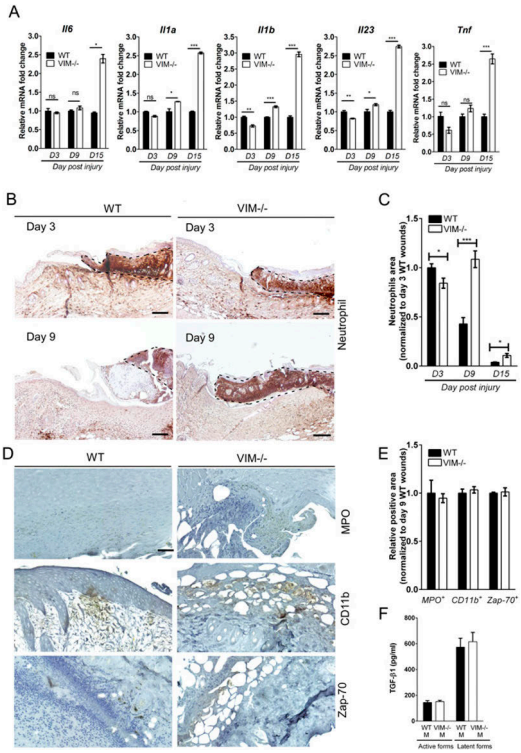

Fig. S4. Inflammatory cytokines and infiltrated inflammatory cells in wounds in WT and VIM$^{-/-}$ mice (related to Fig. 4). (*A*) qRT-PCR analysis of transcripts for IL-6 (Il6), IL-1α (Il1a), IL-1β (Il1b), IL-23 (Il23), and TNF-α (Tnf) in wounds in VIM$^{-/-}$ and WT mice on days 3 (D3), 9 (D9), and 15 (D15) after wounding. Data are shown as means ± SEM; $n = 3$. (*B*) Representative pictures of immunohistochemical labeling of mouse neutrophils in wounds in VIM$^{-/-}$ and WT mice on days 3 and 9 postinjury. The inflamed tissue is indicated by black dashed lines. (Scale bars, 20 mm.) (*C*) Comparison of the temporal regulation of inflammation (the wound-edge regions infiltrated with neutrophils) in wounds in VIM$^{-/-}$ and WT mice. Data are shown as means ± SEM; $n = 3$. (*D* and *E*) Representative pictures (*D*) and quantitative comparison (*E*) of the myeloperoxidase activity of neutrophils (MPO), monocyte/macrophage marker CD11b, and T-cell marker Zap-70 in the wound-edge regions of wounds in VIM$^{-/-}$ and WT mice 9 d after injury. (Scale bar, 100 μm.) Data in *E* are shown as mean ± SEM; $n = 3$. (*F*) Level of active and latent forms of TGF-β1 in the supernatants after 6 d of WT and VIM$^{-/-}$ macrophage cell culture were analyzed by ELISA. Data are shown as means ± SEM; $n = 5$. $^*P < 0.05$; $^{**}P < 0.01$; $^{***}P < 0.001$; ns, not significant.

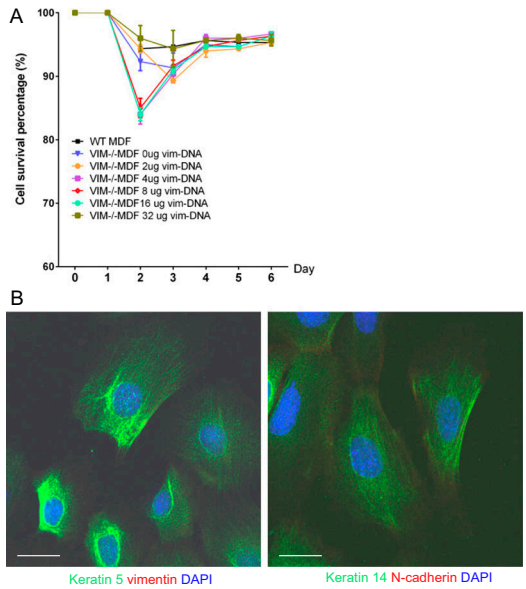

Fig. S5. Vimentin does not influence fibroblast survival (related to Fig. 6). (*A*) The cell-survival curve of VIM$^{-/-}$ and WT MDFs after transfection with different amounts of vectors encoding full-length vimentin (the total DNA per transfection was equalized with the control vector). Data are shown as means ± SEM; $n = 3$. (*B*) Representative confocal pictures of immunofluorescent labeling of DAPI (blue), keratin 5 (green), and vimentin (red) (*Left*) or keratin 14 (green) and N-cadherin (red) (*Right*) from isolated mouse keratinocytes. (Scale bars, 20 μm.)

Table S1. Sex and age of mice used in wound-healing experiments

Experiment	Genotype	Sex	Age, wk	No. of mice
Burn injury	WT	Male	9	8
	WT	Female	9	6
Burn injury	VIM$^{-/-}$	Male	9	6
	VIM$^{-/-}$	Female	9	6
Burn injury	WT	Male	10	4
	WT	Female	10	5
Burn injury	VIM$^{-/-}$	Male	10	4
	VIM$^{-/-}$	Female	10	5
Excisional injury	WT	Male	8	3
	WT	Female	8	3
Excisional injury	VIM$^{-/-}$	Male	8	3
	VIM$^{-/-}$	Female	8	3

Table S2. siRNA Slug (Snai2) sequences

Oligo 1:	CUAUGAAAGUUACCCUAUA
Oligo 2:	GGAUCACAGUGGUUCAGAA
Oligo 3:	GGAGCAUACAGCCCUAUUA
Oligo 4:	UAAGACCUAUUCUACGUUC

Table S3. Primers used for qPCR

Gene name (protein name)	Forward sequence	Reverse sequence	NCBI Gene ID
Vim (Vimentin)	CGTCCACACGCACCTACAG	GGGGGATGAGGAATAGAGGCT	22352
Fn1 (Fibronectin)	GATGTCCGAACAGCTATTTACCA	CCTTGCGACTTCAGCCACT	14268
S100a4 (FSP-1)	TCCACAAATACTCAGGCAAAGAG	GCAGCTCCCTGGTCAGTAG	20198
Cdh2 (N-Cadherin)	AGCGCAGTCTTACCGAAGG	TCGCTGCTTTCATACTGAACTTT	12558
Snai2 (Slug)	TGGTCAAGAAACATTTCAACGCC	GGTGAGGATCTCTGGTTTTGGTA	20583
Gapdh (GAPDH)	AGGTCGGTGTGAACGGATTTG	TGTAGACCATGTAGTTGAGGTCA	14433
Il6 (IL-6)	TAGTCCTTCCTACCCCAATTTCC	TTGGTCCTTAGCCACTCCTTC	16193
Il23 (IL-23)	ATGCTGGATTGCAGAGCAGTA	ACGGGGCACATTATTTTTAGTCT	83430
Tgfb1 (TGF-β1)	CTCCCGTGGCTTCTAGTGC	GCCTTAGTTTGGACAGGATCTG	21803
Tnf (TNF-α)	CCCTCACACTCAGATCATCTTCT	GCTACGACGTGGGCTACAG	21926
Il1a (IL-1α)	CGTCAGGCAGAAGTTTGTCA	TGATGAGTTTTGGTGTTTCTGG	16175
Il1b (IL-1β)	GCAACTGTTCCTGAACTCAACT	ATCTTTTGGGGTCCGTCAACT	16176

Mohanasundaram P#, Coelho-Rato LS#, Modi MK, Urbanska M, Lautenschläger F, Cheng F, Eriksson JE. 2022. Cytoskeletal vimentin regulates cell size and autophagy through mTORC1 signaling. *PLOS Biology* 20:e3001737. # Equal contributions

II

PLOS BIOLOGY

RESEARCH ARTICLE

Cytoskeletal vimentin regulates cell size and autophagy through mTORC1 signaling

Ponnuswamy Mohanasundaram[1,2☯], Leila S. Coelho-Rato[1,2☯], Mayank Kumar Modi[1,2], Marta Urbanska[3,4¤], Franziska Lautenschläger[5,6], Fang Cheng[1,2,7], John E. Eriksson[1,2]*

1 Turku Bioscience Centre, University of Turku and Åbo Akademi University, Turku, Finland, **2** Cell Biology, Faculty of Science and Engineering, Åbo Akademi University, Turku, Finland, **3** Biotechnology Center, Center for Molecular and Cellular Bioengineering, Technische Universität Dresden, Dresden, Germany, **4** Max Planck Institute for the Science of Light & Max-Planck-Zentrum für Physik und Medizin, Erlangen, Germany, **5** Saarland University, NT Faculty, Experimental Physics, Saarbrücken, Germany, **6** Center for Biophysics, Saarland University, Germany, **7** School of Pharmaceutical Sciences (Shenzhen), Shenzhen Campus of Sun Yat-sen University, Shenzhen, Guangdong, P.R. China

☯ These authors contributed equally to this work.
¤ Current address: Department of Physiology, Development and Neuroscience, University of Cambridge, Cambridge, United Kingdom
* john.eriksson@bioscience.fi

Citation: Mohanasundaram P, Coelho-Rato LS, Modi MK, Urbanska M, Lautenschläger F, Cheng F, et al. (2022) Cytoskeletal vimentin regulates cell size and autophagy through mTORC1 signaling. PLoS Biol 20(9): e3001737. https://doi.org/10.1371/journal.pbio.3001737

Academic Editor: Alex P. Gould, The Francis Crick Institute, UNITED KINGDOM

Received: December 30, 2021

Accepted: July 1, 2022

Published: September 13, 2022

Peer Review History: PLOS recognizes the benefits of transparency in the peer review process; therefore, we enable the publication of all of the content of peer review and author responses alongside final, published articles. The editorial history of this article is available here: https://doi.org/10.1371/journal.pbio.3001737

Data Availability Statement: The authors confirm that all data underlying the findings are fully available without restriction. Flow cytometry files are available in the Flowrepository database https://

Abstract

The nutrient-activated mTORC1 (mechanistic target of rapamycin kinase complex 1) signaling pathway determines cell size by controlling mRNA translation, ribosome biogenesis, protein synthesis, and autophagy. Here, we show that vimentin, a cytoskeletal intermediate filament protein that we have known to be important for wound healing and cancer progression, determines cell size through mTORC1 signaling, an effect that is also manifested at the organism level in mice. This vimentin-mediated regulation is manifested at all levels of mTOR downstream target activation and protein synthesis. We found that vimentin maintains normal cell size by supporting mTORC1 translocation and activation by regulating the activity of amino acid sensing Rag GTPase. We also show that vimentin inhibits the autophagic flux in the absence of growth factors and/or critical nutrients, demonstrating growth factor-independent inhibition of autophagy at the level of mTORC1. Our findings establish that vimentin couples cell size and autophagy through modulating Rag GTPase activity of the mTORC1 signaling pathway.

Introduction

Cell size regulation is intricately related to nutrient availability and the rate by which macromolecules are synthesized [1]. To maintain stable cell growth, cells require nutrients and growth factors. On the other hand, when cells are deprived from nutrients or growth factors, or if they are exposed to stress, cell growth will be inhibited and autophagy will be triggered in order to recycle cellular components to ensure cell survival. These processes, both cell growth and autophagy, are primarily governed by the mechanistic target of rapamycin kinase complex 1 (mTORC1) signaling complex. mTORC1 acts as central signaling hub in regulating cell size

flowrepository.org/id/FR-FCM-Z5FK. The gating strategy used to analyze the cell populations is deposited in Figshare (https://doi.org/10.6084/m9.figshare.20024534.v1). All other relevant data are within the paper and its Supporting Information files.

Funding: This study was supported by following funders below: Academy of Finland #317867 (https://www.aka.fi/en/) to JEE, Sigrid Jusélius Foundation (https://www.sigridjuselius.fi/en/) to JEE, Magnus Ehrnrooth Foundation (https://www.magnusehrnroothinsaatio.fi/en/) to PM, LSCR, The Endowment of the Åbo Akademi University (https://stiftelsenabo.fi/) to JEE, K. Albin Johanssons stiftelse (https://www.foundationweb.net/johansson/) to PM, LSCR, Maud Kuistila Memorial Foundation (https://mkmsaatio.fi/en/the-maud-kuistila-memorial-foundation/) to LSCR, Liv och Hälsa Foundation (http://www.livochhalsa.fi/) to PM, Otto A Malm Foundation (https://en.ottomalm.fi/) to LSCR, Finnish Cultural Foundation (https://skr.fi/en) to LSCR, Swedish Cultural Foundation (https://www.kulturfonden.fi/in-english/) to LSCR, Ella and Georg Ehrnrooth Foundation (https://www.ellageorg.fi/en) to LSCR, The Foundation "Konung Gustaf V:s och Drottning Victorias Frimurarestiftelse" (https://www.kungahuset.se/kungliga-stiftelser/forskning) to JEE, The DFG German Research Foundation # CRC 1027(https://www.dfg.de/en/) to FL. The funders had no role in study design, data collection and analysis, decision to publish, or preparation of the manuscript.

Competing interests: The authors have declared that no competing interests exist.

Abbreviations: BMDCs, bone marrow-derived dendritic cells; EAAs, essential amino acids; EMT, epithelial to mesenchymal transition; FCS, fetal calf serum; IFs, intermediate filaments; mTORC1, mechanistic target of rapamycin kinase complex 1; NEAAs, non-essential amino acids; PFA, paraformaldehyde; RT-DC, real-time deformability cytometry; SFM, serum-free media.

and metabolism by sensing and coordinating stimuli derived from nutrients, energy, stress, and growth factors [2]. Amino acids mediate mTORC1 signaling through Rag GTPases: Presence of amino acids activate Rag GTPases leading to recruitment of mTORC1 to the lysosomal membrane where it is activated by Rheb [3–5]. This allows mTORC1 to promote protein synthesis by controlling downstream effectors, 4-EBP1 and p70S6K [6] and by inhibiting autophagy via phosphorylation of ULK1, a known promoter of autophagy [7–9].

Vimentin, an intermediate filaments (IFs) protein, has been reported to act as signaling scaffold in key cellular processes required to maintain tissue integrity and facilitate tissue repair [10,11]. These include cell migration, adhesion, proliferation, and invasion [12]. In this respect, vimentin is a well-established marker for epithelial to mesenchymal transition (EMT), a crucial step in wound healing and metastasis [13]. Vimentin-deficient (Vim −/−) mice exhibit delayed wound healing due to defects in EMT signaling, cell migration, and cell proliferation [14]. Furthermore, vimentin regulates autophagy by forming a complex with the autophagy regulator Beclin and the adaptor protein 14-3-3 [15]. Another link between cell size and vimentin was provided by a recent study showing that Vim −/− mice have deficient accumulation of body fat [16] and by the first report on a human vimentin mutation leading to lipodystrophy [17]. Keratin 17, another member of the IF family, was implicated in cell size signaling, as mouse-derived skin keratinocytes lacking keratin 17 are smaller than corresponding WT cells and display lower AKT/mTOR activation [18]. Related to all these studies, we report here that cell size regulation is coupled to vimentin, both in terms of enlargement and reduction.

Results and discussion

Loss of vimentin reduces cell size

When reporting that vimentin has a role in fibroblast proliferation and in EMT [14,19], we observed that not only do Vim −/− fibroblasts grow slower, but also they were significantly smaller (S1 Video). Correspondingly, when examining the Vim −/− mice in greater detail, we observed that they were leaner, as reflected in remarkable reductions in weight, body mass index, as well as Lee's index (Fig 1A–1C), in line with an initial recent report [16]. These mice also had markedly lower fat content (Fig 1D) and smaller size of adipocytes (Fig 1E). Likewise, some of the organs (heart and kidney) were also smaller in size (Fig 1F). As all these effects point toward a potential disturbance in cell size regulation, we quantified in detail the effects of vimentin on cell size. We found that Vim −/− MEFs are significantly smaller than WT MEFs (Fig 2A and 2B). This effect was seen in cells in their active growth phase and cells in confluent state (S1 Video), indicating that the effect is not coupled to cell spreading. To eliminate the effect of cell spreading, we next measured the cell volume of trypsinized MEFs and found that the volume of Vim −/− MEFs is considerably lower than that of WT MEFs (Fig 2C and 2D). To minimize cell cycle-dependent size variation, we employed thymidine-induced cell cycle arrest, which revealed an even more pronounced cell volume reduction in the Vim −/− MEFs as compared to the WT MEFs, demonstrating that the size effect on cell volume is cell cycle independent (Fig 2E). To ensure that these effects were not specific for the immortalized MEFs, we assessed the size of primary MEFs isolated from WT and Vim −/− mice, which showed a similar size reduction in the Vim −/− primary MEFs (Fig 2F). We also investigated the size of primary bone marrow-derived dendritic cells (BMDCs) using a high-throughput microfluidics-based method [20] to compare the results acquired from adherent fibroblasts with a non-adherent and spherical cell type. These cells possess a less extensive cytoskeleton, which implies that the possibility of mere size effects from removing vimentin as a cytoskeletal element is minimized. Furthermore, we used a

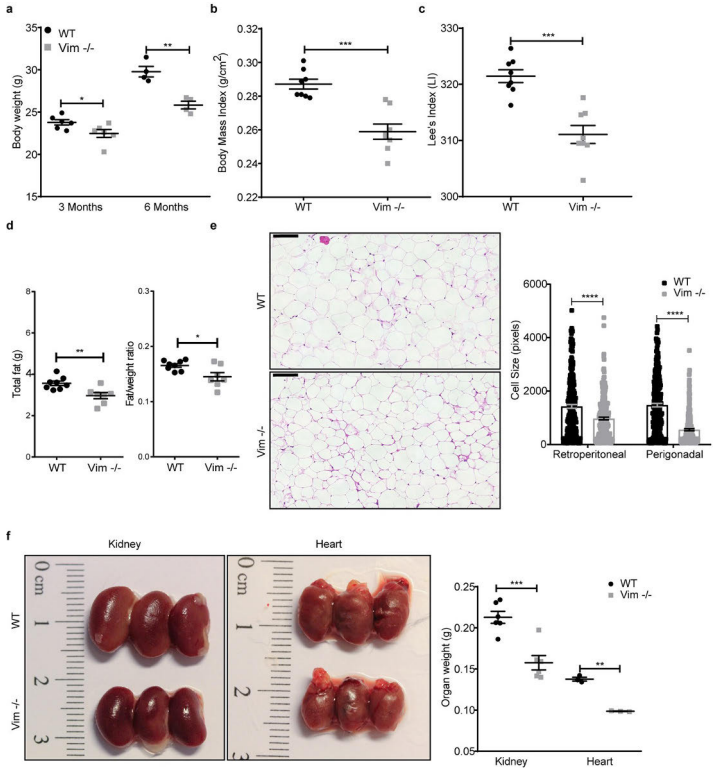

Fig 1. Vim −/− mice are smaller than WT. (a) Body weight of WT and Vim −/− male mice of 3 ($n = 6$) and 6 months old ($n = 4$). (b) BMI and (c) Lee's indexes were calculated for 6 months old mice ($n = 8$). (d) Total fat mass determined by EcoMRI and ratio of fat/weight of 6 months old male mice ($n = 7–8$). (e) Micrograph of adipocytes from 3 months old WT and Vim −/− male mice. The size of retroperitoneal and perigonadal adipocytes were quantified using Fiji ($n = 3$, 250 cells in total). (f) Organ weight of kidney ($n = 6$) and heart ($n = 3$) from 3 months old male mice. The results are presented in the form of mean ± standard deviation of the mean of the biological replicates. Scale bar = 100 μm, $^{*}p < 0.05$; $^{**}p < 0.01$, $^{***}p < 0.001$, $^{****}p < 0.0001$. The data underlying the graphs shown in Fig 1A–1F can be found in S1 Data.

https://doi.org/10.1371/journal.pbio.3001737.g001

microfluidic method to image the cells not only in the initial state, but also upon deformation in a narrow constriction of a microfluidic channel, where cytoskeletal structures are strained. Consistently with the above results, BMDCs lacking vimentin showed decreased size in both normal and deformed state (S1a and S1b Fig). These results emphasize that the vimentin-dependent effect on cell size is a generic effect irrespective of cell type. Furthermore, these results do not support the assumption of the cell size reduction stemming merely from the loss of the cytoskeletal component. To demonstrate that the effects were due to vimentin, we also show that the reduced cell volume could be rescued by reintroducing WT vimentin into Vim −/− MEFs (Fig 2G and 2H).

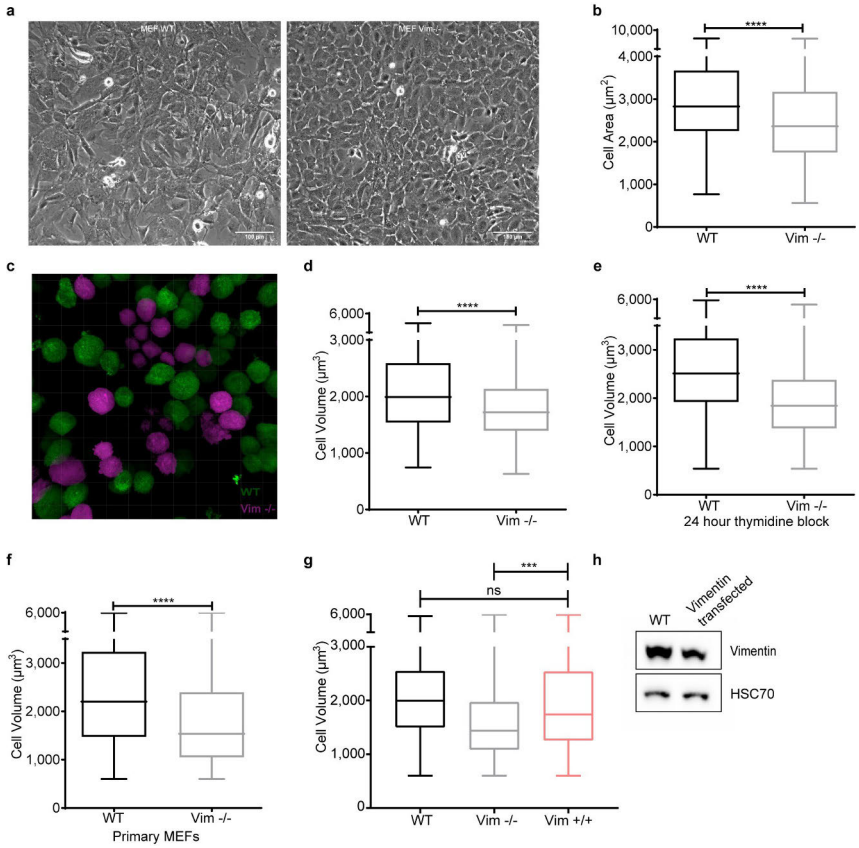

Fig 2. Loss of vimentin reduces cell size. (**a**) Phase contrast representative images of WT and Vim −/− MEFs (scale bar = 100 μm). (**b**) Distribution of the cell area obtained from phase contrast images measured using Fiji ($n = 3$). (**c**) Micrograph of WT (green) and Vim −/− (magenta) MEFs image made with Imaris software for cell volume analysis. (**d**) Cell volume distribution of WT and Vim −/− MEFs obtained from z-stacks from cells in suspension stained with CellTracker ($n = 3$). (**e**) Cell volume distribution of WT and Vim −/− cells treated with 1 mM of thymidine for 24 hours ($n = 3$). (**f**) Cell volume distribution of primary MEFs isolated from WT and Vim −/− mice ($n = 3$). (**g**) Cell volume distribution of WT, Vim −/−, and pCMV script-vimentin transfected (48 hours post transfection) in Vim −/− MEFs ($n = 3$). (**h**) Western blot analysis of WT and Vim −/− MEFs transfected with wild-type vimentin. $^{***}p < 0.001$, $^{****}p < 0.0001$. The data underlying the graphs shown in Fig 2B and 2D–2G can be found in S1 Data.

https://doi.org/10.1371/journal.pbio.3001737.g002

mTORC1 activation is impaired in Vim −/− MEFs

As cell size is tightly regulated by nutrients and growth factors [1], we wanted to assess whether the effect seen on cell size is linked to these stimuli. To this end, cells were serum starved for 2 to 3 days, then transferred to fresh serum-free media, and subsequently stimulated with insulin or fetal calf serum (FCS) for 24 hours. Importantly, we found that serum starvation reduced the size of WT MEFs to the same as Vim −/− MEFs (Fig 3A). Stimulation with insulin only, which rules out the influence of other growth factors, increased cell size only in WT MEFs and

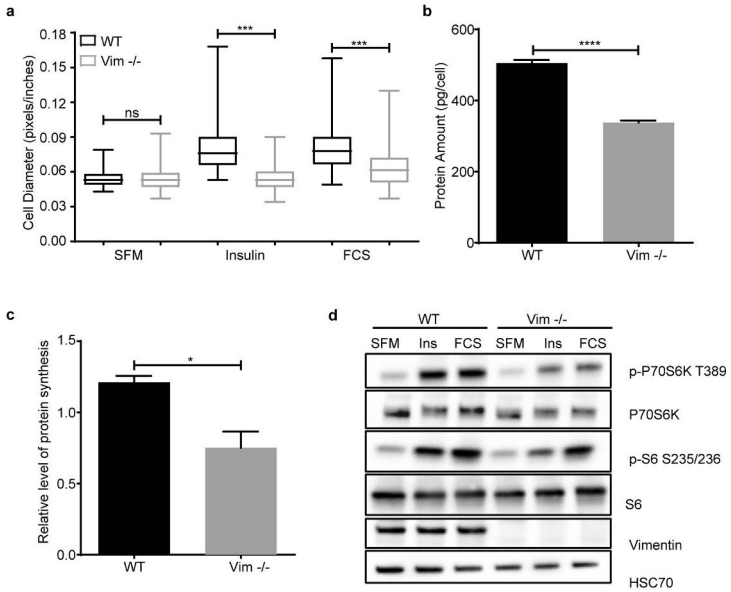

Fig 3. mTORC1 activation is impaired in Vim −/− MEFs. (**a**) Distribution of the cell diameter of WT and Vim −/− MEFs serum starved for 2 to 3 days and treated with 100 μg/ml insulin or 5% FCS for 24 hours ($n = 3$). (**b**) Protein amount per cell is represented as mean ± SEM of protein concentration. A same number of cells were lysed, and protein concentration was measured using a commercial BCA kit ($n = 3$). (**c**) Protein synthesis is represented as mean ± SEM of WT and Vim −/− MEFs stimulated with insulin for 30 minutes and it was measured by using the Click-iT HPG Alexa Fluor Protein Synthesis Assay Kit ($n = 3$). Protein synthesis was quantified using the mean fluorescence intensity normalized to the serum-starved treatment. (**d**) Western blotting analysis of serum-starved cells (overnight) treated with 100 nM of insulin or 5% serum for 15 minutes ($n = 3$). $^{*}p < 0.05$, $^{***}p < 0.001$, $^{****}p < 0.0001$, ns = nonsignificant. The data underlying the graphs shown in Fig 3A–3C can be found in S1 Data. SFM, serum-free media; FCS, fetal calf serum; mTORC1, mechanistic target of rapamycin kinase complex 1.

https://doi.org/10.1371/journal.pbio.3001737.g003

not in Vim −/− MEFs (Fig 3A). Consistently, when the cells were stimulated with FCS, there was a significant increase in WT MEFs, whereas Vim −/− MEFs were unaffected (Fig 3A). Our results show that the reduction in cell size in Vim −/− MEFs is linked to a disruption in insulin-dependent signaling. Thus, the smaller size stems from abrogation of the cellular signaling mechanisms regulating this attribute and not from structural effects of a missing cytoskeletal component. Since cell size depends on the balance between synthesis and degradation of macromolecules [1], we measured protein amount per cell and found that it was significantly lower in Vim −/− MEFs (Fig 3B), indicating that the reduction in cell size is directly coupled to the anabolic state of the cells. To link this observation to growth signaling, we measured the level of protein synthesis after insulin stimulation and observed that it was significantly lower in Vim −/− MEFs (Fig 3C). These results demonstrate that vimentin participates in signaling stimulating cell size. Interestingly, starvation reduced the size of WT MEFs to the size of vimentin-deficient cells, while the size of the Vim −/− MEFs was not affected. This implies that the Vim −/− MEFs behave as if they would be in a compromised nutritional state already without starvation, due to deficient nutrient-coupled signaling.

It is well established that mTORC1 is one of the main pathways regulating cell size and metabolism in response to nutrients, growth factors, and other extracellular cues [21]. To investigate the relationship between mTORC1 signaling and the role of vimentin in cell size, we analyzed mTORC1 activity after overnight serum starvation of cells and subsequent stimulation with insulin or FCS for 15 minutes. Intriguingly, we found that already without stimulation, the phosphorylation of mTORC1 downstream targets were lower in Vim −/− MEFs. Strikingly, Vim −/− MEFs stimulated with insulin or FCS showed only negligible mTORC1 activation (Fig 3D), indicating that the observed faulty cell size signaling is due to a defect in mTORC1 activation. Together, these results show that the cell size reduction in Vim −/− cells is due to abrogated mTORC1 signaling.

Vimentin modulates the mTORC1 pathway through nutrient and insulin signaling

Along with insulin and growth factor signaling, mTORC1 is activated by nutrients [6]. To understand how the combination of nutrients and insulin signaling modulates vimentin-mediated mTORC1 signaling, we starved the cells for 1 hour in culture media without amino acids, glucose, and serum, followed by stimulation with amino acids L-glutamine with minimum essential amino acids (EAAs) alone or with non-EAAs, glucose, and insulin. As Vim −/− MEFs displayed a striking defect in the insulin-mediated stimulation of mTORC1 signaling, we first studied what are the differences in the presence of insulin while the nutrient sources are varied (Fig 4A). By maximal stimulation of insulin-mediated signaling, we wanted to reveal possible differential effects of variable nutrient sources and, in this way, examine the upstream parts of the insulin signaling pathway. The lack of a difference in AKT phosphorylation (Fig 4A), implies that vimentin does not regulate mTORC1 signaling in the upstream parts of the pathway. Importantly, when examining the downstream targets, we saw that when insulin signaling is pushed to the maximum, the downstream signaling is significantly suppressed regardless of the nutrient source (Fig 4A). This outcome demonstrates that the capacity of insulin signaling to amplify the mTORC1 pathway is always dependent on vimentin, regardless of which additional stimuli are provided by individual nutrients.

When examining the effect of nutrients alone, the overall finding is that in Vim −/− fibroblasts, there is very little signaling passing down to the targets downstream of mTORC1 (Fig 4B). While the addition of glucose to WT MEFs boosted the amino acid-mediated activation of P70S6K and the ribosomal protein S6, this amplification was basically absent in Vim −/− MEFs (Fig 4B). Although, the S6 activation stayed overall at very low levels in the Vim −/− MEFs, some residual S6 activation could be observed, with slight variation between different nutrient treatments (Fig 4B). The phosphorylation level of the mTORC1 downstream target 4EBP1 is also reduced in Vim −/− MEFs (Fig 4B). 4EBP1 is an inhibitory protein, whose functions are regulated by mTORC1-mediated phosphorylation. In a hypophosphorylated state, 4EBP1 blocks protein synthesis by binding to the eIF4E complex. mTORC1 inhibits this interaction through phosphorylation and promotes protein synthesis [2,22]. Importantly, we were able to rescue the phosphorylation of S6 in Vim −/− MEFs by transfecting WT vimentin (S1C–S1E Fig). Together, these results imply that vimentin deletion abrogates mTORC1 signaling impairing the phosphorylation of both S6K and 4EBP1, which are both likely to contribute to the reduced protein synthesis rates in the Vim −/− cells, with the consequent reduction in cell size.

To verify that only mTORC1 downstream signaling is affected, we performed the same experiment on cells treated with 100 nM of rapamycin, an inhibitor of mTORC1. We found that this treatment inhibits mTORC1 activation in WT MEFs and the residual mTORC1

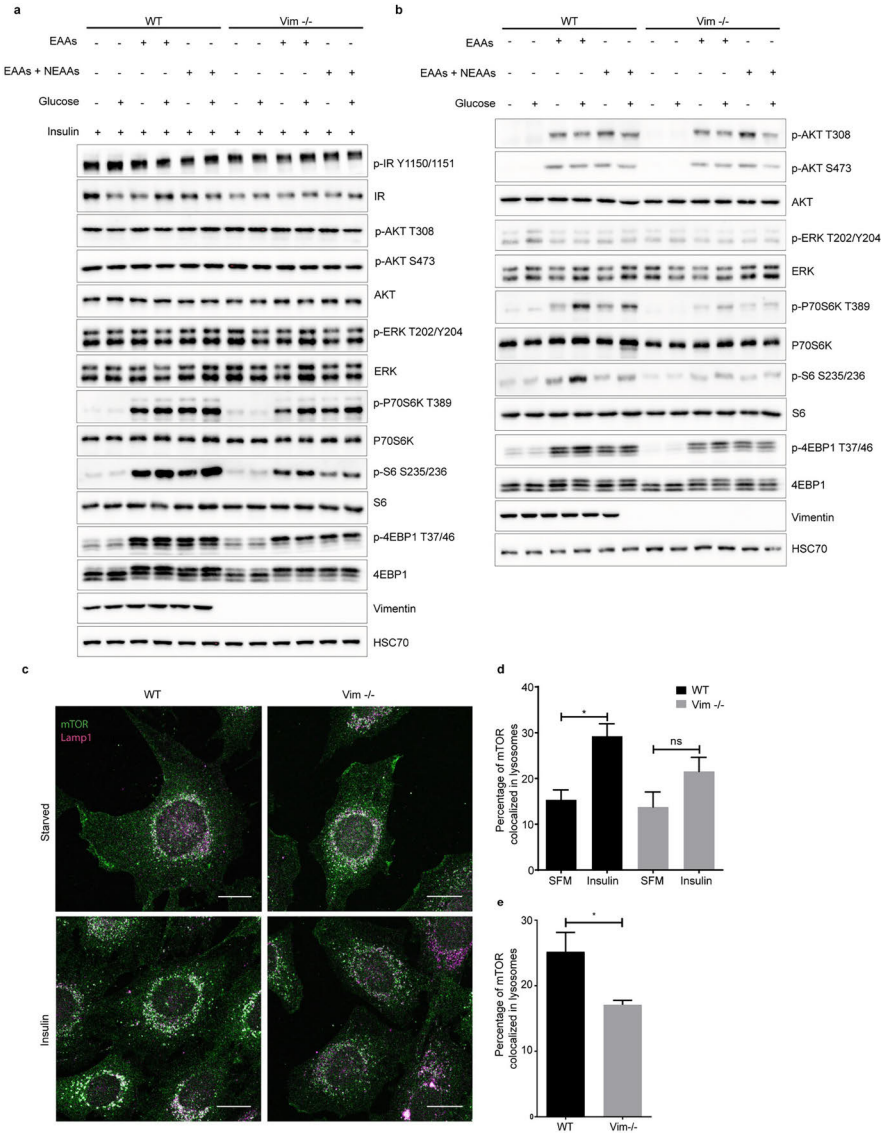

Fig 4. Vimentin modulates the mTORC1 pathway through nutrient and insulin signaling. (**a**) Western blot analysis of WT and Vim −/− MEFs starved with RPMI media lacking amino acids, glucose, and growth factors for 1 hour, followed by a 30-minute stimulation with 1 mM L-glutamine plus 1× EAAs alone or with NEAAs, plus 2.5 mM glucose and 100 nM insulin ($n = 3$). (**b**) Same experiment as in (**a**) performed without insulin. (**c**) Representative images of WT and Vim −/− MEFs serum starved overnight and stimulated with 100 nM insulin for 15 minutes. The cells were stained for mTOR and the lysosomal marker LAMP1 (scale bar = 20 μm). (**d**) The colocalization

analysis is represented as mean ± SEM of the percentage of colocalized pixels before and after insulin stimulation and it was performed using BioImageXD ($n = 3$). (**e**) Same as in (**d**) but in steady-state conditions. $^{*}p < 0.05$, ns = nonsignificant. The data underlying the graphs shown in Fig 4D and 4E can be found in S1 Data. SFM, serum-free media; EAAs, essential amino acids; NEAAs, Non essential amino acids; mTORC1, mechanistic target of rapamycin kinase complex 1.

https://doi.org/10.1371/journal.pbio.3001737.g004

activation in Vim −/− MEFs (S2A and S2B Fig), validating that vimentin modulates mTORC1 activation by regulating its capability to activate downstream effectors. Altogether, these results show that vimentin is required for the phosphorylation of mTORC1 downstream effectors to take place, pointing to a role of vimentin in mTORC1 activation itself.

S6 is phosphorylated at serine 234/235 through P70S6K, which is downstream of the AKT-mTORC1 signal transduction pathway [21]. S6 can also be activated by P90S6K, a downstream effector of ERK signaling [23]. Therefore, we used AKT and ERK kinase inhibitors to determine whether these kinases play a role in amplifying S6 phosphorylation in a vimentin-dependent manner. We treated WT and Vim −/− MEFs with either an ERK or AKT inhibitor after 40 minutes of full starvation and performed the nutrient and insulin stimulation protocol described before. In both WT and Vim −/− MEFs, AKT inhibition completely blocked AKT and its downstream mTORC1 signaling, including phosphorylation of P70S6K, and S6 (S2C Fig). However, ERK inhibition had no effect on mTORC1 downstream signaling (S2C Fig). Thus, vimentin modulates mTORC1 downstream signaling independently of ERK signaling and the phosphorylation of S6 requires an active mTORC1.

mTOR translocation to lysosomes is impaired in Vim −/− MEFs

Since the effect of vimentin was narrowed down to direct targeting of mTORC1, we wanted to examine the mechanisms underlying this effect. In this respect, mTORC1 translocate from the cytosol to lysosomes for its activation [5,24]. This is an essential step for mTORC1 activation by Rags [24]. Therefore, we measured mTORC1 translocation in serum-starved MEFs upon insulin stimulation using confocal imaging and colocalization analysis. While insulin stimulation strongly increases colocalization of mTOR with the lysosomal marker LAMP1 in WT MEFs, there was no significant colocalization increase in Vim −/− MEFs (Figs 4C, 4D and S3A). Moreover, also at steady-state conditions, colocalization of mTOR to lysosomes is significantly reduced in Vim −/− MEFs, when compared to their WT counterpart (Figs 4E and S3B). This demonstrates that the translocation machinery requires vimentin. Thus, vimentin has the ability to support mTORC1 localization to the lysosomal membrane. This modus operandi is in agreement with the established signaling functions of vimentin, which has been identified as a scaffolding system for many signaling events and pathways [25–28].

Constitutively active Rag GTPase rescues mTOR localization in Vim −/− MEFs

The level of amino acids in the cytosol and lysosomes determine mTORC1 translocation and activation. Rag GTPases sense the levels of amino acids in the cytoplasm and lysosomal lumen [5,29], leading to recruitment of mTORC1 to lysosomes for activation [29]. To understand the molecular mechanisms underlying the vimentin-mediated mTORC1 translocation, we measured the colocalization of mTOR on the lysosomal membrane upon transfection of WT Rag GTPase or constitutively active Rag GTPase, the latter which recruits mTOR to lysosomes even in the absence of amino acids [5,30]. Vim −/− MEFs shows significantly lower mTOR colocalization to the lysosome membrane than WT upon expression of exogenous WT Rag GTPase (Figs 5A, 5B and S4). Importantly, expression of constitutively active Rag GTPase rescued the mTOR colocalization in Vim −/− MEFs (Figs 5A, 5B and S4). Based on these results,

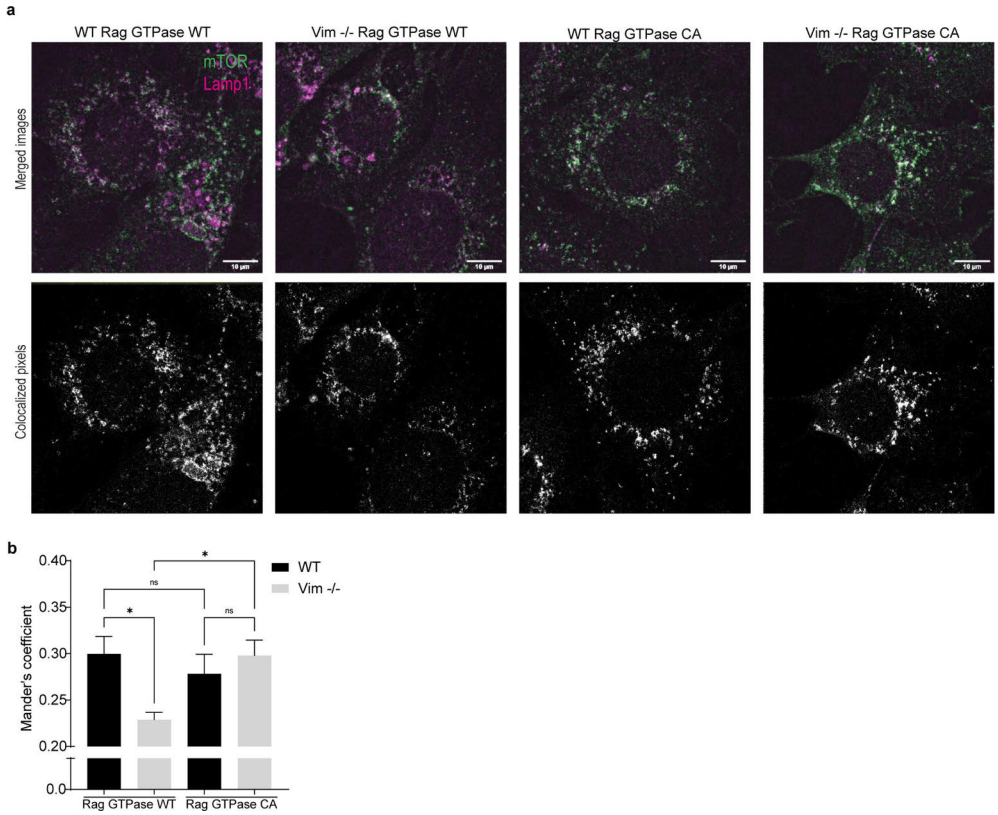

Fig 5. Constitutively active Rag GTPase rescues mTOR localization in Vim −/− MEFs. (**a**) mTOR and LAMP1 were stained in WT and Vim −/− MEFs transfected with either normal Rag GTPase or constitutively active Rag GTPase. Representative images show the merged channels of mTOR and LAMP1 (scale bar = 10 μm). (**b**) Quantification of mTOR and LAMP1 colocalization measured from the images in (a) using Fiji. Mander's coefficient is represented as mean ± SEM of mTOR colocalization on lysosome membrane ($n = 3$). $^{*}p < 0.05$, ns = nonsignificant. The data underlying the graphs shown in the Fig 5B can be found in S1 Data.

https://doi.org/10.1371/journal.pbio.3001737.g005

vimentin determines mTORC1 signaling by regulating Rag GTPase activation. Thus, vimentin could affect nutrient sensing, through which it modulates mTORC1 signaling.

Vimentin inhibits autophagy through mTORC1

As vimentin has been shown to regulate autophagy [15] and autophagy is also closely coupled to mTORC1 signaling, we wanted to determine whether the results we obtained with mTORC1 signaling could be coupled to the vimentin-mediated regulation of autophagy. During autophagy, LC3I, a cytosolic protein, is conjugated with phosphatidylethanolamine to form LC3-II, which is recruited to phagophores, then moved into autophagosomes and is finally degraded in autolysosomes. Thus, the autophagic flux can be obtained by measuring

the rate of conversion of LC3I to LC3II [31]. p62 interacts with autophagy substrates and it selectively transports ubiquitinated proteins to lysosomal cargo for autophagy, a process during which p62 also gets degraded. Therefore, inhibition of autophagy will increase p62 levels, while activation of autophagic flux will reduce the p62 levels [32]. Importantly, we observed that nutrient starvation significantly decreased p62 levels in Vim −/− MEFs, suggesting activation of the autophagic flux, with prominently lower p62 levels as compared to the samples from starved WT MEFs (Fig 6A). In Vim −/− MEFs, this could be partly inhibited in cells stimulated with insulin, amino acids, and glucose (Fig 6A). To further investigate the role of vimentin in autophagy, we subjected cells to depletion of various nutrient sources (glucose, EAAs or EAAs and NEAAs). WT MEFs appeared to be well protected against autophagic flux, as reflected by the steady levels of p62. Strikingly, in Vim −/− MEFs, the levels of p62 are significantly lower than in all the corresponding WT MEF samples, indicating that without vimentin, the cells are significantly more susceptible to autophagy (Fig 6B). Notably, the p62 depletion data can be coupled to the inhibition of the mTORC1 pathway (Fig 6B). To further strengthen these observations and to determine autophagic flux, we measured the conversion of the LC3I and LC3II by using a pMRX-IP-GFP-LC3-RFP-LC3ΔG vector. GFP-LC3 undergoes cleavage and enters lysosome during autophagy; however, RFP-LC3ΔG lacks the cleavage site and remains in the cytosol. In this way, the GFP/RFP fluorescent intensity ratio is a measure of the autophagic flux [33]. While starvation, surprisingly, increases the conversion of LC3I to LC3II in both WT and Vim −/− MEFs (Figs 6C, S5A and S5B), in Vim −/− MEFs, the rate of conversion is significantly faster. This suggests that Vim −/− MEFs cannot withstand limited nutrient levels and are more prone to autophagy than WT MEFs. Importantly, our results show that WT MEFs can sustain p62 levels even in the absence of insulin and that, conversely, Vim −/− MEFs activate autophagy even in the presence of nutrients (Fig 6B). Thus, the inhibition of autophagy we observe here takes place by mechanism different from the AKT and 14-3-3-dependent mechanism previously described [15], in which vimentin and Beclin 1 are phosphorylated by AKT [15]. This notion is especially relevant as in these experiments following nutrient starvation, we saw no difference in AKT activation [15]. It is well established that mTORC1 can be activated by nutrients alone [6] and that mTORC1 inhibits autophagy by phosphorylating ULK1 [8], the autophagy-activating kinase that is required to trigger autophagy by Beclin-1 phosphorylation [9]. To determine to what extent vimentin also regulates cell size through mTORC1-mediated regulation of autophagy, we assessed the ULK1 serine 757 phosphorylation level, the phosphorylation of which is mediated by mTORC1 to inhibit autophagy. We found that this phosphorylation level is reduced in Vim −/− MEFs, whereas in WT MEFs the phosphorylation is increased and sustained, both under stimulation (Fig 6A) and nutrient limitation (Fig 6D). This implies that vimentin controls autophagy through mTORC1-mediated phosphorylation of ULK1, leading to its inhibition. To examine this pathway in greater detail, we also tested whether normal cell volume could be rescued in Vim −/− MEFs using dominant-negative ULK1 K46N, which inhibits autophagy independently of mTORC1 [34]. Overexpressing dominant-negative ULK1 K46N did not rescue cell size in Vim −/− MEFs (S6 Fig). These results demonstrate that, although the Vim −/− are more prone to autophagy due to reduced mTORC1 activity, inhibiting autophagy through dn-ULK1 is not sufficient to increase cell size, but it would require up-regulation of mTORC1 activity. These results show that the vimentin-mediated regulation of mTORC1 activation will also control autophagy, but that autophagy alone is not the primary reason for the reduced cell size in Vim −/− cells but rather the inhibited protein synthesis due to inhibition mTORC1 signaling. Therefore, vimentin regulates both mTORC1-mediated protein synthesis as well as autophagic flux by mTORC1-mediated ULK1 inhibition.

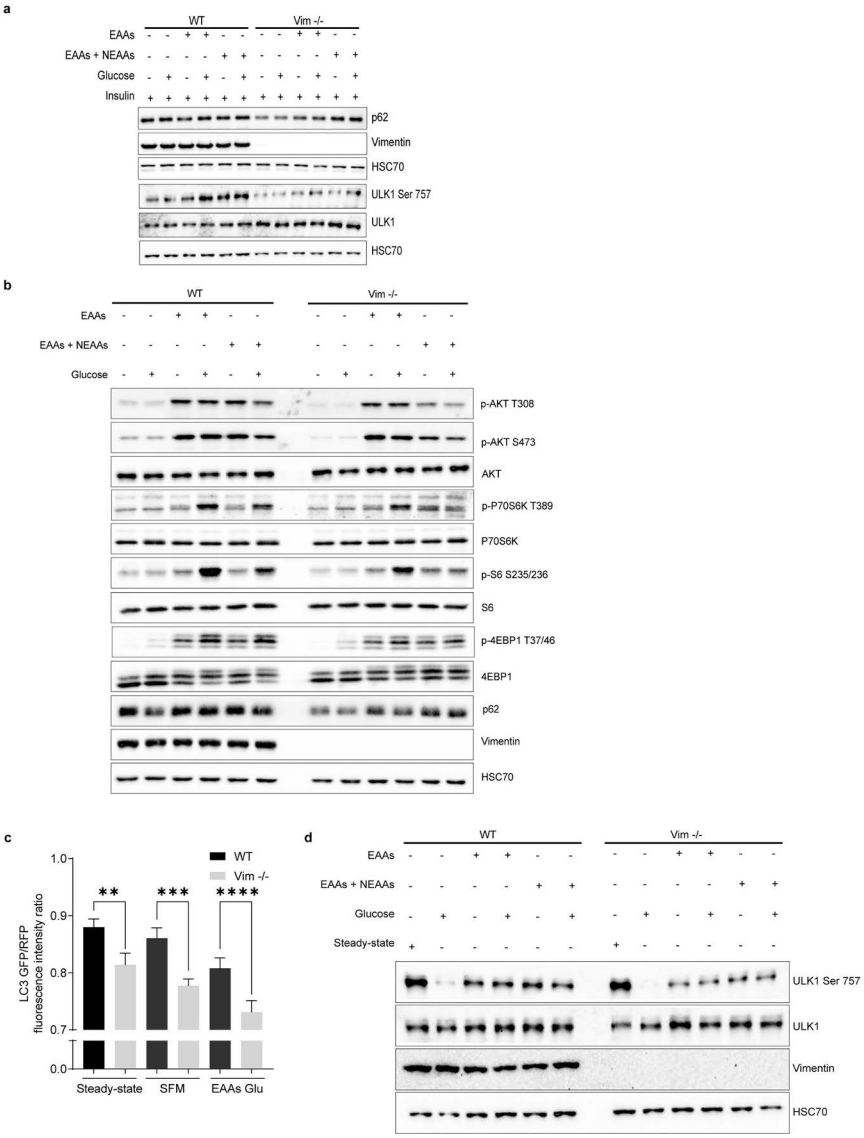

Fig 6. Vimentin protects MEFs from autophagy. (**a**) Western blot analysis of WT and Vim −/− MEFs starved with RPMI media lacking amino acids, glucose, and growth factors for 1 hour, followed by a 30-minute stimulation with 1 mM L-glutamine plus EAAs alone or with NEAAs and 2.5 mM glucose, 100 nM insulin ($n = 3$). (**b**) Western blot analysis of WT and Vim −/− MEFs grown 1 hour in RPMI media with different nutrients (1 mM of L-glutamine plus EAAs alone or with NEAAs and 2.5 mM glucose; $n = 3$). (**c**) Autophagic flux measured through LC3 GFP/RFP fluorescent intensity ratio in cells transfected with 7.5 μg of pMRX-IP-GFP-LC3-RFP-LC3ΔG. Graph represents

mean ± SEM of LC3 GFP and RFP fluorescence intensity ratio of WT and Vim −/− MEFs under normal conditions (steady state, DMEM with serum) or with either SFM or RPMI media lacking amino acids, glucose, and growth factors supplemented with 2 mM of L-glutamine, 1× EAAs and 2.5 mM glucose for 3 hours. Fluorescent intensities were measured with Fiji ($n = 3$). (**d**) Western blot analysis of WT and Vim −/− MEFs grown for 1 hour in normal DMEM with serum or RPMI media lacking amino acids, glucose, and growth factors supplemented with nutrients in different combinations (1 mM L-glutamine plus 1× EAAs alone or with NEAAs and 2.5 mM glucose, $n = 3$). $^{*}p < 0.05$, ns = nonsignificant. The data underlying the graphs shown in Fig 6C can be found in the S1 Data. EAAs, essential amino acids; NEAAs, Non essential amino acids; SFM, serum-free media.

https://doi.org/10.1371/journal.pbio.3001737.g006

Conclusions

Here, we unravel a novel role of vimentin in cell size regulation, as the whole cell size machinery seems to be guarded and concerted by the presence of vimentin. Moreover, we provide evidence that vimentin regulates these processes by mediating mTORC1 lysosomal localization and activation through Rag (Fig 7). We also show that vimentin thereby also regulates autophagy by mTORC1-mediated inhibition of the autophagy-activating kinase ULK1. During wound healing and regeneration, the presence of nutrients and growth factors is crucial for cell growth and proliferation. Fibroblasts are rapidly proliferating cells that are crucial for the formation of granulated tissue in injury areas [35]. In these dynamic but stressful conditions, vimentin levels and its organization are actively coordinated. Our results show that vimentin is the critical link between cell size signaling and other processes critical for repair. The advantage of a vimentin-based link to cell size signaling is that vimentin is also coupled to cytoskeleton-mediated sensing of cell shape [36] and to interactions with both the surface and other cells [11]. High expression of vimentin is a hallmark of many types of cancer cells. Providing an active regulation of cell size coupled to resistance to autophagy is, obviously, an additionally important and advantageous function of vimentin when present in cells in dynamic transition or in cancer cells.

Materials and methods

Plasmids and antibodies

The pCMV-script-vimentin plasmid was a kind gift from Professor Johanna Ivaska [37]. pCMV4-HA was a gift from Shao-Cong Sun (Addgene plasmid # 27553; http://n2t.net/addgene:27553; RRID:Addgene_27553) [38]. pME18S-3HA-mULK1(K46N) was a gift from Masaaki Muramatsu (Addgene plasmid # 22897; http://n2t.net/addgene:22897; RRID:Addgene_22897) [39]. The antibodies used for the experiments are listed in S1 Data.

Mice and ethical statement

WT and Vim −/− mice were generated from heterozygous mice by crossing 129/SV × C57BL/6 strains [14]. The mice were held at the central animal laboratory, Biocity unit (KEK/2010-2112-Eriksson) and it follows good laboratory practice and it routinely inspect by Finish Medicines Agency (Fimea) to monitor standard operating procedures. Mice were fed with standard diet and free access to water. Mice were sacrificed by cervical dislocation. All experiments were performed according to the guidelines set by the Ethical Committee of central animal laboratory. Genotyping was determined by polymerase chain reaction. The body weight was measured at 3 ($n = 6$) and 6 ($n = 4$) months old. BMI and Lee's index of 6 months old mice ($n = 8$) were calculated accordingly. The total fat mass was measured by EcoMRI and normalized to the body weight ($n = 7$ to 8). To evaluate organ size and weight, WT and Vim −/− mice of 3 months of age ($n = 3$) were sacrificed. The white adipose tissues were fixed in 4% paraformaldehyde (PFA) and embedded in paraffin. The sectioning and hematoxylin-eosin staining was carried out by Lounais-Suomen pathology laboratory. The sections were imaged using the

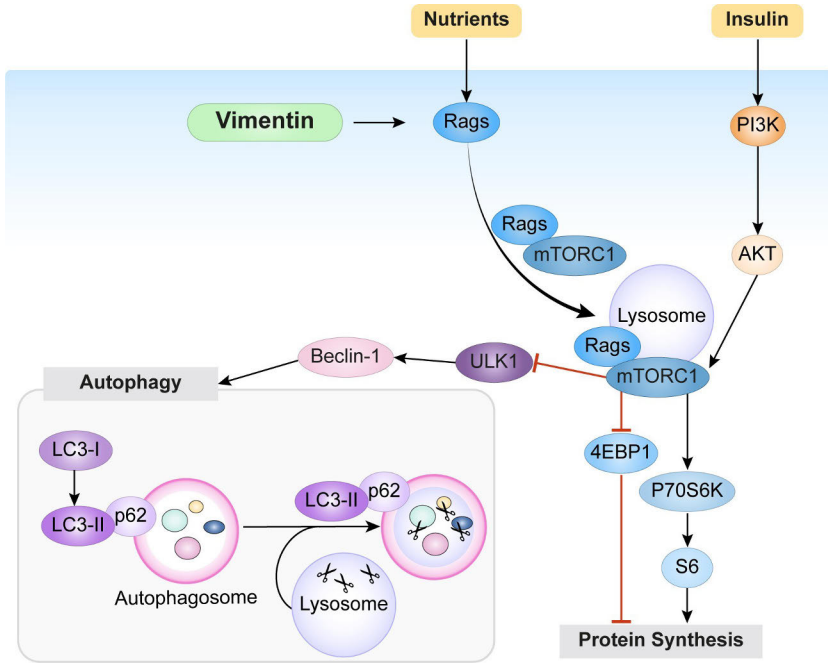

Fig 7. Vimentin regulates mTORC1 signaling by facilitating mTORC1 localization to lysosomes. A simplified scheme of the mTORC1 signaling system. Our results demonstrate that in the presence of nutrients, vimentin facilitates mTORC1 activation by regulating Rag GTPase activation. This results in the phosphorylation of 4EBP1 and P70S6K downstream targets, which lead to protein synthesis. Moreover, activation of mTORC1 results in decreased autophagy, as demonstrated by higher levels of the autophagic flux indicator p62 and reduced LC3I conversion to LC3II. As this autophagy inhibition works even under nutrient-starved condition, in the absence of AKT activation, the results imply that vimentin inhibits autophagy by mTORC1-mediated inhibition of ULK1-Beclin pathway. In this way, vimentin promotes cell size in 2 directions: by boosting protein synthesis through mTORC1 activation and by inhibiting of protein degradation through inhibition of autophagic flux. mTORC1, mechanistic target of rapamycin kinase complex 1.

https://doi.org/10.1371/journal.pbio.3001737.g007

Panoramic Slide Scanner (3DHISTECH, Hungary) and Fiji was used to measure cell size (n = 3, 250 cells in total).

Cell culture and treatments

SV40-immortalised WT and Vim −/− MEFs were cultured in Dulbecco's modified media (DMEM, Sigma #D6171) supplemented with 10% fetal bovine serum (FBS, Biowest #S1810), 2 mM of L-glutamine (Biowest #X0550), 100 U/ml of penicillin, and 100 μg/ml of streptomycin (Sigma #P0781) at 37˚C in a 5% CO_2 incubator and passaged when they were about 80% confluent.

To test if the size phenotype could be rescued, Vim −/− MEFs were seeded in 6-well plates on the day prior to transfection. Using XfectTM (Clontech Laboratories, United States of America #631318) 7.5 μg of pCMV script-vimentin, pCMV4-HA and pME18S-3HA-mULK1 K46N were transfected separately in Vim −/− MEFs according to instructions of the manufacturer. The cells were used for cell volume analysis 48 hours post-transfection.

To assess how growth factors affect the cell size in WT and Vim −/− MEFs, the cells were incubated in serum-free media (SFM) for 2 to 3 days. Then, the media was replaced with fresh SFM, and the cells were stimulated either 100 μg/ml insulin (Sigma #I0516) or 5% fetal calf serum (FCS, Biowest #S1710) for 24 hours. To study mTORC1 activation, 200,000 cells were seeded in 6-well plates and serum starved overnight. Next, the cells were treated either with 100 nM insulin or 5% FCS for 15 minutes. Alternatively, the cells were fully starved for 1 hour with RPMI media (Life Science #R9010-01) lacking glucose, amino acids, and serum. Then, the cells were treated for 30 minutes with 1 mM of L-glutamine plus 1× concentration of either minimum EAAs, (Thermo Fisher Scientific #11130036) or EAAs and non-essential amino acids (NEAAs) mix (1:1 mix of EAAs with NEAAs, Sigma #M7145) either in the presence or absence of 2.5 mM of glucose (Thermo Fisher Scientific #A2494001) for 30 minutes. This experiment was repeated with 100 nM of insulin along with amino acids and glucose. To further investigate mTORC1 signaling, the cells were treated with 100 nM of rapamycin (Tocris #1292) for 20 minutes. This was conducted after 40 minutes of full starvation and was followed by stimulation with amino acids, insulin, and glucose as described above. Alternatively, 2 other kinase inhibitors were used: 1 μm and 1.5 μm of AKT VIII (Calbiochem #124018) or 100 nM and 200 nM of trametinib (Selleckchem #GSK1120212). To study autophagy, 200,000 WT and Vim −/− were seeded in 6-well plates and incubated for 16 hours. On the next day, the media was replaced with RPMI media containing 1 mM glutamine plus EAAs, with or without NEAAs and glucose for 1 hour. The protein levels were evaluated using immunoblotting. To study the role of Rag GTPase in mTOR translocation, WT and Vim −/− MEFs were transfected with either 4.5 μg of pRK5-HA GST RagB WT (Addgene plasmid #19301; http://n2t.net/addgene:19301; RRID:Addgene_19301) and pRK5-HA GST RagC WT (Addgene plasmid #19304; http://n2t.net/addgene:19304; RRID:Addgene_19304) or 4.5 μg of pRK5-HA GST RagB 99L (Addgene plasmid #19303; http://n2t.net/addgene:19303; RRID:Addgene_19303) and pRK5-HA GST RagC 75L (Addgene plasmid #19305; http://n2t.net/addgene:19305; RRID:Addgene_19305) using Xfect (Clontech Laboratories, USA) according to manufacturer's instructions [5].

Primary MEFs isolation

The primary MEFs were isolated according to a previously described method [40]. Briefly, the mice were sacrificed 13 to 14 days post-coitum by cervical dislocation, the uterine horns were dissected, rinsed with 70% ethanol, and kept in PBS. Under the laminar hood, the embryos were separated, and both head and red organs of the embryos were stored for genotyping. The remaining tissue was washed with PBS and minced until it became possible to pipette it. The tissues were incubated for 15 minutes at 37˚C with 2 ml of 0.05% trypsin/EDTA containing 100 K units of DNaseI, and the cells were dissociated by pipetting every 5 minutes. Trypsin was inactivated by adding about 1 volume of freshly prepared DMEM complete media and the cells were centrifuged (100 g) for 5 minutes. The supernatant was carefully removed; the cell pellet was resuspended in pre-warmed DMEM complete media and plated approximately 1 embryo per plate.

Bone marrow-derived dendritic cells (BMDCs)

Primary dendritic cells were differentiated from bone marrow precursors isolated from WT and Vim −/− mice. The differentiation was performed using IMDM medium containing FCS (10%), glutamine (20 mM), penicillin–streptomycin (100 U/ml), 2-ME (50 μm) further supplemented with granulocyte-macrophage colony-stimulating factor (50 ng/ml)-containing supernatant obtained from transfected J558 cells, as previously described [41]. The semi-adherent

cell fraction, corresponding to the $CD86^+$ dendritic cells, was retrieved from the cell culture dishes at the differentiation days 10 to 12 by gentle flushing and used for the measurements. All cell culture reagents were purchased from Thermo Fisher Scientific (Waltham, Massachusetts, USA).

Cell area and diameter

Phase contrast images from WT and Vim −/− MEFs were taken using CellIQ (ChipMan Technologies, Finland) using a 10× objective. The cell area was manually measured using the freehand tool in Fiji ($n = 3$, 200 cells in total) [42]. Cell area of WT and Vim −/− BMDCs was evaluated based on images taken for undeformed (inlet) or deformed (using 2 different flow rates; fr1 = 0.16 μl/s and fr2 = 0.32 μl/s) cells in a real-time deformability cytometry (RT-DC) setup [20] using 40× objective (EC-Plan-Neofluar, 40×/0.75; #420360–9900, Zeiss, Germany). The RT-DC measurements were performed according to previously established protocol [43] using a 30-μm channel. The cell contours were identified using thresholded images, and the cell cross-sectional area was derived from a convex hull of the fitted contours. After the treatment, WT and Vim −/− MEFs were trypsinized and imaged under Lecia DMIL light microscope using 10× objective. The cell diameter was manually measured using the freehand tool in Fiji ($n = 3$, 50 cells in total).

Cell volume

Immortalized and primary WT and Vim −/− MEFs were grown in 6-well plates overnight. The samples were harvested and fixed with 3% PFA for 15 minutes and then stained with 2 μm of CellTracker fluorescent probes (Thermo Fisher Scientific #C34552). Z-stacks were taken using a Leica TCS SP5 Matrix confocal microscope with the 20× objective. The cell volume was measured using Imaris software 8.1 (BITPLANE, Switzerland). Three clones of MEFs were used for the analysis ($n = 3$, 1,800 to 1,900 cells in total). Cell volume analysis was also performed in cells treated for 24 hours with 1 mM thymidine ($n = 3$, 250 to 400 cells) (Sigma #T1895) and in Vim −/− MEFs transfected with pCMV-script-vimentin ($n = 3$, 1,000 to 1,300 cells). To measure cell volume in cells transfected with HA-tag-dnULK1 K46N or HA-tag without insert, cells were immunolabeled for the HA tag with a fluorescent dye Alexa Fluor 488 and stained with CellTracker Red CMTPX Dye (Thermo Fisher Scientific #C34552). Then, cells were imaged as we mentioned before and cell volume of transfected cells were measured by Fiji ImageJ using 3D object counter ($n = 3$, 300 to 600 cells in total). For WT and Vim −/− BMDCs, the volume was calculated by rotation of the 2D cell contours obtained from RT-DC measurements. RT-DC data were reanalyzed from recently published measurements [44]. The calculation was performed using ShapeOut software (ShapeOut 0.9.5; https://github.com/ZELLMECHANIK-DRESDEN/ShapeOut; Zellmechanik Dresden, Germany) according to a previously described approach [45].

Protein concentration

Three different WT and Vim −/− MEFs clones were seeded in 6-well plates and incubated overnight. Then, the cells were trypsinized and 3.0×10^5 cells were lysed for 1 hour at 4˚C in a buffer containing 150 mM NaCl, 1% Triton X-100, 0.2% SDS, 50 mM Tris (pH 8.0), and 0.5% of sodium deoxycholate. The protein concentration was measured using a BCA (Thermo Fisher Scientific #23227) according to the manufacturer's instructions. The protein concentration was normalized to the number of cells.

Immunoblotting

WT and Vim −/− MEFs (treated as described above) were washed 3 times with ice cold PBS and lysed with 3× sample buffer (0.625 M Tris-HCL (pH 6.8), 3% sodium dodecyl sulfate, 30% glycerol, 0.015% bromophenolblue, 3% β-mercaptoethanol). The lysates were heated for 10 minutes at 98˚C. The samples were separated by SDS-PAGE, transferred to nitrocellulose membranes (or methanol-activated polyvinylidene difluoride membranes for LC3), and blocked 1 hour with 5% milk in TBS 0.3% Tween20. The membranes were incubated with primary antibody overnight at 4˚C. All primary antibodies used for western blot were diluted 1:1,000 in TBS 0.3% Tween20 3% BSA 0.02% sodium azide. The membranes were washed 20 minutes with TBS 0.3% Tween20 and incubated for 1 hour at room temperature with secondary antibody (diluted 1:10,000 in TBS 0.3% Tween20 5% milk). The antibody signals were probed with enhanced chemiluminescence (Amersham #RPN2236) and detected in a BioRad Chemidoc machine.

Immunostaining

For the mTOR translocation assay, WT and Vim −/− MEFs were seeded on top of glass coverslips and serum starved overnight. The cells were treated with 100 nM of insulin for 15 minutes, were washed once with PBS, and were fixed with 3% PFA in PBS for 15 minutes at room temperature. Then, the cells were permeabilized with PBS 0.2% Triton X-100 for 5 minutes and blocked with 3% BSA in PBS 0.2% Tween20 for 1 hour. The coverslips were incubated overnight in a humidified chamber with primary antibody diluted 1:200 (mTOR), 1:20 (LAMP1), and 1:2,000 (vimentin) in PBS 3% BSA 0.2% Tween20. On the next day, the coverslips were washed 3 times with PBS 0.2% Tween20, for 5 minutes each, and incubated with secondary antibody in PBS 3% BSA 0.2% Tween20 for 1 hour in the dark, at room temperature. The coverslips were washed as described before and dipped in Milli-Q water once. The excess water was removed, the coverslips were mounted on the slides with mowiol 4–88 and left to dry overnight. The imaging was performed using a Leica SP5 TCS confocal microscope with the 63× immersion oil objective numerical aperture 1.32. The colocalization analysis of LAMP1 and mTOR ($n = 3$, 12 to 15 cells per trial) was carried out with the colocalization tool on BioImageXD [46]. For the Rag activity experiment, cells were seeded on glass cover slips 24 hours after transfection and, on the next day, cells were fixed with 3% PFA. Cells were stained and imaged as described above. The antibody dilutions were as follows: 1:200 (mTOR), 1:20 (LAMP1), and 1:200 (HA-tag). Fiji JaCoP tool was used for the colocalization analysis of mTOR and LAMP1. This was performed in cells which expressed exogenous Rag GTPase by calculating the Mander's coefficient ($n = 3$, 8 to 12 cells per repeat).

Protein synthesis assay

WT and Vim −/− MEFs were seeded in 96-well plates and serum starved overnight. The assay was carried out using the Click-iT HPG Alexa Fluor Protein Synthesis Assay Kits (Thermo Fisher Scientific #C10428). Briefly, the media was changed to methionine-free media with 50 μm of a methionine analogue. The cells were treated with 100 nM of insulin for 30 minutes and were washed once with PBS. The cells were fixed with 3% PFA in PBS and permeabilized with PBS 0.3% Triton X-100. The Click-it reaction was prepared according to the instructions of the manufacturer and added to the cells for 30 minutes in dark. Then, the cells were washed and kept in PBS. The imaging was performed with Cell-IQ (Chip-Man Technologies, Finland) using the green channel and the 10× objective. The image analysis ($n = 3$, 100 cells in total) was carried out with the Cell-IQ Analyzer software by measuring the signal intensity.

Autophagy flux

To measure the autophagic flux, WT and Vim −/− MEFs were seeded in 6-well plates and allowed to grow overnight. Then, 7.5 μg of the pMRX-IP-GFP-LC3-RFP-LC3ΔG vector (Addgene plasmid # 84572; http://n2t.net/addgene:84572; RRID: Addgene_84572) was transfected using Xfect (Clontech Laboratories, USA) according to manufacturer's instructions. After 24 hours, cells were seeded on glass cover slips and, on the next day, switched to SFM (DMEM, Sigma #D6171) or RPMI media (Life Science #R9010-01) supplemented with 1 mM of L-glutamine plus minimum EAAs mix (Thermo Fisher Scientific #11130036) and 2.5 mM glucose (Thermo Fisher Scientific #A2494001) for 3 hours. Cells were fixed with 3% PFA for 15 minutes and imaged with Leica SP5 TCS confocal microscope under a 63× immersion oil objective with a numerical aperture of 1.32. In transfected cells, fluorescent intensity of GFP and RFP were measured with Fiji using the free hand tool, and ratios of GFP/RFP fluorescent intensity were calculated as a measure of autophagic flux ($n = 3$, 100 to 120 cells in total).

Flow cytometry

Vim −/− MEFs were transfected as described in previously to assess whether mTORC1 activity could be rescued. After 24 hours, cells were fully starved for 1 hour with RPMI media without amino acids, glucose, and serum (Life Science #R9010-01). Then, cells were treated for 30 minutes with 1 mM of L-glutamine plus 1× concentration of minimum EAAs mix (Thermo Fisher Scientific #11130036), 2.5 mM of glucose (Thermo Fisher Scientific #A2494001), and 100 nM insulin. Then, cells were fixed with 3% PFA for 20 minutes and permeabilized with 0.2% Triton X-100 for 10 minutes. Cells were incubated in a primary antibody against S6 Ser235/236 (1:100) in PBS 3% BSA 0.2% Tween20 for 1 hour and washed twice with PBS 0.2% Tween20. Samples were incubated with secondary antibody (anti-rabbit Alexa 488, 1:500) in PBS 3% BSA 0.2% Tween20 for 30 minutes and then washed twice. Cells were labeled with vimentin Alexa Fluor 647 for 30 minutes in PBS 3% BSA 0.2% Tween20 and washed twice. Data acquired with BD LSRFortessa (BD Biosciences) using FITC 530/30 (515 to 545 nm) and APC 670/14 (663 to 677 nm). Data were analyzed with FlowJo by measuring the median fluorescent intensity of S6 Ser235/236 in vimentin positive and vimentin null cells gated populations.

Statistical analysis

All the statistical analysis was carried out with GraphPad Prism 7 (GraphPad Software, USA). Three independent trials were carried out for each experiment unless it is stated otherwise. The statistical significance between 2 groups were measured by unpaired Student *t* test with Welch correction. The Mann–Whitney test was used for samples not following a normal distribution. Multiple comparisons were performed using either 1-way ANOVA or Welch ANOVA test with Holm–Sidak correction for multiple testing. For BMDC measurements, 5 independent experiment replicates were performed, and the statistical analysis was performed using linear mixed effect model in ShapeOut according to previously described procedures [45].

Supporting information

S1 Video Video on the effect of vimentin on cell size Live cell imaging shows that Vim −/− MEFs are consistently smaller than WT MEFs grown to confluency.
(MP4)

S1 Fig. The size phenotype is not restricted to MEFs. (**a**) Cell area of WT (black) and Vim −/− (gray) BMDCs obtained from RT-DC measurements of undeformed, spherical cells

(initial) and cells deformed in a narrow constriction of a microfluidic channel using 2 different flow rates (fr1 = 0.16 μl/s and fr2 = 0.32 μl/s). (**b**) Cell volume of WT (black) and Vim −/− (gray) BMDCs corresponding to the samples in (**a**). In (**a**) and (**b**), each data point represents a mean of an independent RT-DC measurement ($n = 5$), with at least 1,000 cells evaluated per measurement. $^{*}p < 0.05$, $^{**}p < 0.01$. RT-DC cell size data has been obtained by reanalyzing recently published measurements (44). (**c**) Dot plot of phospho-S6 fluorescent intensity in WT (MFI = 28,274) and Vim −/− MEFs (MFI = 9,906). (**d**) Corresponding dot plot analysis of phospho-S6 fluorescent intensities of Vim −/− MEFs starved (MFI = 895) and nutrient stimulated (MFI = 3,214) compared with (**e**). Vim −/− MEFs transfected with WT vimentin starved (MFI = 29,588) and nutrient stimulated (MFI = 39,099). Nutrient stimulation was done by starving cells for 1 hour without nutrient and growth factors followed by stimulation with 1× EAAs, 1 mM glutamine, 2.5 mM glucose, and 100 nM insulin for 30 minutes. MFI = median fluorescent intensity of Alexa Fluor 488. One representative of several. Gating used for the analysis can be found in the Figshare https://doi.org/10.6084/m9.figshare.20024534.v1. The data underlying the graphs shown in the S1 Fig can be found in S1 Data.
(TIF)

S2 Fig. Phosphorylation of mTORC1 downstream targets requires an active mTORC1. (**a**) Western blot analysis of WT and Vim −/− MEFs starved with RPMI media lacking amino acids, glucose, and growth factors for 1 hour, followed by stimulation with EAAs or EAAs and NEAAs, with or without 2.5 mM glucose in all combinations. Cells were treated with 100 nM of rapamycin after 40 minutes of starvation ($n = 3$). (**b**) Same experiment but including a 100 nM insulin treatment ($n = 3$). (**c**) Western blot analysis of WT and Vim −/− MEFs treated as in S2B Fig in the presence of an ERK (TRAM) or an AKT (AKT VIII) inhibitor ($n = 3$).
(TIF)

S3 Fig. mTOR colocalization to lysosomes is higher in WT MEFs. (**a**) WT and Vim −/− MEFs were serum starved overnight and stimulated with 100 nM insulin for 15 minutes. Cells were stained with mTOR (green channel) and the lysosomal marker LAMP1 (far red channel). (**b**) Same as in (a), but in steady state conditions (scale bar = 20 μm).
(TIF)

S4 Fig. Constitutively active Rag GTPase rescues mTOR localization to lysosomes in Vim −/− MEFs. Images show mTOR, HA tagged WT Rag GTPase, or HA tagged constitutively active Rag GTPase and LAMP1 in WT and Vim −/− MEFs. Merged images represent mTOR and LAMP1 channels.
(TIF)

S5 Fig. Autophagic flux is higher in Vim −/− MEFs. (**a**) Images show GFP and RFP channels and their intensity histograms of WT and Vim −/− MEFs transfected with pMRX-IP-GFP-LC3-RFP-LC3ΔG. Images were taken under steady-state conditions, serum starvation, and nutrient limitation (only EAAs with L-glutamine and glucose in the media) for 3 hours. (**b**) Western blot analysis of WT and Vim −/− MEFs grown for 1 hour in normal DMEM with serum or RPMI media lacking amino acids, glucose, and growth factors supplemented with nutrients in different combinations (1 mM L-glutamine plus 1× EAAs alone or with NEAAs and 2.5 mM glucose, $n = 3$). The data underlying the histogram shown in the S5A Fig can be found in S1 Data.
(TIF)

S6 Fig. Overexpression of dnULK1 K46N did not affect cell size in Vim −/− MEFs. (**a**) Cell volume distribution of Vim −/− MEFs transfected with HAtag-dnULK1 K46N or HA-tag

without insert ($n = 3$). ns = nonsignificant. The data underlying the graphs shown in the S6 Fig can be found in S1 Data.
(TIF)

S1 Data. Numerical values used to generate the graphs.
(XLSX)

S1 Raw images. Uncropped images of the western blots.
(PDF)

S1 Table. List of antibodies.
(PDF)

Acknowledgments

We would like to thank the Cell Imaging Core at Turku Bioscience and Biocenter Finland for the research facilities.

Author Contributions

Conceptualization: Ponnuswamy Mohanasundaram, John E. Eriksson.

Funding acquisition: Franziska Lautenschläger, John E. Eriksson.

Investigation: Ponnuswamy Mohanasundaram, Leila S. Coelho-Rato, Mayank Kumar Modi, Marta Urbanska, Fang Cheng.

Methodology: Ponnuswamy Mohanasundaram, Leila S. Coelho-Rato, Fang Cheng.

Supervision: Franziska Lautenschläger, John E. Eriksson.

Visualization: Ponnuswamy Mohanasundaram, Leila S. Coelho-Rato.

Writing – original draft: Ponnuswamy Mohanasundaram, Leila S. Coelho-Rato.

Writing – review & editing: Ponnuswamy Mohanasundaram, Leila S. Coelho-Rato, John E. Eriksson.

References

1. Lloyd AC. The Regulation of Cell Size. Cell. 2013; 154(6):1194–205. https://doi.org/10.1016/j.cell.2013.08.053 PMID: 24034244
2. Saxton RA, Sabatini DM. mTOR Signaling in Growth, Metabolism, and Disease. Cell. 2017; 168(6):960–76. https://doi.org/10.1016/j.cell.2017.02.004 PMID: 28283069
3. Bar-Peled L, Chantranupong L, Cherniack AD, Chen WW, Ottina KA, Grabiner BC, et al. A Tumor suppressor complex with GAP activity for the Rag GTPases that signal amino acid sufficiency to mTORC1. Science. 2013; 340(6136):1100–6. https://doi.org/10.1126/science.1232044 PMID: 23723238
4. Kim E, Goraksha-Hicks P, Li L, Neufeld TP, Guan KL. Regulation of TORC1 by Rag GTPases in nutrient response. Nat Cell Biol. 2008; 10(8):935–45. https://doi.org/10.1038/ncb1753 PMID: 18604198
5. Sancak Y, Peterson TR, Shaul YD, Lindquist RA, Thoreen CC, Bar-Peled L, et al. The Rag GTPases bind raptor and mediate amino acid signaling to mTORC1. Science. 2008; 320(5882):1496–501. https://doi.org/10.1126/science.1157535 PMID: 18497260
6. Condon KJ, Sabatini DM. Nutrient regulation of mTORC1 at a glance. J Cell Sci. 2019; 132(21). https://doi.org/10.1242/jcs.222570 PMID: 31722960
7. Kim J, Kundu M, Viollet B, Guan KL. AMPK and mTOR regulate autophagy through direct phosphorylation of Ulk1. Nat Cell Biol. 2011; 13(2):132–41. https://doi.org/10.1038/ncb2152 PMID: 21258367
8. Chan EY. mTORC1 phosphorylates the ULK1-mAtg13-FIP200 autophagy regulatory complex. Sci Signal. 2009; 2(84):pe51. https://doi.org/10.1126/scisignal.284pe51 PMID: 19690328

9. Russell RC, Tian Y, Yuan H, Park HW, Chang YY, Kim J, et al. ULK1 induces autophagy by phosphorylating Beclin-1 and activating VPS34 lipid kinase. Nat Cell Biol. 2013; 15(7):741–50. https://doi.org/10.1038/ncb2757 PMID: 23685627
10. Danielsson F, Peterson M, Caldeira Araújo H, Lautenschläger F, Gad A. Vimentin Diversity in Health and Disease. Cell. 2018; 7(10):147. https://doi.org/10.3390/cells7100147 PMID: 30248895
11. Ivaska J, Pallari HM, Nevo J, Eriksson JE. Novel functions of vimentin in cell adhesion, migration, and signaling. Exp Cell Res. 2007; 313(10):2050–62. https://doi.org/10.1016/j.yexcr.2007.03.040 PMID: 17512929
12. Satelli A, Li S. Vimentin as a potential molecular target in cancer therapy Or Vimentin, an overview and its potential as a molecular target for cancer therapy. Cell Mol Life Sci CMLS. 2011; 68(18):3033–46.
13. Ivaska J. Vimentin: Central hub in EMT induction? Small GTPases. 2011; 2(1):51–3. https://doi.org/10.4161/sgtp.2.1.15114 PMID: 21686283
14. Cheng F, Shen Y, Mohanasundaram P, Lindström M, Ivaska J, Ny T, et al. Vimentin coordinates fibroblast proliferation and keratinocyte differentiation in wound healing via TGF-β–Slug signaling. Proc Natl Acad Sci U S A. 2016; 113(30):E4320–7. https://doi.org/10.1073/pnas.1519197113 PMID: 27466403
15. Wang RC, Wei Y, An Z, Zou Z, Xiao G, Bhagat G, et al. Akt-Mediated Regulation of Autophagy and Tumorigenesis Through Beclin 1 Phosphorylation. Science. 2012; 338(6109):956–9. https://doi.org/10.1126/science.1225967 PMID: 23112296
16. Wilhelmsson U, Stillemark-Billton P, Borén J, Pekny M. Vimentin is required for normal accumulation of body fat. Biol Chem. 2019; 400(9):1157–62. https://doi.org/10.1515/hsz-2019-0170 PMID: 30995202
17. Cogné B, Bouameur JE, Hayot G, Latypova X, Pattabiraman S, Caillaud A, et al. A dominant vimentin variant causes a rare syndrome with premature aging. Eur J Hum Genet EJHG. 2020; 28(9):1218–30. https://doi.org/10.1038/s41431-020-0583-2 PMID: 32066935
18. Kim S, Wong P, Coulombe PA. A keratin cytoskeletal protein regulates protein synthesis and epithelial cell growth. Nature. 2006; 441(7091):362–5. https://doi.org/10.1038/nature04659 PMID: 16710422
19. Virtakoivu R, Mai A, Mattila E, De Franceschi N, Imanishi SY, Corthals G, et al. Vimentin-ERK Signaling Uncouples Slug Gene Regulatory Function. Cancer Res. 2015; 75(11):2349–62. https://doi.org/10.1158/0008-5472.CAN-14-2842 PMID: 25855378
20. Otto O, Rosendahl P, Mietke A, Golfier S, Herold C, Klaue D, et al. Real-time deformability cytometry: on-the-fly cell mechanical phenotyping. Nat Methods. 2015; 12(3):199–202. https://doi.org/10.1038/nmeth.3281 PMID: 25643151
21. Liu GY, Sabatini DM. mTOR at the nexus of nutrition, growth, ageing and disease. Nat Rev Mol Cell Biol. 2020; 21(4):183–203. https://doi.org/10.1038/s41580-019-0199-y PMID: 31937935
22. Rousseau D, Gingras AC, Pause A, Sonenberg N. The eIF4E-binding proteins 1 and 2 are negative regulators of cell growth. Oncogene. 1996; 13(11):2415–20. PMID: 8957083
23. Roux PP, Shahbazian D, Vu H, Holz MK, Cohen MS, Taunton J, et al. RAS/ERK Signaling Promotes Site-specific Ribosomal Protein S6 Phosphorylation via RSK and Stimulates Cap-dependent Translation. J Biol Chem. 2007; 282(19):14056–64. https://doi.org/10.1074/jbc.M700906200 PMID: 17360704
24. Sancak Y, Bar-Peled L, Zoncu R, Markhard AL, Nada S, Sabatini DM. Ragulator-Rag Complex Targets mTORC1 to the Lysosomal Surface and Is Necessary for Its Activation by Amino Acids. Cell. 2010; 141(2):290–303. https://doi.org/10.1016/j.cell.2010.02.024 PMID: 20381137
25. Pallari HM, Eriksson JE. Intermediate Filaments as Signaling Platforms. Sci STKE. 2006; 2006(366):pe53–pe53. https://doi.org/10.1126/stke.3662006pe53 PMID: 17179489
26. Hyder CL, Pallari HM, Kochin V, Eriksson JE. Providing cellular signposts—post-translational modifications of intermediate filaments. FEBS Lett. 2008; 582(14):2140–8. https://doi.org/10.1016/j.febslet.2008.04.064 PMID: 18502206
27. Hyder CL, Isoniemi KO, Torvaldson ES, Eriksson JE. Insights into intermediate filament regulation from development to ageing. J Cell Sci. 2011; 124(Pt 9):1363–72. https://doi.org/10.1242/jcs.041244 PMID: 21502133
28. Styers ML, Kowalczyk AP, Faundez V. Intermediate Filaments and Vesicular Membrane Traffic: The Odd Couple's First Dance? Traffic. 2005; 6(5):359–365. https://doi.org/10.1111/j.1600-0854.2005.00286.x PMID: 15813746
29. González A, Hall MN. Nutrient sensing and TOR signaling in yeast and mammals. EMBO J. 2017; 36(4):397–408. https://doi.org/10.15252/embj.201696010 PMID: 28096180
30. Efeyan A, Zoncu R, Chang S, Gumper I, Snitkin H, Wolfson RL, et al. Regulation of mTORC1 by the Rag GTPases is necessary for neonatal autophagy and survival. Nature. 2013; 493(7434):679–83. https://doi.org/10.1038/nature11745 PMID: 23263183

31. Mizushima N, Yoshimori T. How to Interpret LC3 Immunoblotting. Autophagy. 2007; 3(6):542–5. https://doi.org/10.4161/auto.4600 PMID: 17611390

32. Sánchez-Martín P, Komatsu M. p62/SQSTM1—steering the cell through health and disease. J Cell Sci. 2018; 131(21):jcs222836. https://doi.org/10.1242/jcs.222836 PMID: 30397181

33. Kaizuka T, Morishita H, Hama Y, Tsukamoto S, Matsui T, Toyota Y, et al. An Autophagic Flux Probe that Releases an Internal Control. Mol Cell. 2016; 64(4):835–49. https://doi.org/10.1016/j.molcel.2016.09.037 PMID: 27818143

34. Hara T, Takamura A, Kishi C, Iemura SI, Natsume T, Guan JL, et al. FIP200, a ULK-interacting protein, is required for autophagosome formation in mammalian cells. J Cell Biol. 2008; 181(3):497–510. https://doi.org/10.1083/jcb.200712064 PMID: 18443221

35. Lamouille S, Xu J, Derynck R. Molecular mechanisms of epithelial–mesenchymal transition. Nat Rev Mol Cell Biol. 2014; 15(3):178–96. https://doi.org/10.1038/nrm3758 PMID: 24556840

36. Lowery J, Kuczmarski ER, Herrmann H, Goldman RD. Intermediate Filaments Play a Pivotal Role in Regulating Cell Architecture and Function. J Biol Chem. 2015; 290(28):17145–53. https://doi.org/10.1074/jbc.R115.640359 PMID: 25957409

37. Ivaska J, Vuoriluoto K, Huovinen T, Izawa I, Inagaki M, Parker PJ. PKCε-mediated phosphorylation of vimentin controls integrin recycling and motility. EMBO J. 2005; 24(22):3834–45.

38. Xiao G, Sun SC. Negative regulation of the nuclear factor kappa B-inducing kinase by a cis-acting domain. J Biol Chem. 2000; 275(28):21081–5. https://doi.org/10.1074/jbc.M002552200 PMID: 10887201

39. Yan J, Kuroyanagi H, Kuroiwa A, Matsuda Y, Tokumitsu H, Tomoda T, et al. Identification of mouse ULK1, a novel protein kinase structurally related to C. elegans UNC-51. Biochem Biophys Res Commun. 1998; 246(1):222–7. https://doi.org/10.1006/bbrc.1998.8546 PMID: 9600096

40. Qiu LQ, Lai WS, Stumpo DJ, Blackshear PJ. Mouse Embryonic Fibroblast Cell Culture and Stimulation. Bio-Protoc. 2016; 6(13):e1859. https://doi.org/10.21769/BioProtoc.1859 PMID: 28573158

41. Vargas P, Maiuri P, Bretou M, Sáez PJ, Pierobon P, Maurin M, et al. Innate control of actin nucleation determines two distinct migration behaviours in dendritic cells. Nat Cell Biol. 2016; 18(1):43–53. https://doi.org/10.1038/ncb3284 PMID: 26641718

42. Schindelin J, Arganda-Carreras I, Frise E, Kaynig V, Longair M, Pietzsch T, et al. Fiji: an open-source platform for biological-image analysis. Nat Methods. 2012; 9(7):676–82. https://doi.org/10.1038/nmeth.2019 PMID: 22743772

43. Urbanska M, Rosendahl P, Kräter M, Guck J. High-throughput single-cell mechanical phenotyping with real-time deformability cytometry. Methods Cell Biol. 2018; 147:175–198. https://doi.org/10.1016/bs.mcb.2018.06.009 PMID: 30165957

44. Stankevicins LDC, Urbanska M, Flormann DA, Terriac E, Mostajeran Z, Gad AKB, et al. Vimentin provides the mechanical resilience required for amoeboid migration and protection of the nucleus. bioRxiv. 2019; 31:720946.

45. Herbig M, Mietke A, Müller P, Otto O. Statistics for real-time deformability cytometry: Clustering, dimensionality reduction, and significance testing. Biomicrofluidics. 2018; 12(4):042214. https://doi.org/10.1063/1.5027197 PMID: 29937952

46. Kankaanpää P, Paavolainen L, Tiitta S, Karjalainen M, Päivärinne J, Nieminen J, et al. BioImageXD: an open, general-purpose and high-throughput image-processing platform. Nat Methods. 2012; 9(7):683–9. https://doi.org/10.1038/nmeth.2047 PMID: 22743773

Mohammad I, Nousiainen K, Bhosale SD, Starskaia I, Moulder R, Rokka A, Cheng F, **Mohanasundaram P**, Eriksson JE, Goodlett DR, Lähdesmäki H, Chen Z. 2018. Quantitative proteomic characterization and comparison of T helper 17 and induced regulatory T cells. *PLOS Biology* 16:e2004194.

III

PLOS BIOLOGY

METHODS AND RESOURCES

Quantitative proteomic characterization and comparison of T helper 17 and induced regulatory T cells

Imran Mohammad[1,2], Kari Nousiainen[3], Santosh D. Bhosale[1,2], Inna Starskaia[1,2], Robert Moulder[1], Anne Rokka[1], Fang Cheng[4], Ponnuswamy Mohanasundaram[4], John E. Eriksson[4], David R. Goodlett[5], Harri Lähdesmäki[3], Zhi Chen[1]*

1 Turku Centre for Biotechnology, University of Turku and Åbo Akademi University, Turku, Finland, **2** Turku Doctoral Programme of Molecular Medicine, University of Turku, Turku, Finland, **3** Department of Computer Science, Aalto University, Espoo, Finland, **4** Cell Biology, Biosciences, Faculty of Science and Engineering, Åbo Akademi University, Turku, Finland, **5** Department of Pharmaceutical Sciences, University of Maryland School of Pharmacy, Baltimore, Maryland, United States of America

* zchen@utu.fi

Citation: Mohammad I, Nousiainen K, Bhosale SD, Starskaia I, Moulder R, Rokka A, et al. (2018) Quantitative proteomic characterization and comparison of T helper 17 and induced regulatory T cells. PLoS Biol 16(5): e2004194. https://doi.org/10.1371/journal.pbio.2004194

Academic Editor: Paula Oliver, University of Pennsylvania Perelman School of Medicine, United States of America

Received: September 9, 2017

Accepted: April 25, 2018

Published: May 31, 2018

Data Availability Statement: The mass spectrometry proteomics data have been deposited to the ProteomeXchange Consortium via the PRIDE partner repository with the dataset identifier PXD007826. RNA-seq data can be found at the NCBI Gene Expression Omnibus with accession number GSE 104152.

Funding: Academy of Finland www.aka.fi (grant number 258313 (to ZC); Centre of Excellence in Molecular Systems Immunology and Physiology

Abstract

The transcriptional network and protein regulators that govern T helper 17 (Th17) cell differentiation have been studied extensively using advanced genomic approaches. For a better understanding of these biological processes, we have moved a step forward, from gene- to protein-level characterization of Th17 cells. Mass spectrometry–based label-free quantitative (LFQ) proteomics analysis were made of in vitro differentiated murine Th17 and induced regulatory T (iTreg) cells. More than 4,000 proteins, covering almost all subcellular compartments, were detected. Quantitative comparison of the protein expression profiles resulted in the identification of proteins specifically expressed in the Th17 and iTreg cells. Importantly, our combined analysis of proteome and gene expression data revealed protein expression changes that were not associated with changes at the transcriptional level. Our dataset provides a valuable resource, with new insights into the proteomic characteristics of Th17 and iTreg cells, which may prove useful in developing treatment of autoimmune diseases and developing tumor immunotherapy.

Author summary

T helper 17 (Th17) cells and induced regulatory T (iTreg) cells are two subsets of T helper cells differentiated from naïve cells that play important roles in autoimmune diseases, immune homeostasis, and tumor immunity. The differentiation process is achieved by changes in numerous proteins, including transcription regulators, enzymes, membrane receptors, and cytokines, which are critical in lineage commitment. To profile protein expression changes in Th17 and iTreg cells, we polarized murine naïve CD4+ T (Thp) cells in vitro to Th17 and iTreg cells and performed quantitative proteomic analysis of these cells. More than 4,000 proteins, covering almost all subcellular compartments, were detected. Quantitative comparison of the protein expression profiles resulted in the

Research 2012–2017 grant 250114 (to HL)). The funder had no role in study design, data collection and analysis, decision to publish, or preparation of the manuscript. National Technology Agency of Finland (DRG was supported by Finland Distinguished Professor Programme, grant 40398). The funder had no role in study design, data collection and analysis, decision to publish, or preparation of the manuscript. CIMO foundation (to IS). The funder had no role in study design, data collection and analysis, decision to publish, or preparation of the manuscript. University of Turku Foundation (to IM and ZC). The funder had no role in study design, data collection and analysis, decision to publish, or preparation of the manuscript. Finnish Cultural Foundation (to IS). The funder had no role in study design, data collection and analysis, decision to publish, or preparation of the manuscript.

Competing interests: The authors have declared that no competing interests exist.

Abbreviations: ACAA2, acetyl-CoA acyltransferase 2; Actg1, γ-actin 1; ADSSL1, adenylosuccinate synthetase isozyme 1; Aebp2, adipocyte enhancer–binding protein 2; AHR, aryl hydrocarbon receptor; ALDH2, aldehyde dehydrogenase 2; Aldoa, aldolase A; Arid1a, AT-rich interaction domain 1A; ATP5A1, ATP synthase F1 subunit alpha; ATP5B, ATP synthase subunit beta; Bach, BTB domain and CNC homology; BASP1, brain abundant membrane attached signal protein 1; Bcl10, B cell chronic lymphocytic leukemia/lymphoma 10; Brd8, bromodomain-containing 8; C, carbamidomethyl; C1qbp, complement C1q binding protein; Carm1, coactivator-associated arginine methyltransferase 1; Cbfb, core binding factor beta; Ccar1, cell cycle and apoptosis regulator 1; Ccnh, cyclin H; Ccnt1, cyclin T1; CCR7, C-C motif chemokine receptor 7; Cdc5l, cell division cycle 5–like protein; Chd4, chromodomain helicase DNA-binding protein 4; CLP1, cleavage and polyadenylation factor I subunit 1; CNS-1, conserved noncoding DNA sequence 1; Coa6, cytochrome c oxidase assembly factor 6; Cops2, constitutive photomorphogenesis 9 signalosome subunit 2; Coro1a, coronin 1A; COX2, cyclooxygenase 2; COX5A, cyclooxygenase 5A; CNOT2, CCR4-NOT transcription complex subunit 2; cPLA2α, cytosolic phospholipase A2 alpha; cpm, count per million; CPT1A, carnitine palmitoyltransferase 1A; CPT2, carnitine palmitoyltransferase 2; Ctla4, cytotoxic T lymphocyte–associated protein 4; Cxxc1, CXXC finger protein 1; Ddx5, DEAD-box helicase 5; DE, differentially expressed; Dnmt3a, DNA methyltransferase 3 alpha; Eif4a1, eukaryotic translation initiation factor 4a1; ENO1, enolase 1;

identification of proteins specifically expressed in the Th17 and iTreg cells. Importantly, our combined analysis of proteome and gene expression data revealed protein expression changes that were not associated with changes at the transcriptional level. The present study serves as a valuable resource that may prove useful in developing treatment of autoimmune diseases and cancer.

Introduction

Interleukin-17 secreting T helper (T helper 17 [Th17]) cells are involved in neutrophilia, tissue remodeling and repair, and production of antimicrobial proteins. In addition, they play a critical role in inflammation and autoimmunity. Regulatory T (Treg) cells are immunosuppressive and essential for maintaining self-tolerance and homeostasis. Natural regulatory T (nTreg) cells develop in the thymus and are therefore distinct from the cells undergoing parallel thymic differentiation to become the naïve progenitors of T helper 1 (Th1), T helper 2 (Th2), and Th17 cells [1–4]. However, naïve CD4+ T (Thp) cells can be induced in vitro to differentiate into cells with similar characteristics as Treg cells, which are defined as induced regulatory T (iTreg) cells [5–7]. In recent years, considerable interest has been directed toward the targeting of Th17 and/or Treg cells in the treatment of autoimmune diseases and developing tumor immunotherapy [8]. An understanding of the molecular mechanisms of Th17 and iTreg cell differentiation, together with identification of the key molecules in Th17 and iTreg cell function, will help to develop strategies to target or manipulate these two Th cell types.

Characterization of the molecular mechanisms directing the differentiation of naïve Th cells toward their distinct subsets—namely, Th1, Th2, Th17, and Treg cells—has been studied in some depth by using transcriptomic and epigenomic strategies [9–14]. However, the regulation of gene expression is also controlled at the posttranscriptional, translational, and post-translational levels. Accordingly, poor levels of concordance between changes in protein abundance and mRNA expression have been reported, for example, with variation in mRNA quantities accounting for only around 40% of differences at the protein level [15, 16]. As proteins contribute the structural and functional elements of cells, a comprehensive view of the Th17/iTreg cells proteome is thus required. While protein expression profiling in Th1, Th2, and Treg cells has been reported [17–19] [20], there are no large-scale proteomic reports on Th17 cells. In the past, due to lower sensitivity and poorer reproducibility, cellular protein profiling was mostly limited to description of the higher and moderately abundant cellular components, and relatively less protein expression changes were quantified. Importantly, several of the signature molecules of Th cell subsets, such as key transcription factors (TFs) and cytokine receptors, are often present at low levels [21] and were difficult to detect with previous proteomics profiling approaches. However, with continued improvements in proteomic technology, the achievable levels of coverage have begun to approach those from genomic analyses, indicating detection of thousands of proteins from a single analysis. In particular, mass spectrometry coupled with liquid chromatography (LC-MS) provides an integrated system for analyzing protein components with improved sensitivity and moderate throughput.

In this study, label-free quantitative (LFQ) proteomics analysis was used to define the proteins from in vitro cultured murine Th17 and iTreg cells. Over 4,000 proteins were detected, with representation of almost all subcellular compartments. A shared protein signature was observed in the proteomes of the T cell receptor (TCR)-activated helper T cell (Th0), Th17, and iTreg cells, in addition to distinct differences in the proteins expressed in these two subsets. Importantly, protein expression changes were found that were not otherwise implicated

ENO3, enolase 3; ETV6, ETS variant 6; FAM129B, family with sequence similarity 129 member B; Fasn, fatty acid synthase; FDR, false discovery rate; Foxk1, forkhead box K1; FOXO1, forkhead box O1; Foxp1, forkhead box P1; Foxp3, forkhead box P3; FPKM, fragments per kilobase of transcript per million mapped reads; FSCN1, fascin actin-bundling protein 1; Fus, Fus RNA binding protein; Gabpa, GA-binding protein transcription factor subunit alpha; Gapdh, glyceraldehyde-3-phosphate dehydrogenase; Gatad2a, GATA zinc finger domain containing 2A; Gimap4, GTPase IMAP family member 4; Gimap5, GTPase IMAP family member 5; GLUT1, glucose transporter 1; GLUT3, glucose transporter 3; GNG2, G protein unit gamma 2; GSEA, Gene Set Enrichment Analysis; Gtf2a1, general transcription factor IIA subunit 1; Gtf2e1, general transcription factor IIE subunit 1; H2afx, histone 2A family member X; HACD3, 3-hydroxyacyl-CoA dehydratase 3; HADH, hydroxyacyl-CoA dehydrogenase; HCD, higher-energy C-trap dissociation; Hcfc1, host cell factor C1; HDAC1, histone deacetylase 1; HDAC3, histone deacetylase 3; Hexim1, hexamethylene bisacetamide inducible 1; HIF1α, hypoxia-inducible factor 1 subunit alpha; Hist1h1e, histone cluster 1 H1 family member E; Hk1, hexokinase 1; Hmgb1, high-mobility group box 1; Hprt, hypoxanthine phosphoribosyltransferase; Hnrnpd, heterogeneous nuclear ribonucleoprotein D; Hnrnpk, heterogeneous nuclear ribonucleoprotein K; Hspd1, heat shock protein family D1; IBD, inflammatory bowel disease; ICAM1, intercellular adhesion molecule 1; ICAM2, intercellular adhesion molecule 2; Iigp1, interferon-inducible GTPase 1; IKZF3, IKAROS family zinc finger 3; IKZF4, IKAROS family zinc finger 4; IL2, interleukin 2; IL2RA, interleukin 2 receptor alpha; IL2RG, interleukin 2 receptor gamma; IL4r, interleukin 4 receptor; IL6, interleukin 6; IL16, interleukin 16; IL17, interleukin 17; IL17A, interleukin 17A; IL17F, interleukin 17F; IPA, Ingenuity Pathway Analysis; Irf3, interferon regulatory factor 3; IRF4, interferon regulatory factor 4; Isg15, interferon-stimulated gene 15; ITGAE, integrin subunit alpha E; ITGAL, integrin alpha L; ITGB1, integrin beta 1; ITGB2, integrin beta 2; ITGB7, integrin beta 7; iTreg, induced regulatory T; Jak3, Janus kinase 3; KEGG, Kyoto Encyclopedia of Genes and Genomes; Khdrbs1, KH RNA binding domain containing, signal transduction–associated 1; Lag3, lymphocyte activating 3; Lck, lymphocyte cell-specific protein tyrosine kinase; LC-MS, mass spectrometry coupled with liquid chromatography; LC-MS/MS, liquid chromatography–tandem mass spectrometry; LFQ, label-free quantitative; Lgals3, galectin 3; Lgals7, galectin 7; MALT1, mucosa-associated lymphoid tissue 1; MAPK11, mitogen-

from transcriptomics data. Pathway enrichment and network analysis improved the understanding of the functional context and organization of proteins in Th17 and iTreg cells. Our dataset provides a valuable resource for studying Th cell specification and further developing novel therapies to treat autoimmune diseases, inflammation, and tumors by manipulating or targeting Th17 or iTreg cells.

Results

Proteomic profiles of polarizing Th17 and iTreg cells

To identify the proteome of Th17 cells, Thp cells were isolated and polarized toward Th17 cells for 72 h using standard culture protocols. Interleukin 2 (IL2) was not added to the in vitro Th17 cultures on account of its reported suppression of Th17 polarization [22]. Under these conditions, approximately 40% of interleukin 17 (IL17)-producing cells were established after 72 h of polarization. The 72 h time point was therefore chosen to study the proteome of polarizing Th17 cells. To compare the proteomics of the two closely linked Th cell subsets iTreg and Th17 cells, iTreg cells were polarized for 7 d followed by restimulation and polarization for another 3 d, after which 87% of the cells expressed forkhead box P3 (Foxp3) (Fig 1A and 1B). The expression of IL17 and Foxp3 were detected by intracellular protein staining followed by flow cytometry analysis of the Th17- and iTreg-polarized cells, respectively (Fig 1B). Following cell lysis with NP-40 and trypsin digestion, the samples were analyzed by liquid chromatography–tandem mass spectrometry (LC-MS/MS) (Fig 1A). Overall, from the analyses of 3 independent cultures of polarizing Th17, iTreg, activated (Th0) and Thp cells, 4,287 protein groups were detected. Principle component analysis showed that the Th17, iTreg, and Th0 subsets could be distinguished based on their protein expression profiles in all 3 of the independent cultures (S1A Fig). Furthermore, high Pearson's correlation coefficients were observed for the 3 independent cultures (0.9–0.95) in all the cultured subsets (Fig 1C and S1B Fig). The identified proteins span a concentration range of 6 orders of magnitude, indicating detection of proteins across a wide range of expression (S1C Fig and S1 Data). To obtain an overview of the detected T helper cell proteomes, the cumulative contribution of each protein to total detected proteins was plotted. The 3 in vitro cultured Th cell subsets showed similar patterns for the protein cumulative intensities, in which the first quarter was mostly attributed to the cytoskeleton and glycolytic enzymes (Fig 1D and S1 Data). Analysis of protein location in terms of the cellular compartment indicated about half of the detected proteins were cytoplasmic and 31% were from the nucleus. Cytokines were identified amongst the 2% of proteins that were categorized as located from the extracellular space, such as interleukin 17F (IL17F) and interleukin 16 (IL16) in Th17 cells (Fig 1E and S1 Data). Cytokines and cytokine receptors are important for fate decision of Th cell differentiation. In order to facilitate the determination of plasma membrane proteins, the nonionic detergent NP-40 was used for sample preparation in this study, resulting in the identification of 317 and 312 plasma membrane proteins in Th17 or iTreg cells, respectively (Fig 1E and S1 Data). Importantly, some cytokine receptors and integrins—such as interleukin 2 receptor alpha (IL2RA), interleukin 2 receptor gamma (IL2RG), tumor necrosis factor receptor superfamily member 18 (TNFRSF18), intercellular adhesion molecule 1 (ICAM1), intercellular adhesion molecule 2 (ICAM2), integrin alpha L (ITGAL), integrin beta 1 (ITGB1), integrin beta 2 (ITGB2), and integrin beta 7 (ITGB7)—were detected both in Th17 and iTreg cells (S1 Data). As shown in Fig 1F and S1 Data, 3,589 proteins—including the expected CD3E, CD3G, CD2, CD4, CD5, CD6, CD28, CD44, and CD69—were detected in cells cultured under all of the 3 polarizing conditions. This supported the concept that although these cells are polarizing toward distinct functional subsets, they still carry a basic T cell signature. Furthermore, the analysis of these data revealed that proteins

activated protein kinase; Max, MYC-associated factor X; Mecp2, methyl-CpG binding protein 2; Mif, macrophage migration inhibitory faction; Mta2, metastasis-associated 1 family member 2; Mybbp1a, MYB binding protein 1A; Myh9, myosin heavy chain 9; MYH11, myosin heavy chain 11; NAFLD, nonalcoholic fatty liver disease; Ncl, nucleolin; NCoR, nuclear receptor corepressor; NDUFS1, NADH:ubiquinone oxidoreductase core subunit S1; NFAT1, TF NFATC2, NFATC2, nuclear factor of activated T cells 2; NFKB1, nuclear factor kappa B subunit 1; Nfkbia, nuclear factor of kappa light polypeptide gene enhancer in B cells inhibitor alpha; Nfyb, nuclear transcription factor Y beta; Nmi, N-myc and STAT interactor; NR3C1, nuclear receptor subfamily 3 group C member 1; nTreg, natural regulatory T; OXPHO, oxidative phosphorylation; P4HA1, prolyl 4-hydroxylase subunit alpha 1; PDE5A, phosphodiesterase 5A; Phb, prohibitin; Phb1, prohibitin 1; Phb2, prohibitin 2; Phf5a, PHD finger protein 5a; Pkm, pyruvate kinase M; Pml, promyelocytic leukemia; Ppia, peptidylprolyl isomerase A; Pqpb1, polyglutamine-binding protein 1; PXN, paxillin; Psmd9, proteasome 26S subunit, non-ATPase 9; Rac2, ras-related C3 botulinum toxin substrate 2; Ran, Ras-related nuclear protein; Rbbp7, retinoblastoma binding protein 7; Rbm39, RNA binding motif 39; REXO4, RNA exonuclease 4; RIOK1, right open reading frame kinase 1; ROMO1, reactive oxygen species modulator 1; RORγt, retinoic acid receptor–related orphan receptor gamma T; Rorc, retinoic acid receptor–related orphan receptor C; RUNX1, runt-related transcription factor 1; RUNX3, runt-related transcription factor 3; Ruvbl1, RuvB-like AAA ATPase 1; Ruvbl2, RuvB-like AAA ATPase 2; Sap130, Sin3A-associated protein 130; SATB1, special AT-rich sequence-binding protein 1; Serpinb5, Serpin Family B Member 5; SIRT2, sirtuin 2; SLC2A1, solute carrier family 2 member 1; SLC2A3, solute carrier family 2 member 3; SLC4A2, solute carrier family 4 member 2; Slc25a2, solute carrier family 25 member 2; SMARCA4, SWI/SNF-related matrix-associated actin-dependent regulator of chromatin subfamily A member 4; SMARCA5, SWI/SNF-related matrix-associated actin-dependent regulator of chromatin subfamily A member 5; SMARCB1, SWI/SNF-related matrix-associated actin-dependent regulator of chromatin subfamily B member 1; SMARCC2, SWI/SNF-related matrix-associated actin-dependent regulator of chromatin subfamily C member 2; Smarcd, SWI/SNF-related matrix-associated actin-dependent regulator of chromatin subfamily D; SMARCD1, SWI/SNF-related matrix-associated actin-dependent regulator of chromatin subfamily D member 1; SMARCE1, SWI/SNF-

from almost all cellular compartments were detected, adding to the value of these data as a resource to further study candidate proteins potentially contributing to Th17 and iTreg cell differentiation and function.

Protein expression changes during Th17/iTreg cell differentiation

Since Th17 and Treg cells play an important role in autoimmunity and inflammation [8, 23–25], detailed gene expression profiling studies have been carried out in them [10, 14, 26–28]. However, there are no reports using proteomics to profile protein expression during Th17 cell differentiation. In this study, quantitative proteomics of Th17, iTreg, and Th0 cells enabled the comparison of protein expression in differentiating Th17 and iTreg cells. Of the proteins detected in this study, 93% were detected in all 3 T cell subsets. However, 40 proteins were selectively expressed in response to Th17 polarizing cytokines (Fig 1F). Among these, cytokine IL17F and TF retinoic acid receptor–related orphan receptor C (RORC) have been previously well characterized as Th17 cell signature molecules [29–31]. Both of these were detected only in Th17 cells and not in activated Th0 cells (Fig 2A and S2 Data), confirming that our in vitro cultured Th cells were successfully polarized. The other proteins detected only in Th17 cells included aryl hydrocarbon receptor (AHR) and phosphodiesterase 5A (PDE5A). Amongst these, in the PDE5A gene, the active enhancer mark H3K27ac was detected in PMA-Ionomycin-stimulated Th17 primary cells [32]. Solute carrier family 4 member 2 (SLC4A2, also known as AE2) was also only detected in Th17 cells. It has been reported that the activity of SLC4A2 is sensitive to pH, and its mutation is associated with primary biliary cirrhosis and autoimmune disease of the urogenital tract [33, 34]. However, whether these genes play roles in Th17 cells has not been thoroughly studied. When comparing proteins detected in Th17 cells with TCR-activated Th0 cells, we found that there were statistically significant changes (false discovery rate [FDR] < 0.05) in the expression of 25.9% of all detected proteins in Th0 and Th17 cells (1,005 out of 3,880 proteins) (see Methods). Amongst these, the expression of 414 proteins—including IL17F, RORC, AHR, and IKAROS family zinc finger 3 (IKZF3)—were up-regulated, whereas 591 proteins—such as TNFRSF18 (GITR) and tumor necrosis factor receptor superfamily member 4 (TNFRSF4, OX40)—were down-regulated (Fig 2B and 2C upper panel, S2 Data).

The role of iTreg cells is to control the effector cells (including Th17, Th1, or Th2 cells) and to suppress immune response [2, 8]. Foxp3 is the key TF for iTreg cell subset differentiation, as well as having a suppressive function [8, 23]. With the proteomics analysis of in vitro cultured iTreg cells, FOXP3 protein was detected in all 3 independent cultures, whereas it was not in TCR-activated Th0 cells (Fig 2A and S2 Data). Comparing the proteomes of Th0 cells and polarized iTreg cells, in addition to FOXP3, the expression of, for example, runt-related transcription factor 3 (RUNX3), integrin subunit alpha E (ITGAE), G protein unit gamma 2 (GNG2), and vimentin (VIM) were also up-regulated, whereas the expression of such proteins as special AT-rich sequence-binding protein 1 (SATB1) and CD69 were down-regulated (Fig 2C upper panel, S2 Data). Altogether, quantitative proteomics from 3 independent in vitro cell cultures revealed expression changes of 675 proteins after 10 d differentiation toward iTreg cells compared to Th0 cells (FDR < 0.05). On the basis of functional annotation with Ingenuity Pathway Analysis (IPA, QIAGEN Bioinformatics, https://www.qiagenbioinformatics.com), the differentially expressed (DE) proteins were classified into 12 functional groups (Fig 2D and S2 Data). Similarly as with Th17 cells, the enzyme was the functional group represented with the most protein expression changes when compared to Th0 cells.

Following the activation via TCR and costimulatory receptors, the fate decision of Th cell subsets is largely determined by TFs. After 72 h of in vitro polarization of Th17 cells and 10 d

related matrix-associated actin-dependent regulator of chromatin subfamily E member 1; SMRT, silencing mediator for retinoid and thyroid receptors; SMYD3, SET and MYND domain containing 3; Sqstm1, sequestosome 1; Srsf2, serine- and arginine-rich splicing factor 2; Stat1, signal transducer and activator of transcription 1; Stat2, signal transducer and activator of transcription 2; STAT3, signal transducer and activator of transcription 3; Stat5a, signal transducer and activator of transcription 5A; Stat6, signal transducer and activator of transcription 6; Stip1, stress-induced phosphoprotein 1; STMN2, stathmin 2; Supt16h, SPT16 homolog; Tbl1xr1, transducin beta like 1 X-linked receptor 1; Tcea1, transcription elongation factor A polypeptide 1; Tceb3, transcription elongation factor B polypeptide 3; Tcf7, transcription factor 7; TCR, T cell receptor; TF, transcription factor; TGFβ, transforming growth factor beta; TGFβR, transforming growth factor beta receptor type 1; TGM2, transglutaminase 2; Th0, T cell receptor–activated helper T; Th1, T helper 1; Th2, T helper 2; Th17, T helper 17; Thoc1, THO complex 1; Thp, naïve CD4+ T; TNFRSF4, tumor necrosis factor receptor superfamily member 4; TNFRSF18, tumor necrosis factor receptor superfamily member 18; Traf6, tumor necrosis factor receptor–associated factor 6; Treg, regulatory T; Trrap, transformation/transcription domain–associated protein; Uba1, ubiquitin 1; Uba52, ubiquitin 52; Ube2v1, ubiquitin conjugating enzyme E2 V1; Ubtf, upstream binding transcription factor; VIM, vimentin; Wdr1, WD repeat domain 1; WT, wild-type; Yy1, yin yang 1; Zap70, zeta chain of T cell receptor–associated protein kinase 70.

of polarization of iTreg cells, the expression of 75 and 50 transcription regulators and ligand-dependent nuclear receptors were significantly changed, respectively (Fig 2D, S2A Fig and S2 Data), including RORC, FOXP3, AHR, nuclear factor of activated T cells 2 (NFATC2), and IKZF3. Some of these differentially expressed TFs, such as CCR4-NOT transcription complex subunit 2 (CNOT2) and family with sequence similarity 129 member B (FAM129B), were proteins whose expression level was induced after both differentiation of Th17 and iTreg cells. As transcription regulators, their functions in Th17/iTreg cell differentiation are largely unknown. Further functional characterization of these TFs or identification of their target genes in Th17/iTreg cells may help to understand transcriptional mechanisms of the Th17/iTreg cell differentiation process. Kinases are important contributors to cell fate decisions. Many protein kinase inhibitors have been developed to treat diseases such as cancer, inflammation, and autoimmune disorders [35, 36]. In our data, both in Th17 and iTreg cells, we found the protein expression of a group of kinases was changed, such as mitogen-activated protein kinase 11 (MAPK11), right open reading frame kinase 1 (RIOK1), and cleavage and polyadenylation factor I subunit 1 (CLP1) (Fig 2D, S2 Data). Many of these have not been previously reported in the context of Th17/iTreg cell function or differentiation. Follow-up studies on these kinases or candidate proteins from the other functional groups (Fig 2D, S2 Data) could provide further insight on the development of novel therapeutic targets to modify Th17/Treg-mediated diseases.

Pathway enrichment analysis of the DE proteins detected from the comparison of polarizing Th17 and Th0 cells indicated that their association with a number of different biological processes. Notably, oxidative phosphorylation (OXPHO), antigen processing and presentation and metabolic pathways were the top enriched pathways (S2B Fig; S2 Data), suggesting that the Th17 cell differentiation process is accompanied with antigen processing and metabolic changes, and especially OXPHO. Pathway analysis in the DE proteins from the comparison of iTreg and Th0 cells only revealed 2 enriched pathways, systemic lupus erythematosus and alcoholism, which both included changes of several histone cluster 1 h2 and h4 family members (S2 Data).

Distinct protein expression changes in iTreg and Th17 cells

Although Th17 and iTreg cells have different functions, they share transforming growth factor β (TGFβ) as a common cytokine, which is required for both iTreg and Th17 cell differentiation. To gain further insight into these differences, we next evaluated which proteins showed distinct changes in these 2 cell lineages. Comparing the proteomes detected for the Th17 and iTreg cells, we found 2,040 proteins with a statistically significant (FDR < 0.05) expression difference. Of the 2,040 DE proteins, 1,067 proteins were expressed higher in Th17 cells, and 973 proteins were expressed higher in iTreg cells (Fig 3A and S3 Data). Similarly to FOXP3, which was highly up-regulated in iTreg cells, other TFs—such as IKAROS family zinc finger 4 (IKZF4) and RUNX3—were also highly expressed in iTreg cells. Importantly, we found that the chromatin organizer SATB1 was highly expressed in Th17 cells when compared to TCR-activated Th0 cells, and its expression changed in an opposite direction in cells cultured under Th17/iTreg polarizing conditions (Fig 3A and S3A and S3B Fig). The down-regulation of SATB1 in iTreg cells was consistent with a previous finding that expression of SATB1 was suppressed by Foxp3 [37], whilst in Th17 differentiating cells, we observed that it was up-regulated. Most interestingly, expression of another 19 proteins, such as ETS Variant 6 (ETV6) and transglutaminase 2 (TGM2), showed the same pattern as SATB1. In contrast, 26 proteins—including C-C motif chemokine receptor 7 (CCR7), brain abundant membrane attached signal protein 1 (BASP1), adenylosuccinate synthetase isozyme 1 (ADSSL1), enolase 3 (ENO3),

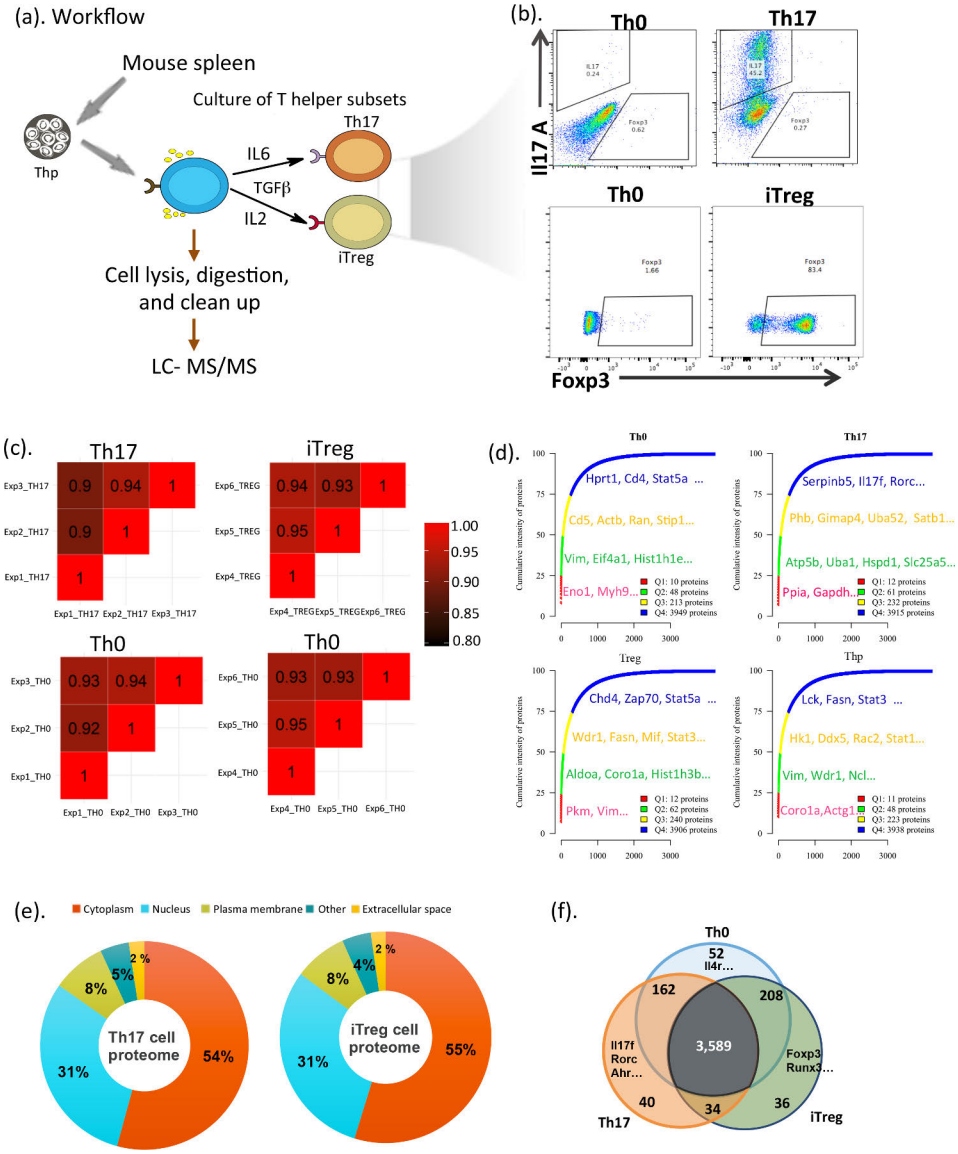

Fig 1. Th17 and iTreg cell proteome. (a) Illustration of experimental and proteomic workflow in the study. (b) Representative flow cytometry plots showing the expression of murine IL17 in Th0 and Th17 cells cultured for 3 d and Foxp3 in Th0 and iTreg cells cultured for 7 d followed by restimulation with anti-CD3/CD28 and polarizing cytokines for additional 3 d. Percentages of positive cells were indicated. (c) Pearson's correlation plots showing the correlation value of biological triplicates for Th17, iTreg, Th0 paired with Th17, and Th0 paired with iTreg cells. (d) Cumulative protein abundances

plotted against ranked proteins. The number of proteins in each quantile was shown on the lists and in S1 Data. (e) Pie chart with percentages of proteins identified across different cell compartments in Th17 and iTreg cells. The complete lists of proteins are in S1 Data. (f) Venn diagram with quantified proteins across Th0, Th17, and iTreg cells. The complete lists of proteins are in S1 Data. Actb, β-actin; Actg1, γ-actin 1; Ahr, aryl hydrocarbon receptor; Aldoa, aldolase A; Atp5b, ATP synthase subunit beta; Chd4, chromodomain helicase DNA-binding protein 4; Coro1a, coronin 1A; Ddx5, DEAD-box helicase 5; Eif4a1, eukaryotic translation initiation factor 4a1; Eno1, enolase 1; Fasn, fatty acid synthase; Foxp3, forkhead box P3; Gapdh, glyceraldehyde-3-phosphate dehydrogenase; Gimap4, GTPase IMAP family member 4; Hist1h1e; histone cluster 1 H1 family member E; Hk1, hexokinase 1; Hprt, hypoxanthine phosphoribosyltransferase; Hspd1, heat shock protein family D1; IL2, interleukin 2; Il4r, interleukin 4 receptor; IL6, interleukin 6; Il17 A, interleukin 17 A; IL17f, interleukin 17f; iTreg, induced regulatory T; Lck, lymphocyte cell-specific protein tyrosine kinase; LC-MS/MS, liquid chromatography–tandem mass spectrometry; Mif, macrophage migration inhibitory faction; Myh9, myosin heavy chain 9; Ncl, nucleolin; Phb, prohibitin; Pkm, pyruvate kinase M; Ppia, peptidylprolyl isomerase A; Rac2, ras-related C3 botulinum toxin substrate 2; Ran, Ras-related nuclear protein; Rorc, retinoic acid receptor–related orphan receptor C; Runx3, runt-related transcription factor 3; Satb1, special AT-rich sequence-binding protein 1; Serpinb5, Serpin Family B Member 5; Slc25a2, solute carrier family 25 member 2; Stat1, signal transducer and activator of transcription 1; Stat3, signal transducer and activator of transcription 3; Stat5a, signal transducer and activator of transcription 5A; Stip1, stress-induced phosphoprotein 1; TGFβ, transforming growth factor β; Th0, T cell receptor–activated helper T; Th17, T helper 17; Uba1, ubiquitin 1; Uba52, ubiquitin 52; Vim, vimentin; Wdr1, WD repeat domain 1; Zap70, zeta chain of T cell receptor–associated protein kinase 70.

https://doi.org/10.1371/journal.pbio.2004194.g001

RIOK1, fascin actin-bundling protein 1 (FSCN1), and myosin heavy chain 11 (MYH11)—were expressed in an opposite manner: repressed in Th17 and induced in iTreg cells (S3C Fig). It would be interesting to investigate whether and how these proteins contribute to Th17 and iTreg cell function.

Since Th17 cells produce inflammatory cytokines and since iTreg cells are immunosuppressive, in order to explore how the observed protein expression changes in Th17 and in iTreg cells are linked with the cell functions, we performed a Kyoto Encyclopedia of Genes and Genomes (KEGG) pathway enrichment analysis of DE proteins in the comparison of Th17 and iTreg cells. We found that several pathways were enriched in the proteins highly expressed in Th17 cells, including spliceosome, ribosome, and OXPHO (Fig 3B and S3 Data). Importantly, the most significantly enriched pathways for the proteins highly expressed in iTreg cells were the metabolic pathway and fatty acid metabolism pathways (Fig 3B and S3 Data). To further illustrate functional impact of protein expression differences in Th17 and iTreg cells, we constructed an enrichment map using core enrichment genes of the Gene Set Enrichment Analysis (GSEA) (S3D Fig). The protein–protein interactions were derived from the String database [38] using confidence level 0.7. As shown in S3D Fig, the module named "pathways whose core enrichment genes overlap with Oxidative phosphorylation" including a group of proteins such as ATP synthase subunit beta (ATP5B), ATP synthase F1 subunit alpha (ATP5A1), cyclooxygenase 2 (COX2), cyclooxygenase 5A (COX5A), and NADH:ubiquinone oxidoreductase core subunit S1 (NDUFS1) were highly expressed in Th17 cells and were closely associated with each other. Based on previous studies, these proteins have been involved in OXPHO as well as in Huntington disease, Alzheimer disease, Parkinson disease, retrograde endocannabinoid signaling, and nonalcoholic fatty liver disease (NAFLD) (Fig 3B, S3D Fig and S3 Data), whereas a group of proteins including acetyl-CoA acyltransferase 2 (ACAA2), aldehyde dehydrogenase 2 (ALDH2), hydroxyacyl-CoA dehydrogenase (HADH), carnitine palmitoyltransferase 2 (CPT2), and 3-hydroxyacyl-CoA dehydratase 3 (HACD3) were highly expressed in iTreg cells and were clustered as a module named fatty acid metabolism. This module comprised pathways of fatty acid metabolism, fatty acid elongation, and fatty acid degradation (S3D Fig, S3 Data). Additionally, the group of proteins involved in ribosome biogenesis was highly expressed in Th17 cells and formed the "ribosome" module. Results from pathway analysis indicate that Th17 and iTreg cells use a distinct energy resource to maintain their functions.

Among the DE proteins in the comparison of Th17 and iTreg cells, there were a group of 155 TFs and ligand-dependent nuclear receptors, including the 2 lineage-specific TFs, Foxp3 and RORC. In order to investigate the highly complex interaction patterns of these TFs in

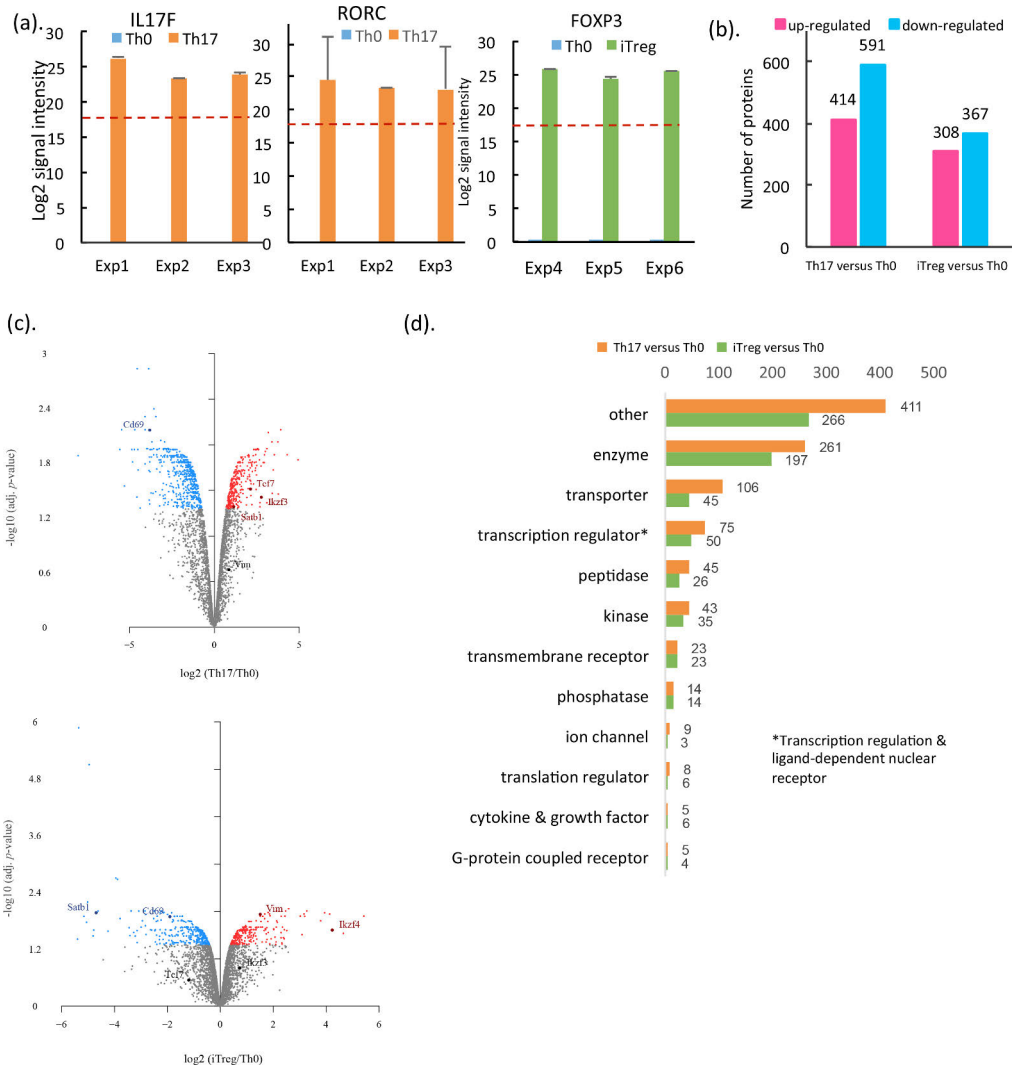

Fig 2. Protein Exp changes during Th17 and iTreg cell differentiation. (a) LC-MS/MS log2 median intensity values of cytokine IL17F, TF Rorc in Th0 and Th17, and TF Foxp3 in Th0 and iTreg cells from 3 replicates. Data shown are median values from 3 technical replicates (in S2 Data) with the SEM. Dotted line showing the minimum of LC-MS/MS signal intensity detections. (b) Number of DE proteins of Th17 and iTreg in comparison to Th0 cells. The complete lists of DE proteins can be found in S2 Data. (c) Volcano plots of statistical significance against fold-change of proteins between cell types (in S2 Data). Blue and red dots indicate statistically differentially abundant proteins. (d) Functional groups of significantly DE proteins in Th17 or iTreg cells compared to Th0 cells. Functional groups were annotated by using IPA (Qiagen Bioinformatics. www.qiagenbioinformatics.com). The complete lists of DE proteins are in S2 Data. DE, differentially expressed; Exp, expression; Foxp3, forkhead box P3; IKZF3, IKAROS family zinc finger 3; IKZF4, IKAROS family zinc finger 4; IL17F, interleukin 17F; IPA, Ingenuity Pathway Analysis; iTreg, induced regulatory T; LC-MS/MS, liquid chromatography–tandem mass spectrometry; Rorc, retinoic acid receptor–related orphan receptor C; Satb1, special AT-rich sequence-binding protein 1; SEM, standard error of the mean; Tcf7, transcription factor 7; TF, transcription factor; Th0, T cell receptor–activated helper T; Th17, T helper 17; Vim, vimentin.

https://doi.org/10.1371/journal.pbio.2004194.g002

regulating Th17 and iTreg lineage commitment, we constructed a transcriptional regulatory network in Th17 and iTreg cells using these DE TFs. The histone deacetylase 1 (HDAC1) was responsible for the deacetylation of lysine residues on the N-terminal of the core histones (H2A, H2B, H3, and H4). HDAC1 was slightly but significantly more highly expressed in Th17 cells compared to iTreg cells (S3 Data). A study in human Th17 cells has indicated that HDAC1 interacts with and deacetylates retinoic acid receptor–related orphan receptor γ T (RORγt) [39]. Protein–protein association network analysis using String *Mus musculus* database showed the association of HDAC1 with multiple TFs, including signal transducer and activator of transcription 3 (STAT3), nuclear factor kappa B subunit 1 (NFKB1), runt-related transcription factor 1 (RUNX1), and sirtuin 2 (SIRT2) (Fig 3C). Given the essential role of histone deacetylation for epigenetic repression of gene expression, HDAC1 was at the highest regulatory level in the hierarchical view of the transcriptional regulatory network in Th17 and iTreg cells. The critical role of STAT3 in Th17 and iTreg differentiation has been established by several studies [22, 30, 40–43]. Consistent with previous findings, the network analysis demonstrated the association of STAT3 with other STATs as well as with interferon regulatory factor 4 (IRF4), JUNB, FOXP3, REL, forkhead box O1 (FOXO1), and nuclear receptor subfamily 3 group C member 1 (NR3C1) (Fig 3C). In the constructed network, the size of each node correlates with its connectivity. Interestingly, one of the biggest nodes in the network was SWI/SNF-related matrix-associated actin-dependent regulator of chromatin subfamily A member 4 (SMARCA4), which was expressed more highly in Th17 compared to iTreg cells (Fig 3C). It has been reported that Smarca4 was among the Th17 positive module. Knockdown of Smarca4 regulator down-regulated Th17 marker genes in Th17 cells [28]. Notably, in the constructed network, in addition to SMARCA4, several other members of the SWI/SNF family—including SWI/SNF-related matrix-associated actin-dependent regulator of chromatin subfamily A member 5 (SMARCA5), SWI/SNF-related matrix-associated actin-dependent regulator of chromatin subfamily D member 1 (SMARCD1), SWI/SNF-related matrix-associated actin-dependent regulator of chromatin subfamily B member 1 (SMARCB1), SWI/SNF-related matrix-associated actin-dependent regulator of chromatin subfamily C member 2 (SMARCC2), SMARCE1—were all highly expressed in Th17 cells (Fig 3C), suggesting the SWI/SNF family may play an import role in regulating Th17 differentiation or function. As such, the transcriptional regulatory network analysis not only confirmed previous findings but also predicts potential regulators that have not been previously appreciated.

Collectively, Th17 and iTreg cells have distinct protein expression profiles that are associated with differently enriched pathways. Pathway enrichment and network analysis improved the understanding of the functional context and organization of proteins in Th17 and iTreg cells. Follow up functional characterization of these molecules may provide novel potential targets influencing Th17/iTreg balance.

Correlation of protein and RNA expression changes during Th17 and iTreg cell differentiation

Characterization of molecular mechanisms involved in regulating Th17 cell differentiation has been studied at the transcriptional and epigenetic level [10, 26–28]. To identify protein expression changes not previously detected in mRNA expression–profiling studies, we generated an RNA-seq data set from in vitro cultured murine Th0 and Th17 cells with the same culture conditions as the proteomics study. Firstly, transcripts from 96.7% of the proteins detected by LC-MS/MS could be found in RNA-seq data (S4 Data). As expected, increased expression of IL17F and RORC in Th17 cells was observed both in quantitative proteomics as well as RNA-seq data. To address the question of which protein expression changes were not seen at mRNA

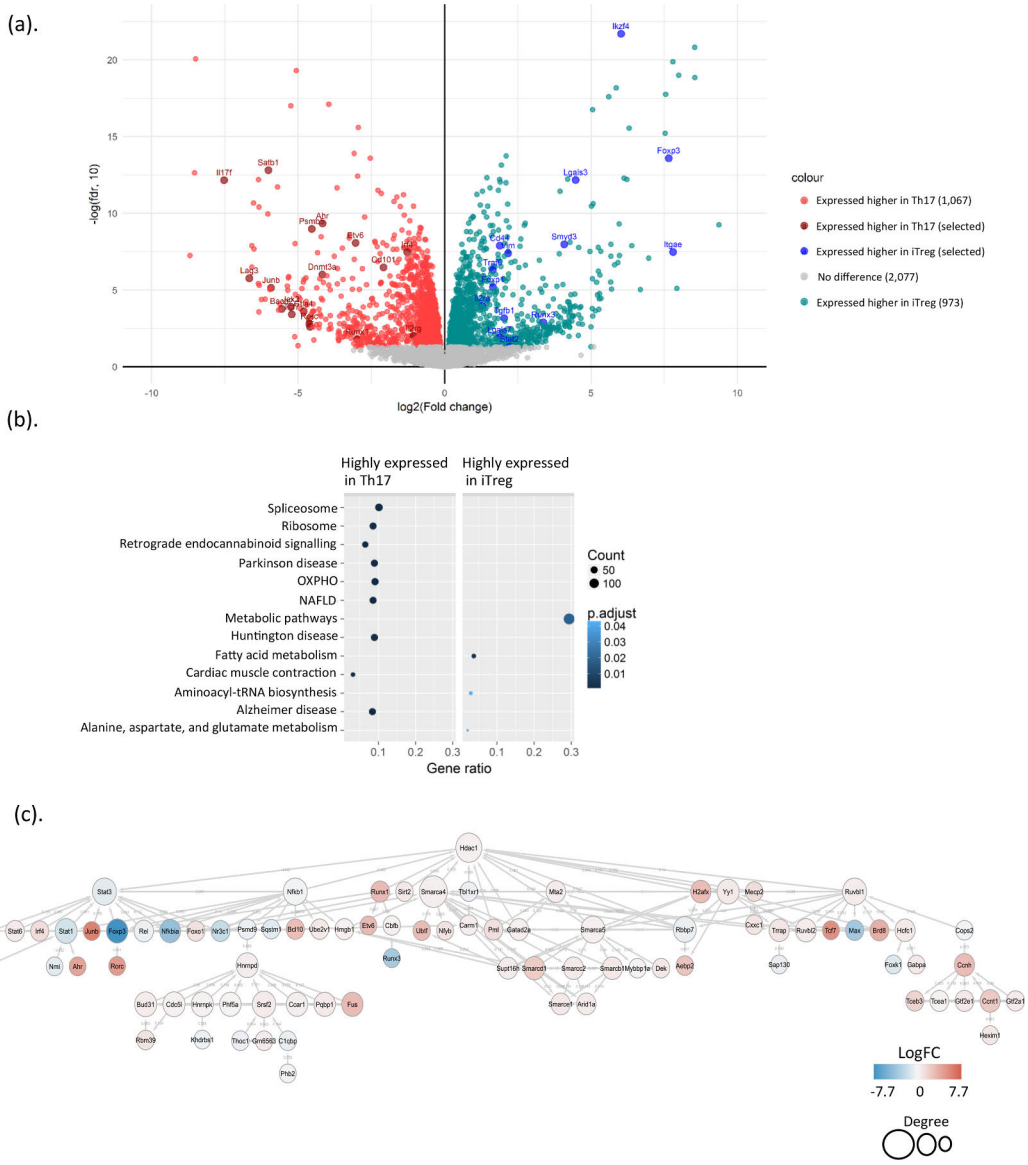

Fig 3. DE proteins in Th17 and iTreg cell differentiation. (a) Volcano plot of the comparison of proteome from Th17 versus iTreg cell. Green and red dots indicate statistically DE proteins. The complete lists of DE proteins in Th17 and iTreg cells are in S3 Data. (b) KEGG pathway analysis was performed on up-regulated (highly expressed in Th17) and down-regulated (highly expressed in iTreg) proteins in Th17 versus iTreg comparison. The pathways presented in the plot are significantly (Benjamini-Hochberg adjusted $p < 0.05$) enriched; size and color of dot indicate the number of proteins detected for that pathway and adjusted p-value respectively. The

lists of pathways and proteins are in S3 Data. (c) Transcriptional regulatory network of Th17 and iTreg cells is shown. The TF annotation for DE proteins in comparison of Th17 and iTreg cells was obtained using IPA. The lists of TFs are in S3 Data. Hierarchical layout of String network is displayed. The red and blue nodes indicate proteins highly expressed in Th17 and iTreg cells, respectively. The size of nodes indicates the degree of connectivity of the nodes. Aebp2, adipocyte enhancer–binding protein 2; Ahr, aryl hydrocarbon receptor; Arid1a, AT-rich interaction domain 1A; Bach, BTB domain and CNC homology; Bcl10, B cell chronic lymphocytic leukemia/lymphoma 10; Brd8, bromodomain-containing 8; C1qbp, complement C1q binding protein; Carm1, coactivator-associated arginine methyltransferase 1; Cbfb, core binding factor beta; Ccar1, cell cycle and apoptosis regulator 1; Ccnh, cyclin H; Ccnt1, cyclin T1; Cdc5l, cell division cycle 5–like protein; Cops2, constitutive photomorphogenesis 9 signalosome subunit 2; Ctla4, cytotoxic T lymphocyte–associated protein 4; Cxxc1, CXXC finger protein 1; DE, differentially expressed; Dnmt3a, DNA methyltransferase 3 alpha; Etv6, ETS Variant 6; fdr, false discovery rate; Foxk1, forkhead box K1; Foxo1, forkhead box O1; Foxp1, forkhead box P1; Foxp3, forkhead box P3; Fus, Fus RNA binding protein; Gabpa, GA-binding protein transcription factor subunit alpha; Gatad2a, GATA zinc finger domain containing 2A; Gtf2a1, general transcription factor IIA subunit 1; Gtf2e1, general transcription factor IIE subunit 1; H2afx, histone 2A family member X; Hcfc1, host cell factor C1; Hdac1, histone deacetylase 1; Hexim1, hexamethylene bisacetamide inducible 1; Hmgb1, high-mobility group box 1; Hnrnpd, heterogeneous nuclear ribonucleoprotein D; Hnrnpk, heterogeneous nuclear ribonucleoprotein K; IKZF4, IKAROS family zinc finger 4; Il2, interleukin 2; Il2ra, interleukin 2 receptor alpha; Il2rg, interleukin 2 receptor gamma; Il17f, interleukin 17f; IPA, Ingenuity Pathway Analysis; Irf3, interferon regulatory factor 3; Irf4, interferon regulatory factor 4; ITGAE, integrin subunit alpha E; iTreg, induced regulatory T; Jak3, Janus kinase 3; KEGG, Kyoto Encyclopedia of Genes and Genomes; Khdrbs1, KH RNA binding domain containing, signal transduction–associated 1; Lag3, lymphocyte activating 3; Lgals3, galectin 3; Lgals7, galectin 7; Max, MYC-associated factor X; Mecp2, methyl-CpG binding protein 2; Mta2, metastasis-associated 1 family member 2; Mybbp1a, MYB binding protein 1A; Nfkbia, nuclear factor of kappa light polypeptide gene enhancer in B cells inhibitor alpha; Nfyb, nuclear transcription factor Y beta; Nmi, N-myc and STAT interactor; NR3C1, nuclear receptor subfamily 3 group C member 1; OXPHO, oxidative phosphorylation; Phb1, prohibitin 1; Phb2, prohibitin 2; Phf5a, PHD finger protein 5a; Pml, promyelocytic leukemia; Pqpb1, polyglutamine-binding protein 1; Psmb5, proteasome subunit beta 5; Psmd9, proteasome 26S subunit non-ATPase 9; Rbbp7, retinoblastoma binding protein 7; Rbm39, RNA binding motif 39; Rorc, retinoic acid receptor–related orphan receptor C; Runx1, runt-related transcription factor 1; Runx3, runt-related transcription factor 3; Ruvbl1, RuvB-like AAA ATPase 1; Ruvbl2, RuvB-like AAA ATPase 2; Sap130, Sin3A-associated protein 130; Satb1, special AT-rich sequence-binding protein 1; Sqstm1, sequestosome 1; Sirt2, sirtuin 2; Smarca4, SWI/SNF-related matrix-associated actin-dependent regulator of chromatin subfamily A member 4; Smarca5, SWI/SNF-related matrix-associated actin-dependent regulator of chromatin subfamily A member 5; Smarcb1, SWI/SNF-related matrix-associated actin-dependent regulator of chromatin subfamily B member 1; Smarcc2, SWI/SNF-related matrix-associated actin-dependent regulator of chromatin subfamily C member 2; Smarcd, SWI/SNF-related matrix-associated actin-dependent regulator of chromatin subfamily D; Smarce1, SWI/SNF-related matrix-associated actin-dependent regulator of chromatin subfamily E member 1; Smyd3, SET And MYND domain containing 3; Srsf2, serine- and arginine-rich splicing factor 2; Stat1, signal transducer and activator of transcription 1; Stat2, signal transducer and activator of transcription 2; Stat3, signal transducer and activator of transcription 3; Stat6, signal tranducer and activator of transcription 6; Supt16h, SPT16 homolog; Tbl1xr1, transducin beta–like 1 X-linked receptor 1; Tcea1, transcription elongation factor A polypeptide 1; Tceb3, transcription elongation factor B polypeptide 3; Tcf7, transcription factor 7; TF, transcription factor; Tgfbr-I, transforming growth factor beta receptor type 1; Th17, T helper 17; Thoc1, THO complex 1; Traf6, tumor necrosis factor receptor–associated factor 6; Trrap, transformation/transcription domain–associated protein; Ube2v1, ubiquitin conjugating enzyme E2 V1; Ubtf, upstream binding transcription factor; Vim, vimentin; Yy1, yin yang 1.

https://doi.org/10.1371/journal.pbio.2004194.g003

level, we compared the DE genes and DE proteins (Th17 versus Th0). First, to make the proteomics and transcriptomics data comparable, from DE proteins we removed proteins without corresponding transcripts; similarly, the DE genes without detected corresponding proteins were also removed from DE genes. Interestingly, among the 963 DE proteins with corresponding detected transcripts in Th17 cells, expression changes for 284 (29.5%) proteins agreed with their gene expression changes detected by RNA-seq at the same time point (Fig 4A and S4 Data). This group included 139 molecules that were up-regulated consistently both at mRNA and protein level, such as Il17f, Rorc, and Ahr, and 145 molecules were down-regulated consistently both at mRNA and protein level, including, for example, Tnfrsf18, Cd44, Il2rg, and interferon-inducible GTPase 1 (Iigp1). Therefore, for these 284 genes, our proteomics experiments confirmed their mRNA expression changes at the protein level. Notably, among the 963 DE proteins with corresponding detectable transcripts in Th17 cells, 564 proteins (58.6%) were only found to be DE at the protein but not at mRNA level (Fig 4A, S4 Data) at the same time point. This is comparable with previously reported proteomics studies showing the correlation between mRNA and protein changes [44–47]. Based on protein annotation, the DE proteins with and without consistent mRNA expression changes showed similar composition of functional groups (S4A Fig and S4 Data). To address whether the DE genes encoding non-DE proteins were at relatively low expression levels, we checked the distribution of fragments per kilobase of transcript per million mapped reads (FPKM) values for the group of DE genes encoding DE proteins and the group of only DE genes encoding non-DE protein. We did not observe any major differences, indicating that DE genes encoding non-DE proteins were not relatively lowly expressed (S4B Fig and S4 Data). This indicates translation, protein degradation and export process, and maybe posttranslation modification play an important role in controlling Th17/iTreg cell protein expression. These newly identified DE proteins may also

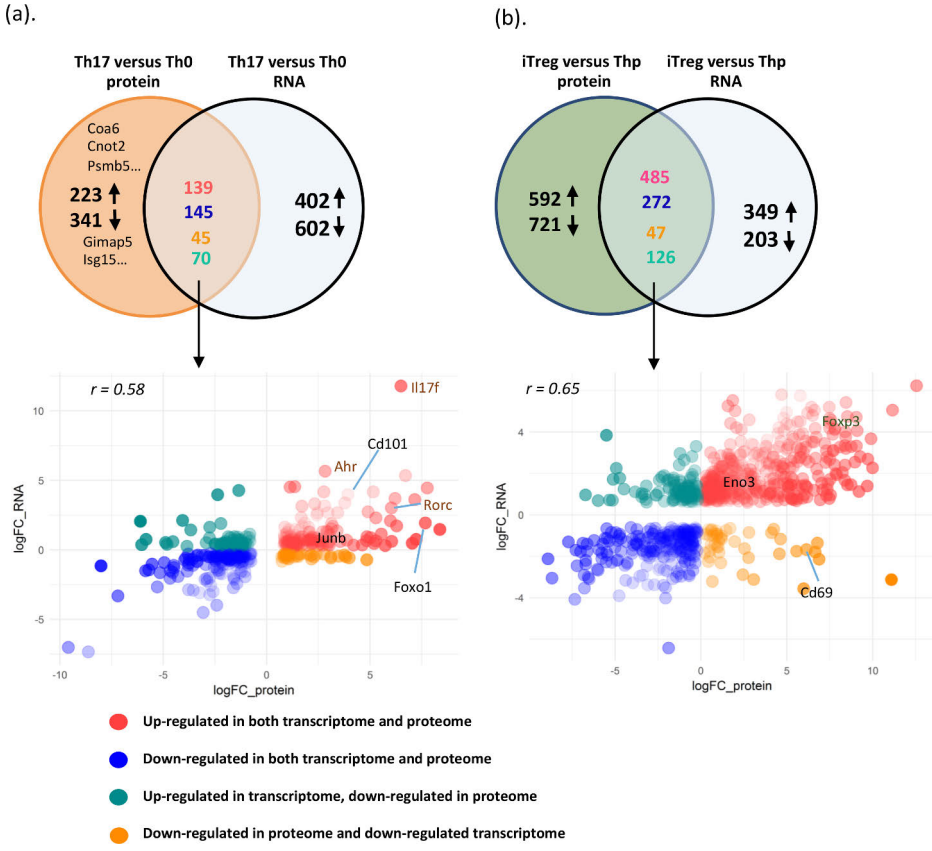

Fig 4. Correlation of protein and RNA expression changes during Th17 and iTreg cell differentiation. Venn diagram showing the comparison of DE proteins with corresponding transcripts and DE transcripts with encoded detected proteins in comparison of Th17 and Th0 cells (a) or iTreg versus Thp cells (b). Scatterplot of proteins that were observed in proteomic and transcriptomic comparison of Th17 versus Th0 cell (a) or iTreg versus Thp cells (b). The lists of detected proteins and transcripts in Th17 versus Th0 cells and in iTreg versus Thp cells are in S4 Data. Ahr, aryl hydrocarbon receptor; Cnot2, CCR4-NOT transcription complex subunit 2; Coa6, cytochrome c oxidase assembly factor 6; DE, differentially expressed; Eno3, enolase 3; Foxo1, forkhead box O1; Foxp3, forkhead box P3; Gimap5, GTPase IMAP family member 5; Il17f, interleukin 17F; Isg15, interferon-stimulated gene 15; iTreg, induced regulatory T; Psmb5, proteasome subunit beta 5; Rorc, retinoic acid receptor–related orphan receptor C; Th0, T cell receptor–activated helper T; Th17, T helper 17; Thp, naïve CD4+ T.

https://doi.org/10.1371/journal.pbio.2004194.g004

contribute to Th17 cell polarization and function. Given the importance of Th17 cells in immune response and disease pathogenesis, it is worth further characterizing their function in Th17 cells.

To compare proteomics and transcriptomics data from in vitro cultured iTreg cells with Thp cells, we used published microarray data [10] and observed increased Foxp3 expression in iTreg cells both at protein level as well as at mRNA level. Comparing our proteomics data with these microarray data generated from iTreg cells with the similar conditions, we observed 757

genes with consistent expression changes at protein and mRNA level. Among the overlapping DE proteins and DE mRNAs, the Pearson's correlation coefficient was 0.65 (Fig 4B, S4 Data). However, we found that for 67.8% of the DE proteins, the changes were inconsistent with the RNA expression changes at the selected time point. Among the DE proteins in iTreg cells, 1,313 proteins were found to be DE at the protein but not the RNA level (Fig 4B, S4 Data)—such as stathmin 2 (STMN2), prolyl 4-hydroxylase subunit alpha 1 (P4HA1), and reactive oxygen species modulator 1 (ROMO1)—for which their contributions to iTreg cells have not yet been characterized. As another example, one of the H3K4 histone methyltransferases, SET and MYND domain containing 3 (SMYD3), was up-regulated only at the protein level. Notably, a recent study has reported that TGFβ induces SMYD3 expression during iTreg differentiation [48]. SMYD3 regulates Foxp3 expression by enhancing the trimethylated state of H3K4 in the promoter and the conserved noncoding DNA sequence 1 (CNS-1) element of Foxp3.

Validation of DE proteins in Th17 and iTreg cells

To confirm the LFQ results, we used either flow cytometry or western blot to quantify expression of selected proteins in 3 additional cultures. Comparing to TCR-activated Th0 cells in our primary proteomics data, we found expression of CD69 to be significantly down-regulated in both Th17 and iTreg cells (Fig 5A and S5 Data). CD69 is widely accepted as a marker of early T cell activation with an immune regulatory role [3, 4, 49, 50]. Compared to Th0 cells, after 72 h culture, CD69 expression was clearly down-regulated in iTreg and especially in Th17 cells (Fig 5B). CD101 is highly expressed in lymphoid and myeloid cells in intestinal tissues, and its expression in T cells was sufficient for Treg function and the inhibition of T cell proliferation [51, 52]. Notably, reduced expression of CD101 has been detected in inflammatory bowel disease (IBD) patients [52]. We found that Th17 culturing conditions induced CD101 expression and that it was expressed at higher levels in Th17 cells than iTreg cells (Figs 3A and 5A). This difference was also confirmed by flow cytometry (Fig 5B).

It has been previously shown that TF NFATC2 (NFAT1) interacts with FOXP3, and the complex suppresses IL2 production and Treg cell function [53]. We found that expression of NFATC2 was induced in Th17 cells from the transcriptomics as well as proteomics data (Fig 5A and S5 Data). Our western blot analyses also validated this expression change of NFATC2 in Th17 cells compared to Th0 cells (Fig 5C, S5 Fig).

We were especially interested in the proteins selectively expressed in iTreg or Th17 cells that may contribute to their lineage-specific functions. Expression levels of SMYD3 and ENO3 were up-regulated in iTreg cells (Fig 5A and S5 Data). Consistent with this observation, western blot analysis on 3 additional murine T cell cultures showed enhanced SMYD3 expression in iTreg cell (Fig 5C, S5 Fig). Protein expression of FOXO1 was increased in both iTreg cells and Th17 cells (Fig 5C, S5 Fig). Taken together, using different technologies, we validated selected protein expression changes detected by LFQ proteomics analysis, indicating the identified protein expression changes in this study are reliable, hence supporting the utility of this dataset to identify novel molecules putatively involved in the regulation of iTreg or Th17 cell function.

VIM is highly expressed in iTreg cells and influences TGFβ-induced Foxp3 expression

From both proteomics and transcriptomics data, we found that the intermediate filament protein VIM is highly expressed in iTreg (Fig 5C and S6 Data). In iTreg proteomics study, we cultured T cells for 10 d, to evaluate whether the VIM is up-regulated in early polarizing iTreg cells, and we extracted FPKM values of Vim mRNA expression from our RNA-seq data in which Thp cells were cultured under Th0, iTreg, and Th17 for 3 d. As shown in Fig 6A and S6

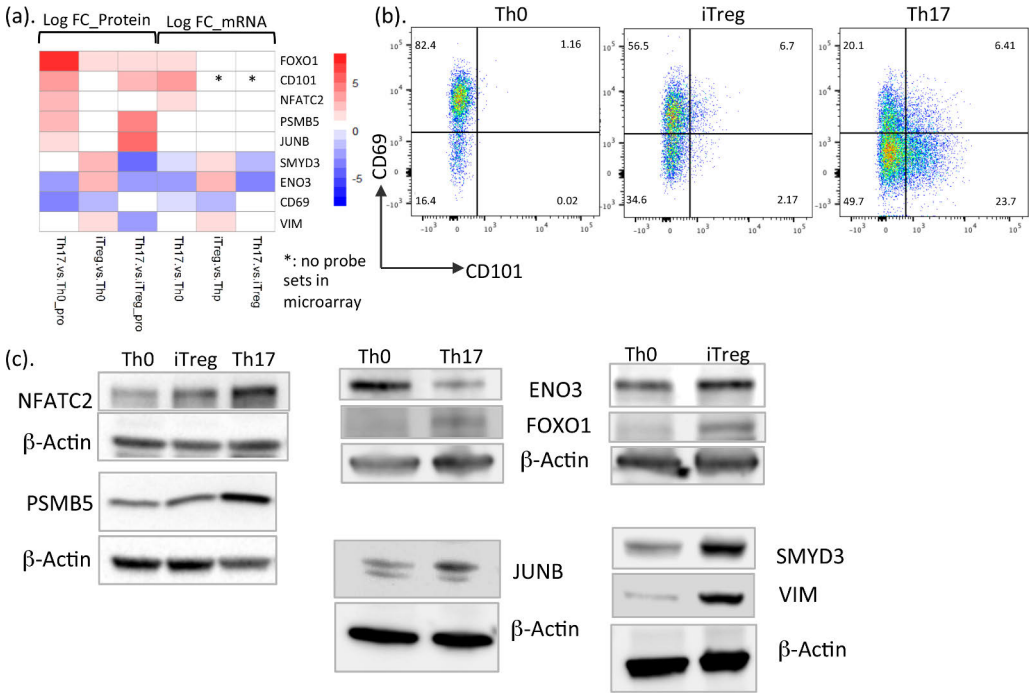

Fig 5. Validation of protein expression changes with different technologies. (a) Heatmap showing the log fold change values (in S5 Data) of proteins and mRNA DE in Th17 and iTreg cells in comparison with Th0 cells and Th17 compared with iTreg cells. (b) Flow cytometry analysis demonstrating the expression of surface molecules CD69 and CD101 in murine Th0, iTreg, and Th17 cells. One replicate is shown. (c) Immunoblot analysis of DE proteins in iTreg and Th17 cells compared to Th0 cells. Representative blots from 2–3 independent experiments are shown. DE, differentially expressed; ENO3, enolase 3; FOXO1, forkhead box O1; iTreg, induced regulatory T; NFATC2, nuclear factor of activated T cells 2; PSMB5, proteasome subunit beta 5; SMYD3, SET and MYND domain containing 3; Th0, T cell receptor–activated helper T; Th17, T helper 17; Thp, naïve CD4+ T; VIM, vimentin.

https://doi.org/10.1371/journal.pbio.2004194.g005

Data, expression of Vim was significantly up-regulated in polarizing iTreg cells compared to Th0 cells. Because TGFβ is the key cytokine to induce Foxp3 expression and iTreg differentiation, we tested whether the enhanced expression of VIM in iTreg cells was dependent on TGFβ. LY2109761 is a transforming growth factor β receptor type 1 (TGFβR-I) kinase inhibitor [54–56]. Consistent with the proteomics data, in western blot, we also detected high VIM expression in iTreg cells compared with Th0 (Fig 6B). Importantly, we observed that addition of LY2109761 diminished Foxp3 as well as VIM expression (Fig 6B), indicating that the up-regulation of VIM in iTreg cells is induced by TGFβ.

Next, we assessed whether VIM plays a role in regulating Foxp3 expression. Thp cells from wild-type (WT) and Vim−/− mice [57] were isolated and activated with plate-bound anti-CD3/CD28 and cultured under Th0 (anti-CD3/CD28) and iTreg (anti-CD3/CD28 combined with TGFβ+IL2) polarizing condition. We observed the absence of VIM in Vim−/− T cells and again detected enhanced expression of VIM in WT iTreg cells (Fig 6C). However, we did not observe significant change of Foxp3 expression in iTreg cells cultured from Vim−/− CD4+ T cells compared to control T cells (Fig 6C). To dissect the effect of VIM on TGFβ- and

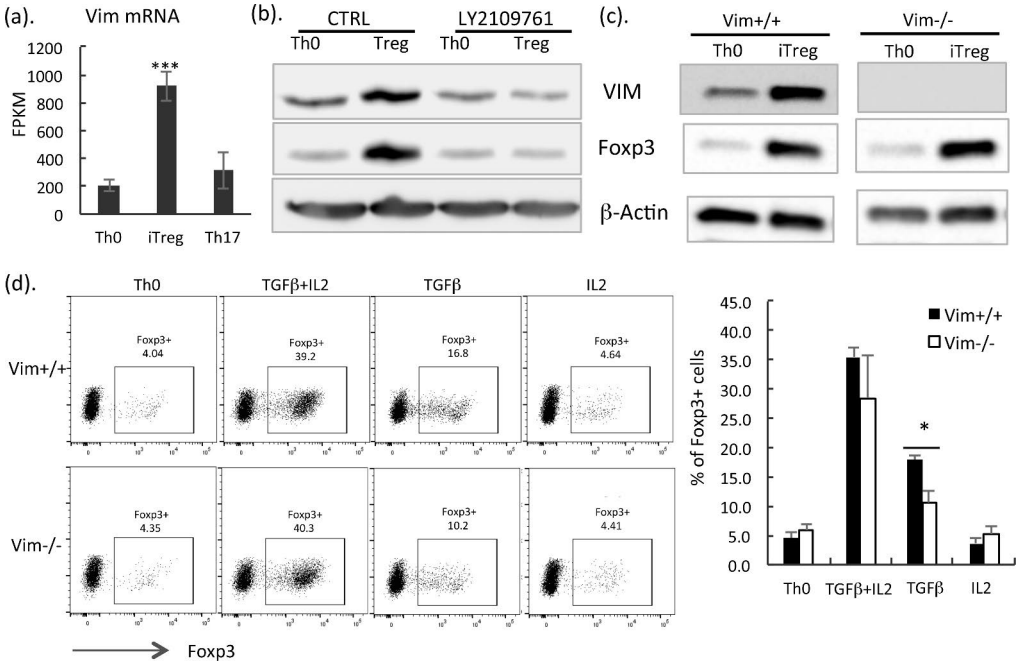

Fig 6. VIM is highly expressed in iTreg cells and influences TGFβ-induced Foxp3 expression. (a) mRNA expression of Vim from RNA-seq data generated in the present study. WT Thp cells were cultured under Th0, iTreg, and Th17 polarizing condition for 3 d. RNAs were isolated and processed for RNA-seq. Data shown are median FPKM values from 3 independent experiments (in S6 Data) with the SEM. Statistical analysis was performed by using paired Student *t* test. ***: $p < 0.01$. (b) Immunoblot analysis of Thp cells cultured to Th0 and iTreg with and without 1 μM LY2109761 for 3 d. VIM, Foxp3, and loading control **β**-actin were shown. Representative of 3 independent experiments is shown. (c) Thp cells cultured to Th0 and iTreg for 3 d. Vim, Foxp3, and loading control **β**-actin were shown. Representative blots of 3 independent experiments are shown. (d) Flow cytometry analysis of WT and Vim-deficient CD4+ T cells cultured with TCR activation (Th0) and with cytokines (IL2+ TGFβ1, TGFβ1, IL2) for 3 d. Representative intracellular cytokine staining for Foxp3 was shown on left panel, and percentage of Foxp3 expression cells detected from 4 independent experiments (in S6 Data) was shown on right panel. CTRL, control; Foxp3, forkhead box P3; FPKM, fragments per kilobase of transcript per million mapped reads; IL2, interleukin 2; iTreg, induced regulatory T; SEM, standard error of the mean; TCR, T cell receptor; TGFβ, transforming growth factor beta; Th0, T cell receptor–activated helper T cell; Th17, T helper 17; Thp, naïve CD4+ T; VIM, vimentin; WT, wild-type.

https://doi.org/10.1371/journal.pbio.2004194.g006

IL2-induced Foxp3 expression, we cultured control and Vim−/− Thp cells in the presence of only TGFβ, only IL2, or TGFβ combined with IL2 for 3 d. Results from intracellular Foxp3 staining showed significantly reduced Foxp3 expression in Vim−/− T cells cultured with TGFβ compared to control T cells (Fig 6D). Interestingly, after addition of IL2 and TGFβ or only with IL2 from 4 independent cultures in Vim−/− cells, no significant expression change of Foxp3 was detected (Fig 6D), indicating that IL2 prevented the effect of VIM in TGFβ-induced Foxp3 expression. Collectively, these data suggest that TGFβ up-regulates VIM expression in iTreg cells. VIM contributes to TGFβ-induced Foxp3 expression.

Discussion

In recent years, next-generation sequencing technology has been widely applied to study the transcriptome of many cellular types and changes, including the differentiation of Th subsets

[14, 27, 58, 59]. In the present study, the application of LFQ proteomics technology provided successful detection and LFQ of the master TF of Treg cells, Foxp3 in cultured iTreg cells, and the hallmark cytokine IL17F and TF RORC in Th17 polarizing cells. To our knowledge, this is the first quantitative proteome profile study in Th17 cells. Given the importance of Th17 and Treg cells in inflammation, autoimmunity, and cancer, development of novel strategies to modulate Th17/Treg cell balance to treat immune-associated diseases and cancer is a subject of interest.

In this study, we chose to study protein profiles of the Th17 cell after in vitro polarization for 3 d. As mentioned above, because of the suppressive effect of IL2 for Th17 differentiation [22], IL2 was not added to the Th17 polarizing cytokine cocktail. Under these conditions, using intracellular cytokine staining, IL17 was detected in approximately 40% of the polarizing Th17 cells. To achieve full polarization of the iTreg cells, we cultured Thp cells for 7 d and restimulated with anti-CD3/CD28 and cultured with TGFβ combined with IL2 for another 3 d. From 3 independent cultures, approximately 87% of cells express Foxp3. These conditions were subsequently chosen for the proteomics profiling of the Th17 and iTreg cells on account of the levels of polarization achieved.

For Th cell subsets, a large amount of gene expression data has been generated using microarray or more recently developed RNA-seq technology. Since intracellular protein levels are balanced through protein biosynthesis, degradation, and export, transcriptomics analysis cannot capture protein-level changes in these processes, and accordingly, many of the detected gene expression changes cannot be confirmed at protein level. Therefore, we took a step beyond mRNA measurement and used LFQ proteomics to construct a protein landscape for Th17 and iTreg cells. With the comparison of proteomics and transcriptomics data from cells cultured in vitro with the same conditions, we quantitatively confirmed 284 and 757 of the DE genes at the protein level in differentiated Th17 compared to Th0 and in iTreg compared to Thp cell, respectively. Some of these proteins have been identified in previous studies to play an important role in regulating Th17/iTreg cell differentiation, such as RORC, IL17F, Foxp3, CD101, NFATC2, mucosa-associated lymphoid tissue 1 (MALT1), and AHR. We also identified a panel of proteins—such as RNA exonuclease 2 (REXO2), paxillin (PXN), and FAM129B—with both RNA and protein expression changes in Th17 cells, whose role in Th17 cell differentiation or function yet needs to be defined. These proteins with consistent changes both at the RNA and protein level in Th17 and iTreg cells provide novel candidates for further functional characterization. Therefore, combining mRNA and protein profiling data can identify potentially relevant targeting molecules.

From further comparisons of the proteomics and transcriptomics data within the same cell types, we found that more than half of the protein-level changes were not detected at the mRNA level. For example, CNOT2 is a subunit of the CCR4-NOT complex, which regulates mRNA synthesis and degradation and is also involved in mRNA splicing, transport, and localization. CNOT2 interacts with histone deacetylases and functions as a repressor of polymerase II transcription [60]. It interacts with several subunits of the silencing mediator for retinoid and thyroid receptors (SMRT)/nuclear receptor corepressor (NCoR)-histone deacetylase 3 (HDAC3) complex and contributes to transcription repression [61]. However, as a transcription regulator, the function of CNOT2 in primary T cells, especially in the differentiation of Th subsets, is largely unknown. In the present study, we found for the first time that the CNOT2 protein is up-regulated in polarizing Th17 cells, but the similar induction of Cnot2 mRNA was not detected by RNA-seq at the same time point. This warrants further characterization of the function of CNOT2 in Th17 cell differentiation and its contribution to autoimmune inflammation.

In this study, pathway enrichment analysis of the proteins DE in Th17 and iTreg cells showed that the OXPHO pathway was enriched in proteins highly expressed in Th17 cells, whereas fatty acid metabolism pathway was enriched in proteins highly expressed in iTreg cells. In the past few years, several studies have demonstrated that the cellular metabolism pathways have a critical role in regulating Th17/iTreg cell differentiation [62–64]. It has been reported that hypoxia-inducible factor 1 subunit α (HIF1α) is up-regulated in Th17 cells and promotes glycolysis in Th17 differentiation [65]. The transport of glucose across the plasma membranes of mammalian cells is facilitated by the Glut family (also called solute carrier family 2). Studies have shown that effector T cells express higher level of glucose transporter 1 (GLUT1; solute carrier family 2 member 1 [SLC2A1]) than iTreg cells. On the other hand, iTreg cells utilize lipid oxidation as a primary metabolic pathway [63]. Moreover, it has been shown that Th17 cell proliferation and cytokine production are inhibited when glycolysis is blocked [65]. In our data, the glycolysis pathway was not enriched in proteins highly expressed in Th17 cells. However, we found that expression of another GLUT family member, glucose transporter 3 (GLUT3; solute carrier family 2 member 3 [SLC2A3]), but not GLUT1, was significantly higher in Th17 cells compared to iTreg cells. Further characterization of contribution of these 2 glucose transporters in Th17/iTreg balance is needed. OXPHO is an important metabolic process for generating ATP molecules in mitochondria. With the comparison of the Th17 and iTreg cell proteomics data, we detected a group of 52 proteins in the OXPHO pathway—including several COX molecules and NADH dehydrogenases—that were highly expressed. These molecules have also been found to be highly expressed in several neuron diseases, such as Parkinson disease, Huntington disease, and Alzheimer disease. To our knowledge, this is the first study reporting a big group of OXPHO-regulated protein changes in Th17 cells. Further functional characterization of this pathway in Th17 cells and the link with diseases seems to be important. Lastly, we found the enrichment of fatty acid metabolic pathway highly expressed in iTreg cells. In addition to the already reported carnitine palmitoyltransferase 1A (CPT1A) [18], the enriched pathway includes 17 proteins whose functions in Treg cells have not yet been established. Interestingly, a previous proteomics study of human Treg and conventional T cells has shown an increased expression of glycolysis-related enzyme enolase 1 (ENO1) in Treg cells [18]. In our murine T cells, we found that although the expression level of ENO1 was higher than that of ENO3, ENO3 showed greater expression changes in iTreg cells, with a 2.3-fold increase compared to Th0 cells and a 2.6-fold increase when compared to Th17 cells. However, we did not observe significant expression changes of ENO1 in iTreg compared to Th0 cells, and only a minor increase (0.2-fold increase) was observed when comparing to Th17 cells. These results suggest that in murine Th17/iTreg cells, ENO3 but not ENO1 may have a more important role. Taken together, our data showed that a large number of proteins involved in metabolic pathways were differently expressed in Th17 and iTreg cells, suggesting that Th17 and iTreg cells use distinct energy resource to maintain their function.

The comparison of the proteomics and transcriptomics data from iTreg cells led to the recognition of the high differential expression of VIM in iTreg cells. VIM is the major cytoskeletal component of mesenchymal cells with important roles in cell adhesion, migration, differentiation, cytoskeletal rearrangements, and regulation of cell morphology. VIM has an important function in epithelial–mesenchymal transition and tumorigenesis [66–68]. In lymphocytes, VIM provides structural support in circulating human lymphocytes and also plays a role in lymphocyte adhesion and transcellular migration [69]. A recent study demonstrates that in a mouse model, VIM is required for TGFβ-induced wound healing [66]. In the present study, we found that VIM is highly expressed in iTreg cells, and TGFβ up-regulated the expression of VIM. Although Vim mRNA was also slightly up-regulated in Th17 cells, its protein expression level is significantly lower in Th17 cells compared to iTreg cells, suggesting that addition of the

inflammatory cytokine interleukin 6 (IL6) in the cell culture may suppress TGFβ-induced VIM expression. Importantly, we found that VIM was involved in TGFβ-induced Foxp3 expression. However, this effect was prevented by IL2. Since both TGFβ and IL2 have fundamental functions in T cells, it would be interesting to further explore how the expression of VIM in T cells contributes to different immune-associated diseases. In the present study, we show that the metabolic pathway is one of the most enriched pathways in iTreg cells and that VIM is highly expressed in iTreg cells. Interestingly, a previous study has reported that VIM interacts with cytosolic phospholipase A2 α (cPLA2α) and functions as an adaptor of cPLA2α to function properly during the eicosanoid biosynthetic process [70]. It will also be important to further characterize the mechanisms by which VIM influences T cell functions and what signaling pathways are involved, especially whether it is involved in regulating T cell metabolism.

In summary, these proteomics data provide additional information to the transcriptomics data to help better characterization of Th17 cells, an important group of Th cells that are central to autoimmunity and inflammation. In addition, our dataset provides a valuable resource for further functional characterization of novel players involved in Th17/iTreg cell differentiation or function that could also lead to the development of novel therapeutic targets to modulate Th17/iTreg cells to treat human diseases.

Materials and methods

Ethics statement

Mice used in this study were maintained in the Central Animal Laboratory at Turku University. All experiments were carried out in accordance with appropriate guidelines for the care and use of laboratory animals and were approved by the Finnish Animal Ethics Committee.

CD4+ T cell isolation and culture

Mouse splenocytes were isolated from 8–10-wk-old C57BL/6 mice. For VIM study, mouse splenocytes from 6–10-wk-old Vim−/−, and WT mice were isolated. Mice were maintained in the Central Animal Laboratory at Turku University. CD4+CD62L+ T cell Isolation Kit II (Miltenyi Biotec, Bergisch Gladbach, Germany) was used to obtain naïve T cells. The cells were activated with plate-bound anti-CD3 (1 μg/mL, BD PharMingen, San Diego, CA) and anti-CD28 (1 μg/mL) for all Th0, Th17, and iTreg conditions. For Th17 polarization, IL6 (30 ng/ml, PeproTech, UK), TGFβ1 (5 ng/ml), and neutralizing antibodies anti-IL4 and anti-IFNγ (both at 10 μg/mL, BD PharMingen, San Diego, CA) were added, and cells were cultured for 3 d. For iTreg conditions, IL2 (10 ng/ml, R&D system, Minneapolis, MN) and TGFβ1 (20 ng/ml) were used, and cells were cultured for 7 d, followed by restimulation with anti-CD3/CD28 and culturing with fresh cytokine-containing medium for another 3 d. All cell cultures were performed in IMDM supplemented with 10% fetal calf serum, 2 mM glutamine, 100 iu/mL penicillin, 0.1 mg/mL streptomycin (Sigma, St Louis, MO), and 2.5 μM β-mercaptoethanol.

Sample preparation for mass spectrometric analysis and transcriptomics study

In vitro cultured murine CD4+ T cells were collected after 72 h or 10 d of polarization under polarizing conditions indicated above in "CD4+ T cell isolation and culture". The cells were lysed with lysis buffer containing 0.5% (v/v) NP-40, 150 mM NaCl, and 50 mM Tris-HCl. The lysates were sonicated in Bioruptor Sonicator, and the supernatants were precipitated with Acetone. The obtained pellets were dissolved in 25 mM ammonium bicarbonate buffer containing 8 M Urea. The protein concentrations were measured using Bio-Rad DC protein assay

kit. Proteins were reduced with DTT for 1 h at 37˚C and alkylated with Iodoacetamide for 30 min in dark at room temperature and then were digested with trypsin (Promega sequencing grade). The trypsin to protein ratio of 1:30 (w/w) was used, and digestion was performed at 37˚C overnight. The trypsin activity was quenched by adding 10% of triflouroacetic acid. Peptides were desalted with C18 tips (OMIX, Agilent) according to manufacturer's instruction. The detergent was removed with HiPPR Detergent Removal Spin Column Kit (Thermo Scientific) according to manufacturer's recommendations. The peptides were concentrated in Speedvac and resuspended in 2% formic acid and 2% acetonitrile before mass spectrometry analysis.

LC-MS/MS analysis

The trypsin-digested peptides were analyzed by Q Exactive mass spectrometer (Thermo Fisher Scientific, Bremen, Germany) coupled to a nano-flow UHP-LC system (Easy-nLC1200, Thermo Fisher Scientific). Peptides (200 ng) were first loaded on a trapping column and subsequently separated on a C18 column (75 μm × 150 mm, 5 μm 200 Å, Dr. Maisch). The mobile phase consisted of a binary mixture of water and acetonitrile alone with formic acid.

The peptides were separated from 5% to 35% of solvent B in 85 min at a flow rate of 300 nl/min. The tandem mass spectra were acquired automatically by using Thermo Xcalibur software (Thermo Fisher Scientific). An information-dependent acquisition method with higher-energy C-trap dissociation (HCD) fragmentation of top 10 most intense ion in survey scan of mass range 300–1800 m/z was used. Samples were run in triplicate in randomized batches. To establish the consistent performance of the instrument, both a pooled sample and in-house standard digest were analyzed at the beginning and end of the batch.

MS data analysis

The MS data raw files were searched against a mouse (*M. musculus*) UniProt database (downloaded on 18 January 2016) using the Andromeda search engine integrated into MaxQuant software version 1.5.3.30. The specified search parameters included carbamidomethyl (C) as a fixed modification and methionine oxidation and N-terminal acetylation as variable modification together with 1 tryptic missed cleavage. The peptide and protein FDR were set to 1%. Match between run options was enabled to transfer the identification across the samples.

Proteomic data analysis

Samples for each condition (Thp, Th0, Th17, and iTreg) were derived from 3 cultures, all of which were analyzed using 3 technical replicates. Experimental design was paired. The nondetected MaxQuant intensities were imputed with the minimum nonzero intensity value of the corresponding technical replicate. Proteins MaxQuant identified only by site or labeled as potential contaminants were filtered out of the analysis. We preprocessed the data by summarizing technical replicates with medians, transformed the values to a logarithmic scale, and did the quantile normalization. We used Bioconductor package limma [71] to perform moderated *t* test with paired design to detect the differentially abundant proteins between iTreg and Th0 cells and Th17 and Th0 cells. Moderated *t* test with unpaired design was used to detect the differentially abundant proteins between iTreg and Thp cells as well as iTreg and Th17 cells. Statistical tests were done for such proteins that had at least 1 detected protein intensity value in both conditions. We performed the tests separately for the proteins detected in all samples and for the proteins that were not detected in some of the samples. For the latter proteins, we ignored samples whose corresponding sample pairs were not detected. By using Benjamini-Hochberg multiple correction, the differentially abundant proteins were identified with

FDR < 0.05. Those proteins that had detected intensities in only 1 of the conditions were identified without statistical testing and were called as "selectively expressed." All proteins that had at least 2 paired biological replicates are considered detected.

Transcriptomic data analysis

After 72 h of polarization under polarizing conditions indicated above in "CD4+ T cell isolation and culture", 4 independent in vitro cultured murine CD4+ cells were collected. RNAs from these samples were extracted (RNeasy kit, Qiagen). RNA-seq with pair-end 100-nt read length was performed at the Turku Center for Biotechnology with HiSeq 2000 instrument using Illumina TruSeq chemistry according to the manufacture's instruction.

The RNA-seq data were mapped using Tophat (version 2.0.14) with default parameters to the mm10 mouse reference genome. Read counts were computed with HTSeq-count [72], with options stranded false, feature type exon, and sorted by name and mode union. Negative binomial generalized log-linear model to the read counts for each gene was fitted, and gene-wise statistical tests using pair-wise experimental design were performed with Bioconductor edgeR package [73]. The data were normalized using model-based scaling [74]. The tag-wise dispersions for the generalized linear models were empirical Bayes estimates with expression levels specified by a log-linear model [75]. Genes that did not have more than 1 count per million (cpm) at least in 4 samples were filtered out of the analysis.

Pathway enrichment analysis

Hypergeometric tests and GSEAs of GO and KEGG pathways were performed using R package clusterProfiler [76]. In hypergeometric tests, all proteins with FDR < 0.05 were considered differentially regulated, and the background consisted of all proteins detected in samples involved in the corresponding comparison. For GSEA, we ranked the proteins by the common logarithm of adjusted *p*-value, and the sign was derived from the logarithmic fold change. Uniprot identifiers were mapped to Entrez identifiers using R package biomaRt [77, 78].

Western blotting

Cells were lysed by adding Triton X-100 lysis buffer (50 mM Tris-HCl, pH 7.5, 150 mM NaCl, 0.5% Triton X-100, 5% Glycerol, 1% SDS)–containing protease and phosphatase inhibitors (Roche). The protein quantification was carried out by detergent-compatible protein assay kit (Bio-Rad, Hercules, CA), and 30 μg of protein was resolved in 12% SDS-PAGE gel. The antibodies used in this study are NFATC2, PSMB5, VIM (all from Cell Signaling), ENO3 (Sigma), FOXO1 (Immunoway), SMYD3 (Abcam), FOXP3 (eBioscience), and β-actin (CalBioChem).

Flow cytometry

Cultured T cells were stained for surface expression of CD69 and CD101 (both from BD Biosciences, San Diego, CA). Detection of FOXP3+ or IL17-producing cells was determined by intracellular staining. Briefly, cells were stimulated for 4 h with PMA and ionomycin; after 2 h, GolgiStop (BD Biosciences) was added. Stimulated cells were fixed and permeabilized with Transcription Factor Staining Buffer Set (eBioscience, San Diego, CA) stained with anti-IL17-phycoerythrin (BD Biosciences), Foxp3-APC, or FOXP3-FITC (eBioscience) according to manufacturer's instructions and detected in flow cytometer LSRII (Becton Dickinson, San Jose, CA). Events were collected and analyzed by using flowjo software (Tree Star, Ashland, OR).

Key Learning Points

- **The first proteomics characterization of Th17 cells**
- **Identification of proteins differentially expressed in mouse Th17 and iTreg cells**
- **Comparison of proteomic and transcriptomics changes in mouse Th17 and iTreg cells**

Supporting information

S1 Fig. Correlation of 3 biological replicates. (a) PCA plot of proteomes of different in vitro cultured subsets. Symbols represent biological replicates, and color code represents respective subsets. Ellipses were drawn manually. (b) Pearson's correlation plots showing the correlation coefficient of 3 biological replicates for Thp. (c) Distribution of signal intensities. Plots show the expression of all quantified proteins over 6 orders of magnitude form different cell types. The complete lists of detected proteins can be found in S1 Data. PCA, principal component analysis; Thp, naïve CD4+ T cells.
(TIF)

S2 Fig. Functional groups of DE proteins in Th17 versus Th0 or iTreg versus Th0 cells. (a) Heatmaps showing log-fold-change values with selected functional groups of DE proteins in comparison of Th17 versus Th0 and iTreg versus Th0 cells. Protein annotation for functional groups is obtained from IPA. The complete lists of DE proteins can be found in S2 Data. (b) KEGG pathway enrichment analysis was performed on DE proteins of Th17 versus Th0 conditions. The significantly (Fisher exact test, Benjamini-Hochberg adjusted $p < 0.05$) enriched pathways are presented in the plot, color indicates the adjusted p-value, and size of dot indicates the number of proteins enriched for that pathway. The list of pathways and proteins can be found in S2 Data. DE, differentially expressed; IPA, Ingenuity Pathway Analysis; iTreg, induced regulatory T cells; KEGG, Kyoto Encyclopedia of Genes and Genomes; Th0, T cell receptor–activated helper T cell; Th17, T helper 17
(TIF)

S3 Fig. Distinct protein expression changes in Th17 and iTreg cells. (a) Venn diagram showing the comparisons of DE proteins between Th17 (Th17 versus Th0) and iTreg (iTreg versus Th0) cells. (b and c) Log-fold-change heat map of selected proteins of Th17 versus iTreg in comparison with Th0. The white color in the heat map indicates that protein differences were not statistically significant. The lists of DE proteins in Th17 versus iTreg cells are in S3 Data. (d) String network of protein interactions in Th17 and iTreg cells. The modules shown were obtained by performing the gene-set-enrichment analyses of GO and KEGG pathway. The colors of nodes indicate the log fold change of Th17 and iTreg proteins comparison, and size of nodes indicates the degree of connectivity of the nodes. The list of pathways and proteins can be found in S3 Data. DE, differentially expressed; GO, Gene Ontology; iTreg, induced regulatory T; KEGG, Kyoto Encyclopedia of Genes and Genomes; Th0, T cell receptor–activated helper T cell; Th17, T helper 17
(TIF)

S4 Fig. Correlation of protein and RNA expression changes during Th17 differentiation. (a) Functional groups of DE proteins with and without consistent mRNA changes and DE

mRNA without correlated protein changes (in S4 Data). (b) Genes that are regulated likewise in both transcriptomics and proteomics data have similar gene expression values as genes that are DE in transcriptomics data but not in proteomics data. The curves represent Gaussian kernel density estimates of base-2 logarithms of the mean FPKM values of Th17 samples (in S4 Data). DE, differentially expressed; FPKM, fragments per kilobase of transcript per million mapped reads; Th17, T helper 17
(TIF)

S5 Fig. Immunoblot analysis of 2 replicates showing the validated proteins in Th0, iTreg, and Th17 cells. Immunoblot analysis showing the biological replicates for the expression of PSMB5, SMYD3, NFATC2, JUNB, ENO3, FOXO1, VIM, and loading control β-Actin. ENO3, enolase 3; FOXO1, forkhead box O1; iTreg, induced regulatory T cells; NFATC2, nuclear factor of activated T cells 2; PSMB5, proteasome subunit beta 5; SMYD3, SET and MYND domain containing 3; Th0, T cell receptor–activated helper T cell; Th17, T helper 17; VIM, vimentin.
(TIF)

S1 Data. Lists of detected proteins and cumulative protein abundances in Th0, iTreg, Th17, and Thp cells, related to Fig 1, Fig 2A and S1 Fig. iTreg, induced regulatory T; Th0, T cell receptor–activated helper T cell; Th17, T helper 17; Thp, naïve CD4+ T cells.
(XLSX)

S2 Data. Lists of DE proteins in Th17 versus Th0 and iTreg versus Th0 and pathways from pathway enrichment analysis, related to Fig 2 and S2 Fig. DE, differentially expressed; iTreg, induced regulatory T; Th0, T cell receptor–activated helper T; Th17, T helper 17
(XLSX)

S3 Data. Lists of DE proteins in Th17 versus iTreg, pathways from pathway enrichment analysis and proteins for network analysis, related to Fig 3 and S3 Fig. DE, differentially expressed; iTreg, induced regulatory T; Th17, T helper 17.
(XLSX)

S4 Data. Lists of DE genes in Th17 versus Th0 and iTreg versus Th0 cells with detected proteins, DE proteins with encoded genes, and correlated protein and mRNA expression changes, related to Fig 4A and 4B. DE, differentially expressed; iTreg, induced regulatory T; Th0, T cell receptor–activated helper T; Th17, T helper 17
(XLSX)

S5 Data. The log fold change values of selected proteins and mRNA DE in Th17 and iTreg cells in comparison with Th0 cells and Th17 compared with iTreg cells, related to Fig 5A. DE, differentially expressed; iTreg, induced regulatory T; Th0, T cell receptor–activated helper T; Th17, T helper 17
(XLSX)

S6 Data. mRNA expression of Vim in Th17, iTreg and Th0 cells and quantification of Foxp3 expression in Vim+/+ and Vim−/− mice, related to Fig 6A and 6D. Foxp3, forkhead box P3; iTreg, induced regulatory T; Th0, T cell receptor–activated helper T; Th17, T helper 17; Vim, vimentin.
(XLSX)

Acknowledgments

The proteomics core facility and Finnish Functional Genomics Centre at the Turku Center for Biotechnology are acknowledged for their technical assistance. We thank Dr. Natalia

Battchikova from Department of Biochemistry, University of Turku, for sharing knowledge and reagent for proteomics sample preparation.

Author Contributions

Conceptualization: Zhi Chen.

Data curation: Imran Mohammad, Kari Nousiainen, Harri Lähdesmäki.

Funding acquisition: John E. Eriksson, Harri Lähdesmäki, Zhi Chen.

Investigation: Imran Mohammad, Inna Starskaia, Fang Cheng, Ponnuswamy Mohanasundaram, Zhi Chen.

Methodology: Imran Mohammad, Santosh D. Bhosale, Robert Moulder, Anne Rokka, David R. Goodlett.

Project administration: Zhi Chen.

Resources: John E. Eriksson, Harri Lähdesmäki, Zhi Chen.

Software: Kari Nousiainen, Harri Lähdesmäki.

Supervision: John E. Eriksson, David R. Goodlett, Harri Lähdesmäki, Zhi Chen.

Validation: Imran Mohammad.

Visualization: Imran Mohammad, Kari Nousiainen, Zhi Chen.

Writing – original draft: Zhi Chen.

Writing – review & editing: Imran Mohammad, Kari Nousiainen, Santosh D. Bhosale, Inna Starskaia, Robert Moulder, Anne Rokka, Fang Cheng, Ponnuswamy Mohanasundaram, John E. Eriksson, David R. Goodlett, Harri Lähdesmäki, Zhi Chen.

References

1. Sakaguchi S, Sakaguchi N, Asano M, Itoh M, Toda M. Immunologic self-tolerance maintained by activated T cells expressing IL-2 receptor alpha-chains (CD25). Breakdown of a single mechanism of self-tolerance causes various autoimmune diseases. J Immunol. 1995; 155(3):1151–64. PMID: 7636184.
2. Zhu J, Yamane H, Paul WE. Differentiation of effector CD4 T cell populations (*). Annu Rev Immunol. 2010; 28:445–89. 10.1146/annurev-immunol-030409-101212. https://doi.org/10.1146/annurev-immunol-030409-101212 PMID: 20192806.
3. Martín P, Gómez M, Lamana A, Cruz-Adalia A, Ramírez-Huesca M, Ursa MA, et al. CD69 association with Jak3/Stat5 proteins regulates Th17 cell differentiation. Mol Cell Biol. 2010; 30(20):4877–89. Epub 2010/08/09. https://doi.org/10.1128/MCB.00456-10 PMID: 20696842; PubMed Central PMCID: PMCPMC2950549.
4. Martín P, Sánchez-Madrid F. CD69: an unexpected regulator of TH17 cell-driven inflammatory responses. Sci Signal. 2011; 4(165):pe14. Epub 2011/03/22. https://doi.org/10.1126/scisignal.2001825 PMID: 21427408.
5. Chen W, Jin W, Hardegen N, Lei KJ, Li L, Marinos N, et al. Conversion of peripheral CD4+CD25- naive T cells to CD4+CD25+ regulatory T cells by TGF-beta induction of transcription factor Foxp3. J Exp Med. 2003; 198(12):1875–86. jem.20030152 [pii]10.1084/jem.20030152. https://doi.org/10.1084/jem.20030152 PMID: 14676299; PubMed Central PMCID: PMCPMC2194145.
6. Fu S, Zhang N, Yopp AC, Chen D, Mao M, Zhang H, et al. TGF-beta induces Foxp3 + T-regulatory cells from CD4 + CD25—precursors. Am J Transplant. 2004; 4(10):1614–27. AJT566 [pii]10.1111/j.1600-6143.2004.00566.x. https://doi.org/10.1111/j.1600-6143.2004.00566.x PMID: 15367216.
7. Fantini MC, Becker C, Monteleone G, Pallone F, Galle PR, Neurath MF. Cutting edge: TGF-beta induces a regulatory phenotype in CD4+CD25- T cells through Foxp3 induction and down-regulation of Smad7. J Immunol. 2004; 172(9):5149–53. PMID: 15100250.
8. Nishikawa H, Sakaguchi S. Regulatory T cells in cancer immunotherapy. Curr Opin Immunol. 2014; 27:1–7. Epub 2014/01/14. https://doi.org/10.1016/j.coi.2013.12.005 PMID: 24413387.

9. Elo LL, Järvenpää H, Tuomela S, Raghav S, Ahlfors H, Laurila K, et al. Genome-wide profiling of interleukin-4 and STAT6 transcription factor regulation of human Th2 cell programming. Immunity. 2010; 32 (6):852–62. S1074-7613(10)00214-1 [pii]10.1016/j.immuni.2010.06.011. https://doi.org/10.1016/j.immuni.2010.06.011 PMID: 20620947.

10. Wei G, Wei L, Zhu J, Zang C, Hu-Li J, Yao Z, et al. Global mapping of H3K4me3 and H3K27me3 reveals specificity and plasticity in lineage fate determination of differentiating CD4+ T cells. Immunity. 2009; 30 (1):155–67. S1074-7613(08)00555-4 [pii]10.1016/j.immuni.2008.12.009. https://doi.org/10.1016/j.immuni.2008.12.009 PMID: 19144320; PubMed Central PMCID: PMCPMC2722509.

11. Wei L, Vahedi G, Sun HW, Watford WT, Takatori H, Ramos HL, et al. Discrete roles of STAT4 and STAT6 transcription factors in tuning epigenetic modifications and transcription during T helper cell differentiation. Immunity. 2010; 32(6):840–51. S1074-7613(10)00206-2 [pii]10.1016/j.immuni.2010.06.003. https://doi.org/10.1016/j.immuni.2010.06.003 PMID: 20620946; PubMed Central PMCID: PMCPMC2904651.

12. Tuomela S, Lahesmaa R. Early T helper cell programming of gene expression in human. Semin Immunol. 2013; 25(4):282–90. Epub 2013/11/16. https://doi.org/10.1016/j.smim.2013.10.013 PMID: 24246225.

13. Tripathi SK, Lahesmaa R. Transcriptional and epigenetic regulation of T-helper lineage specification. Immunol Rev. 2014; 261(1):62–83. https://doi.org/10.1111/imr.12204 PMID: 25123277; PubMed Central PMCID: PMCPMC4255756.

14. Tuomela S, Rautio S, Ahlfors H, Öling V, Salo V, Ullah U, et al. Comparative analysis of human and mouse transcriptomes of Th17 cell priming. Oncotarget. 2016; 7(12):13416–28. https://doi.org/10.18632/oncotarget.7963 PMID: 26967054; PubMed Central PMCID: PMCPMC4924651.

15. Cenik C, Cenik ES, Byeon GW, Grubert F, Candille SI, Spacek D, et al. Integrative analysis of RNA, translation, and protein levels reveals distinct regulatory variation across humans. Genome Res. 2015; 25(11):1610–21. Epub 2015/08/21. https://doi.org/10.1101/gr.193342.115 PMID: 26297486; PubMed Central PMCID: PMCPMC4617958.

16. Vogel C, Marcotte EM. Insights into the regulation of protein abundance from proteomic and transcriptomic analyses. Nat Rev Genet. 2012; 13(4):227–32. https://doi.org/10.1038/nrg3185 PMID: 22411467.

17. Moulder R, Lönnberg T, Elo LL, Filén JJ, Rainio E, Corthals G, et al. Quantitative proteomics analysis of the nuclear fraction of human CD4+ cells in the early phases of IL-4-induced Th2 differentiation. Mol Cell Proteomics. 2010; 9(9):1937–53. M900483-MCP200 [pii]10.1074/mcp.M900483-MCP200. https://doi.org/10.1074/mcp.M900483-MCP200 PMID: 20467038; PubMed Central PMCID: PMCPMC2938108.

18. Procaccini C, Carbone F, Di Silvestre D, Brambilla F, De Rosa V, Galgani M, et al. The Proteomic Landscape of Human Ex Vivo Regulatory and Conventional T Cells Reveals Specific Metabolic Requirements. Immunity. 2016; 44(2):406–21. https://doi.org/10.1016/j.immuni.2016.01.028 PMID: 26885861; PubMed Central PMCID: PMCPMC4760097.

19. Rosengren AT, Nyman TA, Lahesmaa R. Proteome profiling of interleukin-12 treated human T helper cells. Proteomics. 2005; 5(12):3137–41. https://doi.org/10.1002/pmic.200401151 PMID: 16038020.

20. Duguet F, Locard-Paulet M, Marcellin M, Chaoui K, Bernard I, Andreoletti O, et al. Proteomic analysis of regulatory T cells reveals the importance of Themis1 in the control of their suppressive function. Mol Cell Proteomics. 2017. Epub 2017/04/03. https://doi.org/10.1074/mcp.M116.062745 PMID: 28373295.

21. Rossi D, Zlotnik A. The biology of chemokines and their receptors. Annu Rev Immunol. 2000; 18:217–42. https://doi.org/10.1146/annurev.immunol.18.1.217 PMID: 10837058.

22. Laurence A, Tato CM, Davidson TS, Kanno Y, Chen Z, Yao Z, et al. Interleukin-2 signaling via STAT5 constrains T helper 17 cell generation. Immunity. 2007; 26(3):371–81. S1074-7613(07)00176-8 [pii] https://doi.org/10.1016/j.immuni.2007.02.009 PMID: 17363300.

23. Rudensky AY. Regulatory T cells and Foxp3. Immunol Rev. 2011; 241(1):260–8. https://doi.org/10.1111/j.1600-065X.2011.01018.x PMID: 21488902; PubMed Central PMCID: PMCPMC3077798.

24. Chen Z, O'Shea JJ. Regulation of IL-17 production in human lymphocytes. Cytokine. 2008; 41(2):71–8. S1043-4666(07)00413-9 [pii]10.1016/j.cyto.2007.09.009. https://doi.org/10.1016/j.cyto.2007.09.009 PMID: 17981475.

25. Chen Z, O'Shea JJ. Th17 cells: a new fate for differentiating helper T cells. Immunol Res. 2008; 41 (2):87–102. https://doi.org/10.1007/s12026-007-8014-9 PMID: 18172584.

26. Tuomela S, Salo V, Tripathi SK, Chen Z, Laurila K, Gupta B, et al. Identification of early gene expression changes during human Th17 cell differentiation. Blood. 2012. blood-2012-01-407528 [pii]10.1182/blood-2012-01-407528. https://doi.org/10.1182/blood-2012-01-407528 PMID: 22544700.

27. Ciofani M, Madar A, Galan C, Sellars M, Mace K, Pauli F, et al. A validated regulatory network for Th17 cell specification. Cell. 2012; 151(2):289–303. https://doi.org/10.1016/j.cell.2012.09.016 PMID: 23021777; PubMed Central PMCID: PMCPMC3503487.

28. Yosef N, Shalek AK, Gaublomme JT, Jin H, Lee Y, Awasthi A, et al. Dynamic regulatory network controlling TH17 cell differentiation. Nature. 2013; 496(7446):461–8. https://doi.org/10.1038/nature11981 PMID: 23467089; PubMed Central PMCID: PMCPMC3637864.

29. Ivanov II, McKenzie BS, Zhou L, Tadokoro CE, Lepelley A, Lafaille JJ, et al. The orphan nuclear receptor RORgammat directs the differentiation program of proinflammatory IL-17+ T helper cells. Cell. 2006; 126(6):1121–33. S0092-8674(06)01105-6 [pii]10.1016/j.cell.2006.07.035. https://doi.org/10.1016/j.cell.2006.07.035 PMID: 16990136.

30. Chen Z, Laurence A, O'Shea JJ. Signal transduction pathways and transcriptional regulation in the control of Th17 differentiation. Semin Immunol. 2007; 19(6):400–8. S1044-5323(07)00092-9 [pii]10.1016/j.smim.2007.10.015. https://doi.org/10.1016/j.smim.2007.10.015 PMID: 18166487; PubMed Central PMCID: PMCPMC2323678.

31. Veldhoen M, Hirota K, Westendorf AM, Buer J, Dumoutier L, Renauld JC, et al. The aryl hydrocarbon receptor links TH17-cell-mediated autoimmunity to environmental toxins. Nature. 2008; 453(7191):106–9. nature06881 [pii]10.1038/nature06881. https://doi.org/10.1038/nature06881 PMID: 18362914.

32. Rouillard AD, Gundersen GW, Fernandez NF, Wang Z, Monteiro CD, McDermott MG, et al. The harmonizome: a collection of processed datasets gathered to serve and mine knowledge about genes and proteins. Database (Oxford). 2016;2016. Epub 2016/07/03. https://doi.org/10.1093/database/baw100 PMID: 27374120; PubMed Central PMCID: PMCPMC4930834.

33. Medina JF. Role of the anion exchanger 2 in the pathogenesis and treatment of primary biliary cirrhosis. Dig Dis. 2011; 29(1):103–12. Epub 2011/06/17. https://doi.org/10.1159/000324144 PMID: 21691115.

34. Concepcion AR, Salas JT, Sáez E, Sarvide S, Ferrer A, Portu A, et al. CD8+ T cells undergo activation and programmed death-1 repression in the liver of aged Ae2a,b-/- mice favoring autoimmune cholangitis. Oncotarget. 2015; 6(30):28588–606. https://doi.org/10.18632/oncotarget.5665 PMID: 26396175; PubMed Central PMCID: PMCPMC4745679.

35. Patterson H, Nibbs R, McInnes I, Siebert S. Protein kinase inhibitors in the treatment of inflammatory and autoimmune diseases. Clin Exp Immunol. 2014; 176(1):1–10. https://doi.org/10.1111/cei.12248 PMID: 24313320; PubMed Central PMCID: PMCPMC3958149.

36. Grant SK. Therapeutic protein kinase inhibitors. Cell Mol Life Sci. 2009; 66(7):1163–77. https://doi.org/10.1007/s00018-008-8539-7 PMID: 19011754.

37. Beyer M, Thabet Y, Müller RU, Sadlon T, Classen S, Lahl K, et al. Repression of the genome organizer SATB1 in regulatory T cells is required for suppressive function and inhibition of effector differentiation. Nat Immunol. 2011; 12(9):898–907. ni.2084 [pii]10.1038/ni.2084. https://doi.org/10.1038/ni.2084 PMID: 21841785.

38. Szklarczyk D, Morris JH, Cook H, Kuhn M, Wyder S, Simonovic M, et al. The STRING database in 2017: quality-controlled protein-protein association networks, made broadly accessible. Nucleic Acids Res. 2017; 45(D1):D362–D8. Epub 2016/10/18. https://doi.org/10.1093/nar/gkw937 PMID: 27924014; PubMed Central PMCID: PMCPMC5210637.

39. Wu Q, Nie J, Gao Y, Xu P, Sun Q, Yang J, et al. Reciprocal regulation of RORγt acetylation and function by p300 and HDAC1. Sci Rep. 2015; 5:16355. Epub 2015/11/09. https://doi.org/10.1038/srep16355 PMID: 26549310; PubMed Central PMCID: PMCPMC4817527.

40. Chen Z, Laurence A, Kanno Y, Pacher-Zavisin M, Zhu BM, Tato C, et al. Selective regulatory function of Socs3 in the formation of IL-17-secreting T cells. Proc Natl Acad Sci U S A. 2006; 103(21):8137–42. 0600666103 [pii]10.1073/pnas.0600666103. https://doi.org/10.1073/pnas.0600666103 PMID: 16698929; PubMed Central PMCID: PMCPMC1459629.

41. Durant L, Watford WT, Ramos HL, Laurence A, Vahedi G, Wei L, et al. Diverse targets of the transcription factor STAT3 contribute to T cell pathogenicity and homeostasis. Immunity. 2010; 32(5):605–15. S1074-7613(10)00169-X [pii]10.1016/j.immuni.2010.05.003. https://doi.org/10.1016/j.immuni.2010.05.003 PMID: 20493732; PubMed Central PMCID: PMCPMC3148263.

42. Holland SM, DeLeo FR, Elloumi HZ, Hsu AP, Uzel G, Brodsky N, et al. STAT3 mutations in the hyper-IgE syndrome. N Engl J Med. 2007; 357(16):1608–19. https://doi.org/10.1056/NEJMoa073687 PMID: 17881745.

43. Milner JD, Brenchley JM, Laurence A, Freeman AF, Hill BJ, Elias KM, et al. Impaired T(H)17 cell differentiation in subjects with autosomal dominant hyper-IgE syndrome. Nature. 2008; 452(7188):773–6. https://doi.org/10.1038/nature06764 PMID: 18337720; PubMed Central PMCID: PMCPMC2864108.

44. Zhang B, Wang J, Wang X, Zhu J, Liu Q, Shi Z, et al. Proteogenomic characterization of human colon and rectal cancer. Nature. 2014; 513(7518):382–7. Epub 2014/07/20. https://doi.org/10.1038/nature13438 PMID: 25043054; PubMed Central PMCID: PMCPMC4249766.

45. Foss EJ, Radulovic D, Shaffer SA, Goodlett DR, Kruglyak L, Bedalov A. Genetic variation shapes protein networks mainly through non-transcriptional mechanisms. PLoS Biol. 2011; 9(9):e1001144. https://doi.org/10.1371/journal.pbio.1001144 PMID: 21909241; PubMed Central PMCID: PMC3167781.

46. Straub L. Beyond the transcripts: what controls protein variation? PLoS Biol. 2011; 9(9):e1001146. https://doi.org/10.1371/journal.pbio.1001146 PMID: 21909242; PubMed Central PMCID: PMC3167779.

47. Ghazalpour A, Bennett B, Petyuk VA, Orozco L, Hagopian R, Mungrue IN, et al. Comparative analysis of proteome and transcriptome variation in mouse. PLoS Genet. 2011; 7(6):e1001393. https://doi.org/10.1371/journal.pgen.1001393 PMID: 21695224; PubMed Central PMCID: PMC3111477.

48. Nagata DE, Ting HA, Cavassani KA, Schaller MA, Mukherjee S, Ptaschinski C, et al. Epigenetic control of Foxp3 by SMYD3 H3K4 histone methyltransferase controls iTreg development and regulates pathogenic T-cell responses during pulmonary viral infection. Mucosal Immunol. 2015; 8(5):1131–43. Epub 2015/02/11. https://doi.org/10.1038/mi.2015.4 PMID: 25669152; PubMed Central PMCID: PMCPMC4532649.

49. Bieber T, Rieger A, Stingl G, Sander E, Wanek P, Strobel I. CD69, an early activation antigen on lymphocytes, is constitutively expressed by human epidermal Langerhans cells. J Invest Dermatol. 1992; 98(5):771–6. PMID: 1569326.

50. Sancho D, Gómez M, Sánchez-Madrid F. CD69 is an immunoregulatory molecule induced following activation. Trends Immunol. 2005; 26(3):136–40. https://doi.org/10.1016/j.it.2004.12.006 PMID: 15745855.

51. Fernandez I, Zeiser R, Karsunky H, Kambham N, Beilhack A, Soderstrom K, et al. CD101 surface expression discriminates potency among murine FoxP3+ regulatory T cells. J Immunol. 2007; 179 (5):2808–14. PMID: 17709494.

52. Schey R, Dornhoff H, Baier JL, Purtak M, Opoka R, Koller AK, et al. CD101 inhibits the expansion of colitogenic T cells. Mucosal Immunol. 2016; 9(5):1205–17. Epub 2016/01/27. https://doi.org/10.1038/mi.2015.139 PMID: 26813346; PubMed Central PMCID: PMCPMC4963314.

53. Wu Y, Borde M, Heissmeyer V, Feuerer M, Lapan AD, Stroud JC, et al. FOXP3 controls regulatory T cell function through cooperation with NFAT. Cell. 2006; 126(2):375–87. https://doi.org/10.1016/j.cell.2006.05.042 PMID: 16873067.

54. Li HY, McMillen WT, Heap CR, McCann DJ, Yan L, Campbell RM, et al. Optimization of a dihydropyrrolopyrazole series of transforming growth factor-beta type I receptor kinase domain inhibitors: discovery of an orally bioavailable transforming growth factor-beta receptor type I inhibitor as antitumor agent. J Med Chem. 2008; 51(7):2302–6. Epub 2008/03/04. https://doi.org/10.1021/jm701199p PMID: 18314943.

55. Melisi D, Ishiyama S, Sclabas GM, Fleming JB, Xia Q, Tortora G, et al. LY2109761, a novel transforming growth factor beta receptor type I and type II dual inhibitor, as a therapeutic approach to suppressing pancreatic cancer metastasis. Mol Cancer Ther. 2008; 7(4):829–40. https://doi.org/10.1158/1535-7163.MCT-07-0337 PMID: 18413796; PubMed Central PMCID: PMCPMC3088432.

56. Zhang M, Kleber S, Röhrich M, Timke C, Han N, Tuettenberg J, et al. Blockade of TGF-β signaling by the TGFβR-I kinase inhibitor LY2109761 enhances radiation response and prolongs survival in glioblastoma. Cancer Res. 2011; 71(23):7155–67. Epub 2011/10/17. https://doi.org/10.1158/0008-5472.CAN-11-1212 PMID: 22006998.

57. Colucci-Guyon E, Portier MM, Dunia I, Paulin D, Pournin S, Babinet C. Mice lacking vimentin develop and reproduce without an obvious phenotype. Cell. 1994; 79(4):679–94. PMID: 7954832.

58. Stubbington MJ, Mahata B, Svensson V, Deonarine A, Nissen JK, Betz AG, et al. An atlas of mouse CD4(+) T cell transcriptomes. Biol Direct. 2015; 10:14. Epub 2015/04/03. https://doi.org/10.1186/s13062-015-0045-x PMID: 25886751; PubMed Central PMCID: PMCPMC4384382.

59. Proserpio V, Piccolo A, Haim-Vilmovsky L, Kar G, Lönnberg T, Svensson V, et al. Single-cell analysis of CD4+ T-cell differentiation reveals three major cell states and progressive acceleration of proliferation. Genome Biol. 2016; 17:103. Epub 2016/05/12. https://doi.org/10.1186/s13059-016-0957-5 PMID: 27176874; PubMed Central PMCID: PMCPMC4866375.

60. Haimovich G, Choder M, Singer RH, Trcek T. The fate of the messenger is pre-determined: a new model for regulation of gene expression. Biochim Biophys Acta. 2013; 1829(6–7):643–53. Epub 2013/01/19. https://doi.org/10.1016/j.bbagrm.2013.01.004 PMID: 23337853; PubMed Central PMCID: PMCPMC3891481.

61. Jayne S, Zwartjes CG, van Schaik FM, Timmers HT. Involvement of the SMRT/NCoR-HDAC3 complex in transcriptional repression by the CNOT2 subunit of the human Ccr4-Not complex. Biochem J. 2006; 398(3):461–7. https://doi.org/10.1042/BJ20060406 PMID: 16712523; PubMed Central PMCID: PMCPMC1559471.

62. Pollizzi KN, Powell JD. Integrating canonical and metabolic signalling programmes in the regulation of T cell responses. Nat Rev Immunol. 2014; 14(7):435–46. https://doi.org/10.1038/nri3701 PMID: 24962260; PubMed Central PMCID: PMCPMC4390057.

63. Michalek RD, Gerriets VA, Jacobs SR, Macintyre AN, MacIver NJ, Mason EF, et al. Cutting edge: distinct glycolytic and lipid oxidative metabolic programs are essential for effector and regulatory CD4+ T

cell subsets. J Immunol. 2011; 186(6):3299–303. Epub 2011/02/11. https://doi.org/10.4049/jimmunol.1003613 PMID: 21317389; PubMed Central PMCID: PMCPMC3198034.

64. Barbi J, Pardoll D, Pan F. Metabolic control of the Treg/Th17 axis. Immunol Rev. 2013; 252(1):52–77. https://doi.org/10.1111/imr.12029 PMID: 23405895; PubMed Central PMCID: PMCPMC3576873.

65. Shi LZ, Wang R, Huang G, Vogel P, Neale G, Green DR, et al. HIF1alpha-dependent glycolytic pathway orchestrates a metabolic checkpoint for the differentiation of TH17 and Treg cells. J Exp Med. 2011; 208(7):1367–76. https://doi.org/10.1084/jem.20110278 PMID: 21708926; PubMed Central PMCID: PMCPMC3135370.

66. Cheng F, Shen Y, Mohanasundaram P, Lindström M, Ivaska J, Ny T, et al. Vimentin coordinates fibroblast proliferation and keratinocyte differentiation in wound healing via TGF-β-Slug signaling. Proc Natl Acad Sci U S A. 2016; 113(30):E4320–7. Epub 2016/07/08. https://doi.org/10.1073/pnas.1519197113 PMID: 27466403; PubMed Central PMCID: PMCPMC4968728.

67. Ivaska J, Pallari HM, Nevo J, Eriksson JE. Novel functions of vimentin in cell adhesion, migration, and signaling. Exp Cell Res. 2007; 313(10):2050–62. Epub 2007/04/14. https://doi.org/10.1016/j.yexcr.2007.03.040 PMID: 17512929.

68. Ivaska J. Vimentin: Central hub in EMT induction? Small GTPases. 2011; 2(1):51–3. https://doi.org/10.4161/sgtp.2.1.15114 PMID: 21686283; PubMed Central PMCID: PMCPMC3116616.

69. Nieminen M, Henttinen T, Merinen M, Marttila-Ichihara F, Eriksson JE, Jalkanen S. Vimentin function in lymphocyte adhesion and transcellular migration. Nat Cell Biol. 2006; 8(2):156–62. Epub 2006/01/22. https://doi.org/10.1038/ncb1355 PMID: 16429129.

70. Nakatani Y, Tanioka T, Sunaga S, Murakami M, Kudo I. Identification of a cellular protein that functionally interacts with the C2 domain of cytosolic phospholipase A(2)alpha. J Biol Chem. 2000; 275(2):1161–8. PMID: 10625659.

71. Ritchie ME, Phipson B, Wu D, Hu Y, Law CW, Shi W, et al. limma powers differential expression analyses for RNA-sequencing and microarray studies. Nucleic Acids Res. 2015; 43(7):e47. Epub 2015/01/20. https://doi.org/10.1093/nar/gkv007 PMID: 25605792; PubMed Central PMCID: PMCPMC4402510.

72. Anders S, Pyl PT, Huber W. HTSeq—a Python framework to work with high-throughput sequencing data. Bioinformatics. 2015; 31(2):166–9. Epub 2014/09/25. https://doi.org/10.1093/bioinformatics/btu638 PMID: 25260700; PubMed Central PMCID: PMCPMC4287950.

73. Robinson MD, McCarthy DJ, Smyth GK. edgeR: a Bioconductor package for differential expression analysis of digital gene expression data. Bioinformatics. 2010; 26(1):139–40. Epub 2009/11/11. https://doi.org/10.1093/bioinformatics/btp616 PMID: 19910308; PubMed Central PMCID: PMCPMC2796818.

74. Robinson MD, Oshlack A. A scaling normalization method for differential expression analysis of RNA-seq data. Genome Biol. 2010; 11(3):R25. Epub 2010/03/02. https://doi.org/10.1186/gb-2010-11-3-r25 PMID: 20196867; PubMed Central PMCID: PMCPMC2864565.

75. McCarthy DJ, Chen Y, Smyth GK. Differential expression analysis of multifactor RNA-Seq experiments with respect to biological variation. Nucleic Acids Res. 2012; 40(10):4288–97. Epub 2012/01/28. https://doi.org/10.1093/nar/gks042 PMID: 22287627; PubMed Central PMCID: PMCPMC3378882.

76. Yu G, Wang LG, Han Y, He QY. clusterProfiler: an R package for comparing biological themes among gene clusters. OMICS. 2012; 16(5):284–7. Epub 2012/03/28. https://doi.org/10.1089/omi.2011.0118 PMID: 22455463; PubMed Central PMCID: PMCPMC3339379.

77. Durinck S, Moreau Y, Kasprzyk A, Davis S, De Moor B, Brazma A, et al. BioMart and Bioconductor: a powerful link between biological databases and microarray data analysis. Bioinformatics. 2005; 21(16):3439–40. https://doi.org/10.1093/bioinformatics/bti525 PMID: 16082012.

78. Durinck S, Spellman PT, Birney E, Huber W. Mapping identifiers for the integration of genomic datasets with the R/Bioconductor package biomaRt. Nat Protoc. 2009; 4(8):1184–91. Epub 2009/07/23. https://doi.org/10.1038/nprot.2009.97 PMID: 19617889; PubMed Central PMCID: PMCPMC3159387.

Ponnuswamy Mohanasundaram

The Role of Vimentin in Tissue Repair and Cell Growth

Epithelial-mesenchymal transition (EMT) is a normal development process, and it also occurs during wound healing, cancer, and fibrosis. EMT supports stemness properties by increasing cell proliferation rate, migration, invasion, and extracellular matrix secretion. Vimentin is a cytoskeletal intermediate filament protein and it is widely used as an EMT marker. The role of vimentin in EMT is not explored in-depth, here we found that vimentin deletion impairs EMT signaling, cell proliferation, cell growth and extracellular matrix deposition. mTORC1 signaling plays a vital role in cell growth by coordinating nutrients and growth factor signaling, here we found that vimentin regulates mTORC1 translocation to lysosome and activity by regulating Rag GTPase activity. Along with this we also observed that vimentin protects cells from reactive oxygen species. This thesis work provides new insights of vimentin role in tissue repair and cell growth.

ISBN 978-952-12-4263-2